Contrib. Astron. Obs. Skalnaté Pleso **48**, 15 – 31, (2018)

Stars with a Stable Magnetic Field

L. Ferrario

Mathematical Sciences Institute
The Australian National University
ACT 2601, Australia, (E-mail: Lilia.Ferrario@anu.edu.au)

Received: November 10, 2017; Accepted: November 25, 2017

Abstract. In this review I will summarise what we know about magnetic fields in stars and what the origin of these magnetic fields may be. I will address the issue of whether the magnetic flux is conserved from pre-main sequence to the compact star phase (fossil field origin) or whether fields may be dynamo generated during some stages of stellar evolution or perhaps during stellar merging events.

Key words: stars: magnetic field – stars: protostars – stars: chemically peculiar – white dwarfs – pulsars – stars: magnetars

1. Introduction

Babcock (1947) was the first astronomer to detect a magnetic field in a star (78 Vir). He also discovered what is still now the most highly magnetic main sequence star, HD 215441 whose field strength is about 3.4×10^4 G (Babcock, 1960). This became known as "Babcock's star" (see Fig. 1).

The existence of strong magnetic fields in white dwarfs was revealed much later when Kemp et al. (1970) detected strong circular polarisation in the continuum of Grw+70°8247 while in neutron stars came with the discovery of the first pulsar, a fast spinning neutron star (Pacini, 1968), by Jocelyn Bell in 1967 (Hewish et al., 1968).

Since those early years, major progress has been made on stellar magnetism thanks to high quality data coming from surveys covering the full range of stellar masses and spanning all evolutionary phases, including pre-main sequence (e.g. Alecian et al., 2013a,b; Hubrig et al., 2013), main and post main-sequence (e.g. Hubrig et al., 2011; Aurière et al., 2015; Wade et al., 2016; Mathys, 2017), white dwarfs (e.g., Schmidt et al., 2001; Landstreet et al., 2012; Kepler et al., 2013) and neutron stars (the Parkes multibeam pulsar survey; Manchester et al., 2001). The data secured by these surveys have allowed researchers to explore the incidence of magnetism among stars, probe their magnetic field strength and structure, and study their field evolution and origin.

The origin of large scale and stable magnetic fields in stars remains an open question in astrophysics. In this paper I will review what is currently known about stellar magnetism and the hypotheses that have been advanced to explain the origin of magnetic fields in stars. A comprehensive paper on stable magnetic

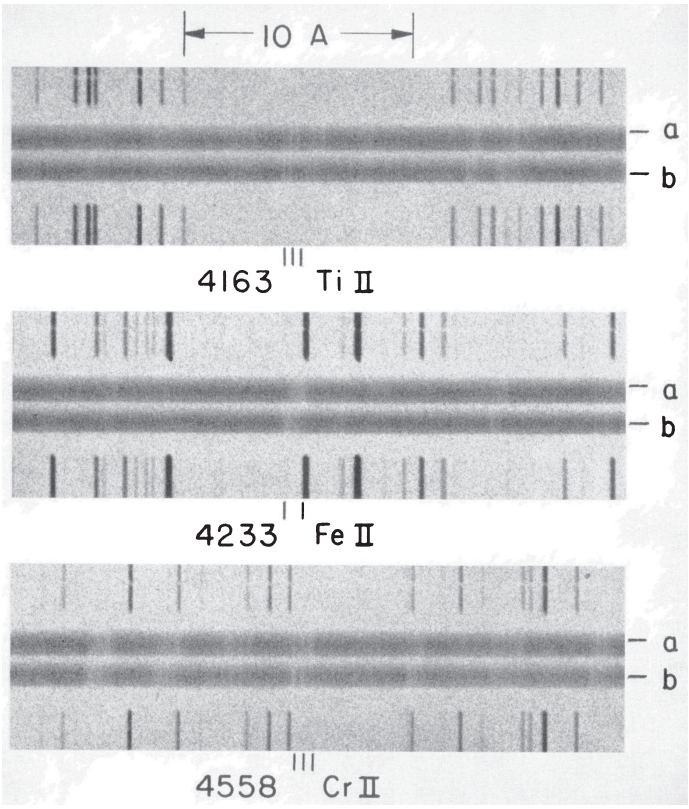

Figure 1. Spectrum of HD 215441 (Babcock, 1947) showing Zeeman split lines in a magnetic field of about 34 000 G. The spectra marked by a and b were photographed simultaneously through the left-hand and right-hand sections of a double circular analyzer. The original dispersion 4.5 Å mm^{-1}; slit width corresponds to 0.14 Å.

equilibria and their evolution in main-sequence and compact stars can be found in Reisenegger (2009) and an extensive review on the origin of stellar magnetic fields in Ferrario et al. (2015b).

2. The Dichotomies of Magnetic Non-Degenerate Stars

Herbig Ae/Be (HAeBe) objects are pre-main sequence stars of $2-15\,M_\odot$ at the later stages of their formation. These objects are still immersed in their protostellar gas-dust envelope and exhibit emission lines of stellar type A/B. Alecian et al. (2013a,b) and Hubrig et al. (2013) conducted large spectro-polarimetric surveys of HAeBe stars to investigate their magnetic and rotational properties

and explore possible evolutionary links between their characteristics to those of the magnetic main sequence Ap/Bp stars. These observations have indeed shown that around 7% of HAeBe objects display large-scale, mainly dipolar magnetic fields with strengths in the range $300 - 2\,100\,\mathrm{G}$ which are similar to those of magnetic main sequence Ap and Bp stars if conservation of magnetic flux is assumed. The incidence of magnetism among HAeBe is also consistent with that observed on the main-sequence. The surveys have also revealed that while the non-magnetic HAeBe objects exhibit rotations $v \sin i = 0 - 300\,\mathrm{km\,s^{-1}}$, the magnetic ones are generally much more slowly rotating with $v \sin i \leq 100\,\mathrm{km\,s^{-1}}$. This dichotomy is reminiscent of that observed in magnetic stars on the main sequence (as first reported by Wolff, 1975) that can have spin periods of up to 1 000 years (see Mathys, 2015). This suggests that those physical processes that are responsible for rotational braking in magnetic main-sequence stars are already at play in the late stages of stellar formation. In this context, Netopil et al. (2017) and Netopil et al. (2018, these proceedings) have studied the rotational characteristics of a sample of more than 500 magnetic main-sequence stars. Their results have confirmed the previous results of North (1998) and Stepien (1998) that the angular momentum is conserved during the evolution on the main-sequence and that no further magnetic braking is observed. Furthermore, they showed that while stars with the highest fields tend to be the slowest rotators, the strongest fields are found only in stars with spin periods shorter than about 150 d, thus confirming the earlier findings of Mathys et al. (1997) and more recently of Mathys (2017).

A second dichotomy exists among A and B type stars with masses of $1.5 - 6\,\mathrm{M_\odot}$, that is, they either exhibit large-scale fields of $300 - 34\,000\,\mathrm{G}$ or they are not magnetic down to the current detection limit of a few Gauss (see Fig. 2). The lack of stars in the 1-300 G field regime has been called the "Ap/Bp magnetic desert" (Aurière et al., 2007). Below the magnetic desert lies another type of magnetic stars, typified by Vega, whose longitudinal field is at the sub-Gauss level (Lignières et al., 2009). Thus this magnetic desert separates intermediate-mass stars with large-scale stable fields from those with unstable fields suggesting that two different mechanisms may be responsible for the generation of their fields. However, Fossati et al. (2015) have reported that massive stars may not have a magnetic desert, although its absence may be linked to mass-dependent field decay (see below Fossati et al., 2016).

A third dichotomy concerns the dearth of close binaries among main-sequence magnetic stars. The aim of the BinaMIcS (Binarity and Magnetic Interactions in various classes of Stars) programme (Alecian et al., 2015) was initiated to explore the incidence of magnetism in binaries with periods shorter than 20 d. Their studies have shown an incidence of magnetism that is about 3 to 5 times lower than in non-magnetic stars, thus confirming the results of Carrier et al. (2002) who first reported that binary systems hosting an Ap star tend to have periods ≥ 3 d.

The above three dichotomies tell us the following. It appears that large-scale

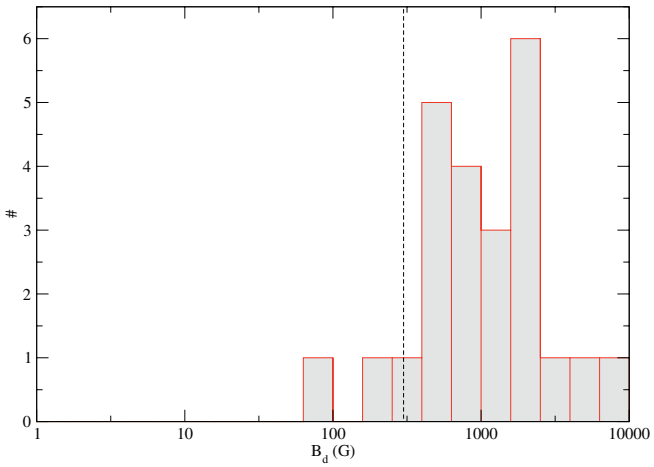

Figure 2. Histogram of the derived dipole strengths B_d of a sample of 28 magnetic Ap/Bp stars from Aurière et al. (2007). Note the dearth of Ap stars with $B_d < 300$ G.

magnetic fields in proto-stars and on the main-sequence are present only in a small fraction ($\sim$ 7%) of stars with radiative envelopes and that these magnetic stars are very rarely found in close binaries. The magnetic field strength dichotomy tells us that the origin of stellar magnetism cannot be attributed to some dynamo action taking place in some evolutionary phases, because if this were the case all stars would be magnetic at some level and there would be no Ap/Bp magnetic desert.

Observations indicate that the magnetic flux is conserved during the evolution from the pre-main sequence to the main sequence. However, if magnetism is a relic of the interstellar field from which the stars formed (see, e.g., Mestel, 1966) then we would expect that the incidence of magnetism should vary across diverse stellar populations. Thus the incidence in the Galactic field should differ from that in clusters and also from cluster to cluster. However, this does not seem to be the case (e.g. Paunzen et al., 2005, 2006). It is also curious that all magnetic stars in binaries (with the exception of ϵ Lupi; Shultz et al., 2015) have non-magnetic companions.

In order to explain the above dichotomies, Ferrario et al. (2009) advanced the hypothesis that magnetic fields could form when two proto-stars merge as they approach the main-sequence and when at least one of them has already developed a radiative envelope. These late mergers would produce a brief period of strong differential rotation and give rise to the large-scale fields observed in the radiative envelopes of Ap, Bp, and Of?p stars. They would also explain the scarcity of close binaries among intermediate-mass main-sequence magnetic stars. One of the merging proto-star predictions is that the incidence of mag-

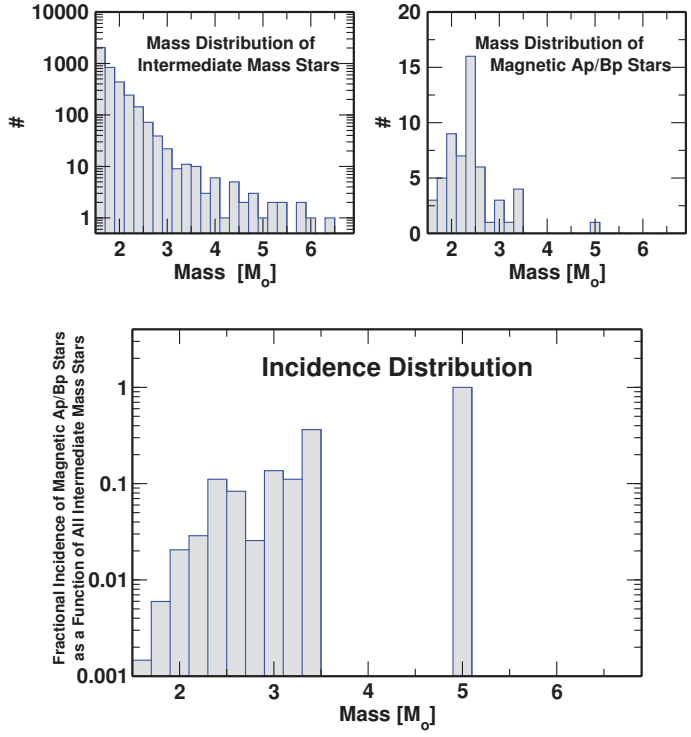

Figure 3. Mass distribution of A/B stars in the solar neighbourhood. *Top left*: mass distribution of all intermediate mass A/B stars. *Top right*: mass distribution of magnetic Ap/Bp stars. *Bottom*: incidence of Ap/Bp stars as a function of mass (Power et al., 2007).

netism should grow with stellar mass, which appears to be validated by the studies of Power et al. (2007) (see Fig. 3) and Sikora et al. (2018, these proceedings) who conducted a volume-limited sample of A/B stars with $M \leq 4\,\mathrm{M}_\odot$.

The question of how fields evolve with stellar age was addressed by Landstreet et al. (2008) who performed surveys of magnetism in A and B type stars in clusters. These observations allowed them to link field strength and structure to stellar mass, fractional ages, and metallicity. Their work revealed that fluxes clearly decrease with age indicating field decay. They also reported that such a decline is faster in stars with a mass larger than about $3\,\mathrm{M}_\odot$. Fossati et al. (2016) conducted a similar study on the field evolution in massive (5-100 $\mathrm{M}_\odot$) main-sequence stars and found an obvious deficiency of evolved magnetic stars which is more prominent at higher masses. So they propose that the absence of a magnetic desert in massive magnetic stars may be caused by the mass-dependent timescales over which field decay occurs. That is, if all magnetic stars are born

with a field above a certain cutoff, the lowest mass stars would retain it as they evolve on the main-sequence. This is because the field decay times in these stars is comparable to or longer than their main-sequence lifetime. However, if field decay acts faster as mass increases (and thus on timescales that are progressively shorter than their main-sequence lifetime), then massive magnetic stars will display, as a class, a smooth magnetic field distribution that extends to very low fields.

Fossati et al. (2016) also noted that field decay may explain the intriguing mismatch between the percentage of massive magnetic stars and that of slowly rotating massive stars. That is, many massive stars that used to be strongly magnetic (and therefore slowly rotating) are no longer magnetic at any measurable level (see also Fossati et al., 2015).

Despite this decay, fields have been observed in some post-main-sequence stars. The first field discovered in an evolved star was that in EK Eridani (Aurière et al., 2011). This is a very slowly rotating red giant ($P = 308.9$ d) with a convective envelope and a large scale poloidal field of about 270 G. Neiner et al. (2017) detected magnetic fields in another two hot evolved stars: ι Car (either on its first crossing of the HR diagram or on a blue loop) and HR 3890 (on its first and only crossing of the HR diagram) and confirmed the field in ϵ CMa (near the end of the main-sequence) first reported by Fossati et al. (2015). Their field strengths are compatible with magnetic flux conservation during stellar evolution indicating that at least in a fraction of stars magnetic fields can persist when a star evolves off the main-sequence.

The magnetic Ap/Bp stars show periodic variabilities caused by the non-uniform distribution of chemical elements on their surface. It is still not clear what causes these inhomogeneities and the viability of theoretical models is mostly restricted to observations of Galactic objects. However, stellar magnetism data obtained in extragalactic systems with different environmental properties would give us additional information that would allow us to better constrain theoretical models. This is what motivated Paunzen et al. (2013) to conduct photometric observations of a sample of magnetic Ap/Bp candidates in the Large Magellanic Cloud (LMC). They discovered that their LMC sample exhibits a low variability amplitude and explained it as due to the absence of regions of the stellar surface that have an overabundance of optically active elements. Paunzen et al. (2005, 2006) also found that while the percentage of chemically peculiar stars in Galactic open clusters is almost identical to that of the Galactic field, in the LMC the incidence is only about 2.2% – less than half of that estimated in the Galaxy. On the other hand, stellar masses and ages do not seem to be dissimilar from Galactic objects. These authors note that the LMC metallicity is about 0.5 dex compared to the Sun thus yielding important insights into the origin of chemical peculiarities and on the origin of magnetic fields in stars.

There are currently no calculations that include fossil fields and follow their evolution as the star ages and all the results highlighted in this section provide

us with valuable constraints for the construction of evolutionary models.

A very comprehensive review of magnetic fields in non-degenerate stars is given by Donati & Landstreet (2009).

3. Magnetic White Dwarfs

Magnetic fields of isolated magnetic white dwarfs lie in the range $10^3 - 10^9$ G. The upper limit cutoff near 10^9 G may be real but the incidence of magnetism below a few 10^3 G still needs to be established (see Landstreet et al., 2012, 2017). Since the discovery of the first magnetic white dwarf (Grw+70°8247; Kemp et al., 1970) the number of objects has been steadily increasing. We now have about 300 isolated and 170 magnetic white dwarfs in interacting binaries (the magnetic cataclysmic variables, MCVs). Extensive reviews on magnetism in white dwarfs can be found in Ferrario et al. (2015a), Wickramasinghe & Ferrario (2000) and also Kawka (2018, these proceedings).

The origin of magnetic fields in white dwarfs has been vigorously debated since their discovery. The proposal that the magnetic Ap/Bp stars are the progenitors of the High Field Magnetic White Dwarfs (HFMWDs; Tout et al., 2004; Wickramasinghe & Ferrario, 2005), as first suggested by Woltjer (1960), has recently been questioned (Liebert et al., 2005, 2015). The point is that there should be the same fraction of HFMWDs in binaries as in single stars. The Sloan Digital Sky Survey has identified thousands of detached white dwarf – M dwarf spectroscopic binaries (e.g., Rebassa-Mansergas et al., 2013, 2016; Ferrario, 2012) but none of these has a field above a few 10^6 G (the detectable limit in the SDSS spectra) even if there are hundreds of HFMWDs known to have fields greater than this detection limit (Liebert et al., 2005, 2015). The sample of white dwarfs within 20 pc (Holberg et al., 2008) has shown that $19.6 \pm 4.5\%$ of white dwarfs have main-sequence companions. Thus, $14 - 24\%$ of the ~ 300 HFMWDs should also have such companions, but none has been identified. The magnitude-limited Palomar-Green survey has shown that $23 - 29\%$ of hot white dwarfs have cool companions. Thus, we expect 7090 of the ~ 300 HFMWDs to have a companion. However, none has been found. The logical conclusion is that the origin of high magnetic fields in white dwarfs is intimately related to their binarity, as first proposed by Tout et al. (2008). We know that some HFMWDs are the result of merging events (EUVE 0317-855 is probably the best example, Vennes et al., 2003). Thus, if magnetic fields in white dwarfs arise as a result of either double degenerate or common envelope mergers, then the complete absence of main sequence (generally M-dwarf) companions to HFMWDs can easily be explained. Despite the total absence of detached binaries composed by a HFMWD and a non-degenerate companion, there are quite a few examples of binaries comprising two white dwarfs, one of which is highly magnetic (see Kawka et al., 2017, and references therein). Close post-common envelope magnetic binaries could have developed their fields during the common envelope

phase (Kawka et al., 2017, e.g., the fast spinning super-Chandrasekhar system NLTT 12758), while distant binaries could have been initially triple systems with two of the three stars merging at some point (e.g., EUVE 0317-855). Following Tout et al. (2008), the stellar merging hypothesis has been explored by Bogomazov & Tutukov (2009), Nordhaus et al. (2011), García-Berro et al. (2012) and Wickramasinghe et al. (2014).

One feature that characterises the HFMWDs is that their mean mass is around $0.78\,M_\odot$, considerably larger than that of non-magnetic white dwarfs ($0.66\,M_\odot$, Tremblay et al., 2013). The population synthesis calculations of Briggs et al. (2015) used the incidence of magnetism among white dwarfs and their mass distribution to constrain their models computed for different values of the common envelope efficiency parameter α. They found that the best agreement with observations is obtained for $\alpha < 0.3$ with the major contribution coming from the merging of a late asymptotic giant branch star with a main-sequence star.

A field distribution similar to that of the isolated HFMWDs is observed in the MCVs. In these interacting systems the mass flowing from the M-dwarf to the magnetic white dwarf is funnelled by the strong fields (a few $10^6 - 10^8$ G, as revealed by photospheric Zeeman lines and/or cyclotron emission features in their UV to IR spectra, e.g., Ferrario et al., 1992, 1993a, 1996, 2003; Schwope et al., 2003; Hoard et al., 2004) to form accretion shocks near the magnetic poles. Truncated accretion discs may or may not be present depending on the accretion rate and field strength (e.g., Ferrario et al., 1993b; Ferrario & Wehrse, 1999). The birth properties of MCVs have been analysed in the context of the common envelope origin of magnetic fields by Briggs et al. (2018, these proceedings). According to this scenario, those systems that emerge from common envelopes as close binaries and about to exchange mass will evolve into MCVs. They found that the best agreement with observations is obtained again for $\alpha < 0.3$. The study by Zorotovic et al. (2010) of the possible evolutionary histories of a sample of SDSS post-common-envelope binaries is in good agreement with the Briggs et al. (2018) results.

I note that there is an interesting parallel between the rarity of close binaries among magnetic main-sequence stars and HFMWDs, supporting a similar (merging) hypothesis for the origin of their fields.

Magnetic white dwarfs are also becoming important tools to investigate the formation and composition of exoplanets. For instance, the suggestion that GD 356 may have an Earth-type planetary companion (Li et al., 1998) is still a tantalising possibility to explain its unique emission line spectrum (Ferrario et al., 1997). Furthermore Kawka & Vennes (2014) have shown that the incidence of magnetism among cool and polluted white dwarfs is much greater than among their non-magnetic counterparts, and proposed a link between crowded planetary systems and the generation of magnetic fields in white dwarfs (see also Kawka, 2018, these proceedings).

4. Neutron Stars

The vast majority of neutron stars is made up by the classical radio pulsars (see the review by Beskin et al., 2015). Pulsars are powered by the loss of rotational energy caused by magnetic braking (remarkably, Pacini, 1967, suggested that a rotating pulsar might emit radio waves just before their discovery). If a pulsar has a spin period P, typically $0.3 - 2\,\mathrm{s}$, and a period derivative $\dot{P}$ (the rate at which the pulsar spins down), typically $10^{-17} - 10^{-13}\,\mathrm{s\,s^{-1}}$, then the dipole radiation formula $B = 3.2 \times 10^{19}\sqrt{P\dot{P}}\,\mathrm{G}$ (Manchester & Taylor, 1977) gives an estimate of a few $10^{11} - 10^{13}\,\mathrm{G}$ for the magnetic field strength. Thus, in the vast majority of cases the magnetic field strength of neutron stars can only be measured indirectly. The only exception arises in those rare cases when the X-ray spectrum of accreting neutron stars shows cyclotron harmonic features, such as those observed in the accreting neutron stars in X0115+63 (Santangelo et al., 1999), Vela X-1 (Kreykenbohm et al., 2002) and 1E1207.4-5209 (Bignami et al., 2003). These fields have been estimated to be a few $10^{10} - 10^{12}\,\mathrm{G}$, thus consistent with the fields inferred in classical pulsars. I show in the left panel of Fig. 4 the X-ray spectrum of X0115+63 and in the right panel, for comparison, the infrared spectrum of the accreting magnetic white dwarf in the MCV VV Puppis showing cyclotron emission features (Visvanathan & Wickramasinghe, 1979).

The millisecond pulsars (MSPs) are very rapidly spinning neutron stars with rotational periods $\gtrsim 30\,\mathrm{ms}$ and magnetic fields typically $\lesssim 10^9\,\mathrm{G}$. The most widely accepted theory regarding the origin of MSPs (mostly found in binary systems with white dwarfs or substellar mass companions) is that they are old neutron stars that have been spun up (recycled) via mass accretion (as first suggested by Backus et al., 1982). However, Ferrario & Wickramasinghe (2007) and Hurley et al. (2010) have demonstrated through population synthesis calculations that the birthrates of binary MSPs via accretion-induced collapse (AIC) of white dwarfs can be as large as, and possibly greater than, those for core collapse. In addition, AIC pulsars can better reproduce the orbital period distributions of some classes of binary MSPs.

At the very high end of the field distribution we find the soft gamma repeaters (SGRs) and the anomalous x-ray pulsars (AXPs), commonly referred to as the magnetars. They are generally characterised by very high fields of a few $10^{13} - 10^{15}\,\mathrm{G}$ (but not always, see below) and spin periods between 2-12 s which are much longer than those of radio-pulsars. The lifetime of magnetars is only a few 10,000 years and they are often found still embedded in their supernova remnants. It is still not clear whether these objects were born rotating very slowly or have spun down rapidly. The persistent and strong X-ray emission of magnetars ($\sim 10^{35}\,\mathrm{erg\,s^{-1}}$) is too large to be powered by their rotational energy. In addition they suffer from violent bursts lasting $0.1 - 40\,\mathrm{s}$ with peak luminosities of up to $\sim 10^{43}\,\mathrm{erg\,s^{-1}}$. SGRs also exhibit giant flares with an energy output of up to $\sim 10^{47}\,\mathrm{erg\,s^{-1}}$ lasting about one second. These activities have been

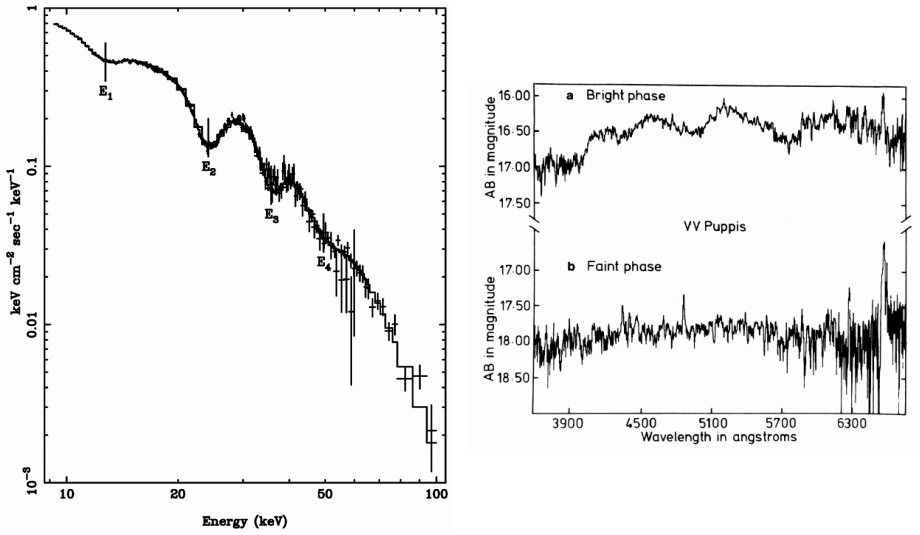

Figure 4. *Left*: Spectrum of X0115+63 showing cyclotron resonant scattering features suggestive that the accreting neutron star has a field of about 10^{12} G (Santangelo et al., 1999). *Right*: The discovery spectrum of VV Puppis exhibiting cyclotron harmonic lines from the accretion shock on the surface of the magnetic white dwarf (Visvanathan & Wickramasinghe, 1979) indicating a field strength of 3.2×10^7 G.

attributed to the decay and instabilities of their magnetic fields (Thompson & Duncan, 1996). Two very comprehensive reviews on the properties of magnetars can be found in Turolla et al. (2015a) and Mereghetti et al. (2015).

We show in Fig. 5 the $P-$ diagram of neutron stars (Manchester et al., 2005).

Another class of neutron stars is that formed by the very quiet and (probably) weakly magnetic ($\leq 10^{10}$ G) central compact objects (CCOs), found in young supernova remnants ($< 10^4$ yr). These are characterised by: (i) thermal X-ray emission (0.4 keV blackbody with dimensions of less than 1 km); (ii) absence of optical or radio emission; and (iii) lack of a pulsar wind nebula. Of the known supernova remnants within 5 kpc, 14 harbour normal radio pulsars, 6 harbour CCOs, and 1 hosts an AXP giving an incidence of CCOs of about 30% (de Luca, 2008). Thus, the birthrate of CCOs may be similar to that of normal radio pulsars. It is still not clear whether these objects were born with a low field (the proposal of Gotthelf & Halpern, 2008, that CCO pulsars anti-magnetars) or whether the field is submerged due to fallback matter from an accretion disc. Viganò & Pons (2012) have shown that some rather moderate accretion of $<< 0.1\,M_\odot$ can bury fields of a few $10^{12} - 10^{14}$ G that may re-emerge on a time-scale of $10^4 - 10^5$ yrs and convert a CCO into a normal radio pulsar (or even a magnetar). Popov & Turolla (2012) suggested that these pulsars would

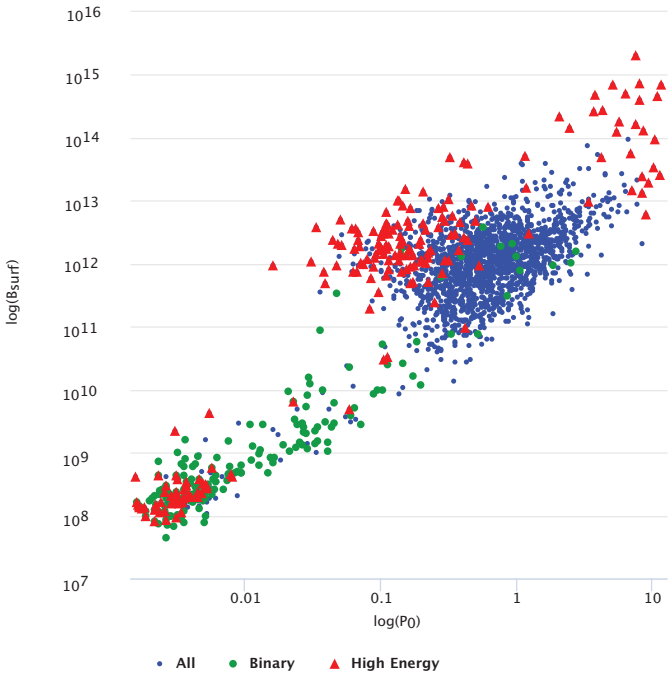

Figure 5. Plot of the surface magnetic field strength $B_{\rm surf}$ against spin period P_0 for pulsars obtained from the ATNF catalogue (Manchester et al., 2005).

be injected into the general population at periods of $0.1 - 0.5\,$s and would be expected to have a negative braking index because their magnetic fields would be increasing. They note that this is indeed the case for $20 - 40$ known pulsars.

As it is for the magnetic white dwarfs, the origin of magnetic fields in neutron stars is still unclear. The convection-driven dynamo of Thompson & Duncan (1993), which was inspired by solar dynamo calculations scaled to neutron stars' physical conditions, predicted fields of up to $10^{16}\,$G and it is still the most widely accepted theory for the origin of neutron stars' magnetic fields. Another avenue for field generation is given by the differential-rotation driven dynamo mechanism where toroidal and poloidal fields grow together until they reach equilibrium values (Braithwaite, 2006). Differential rotation can also be the outcome of stellar merging events, as suggested by Tout et al. (2008) and Wickramasinghe et al. (2014) in the context of magnetism in white dwarfs. Magnetic fields in neutron stars could also be explained according to the fossil field hypothesis (Ferrario & Wickramasinghe, 2006, 2008) which invokes magnetic flux conservation from the main-sequence (or earlier phases) to the compact star stage.

It is curious that neutron stars with similar dipolar field strengths (as inferred from their P and $\dot{P}$) can exhibit a very different array of emission behaviour. For instance, X-ray observations of SGR 0418+5729 by Rea et al. (2010) have revealed a dipolar magnetic field of only 7.5×10^{12} G which is typical of classical radio-pulsars. This indicates that a strong dipolar magnetic field is not necessary for a neutron star to display the violent emission characteristics of a magnetar. Instead, these could be caused by the decay of a large internal toroidal field that does not take part in the spin-down of the star (Thompson & Duncan, 1996; Ferrario & Wickramasinghe, 2008; Rea et al., 2010). It is this toroidal field that could be the differentiating factor among neutron stars of similar P and $\dot{P}$. Interestingly, SGR 0418+5729 is located at a rather high Galactic latitude and its P and $\dot{P}$ indicate that it is close to the death line for radio pulsars. Thus, as suggested by Rea et al. (2010), this SGR is much older than the other magnetars, further supporting the hypothesis that its emission and bursting characteristics (occurring when magnetic stresses overpower the rigid elastic crust causing crust-quakes Lander et al., 2015) may be due to the reservoir of energy amassed in its super-strong toroidal field that is slowly dissipating.

The population synthesis calculations of Ferrario & Wickramasinghe (2008) suggested that massive Of?p stars could be the progenitors of the magnetars because many of them have been associated with young clusters of massive stars. On the other hand, it may even be possible that the stellar merging hypothesis proposed for the explanation of magnetism on the upper main sequence and in the HFMWDs may also be applicable to the magnetars. This would give a unified origin for the fields in most magnetic stars (Wickramasinghe et al., 2014).

An interesting suggestion is that magnetars could also be responsible for short and long gamma-ray bursts (GRBs; Turolla et al., 2015b). For instance, Tout et al. (2011) propounded that the merging of an oxygen-neon white dwarf with the carbon-oxygen core of a naked helium star during a common envelope phase would produce a rapidly spinning magnetar giving rise to long GRBs. However, because the birth rate of magnetars is much higher than that of LGRBs, not all magnetars can be linked to LGRBs and thus the majority of magnetars is expected to originate from single-star evolution.

5. Conclusions

A 5-10% incidence of magnetism in stars is observed at all evolutionary phases, from pre-main-sequence to the compact star stage. Are these magnetic fields of fossil origin? Taken at face value, the observational results seem to support this hypothesis. However, the total absence of HFMWDs paired with non-degenerate companions in detached binaries has shed some serious doubts on this theory. The alternative scenario that would allow us to overcome the problem presented by this lack of duplicity is that HFMWDs could originate from stars that merge

during the common envelope phase or from two merging white dwarfs (double degenerate mergers). Those systems that survive the common envelope evolution and emerge as close binaries just before the onset of accretion will evolve into MCVs. A similar merging scenario could apply to magnetic pre-main-sequence stars, thus explaining the dearth of short-period binaries among Ap/Bp stars.

The origin of fields in neutron stars is more difficult to ascertain, partly because of our incomplete knowledge of their magnetic field strength, structure and evolution. Furthermore, many neutron stars seem to share the same location in the $P-\dot{P}$ diagram, thus suggesting that magnetic field strength alone cannot determine the observed emission behaviour of neutron stars. One proposal is that a hidden (internal) ultra-strong toroidal field that is slowly dissipating could be responsible for most magnetar-like activities observed in neutron stars.

An interesting possibility that has not been fully explored yet is that the fields of magnetars could also have originated through binary interaction, like the mechanism proposed to explain the origin of fields in the progenitors of the Ap/Bp stars and in the HFMWDs. The beauty of this scenario is that it leaves a unified picture for the origin of the highest magnetic fields in all types of stars.

Acknowledgements. L.F. acknowledges support from the Grant Agency of the Czech Republic (15-15943S) and the organisers of the conference "Stars with a stable magnetic field: from pre-main sequence to compact remnants" held in Brno. L.F. also wishes to thank all conference participants for stimulating discussions and in particular Ernst Paunzen, Martin Netopil, Gregg Wade, John Landstreet, Stefano Bagnulo, Stepháne Vennes, Adela Kawka and Alfio Bonanno.

References

Alecian, E., Neiner, C., Wade, G. A., et al. 2015, in IAU Symp., Vol. **307**, *New Windows on Massive Stars*, ed. G. Meynet, C. Georgy, J. Groh, & P. Stee, 330–335

Alecian, E., Wade, G. A., Catala, C., et al. 2013a, *Mon. Not. R. Astron. Soc.*, **429**, 1001

Alecian, E., Wade, G. A., Catala, C., et al. 2013b, *Mon. Not. R. Astron. Soc.*, **429**, 1027

Aurière, M., Konstantinova-Antova, R., Charbonnel, C., et al. 2015, *Astron. Astrophys.*, **574**, A90

Aurière, M., Konstantinova-Antova, R., Petit, P., et al. 2011, *Astron. Astrophys.*, **534**, A139

Aurière, M., Wade, G. A., Silvester, J., et al. 2007, *Astron. Astrophys.*, **475**, 1053

Babcock, H. W. 1947, *Astrophys. J.*, **105**, 105

Babcock, H. W. 1960, *Astrophys. J.*, **132**, 521

Backus, P. R., Taylor, J. H., & Damashek, M. 1982, *Astrophys. J., Lett.*, **255**, L63

Beskin, V. S., Chernov, S. V., Gwinn, C. R., & Tchekhovskoy, A. A. 2015, *Space Sci. Rev.*, **191**, 207

Bignami, G. F., Caraveo, P. A., De Luca, A., & Mereghetti, S. 2003, *Nature*, **423**, 725

Bogomazov, A. I. & Tutukov, A. V. 2009, *Astron. Rep.*, **53**, 214

Braithwaite, J. 2006, *Astron. Astrophys.*, **449**, 451

Briggs, G. P., Ferrario, L., Tout, C. A., Wickramasinghe, D. T., & Hurley, J. R. 2015, *Mon. Not. R. Astron. Soc.*, **447**, 1713

Carrier, F., North, P., Udry, S., & Babel, J. 2002, *Astron. Astrophys.*, **394**, 151

de Luca, A. 2008, in AIP Conf. Ser., Vol. **983**, *40 Years of Pulsars: Millisecond Pulsars, Magnetars and More*, ed. C. Bassa, Z. Wang, A. Cumming, & V. M. Kaspi, 311–319

Donati, J.-F. & Landstreet, J. D. 2009, *Ann. Rev. Astron. Astrophys.*, **47**, 333

Ferrario, L. 2012, *Mon. Not. R. Astron. Soc.*, **426**, 2500

Ferrario, L., Bailey, J., & Wickramasinghe, D. 1996, *Mon. Not. R. Astron. Soc.*, **282**, 218

Ferrario, L., Bailey, J., & Wickramasinghe, D. T. 1993a, *Mon. Not. R. Astron. Soc.*, **262**, 285

Ferrario, L., de Martino, D., & Gänsicke, B. T. 2015a, *Space Sci. Rev.*, **191**, 111

Ferrario, L., Melatos, A., & Zrake, J. 2015b, *Space Sci. Rev.*, **191**, 77

Ferrario, L., Pringle, J. E., Tout, C. A., & Wickramasinghe, D. T. 2009, *Mon. Not. R. Astron. Soc.*, **400**, L71

Ferrario, L. & Wehrse, R. 1999, *Mon. Not. R. Astron. Soc.*, **310**, 189

Ferrario, L. & Wickramasinghe, D. 2006, *Mon. Not. R. Astron. Soc.*, **367**, 1323

Ferrario, L. & Wickramasinghe, D. 2007, *Mon. Not. R. Astron. Soc.*, **375**, 1009

Ferrario, L. & Wickramasinghe, D. 2008, *Mon. Not. R. Astron. Soc.*, **389**, L66

Ferrario, L., Wickramasinghe, D. T., Bailey, J., Hough, J. H., & Tuohy, I. R. 1992, *Mon. Not. R. Astron. Soc.*, **256**, 252

Ferrario, L., Wickramasinghe, D. T., & King, A. R. 1993b, *Mon. Not. R. Astron. Soc.*, **260**, 149

Ferrario, L., Wickramasinghe, D. T., Liebert, J., Schmidt, G. D., & Bieging, J. H. 1997, *Mon. Not. R. Astron. Soc.*, **289**, 105

Ferrario, L., Wickramasinghe, D. T., & Schmidt, G. 2003, *Mon. Not. R. Astron. Soc.*, **338**, 340

Fossati, L., Castro, N., Morel, T., et al. 2015, *Astron. Astrophys.*, **574**, A20

Fossati, L., Schneider, F. R. N., Castro, N., et al. 2016, *Astron. Astrophys.*, **592**, A84

García-Berro, E., Lorén-Aguilar, P., Aznar-Siguán, G., et al. 2012, *Astrophys. J.*, **749**, 25

Gotthelf, E. V. & Halpern, J. P. 2008, in AIP Conf. Ser., Vol. **983**, *40 Years of Pulsars: Millisecond Pulsars, Magnetars and More*, ed. C. Bassa, Z. Wang, A. Cumming, & V. M. Kaspi, 320–324

Hewish, A., Bell, S. J., Pilkington, J. D. H., Scott, P. F., & Collins, R. A. 1968, *Nature*, **217**, 709

Hoard, D. W., Schmidt, G. D., Szkody, P., et al. 2004, *Astron. J.*, **128**, 1894

Holberg, J. B., Sion, E. M., Oswalt, T., et al. 2008, *Astron. J.*, **135**, 1225

Hubrig, S., Ilyin, I., Schöller, M., & Lo Curto, G. 2013, *Astron. Nachr.*, **334**, 1093

Hubrig, S., Schöller, M., Kharchenko, N. V., et al. 2011, *Astron. Astrophys.*, **528**, A151

Hurley, J. R., Tout, C. A., Wickramasinghe, D. T., Ferrario, L., & Kiel, P. D. 2010, *Mon. Not. R. Astron. Soc.*, **402**, 1437

Kawka, A., Briggs, G. P., Vennes, S., et al. 2017, *Mon. Not. R. Astron. Soc.*, **466**, 1127

Kawka, A. & Vennes, S. 2014, *Mon. Not. R. Astron. Soc.*, **439**, L90

Kemp, J. C., Swedlund, J. B., Landstreet, J. D., & Angel, J. R. P. 1970, *Astrophys. J., Lett.*, **161**, L77

Kepler, S. O., Pelisoli, I., Jordan, S., et al. 2013, *Mon. Not. R. Astron. Soc.*, **429**, 2934

Kreykenbohm, I., Coburn, W., Wilms, J., et al. 2002, *Astron. Astrophys.*, **395**, 129

Lander, S. K., Andersson, N., Antonopoulou, D., & Watts, A. L. 2015, *Mon. Not. R. Astron. Soc.*, **449**, 2047

Landstreet, J. D., Bagnulo, S., Valyavin, G., & Valeev, A. F. 2017, *Astron. Astrophys.*, **607**, A92

Landstreet, J. D., Bagnulo, S., Valyavin, G. G., et al. 2012, *Astron. Astrophys.*, **545**, A30

Landstreet, J. D., Silaj, J., Andretta, V., et al. 2008, *Astron. Astrophys.*, **481**, 465

Li, J., Ferrario, L., & Wickramasinghe, D. 1998, *Astrophys. J., Lett.*, **503**, L151

Liebert, J., Ferrario, L., Wickramasinghe, D. T., & Smith, P. S. 2015, *Astrophys. J.*, **804**, 93

Liebert, J., Wickramasinghe, D. T., Schmidt, G. D., et al. 2005, *Astron. J.*, **129**, 2376

Lignières, F., Petit, P., Böhm, T., & Aurière, M. 2009, *Astron. Astrophys.*, **500**, L41

Manchester, R. N., Hobbs, G. B., Teoh, A., & Hobbs, M. 2005, *Astron. J.*, **129**, 1993

Manchester, R. N., Lyne, A. G., Camilo, F., et al. 2001, *Mon. Not. R. Astron. Soc.*, **328**, 17

Manchester, R. N. & Taylor, J. H. 1977, *Pulsars* (San Francisco : W. H. Freeman, c1977.)

Mathys, G. 2015, in ASP Conf. Ser., Vol. **494**, *Physics and Evolution of Magnetic and Related Stars*, ed. Y. Y. Balega, I. I. Romanyuk, & D. O. Kudryavtsev, 3

Mathys, G. 2017, *Astron. Astrophys.*, **601**, A14

Mathys, G., Hubrig, S., Landstreet, J. D., Lanz, T., & Manfroid, J. 1997, *Astron. Astrophys., Suppl.*, **123**, 353

Mereghetti, S., Pons, J. A., & Melatos, A. 2015, *Space Sci. Rev.*, **191**, 315

Mestel, L. 1966, *Mon. Not. R. Astron. Soc.*, **133**, 265

Neiner, C., Oksala, M. E., Georgy, C., et al. 2017, *Mon. Not. R. Astron. Soc.*, **471**, 1926

Netopil, M., Paunzen, E., Hümmerich, S., & Bernhard, K. 2017, *Mon. Not. R. Astron. Soc.*, **468**, 2745

Nordhaus, J., Wellons, S., Spiegel, D. S., Metzger, B. D., & Blackman, E. G. 2011, *Proceedings of the National Academy of Science*, **108**, 3135

North, P. 1998, *Astron. Astrophys.*, **334**, 181

Pacini, F. 1967, *Nature*, **216**, 567

Pacini, F. 1968, *Nature*, **219**, 145

Paunzen, E., Maitzen, H. M., Pintado, O. I., et al. 2006, *Astron. Astrophys.*, **459**, 871

Paunzen, E., Mikulášek, Z., Poleski, R., et al. 2013, *Astron. Astrophys.*, **556**, A12

Paunzen, E., Pintado, O. I., Maitzen, H. M., & Claret, A. 2005, *Mon. Not. R. Astron. Soc.*, **362**, 1025

Popov, S. B. & Turolla, R. 2012, in ASP Conf. Ser., Vol. **466**, *Electromagnetic Radiation from Pulsars and Magnetars*, ed. W. Lewandowski, O. Maron, & J. Kijak, 191

Power, J., Wade, G. A., Hanes, D. A., Aurier, M., & Silvester, J. 2007, in *Physics of Magnetic Stars*, ed. I. I. Romanyuk, D. O. Kudryavtsev, O. M. Neizvestnaya, & V. M. Shapoval, 89–97

Rea, N., Esposito, P., Turolla, R., et al. 2010, *Science*, **330**, 944

Rebassa-Mansergas, A., Agurto-Gangas, C., Schreiber, M. R., Gänsicke, B. T., & Koester, D. 2013, *Mon. Not. R. Astron. Soc.*, **433**, 3398

Rebassa-Mansergas, A., Ren, J. J., Parsons, S. G., et al. 2016, *Mon. Not. R. Astron. Soc.*, **458**, 3808

Reisenegger, A. 2009, *Astron. Astrophys.*, **499**, 557

Santangelo, A., Segreto, A., Giarrusso, S., et al. 1999, *Astrophys. J., Lett.*, **523**, L85

Schmidt, G. D., Vennes, S., Wickramasinghe, D. T., & Ferrario, L. 2001, *Mon. Not. R. Astron. Soc.*, **328**, 203

Schwope, A. D., Thomas, H.-C., Mante, K.-H., Haefner, R., & Staude, A. 2003, *Astron. Astrophys.*, **402**, 201

Shultz, M., Wade, G. A., Alecian, E., & BinaMIcS Collaboration. 2015, *Mon. Not. R. Astron. Soc.*, **454**, L1

Stepien, K. 1998, *Contributions of the Astronomical Observatory Skalnate Pleso*, **27**, 205

Thompson, C. & Duncan, R. C. 1993, *Astrophys. J.*, **408**, 194

Thompson, C. & Duncan, R. C. 1996, *Astrophys. J.*, **473**, 322

Tout, C. A., Wickramasinghe, D. T., & Ferrario, L. 2004, *Mon. Not. R. Astron. Soc.*, **355**, L13

Tout, C. A., Wickramasinghe, D. T., Lau, H. H.-B., Pringle, J. E., & Ferrario, L. 2011, *Mon. Not. R. Astron. Soc.*, **410**, 2458

Tout, C. A., Wickramasinghe, D. T., Liebert, J., Ferrario, L., & Pringle, J. E. 2008, *Mon. Not. R. Astron. Soc.*, **387**, 897

Tremblay, P.-E., Ludwig, H.-G., Steffen, M., & Freytag, B. 2013, *Astron. Astrophys.*, **559**, A104

Turolla, R., Zane, S., & Watts, A. L. 2015a, *Rep. Prog. Phys.*, **78**, 116901

Turolla, R., Zane, S., & Watts, A. L. 2015b, *Rep. Prog. Phys.*, **78**, 116901

Vennes, S., Schmidt, G. D., Ferrario, L., et al. 2003, *Astrophys. J.*, **593**, 1040

Viganò, D. & Pons, J. A. 2012, *Mon. Not. R. Astron. Soc.*, **425**, 2487

Visvanathan, N. & Wickramasinghe, D. T. 1979, *Nature*, **281**, 47

Wade, G. A., Neiner, C., Alecian, E., et al. 2016, *Mon. Not. R. Astron. Soc.*, **456**, 2

Wickramasinghe, D. T. & Ferrario, L. 2000, *Publ. Astron. Soc. Pac.*, **112**, 873

Wickramasinghe, D. T. & Ferrario, L. 2005, *Mon. Not. R. Astron. Soc.*, **356**, 1576

Wickramasinghe, D. T., Tout, C. A., & Ferrario, L. 2014, *Mon. Not. R. Astron. Soc.*, **437**, 675

Wolff, S. C. 1975, *Astrophys. J.*, **202**, 127

Woltjer, L. 1960, *Astrophys. J.*, **131**, 227

Zorotovic, M., Schreiber, M. R., Gänsicke, B. T., & Nebot Gómez-Morán, A. 2010, *Astron. Astrophys.*, **520**, A86

Contrib. Astron. Obs. Skalnaté Pleso **48**, 32 – 39, (2018)

The magnetic field of molecular clouds

P. Padoan[1,2]

[1] *Institut de Ciències del Cosmos, Universitat de Barcelona, IEEC-UB, Martí i Franquès 1, E08028 Barcelona, Spain, (E-mail: ppadoan@icc.ub.edu)*
[2] *ICREA, Pg. Lluís Companys 23, 08010 Barcelona, Spain*

Received: December 11, 2017; Accepted: December 16, 2017

Abstract. The magnetic field of molecular clouds (MCs) plays an important role in the process of star formation: it determines the statistical properties of supersonic turbulence that controls the fragmentation of MCs, controls the angular momentum transport during the protostellar collapse, and affects the stability of circumstellar disks. In this work, we focus on the problem of the determination of the magnetic field strength. We review the idea that the MC turbulence is super-Alfvénic, and we argue that MCs are bound to be born super-Alfvénic. We show that this scenario is supported by results from a recent simulation of supernova-driven turbulence on a scale of 250 pc, where the turbulent cascade is resolved on a wide range of scales, including the interior of MCs.

Key words: ISM: kinematics and dynamics – magnetohydrodynamics (MHD) – stars: formation – turbulence

1. The magnetic-field strength in MCs

The idea that MCs are magnetically supported against their gravitational collapse was reviewed in Shu et al. (1987). In that scenario, the observed random velocities correspond to MHD waves, or perturbations of a strong mean field. Gravitationally bound prestellar cores are initially subcritical and contract because of ambipolar drift until they become supercritical and collapse. Padoan & Nordlund (1997, 1999) proposed an alternative scenario where the mean magnetic field in MCs is weak and the observed turbulence is super-Alfvénic. By comparing results of two simulations, one with a weak field and the other with a strong field, with observational data, they showed that the super-Alfvénic case reproduced the observations better. Further results in support of the super-Alfvénic scenario were later presented in Padoan et al. (2004) and, more recently, by Lunttila et al. (2008, 2009) based on simulated Zeeman measurements.

In this review, we first address the super-Alfvénic nature of the turbulence in MCs in the context of their formation process. To support our scenario, we present results of a large-scale (250 pc) MHD simulation of interstellar medium (ISM) turbulence driven by supernova (SN) explosions. We then show that MC turbulence is super-Alfvénic also with respect to their rms magnetic field, amplified by the turbulence. Finally, we briefly summarize observational results in favour of this picture.

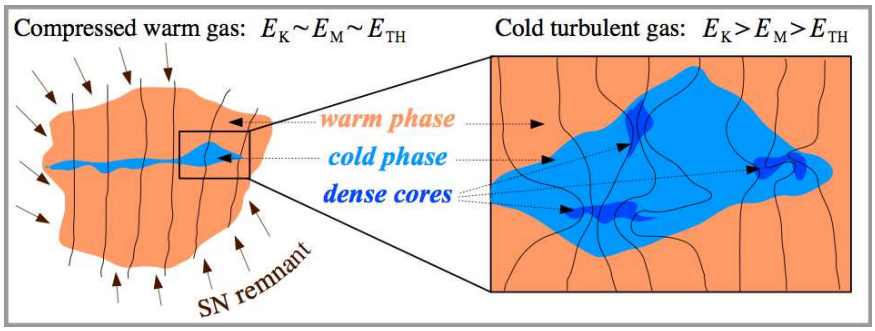

Figure 1. Schematic scenario of the formation of super-Alfvénic MCs.

2. MCs are born super-Alfvénic

Different processes may contribute to the formation of MCs, and a full treatment of this problem should also address the mechanisms of conversion between atomic and molecular gas. For a general picture, we assume that MCs are the result of large-scale compressions of the warm interstellar medium (WISM), driven by the evolution of SN remnants. When such compressions reach the pressure threshold of the thermal instability, the compressed gas rapidly cools and compresses further to a characteristic density of MCs. We can characterize the large-scale turbulence of the WISM by its rms sonic and Alfvénic Mach numbers, M_s and M_A. It is generally believed that the large-scale turbulence in the WISM is transonic and trans-Alfvénic, meaning $M_s \sim 1$ and $M_A \sim 1$.

Because of the transonic nature of the WISM turbulence, the large-scale velocity field can occasionally cause compressions strong enough to bring large regions above the thermal instability threshold. As the gas is further compressed thanks to its cooling, the magnetic field cannot be compressed because of the initially trans-Alfvénic nature of the flow, so the initial compression is forced to be primarily along the magnetic field direction. Assuming that turbulent velocities are not significantly decreased, the characteristic increase in density, $\rho_{cold} \sim 100\,\rho_{warm}$, results in a comparable increase in the turbulent kinetic energy, $E_{K,cold} \sim 100\,E_{K,warm}$, or a corresponding drop in the rms Alfvén velocity, $V_{a,cold} \sim V_{a,warm}/10$. As a consequence, the turbulence in the rapidly cooling gas must be initially super-Alfvénic with respect to the mean magnetic field (Nordlund & Padoan, 2003; Padoan et al., 2010). Compression and stretching in this super-Alfvénic flow can then locally amplify the magnetic field, without affecting the mean field. Because of the reduced temperature, the turbulence in the cold gas is also supersonic, so dense cores with enhanced magnetic field strength are naturally formed by shocks in the turbulent flow. This sequence of events is schematically depicted in Fig. 1.

3. Supernova-driven turbulence

The above scenario of MC formation is supported by a recent SN-driven MHD simulation (Padoan et al., 2016a,b, 2017; Pan et al., 2016) that models a 250-pc ISM region, large enough to address the formation and evolution and MCs. The MHD equations are solved with the Ramses AMR code (Teyssier, 2002; Fromang et al., 2006; Teyssier, 2007) within a cubic region of size $L_{\rm box} = 250$ pc, total mass $M_{\rm box} = 1.9 \times 10^6$ M$_\odot$, and periodic boundary conditions. The mean density is $n_{\rm H,0} = 5$ cm^{-3} and the mean magnetic field $B_0 = 4.6$ μG. The rms magnetic field amplified by the turbulence is 7.2 μG.

The only driving force is from SN feedback. SNe are randomly distributed in space and time during the first period of the simulation without self-gravity, while they are later determined by the position and age of the massive sink particles formed when self-gravity is included. In the initial phase without gravity, the minimum cell size is $dx = 0.24$ pc until $t = 45$ Myr. It is then decreased to $dx = 0.03$ pc, using a root-grid of 512^3 cells and four AMR levels, during an additional period of 10.5 Myr without self-gravity. Finally, at $t = 55.5$ Myr, gravity is introduced and the minimum cell size is further reduced to $dx = 0.0076$ pc by adding two more AMR levels.

To follow the collapse of prestellar cores, sink particles are created in cells where the gas density is larger than 10^6 cm^{-3} if a number of conditions are met (see Haugbølle et al., 2017). When a sink particle of mass larger than 7.5 M$_\odot$ has an age equal to the corresponding stellar lifetime for that mass, a sphere of 10^{51} erg of thermal energy is injected at the location of the sink particle to simulate the SN explosion, as described in detail in Padoan et al. (2016b). We refer to this driving method as *real SNe*, as it provides a SN feedback that is fully consistent with the star-formation rate (SFR), the stellar initial mass function, and the ages and positions of the individual stars whose formation is resolved in the simulation. The simulation has so far been run for approximately 30 Myr with self-gravity, star formation and *real SNe*, generating over 7 000 stars and hundreds of MCs. The SFR in the MCs has realistic values, while the global SFR corresponds to a mean gas-depletion time in the computational volume of almost 1 Gyr, also realistic for a 250-pc scale (Padoan et al., 2017).

4. The mean and rms magnetic-field strength of MCs

The simulation adopts a mean magnetic-field strength consistent with the Galactic one, so the magnetic field inside clouds selected from the simulation should be comparable to that in real MCs. To investigate the role of the magnetic field in individual MCs, in Padoan et al. (2016b) we consider a catalog of 1 547 clouds selected from several snapshots of the simulation, based on a density threshold of $n_{\rm H,min} = 200$ cm^{-3}. The mean and rms magnetic field of each cloud is computed using the values sampled by tracer particles embedded in the simula-

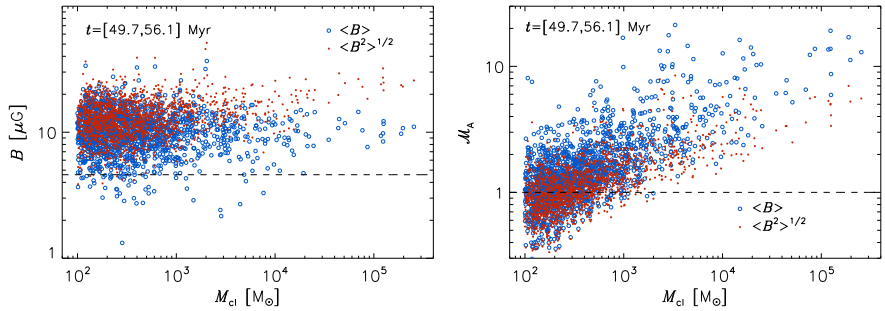

Figure 2. *Left*: Magnetic field strength versus cloud mass for a sample of 1 547 MCs selected from our SN-driven simulation. The dashed line shows the mean magnetic field averaged over the whole computation volume (also the initial mean field). Empty circles correspond to the mean value of the magnetic field of all tracer particles in each cloud, while filled circles give the rms value. *Right*: Alfvénic rms Mach number versus cloud mass for the same clouds as in the left panel, computed with the cloud mean magnetic field (empty circles), or the cloud rms magnetic field (filled circles).

tion, $\langle B\rangle = \Sigma_{\rm i} B_{\rm i}/N$ and $\langle B^2\rangle^{1/2} = (\Sigma_{\rm i} B_{\rm i}^2/N)^{1/2}$, where $B_{\rm i}$ is the magnetic field strength sampled by the particle i in a given cloud, and N is the total number of particles in that cloud. These magnetic field values are plotted versus the cloud mass in the left panel of Fig. 2, where the horizontal dashed line represents the mean magnetic field in the computational volume, $B_0 = 4.6$ μG.

The mean field in the clouds (empty circles) is approximately 10 μG on average, only twice larger than the large-scale magnetic-field strength, B_0, and independent of cloud mass. We have verified that the mean magnetic-field strength of the clouds is also independent of their mean gas density. The relatively small increase of the cloud mean magnetic field relative to B_0 and its independence of gas density are characteristic of trans-Alfvénic supersonic turbulence (Padoan & Nordlund, 1997, 1999), and illustrates that MCs must be formed by compressive motions primarily along magnetic field lines, due to the non-negligible magnetic pressure prior to the compression and cooling of the low-density gas, as discussed above.

Because in super-Alfvénic turbulence the magnetic field is amplified by compressions, as shown by a positive $B - n$ correlation (Padoan & Nordlund, 1997, 1999), our scenario also predicts the formation of dense cores, formed by shocks within MCs (Padoan et al., 2001), with an enhanced magnetic-field strength. The small-scale enhancement of the magnetic field within MCs is illustrated in the left panel of Fig. 2, where the values of the rms field in the clouds (filled circles) is approximately a factor of two larger than the mean field. The rms field increases slightly with cloud mass, due to the correlation between rms velocity and cloud mass: Larger, more massive clouds have larger rms velocity

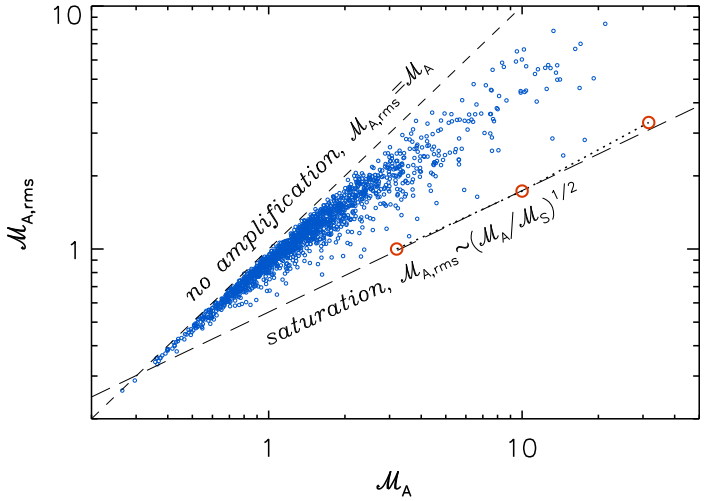

Figure 3. The rms Alfvénic Mach number computed with the rms magnetic field, $\mathcal{M}_{\rm A,rms}$, versus the Alfvénic Mach number based on the mean magnetic field, $\mathcal{M}_{\rm A}$, for the same MCs selected from the SN-driven simulation as in Fig. 2. The long-dashed line shows the saturation value from Eq. (1), while the open circles indicate the saturation values from randomly driven simulations (Kritsuk et al., 2009a,b; Padoan et al., 2010).

than smaller clouds, on average, so the rms field is amplified to a larger value.

As a more direct demonstration of the super-Alfvénic nature of MC turbulence, the right panel of Fig. 2 shows the cloud rms Alfvénic Mach number versus the cloud mass. The Mach number is computed as the ratio of the cloud rms velocity and the cloud Alfvén velocity, where the latter is computed either with the mean magnetic field (empty circles) or with the rms magnetic field (filled circles), and using the mean density sampled by the tracer particles. Nearly all clouds with mass larger than 10^3 $M_\odot$ are super-Alfvénic, even considering their amplified field strength. For the 41 MCs with masses larger than 10^4 $M_\odot$, the average Alfvénic Mach number is 8.3 with respect to the mean field, and 3.9 with respect to the rms field.

The inability of supersonic turbulence to amplify the magnetic field to equipartition with the kinetic energy, as in the MCs of our simulation, was already established with idealized simulations of randomly-driven MHD turbulence. Simulations by Haugen et al. (2004) suggested that the growth rate of the turbulent dynamo in the supersonic regime may be significantly reduced compared to the incompressible case. Later on, simulations with rms sonic Mach number $\mathcal{M}_{\rm s}\approx 10$ and different values of the rms Alfvénic Mach number, $\mathcal{M}_{\rm A}\approx 30$, 10, and 3 (Kritsuk et al., 2009a,b; Padoan et al., 2010), also showed that the saturated rms magnetic field is a function of the mean field, and it is consistent with

amplification by compression, with no contribution from a turbulent dynamo (see Eq. (20) in Padoan & Nordlund, 2011). As firmly established in the comprehensive parameter study by Federrath et al. (2011), a supersonic turbulent dynamo plays a role in the field amplification only when the mean magnetic field is very small, as the saturated value of the magnetic energy is only a few percent of the kinetic energy.

Equation (20) in Padoan & Nordlund (2011) corresponds to the following relation between the rms Alfvénic Mach number computed with the rms magnetic field, $\mathcal{M}_{\rm A,rms}$, and the ratio of Alfvénic to sonic Mach numbers based on the mean magnetic field, $\mathcal{M}_{\rm A}$ and $\mathcal{M}_{\rm s}$ respectively:

$$\mathcal{M}_{\rm A,rms} \sim (\mathcal{M}_{\rm A}/\mathcal{M}_{\rm s})^{1/2}. \quad (1)$$

This predicted saturation level is shown by the long-dashed line in Fig. 3. One can see that it defines the lower envelope of the scatter plot of $\mathcal{M}_{\rm A,rms}$ versus $\mathcal{M}_{\rm A}$ for the MCs selected from our SN-driven simulation. Many clouds are found well above the saturation level, which may be due to their relatively young age, or to an insufficient numerical resolution in the case of the smallest clouds.

5. Comparison with Observations

The super-Alfvénic nature of the turbulence in the clouds from our simulation is consistent with the observational evidence. Based on the comparison between simulations of MHD turbulence and MC observations, Padoan & Nordlund (1997, 1999) suggested that MC turbulence was better characterized by supersonic turbulent flows with $\mathcal{M}_A \gg 1$ than flows with $\mathcal{M}_A \approx 1$. This result was later confirmed with the aid of synthetic observations (Padoan et al., 2004) and synthetic Zeeman splitting measurements (Lunttila et al., 2008). It was shown that a super-Alfvénic turbulence simulation with the characteristic size, density, and velocity dispersion of star-forming regions could produce dense cores with the same relation between magnetic-field strength and column density as observed cores. Lunttila et al. (2008) also computed the relative mass-to-flux ratio $\mathcal{R}_\mu$, defined as the mass-to-flux ratio of a core divided by that of its envelope, as proposed by Crutcher et al. (2009). They found a large scatter in the value of $\mathcal{R}_\mu$, and an average value of $\mathcal{R}_\mu < 1$, in contrast to the ambipolar-drift model of core formation, where the mean magnetic field is stronger and only $\mathcal{R}_\mu > 1$ is allowed. Crutcher et al. (2009) confirmed that $\mathcal{R}_\mu < 1$ in observed cores, as predicted by Lunttila et al. (2008).

In a separate work, Lunttila et al. (2009) used simulated OH Zeeman measurements to compute the mass-to-flux ratio relative to the critical one, λ, and the ratio of turbulent to magnetic energies, $\beta_{\rm turb}$, in molecular cores selected from a super-Alfvénic simulation. They found both mean values and scatter of λ and $\beta_{\rm turb}$ in good agreement with the observational results of Troland & Crutcher (2008). In our super-Alfvénic scenario, the scatter originates partly

from intrinsic variations of the magnetic field strength from core to core, which are not expected in the traditional picture of MCs were the mean magnetic field is strong (Shu et al., 1987).

Taking advantage of the anisotropy of MHD turbulence, Heyer & Brunt (2012) demonstrated that the densest regions of the Taurus MC complex are characterized by super-Alfvénic turbulence, while in low density regions the motions are sub or trans-Alfvénic, also consistent with the picture from our simulation, where MCs are formed by large-scale trans-Alfvénic turbulence, and thus fed preferentially by motions along magnetic field lines, as discussed above (Nordlund & Padoan, 2003; Padoan et al., 2010). Recent dust polarization measurements have shown that the magnetic field has a relatively constant orientation in low-density regions surrounding MCs, with the mean direction mainly parallel to low-density filaments, while the field becomes predominantly perpendicular to the direction of dense filaments in regions of larger column density (Soler et al., 2017). This change is suggestive of the transition from trans-Alfvénic to super-Alfvénic turbulence found by Heyer & Brunt (2012).

6. Conclusions

We have argued that MCs are born super-Alfvénic with respect to their mean magnetic field, because of the trans-Alfvénic nature of the turbulence in the WISM. We have shown that this scenario is supported by the results of a SN-driven simulation meant to represent an overdense region (e.g. a spiral arm) of the ISM on a scale of 250 pc, with a realistic mean magnetic field. MCs selected from the simulation have a mean magnetic-field strength of approximately 10 μG, only a factor of two larger than the mean field averaged over the whole computational volume. Their internal rms velocity is super-Alfvénic with respect to both their mean and rms magnetic field strength.

Despite the small value of their mean magnetic field strength, super-Alfvénic MCs are expected to naturally generate dense cores with stronger magnetic field as the result of compression by turbulent shocks. The properties of such cores measured in simulations of super-Alfvénic turbulence are consistent with those of real MC cores.

Acknowledgements. Computing resources for this work were provided by the NASA High-End Computing (HEC) Program through the NASA Advanced Supercomputing (NAS) Division at Ames Research Center. PP acknowledges support by the Spanish MINECO under project AYA2014-57134-P.

References

Crutcher, R. M., Hakobian, N., & Troland, T. H. 2009, *Astrophys. J.*, **692**, 844

Federrath, C., Chabrier, G., Schober, J., et al. 2011, *Phys. Rev. Lett.*, **107**, 114504

Fromang, S., Hennebelle, P., & Teyssier, R. 2006, *Astron. Astrophys.*, **457**, 371

Haugbølle, T., Padoan, P., & Nordlund, A. 2017, *ArXiv e-prints* [arXiv:1709.01078]

Haugen, N. E. L., Brandenburg, A., & Mee, A. J. 2004, *Mon. Not. R. Astron. Soc.*, **353**, 947

Heyer, M. H. & Brunt, C. M. 2012, *Mon. Not. R. Astron. Soc.*, **420**, 1562

Kritsuk, A. G., Ustyugov, S. D., Norman, M. L., & Padoan, P. 2009a, J. Phys.: Conf. Ser, **180**, 012020

Kritsuk, A. G., Ustyugov, S. D., Norman, M. L., & Padoan, P. 2009b, in ASP Conf. Ser., Vol. **406**, *Numerical Modeling of Space Plasma Flows: ASTRONUM-2008*, ed. N. V. Pogorelov, E. Audit, P. Colella, & G. P. Zank, 15

Lunttila, T., Padoan, P., Juvela, M., & Nordlund, Å. 2008, *Astrophys. J., Lett.*, **686**, L91

Lunttila, T., Padoan, P., Juvela, M., & Nordlund, Å. 2009, *Astrophys. J., Lett.*, **702**, L37

Nordlund, Å. & Padoan, P. 2003, in Lecture Notes in Physics, Berlin Springer Verlag, Vol. **614**, *Turbulence and Magnetic Fields in Astrophysics*, ed. E. Falgarone & T. Passot, 271–298

Padoan, P., Haugbølle, T., Nordlund, Å., & Frimann, S. 2017, *Astrophys. J.*, **840**, 48

Padoan, P., Jimenez, R., Juvela, M., & Nordlund, Å. 2004, *Astrophys. J., Lett.*, **604**, L49

Padoan, P., Juvela, M., Goodman, A. A., & Nordlund, Å. 2001, *Astrophys. J.*, **553**, 227

Padoan, P., Juvela, M., Pan, L., Haugbølle, T., & Nordlund, Å. 2016a, *Astrophys. J.*, **826**, 140

Padoan, P., Kritsuk, A. G., Lunttila, T., et al. 2010, in AIP Conf. Ser, Vol. **1242**, *Plasmas in the Laboratory and the Universe: Interactions, Patterns, and Turbulence*, ed. G. Bertin, F. de Luca, G. Lodato, R. Pozzoli, & M. Romé, 219–230

Padoan, P. & Nordlund, Å. 1997, *ArXiv e-prints* [arXiv:astro-ph/9706176]

Padoan, P. & Nordlund, Å. 1999, *Astrophys. J.*, **526**, 279

Padoan, P. & Nordlund, Å. 2011, *Astrophys. J.*, **730**, 40

Padoan, P., Pan, L., Haugbølle, T., & Nordlund, Å. 2016b, *Astrophys. J.*, **822**, 11

Pan, L., Padoan, P., Haugbølle, T., & Nordlund, Å. 2016, *Astrophys. J.*, **825**, 30

Shu, F. H., Adams, F. C., & Lizano, S. 1987, *Ann. Rev. Astron. Astrophys.*, **25**, 23

Soler, J. D., Ade, P. A. R., Angilè, F. E., et al. 2017, *Astron. Astrophys.*, **603**, A64

Teyssier, R. 2002, *Astron. Astrophys.*, **385**, 337

Teyssier, R. 2007, *Geophysical and Astrophysical Fluid Dynamics*, **101**, 199

Troland, T. H. & Crutcher, R. M. 2008, *Astrophys. J.*, **680**, 457

Contrib. Astron. Obs. Skalnaté Pleso **48**, 40 – 47, (2018)

Modeling the magnetized accretion and outflows in young stellar objects

Ch. Fendt

Max Planck Institute for Astronomy, Heidelberg, Germany
(E-mail: fendt@mpia.de)

Received: October 11, 2017; Accepted: October 29, 2017

Abstract. Recent results of magnetohydrodynamic (MHD) simulations are presented treating the launching of jets from young stellar object accretion disks. The simulations consider the evolution of magnetically diffusive disks that eject high-speed outflows. A few exemplary results are presented: (i) the disk structural evolution that leads to different launching conditions over time, (ii) a general interrelation between the disk magnetization at the outflow launching radius and the outflow asymptotic properties, (iii) jet launching within a self-generated disk magnetic field amplified by a disk mean field dynamo, and (iv) simulations of jets from orbiting jet sources.

Key words: accretion, accretion disks – magnetohydrodynamics (MHD) – ISM: jets and outflows – stars: mass loss – stars: pre-main sequence

1. Introduction

Jets are powerful signatures of astrophysical activity and can be observed over a wide range of energy output and spatial extent. Among other jet sources - mainly relativistic sources such as active galactic nuclei - young stellar objects are particularly interesting, as they allow to observe certain dynamical properties that are essential for modeling. For relativistic jets, mainly observed in synchrotron radio emission, we do not know their exact velocities or mass fluxes.

For protostellar outflows, outflow mass fluxes were found that are proportional to the accretion rate, suggesting a physical link between accretion and ejection (e.g. Edwards et al., 2006). Observations also indicate the existence of a strong magnetic field in the regions where jets are formed (Carrasco-González et al., 2010), and for the jet-launching source (e.g. Edwards et al., 1994).

To summarize, the following observationally confirmed features are essential for our understanding of jet formation and are therefore important ingredients for any theoretical modeling of disks and jets. These are (i) the existence of an *accretion disk* in jet sources, and estimates of the accretion rates, (ii) the existence of a strong *magnetic field* in jets and jet sources, and (iii) jet *knots* that are believed to be shocked gas, from which essential dynamical parameters such as jet *velocity* and *density* can be derived.

It is commonly accepted that MHD processes are essential for launching, acceleration and collimation of outflows from accretion disks (Blandford & Payne, 1982; Pudritz & Norman, 1983; Pudritz et al., 2007).

Considering the topic of this conference, jets from young stars indeed require the existence of a considerably *stable magnetic field* over the jet life time. However, the observations of jet knots (however being generated) also indicate some *time-dependent* variation of the field structure.

2. Jet launching - from accretion to ejection

We distinguish between *jet launching* - the transition from accretion to ejection - and *jet formation* standing for the acceleration and collimation process of a disk wind into a narrow jet. Jet *formation* is usually understood as due to the magneto-centrifugal slingshot mechanism. Outflows of lower velocity are built up as so-called tower jets accelerated by the magnetic pressure gradient of the toroidal field. Jet *launching* is more difficult to treat as interrelating the disk physics with the jet physics. Both differ in several aspects, in particular concerning their time scales. For example, disks are viscous and magnetically diffusive, while jets and outflows can be treated in ideal MHD. Further, disks may have a turbulent, strongly tangled field component, while fast jets rely on the existence of a smooth, large-scale magnetic field.

3. Basic physical processes

The outflow launching is not yet fully understood in all detail. However both, analytical modeling (Li, 1995; Ferreira, 1997) and numerical simulations (Casse & Keppens, 2002; Kuwabara et al., 2005; Zanni et al., 2007) agree on the main launching mechanisms involved. The general idea is visualized in Fig. 1: gas is advected along the disk. A large-scale magnetic field penetrates the disk. The magnetic flux distribution is affected by advection and diffusion of the field through the disk. The launching conditions vary along the disk and in time.

Disk material can be accreted across the magnetic field as the disk plasma is magnetically diffusive. In other words, the existence of magnetic diffusivity is essential in order to allow the material to be exchanged between magnetic flux surfaces. The magnetic diffusivity η is believed to be of turbulent origin. Figure 1 shows how the streamlines cross the magnetic field lines, and how they connect different field lines in disk and outflow.

The very launching process, the lifting of disk material into the outflow is a magnetic process (Ferreira, 1997; Ferreira et al., 2006), where Lorentz forces $\boldsymbol{F}_{\mathrm{L}} \propto \boldsymbol{j} \times \boldsymbol{B}$ play a leading role. If the vertical Lorentz force decreases vertically, gas pressure gradients may lift the material. The toroidal Lorentz force accelerates the plasma azimuthally, leading to a radial centrifugal acceleration.

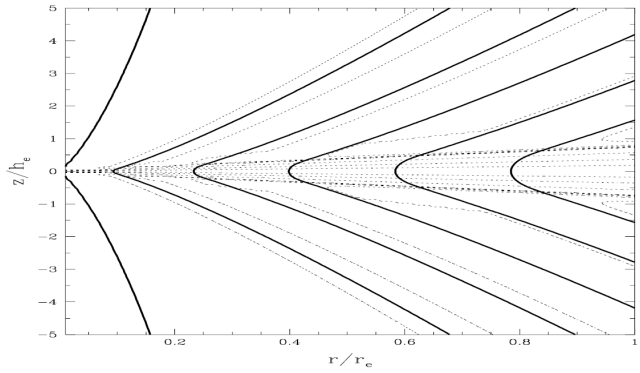

Figure 1. Streamlines of gas (dashed) and magnetic field lines (solid) of a self-similar accretion-ejection solution (taken from Ferreira, 1997).

Modeling the launching process means figuring out (either analytically by numerical simulations) certain magnetic field configurations that provide favorable Lorentz forces for launching and acceleration.

Once lifted above the disk surface, the further acceleration is by the magneto-centrifugal effect (Blandford & Payne, 1982; Pudritz & Norman, 1983) in case of strong poloidal magnetic fields, or by the vertical magnetic pressure (tower jets; Lynden-Bell, 1996) in case of low magnetic flux. The collimation into a narrow beam is accomplished by the pinching forces of the toroidal magnetic field B_ϕ. Simulations of the acceleration and collimation processes of jets forming from the disk surface have been performed in great detail by a number of authors (see e.g. Ustyugova et al., 1995; Ouyed & Pudritz, 1997; Romanova et al., 1997).

Note that while the magnetic field is essentially driving the jet, its role is merely to convert potential energy from disk material into kinetic outflow energy.

4. Simulations of jet launching

Here we present example results of recent jet launching simulations. In general, Fig. 2 shows the evolution of the inner part of a jet launching accretion disk. The magnetic field first diffuses outwards (shown are flux surfaces $\Psi \propto \int B_z dr$), until accretion begins and leads to advection of flux. Obviously, the launching conditions change over time.

4.1. Jet launching and disk magnetization

We applied a novel approach to the jet-launching problem to obtain correlations between the physical properties of the jet and the underlying disk. We have investigated a wide parameter range of disk magnetization $\mu_{\rm D}(r_0) =$

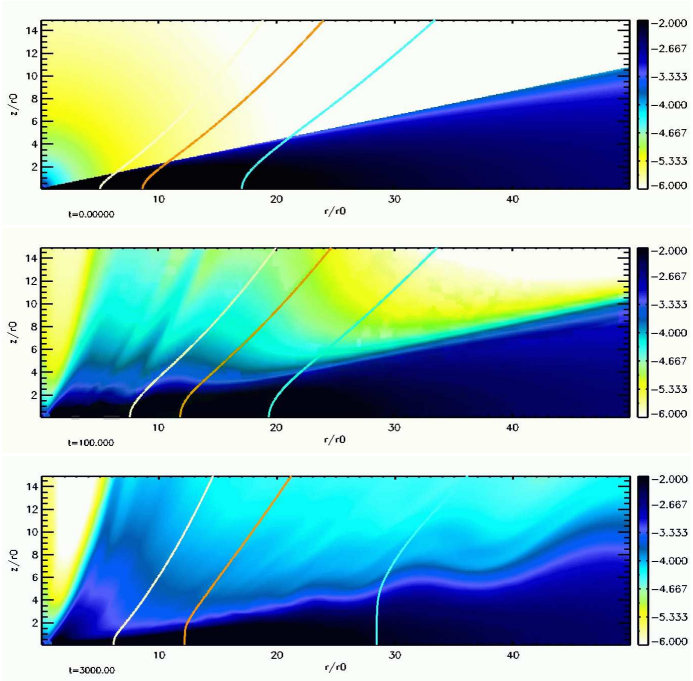

Figure 2. Advection and diffusion of outflow-launching magnetic flux surfaces. Three flux surfaces are shown (disk density in color). The panels show the inner part (length scale normalized to inner disk radii) of a simulation reaching $r = 100$, $z = 300$ in extend (Sheikhnezami et al., 2012).

$10^{-3.5}...10^{-0.7}$ at the outflow launching point r_0. The magnetization μ measures the ratio of magnetic pressure to gas pressure. This study is complementary to the works of Tzeferacos et al. (2009) and Murphy et al. (2010) who investigated the jet launching along a disk surface with decreasing $\mu_{\rm D}(r)$.

As our main result, we have disentangled the disk magnetization at the outflow origin as the main parameter governing the outflow properties. Strongly magnetized disks launch more energetic and faster jets and, due to a larger Alfvén lever arm, these jets extract more angular momentum from the disk. These kinds of systems have, however, a weaker mass loading and a lower mass ejection-accretion ratio. Jets are launched at the disk surface where the magnetization is $\mu(r, z) \simeq 0.1$.

As an example, Fig. 3 shows the tight correlations between the total jet energy e and the mass loading k with the disk magnetization $\mu_{\rm D}$, respectively. The mass loading parameter k measures the amount of matter ejected per unit magnetic flux. Each differently colored line corresponds to a simulation with a

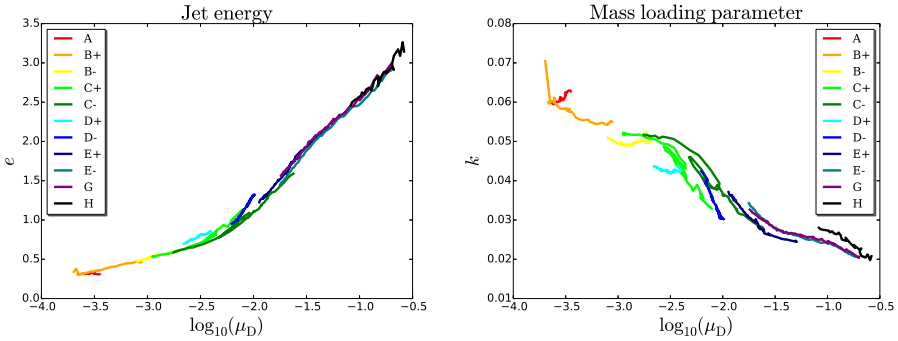

Figure 3. Jet properties with respect to the disk magnetization μ_D. The jet energy e, and the mass loading parameter k are shown. Each colored line represents the evolution of a single simulation up to 10,000 time units. Taken from Stepanovs & Fendt (2016).

different initial disk magnetization.

We also find indication of a critical disk magnetization $\mu_D \simeq 0.01$ separating the regimes of magneto-centrifugally driven and magnetic pressure-driven jets (indicated by the change in slope in Fig. 3). The existence of these two regimes has been discussed by Ferreira (1997), however, we obtain these correlations from simulations that include the dynamical evolution of disk and jet.

4.2. Launching by a disk-dynamo generated magnetic field

Most simulations of jet launching have been set up prescribing a large-scale initial magnetic flux. Exceptions are e.g. Bardou et al. (2001) or von Rekowski et al. (2003) considering a disk dynamo or a stellar dynamo that generate the jet driving magnetic field.

More recently we have presented MHD simulations exploring the launching, acceleration, and collimation of jets and disk winds considering the generation of the magnetic field by an α^2-Ω mean-field disk dynamo (Stepanovs et al., 2014). We found a dynamo-generated magnetic field of the inner disk similar to the commonly prescribed open field structure, favoring magneto-centrifugal launching. The outer disk field is highly inclined and predominantly radial. Here, differential rotation induces a strong toroidal field. Outflows from the outer disk are slower, denser, and less collimated.

We have further applied a toy model triggering a time-dependent mean-field dynamo. When the dynamo is suppressed as the magnetization falls below a critical value, the generation of the outflows and also accretion is inhibited.

Figure 4 shows snapshots of our simulation applying a time-dependent dynamo model. We display the density and velocity structure overlaid with magnetic field lines. Dynamo-active times follow dynamo-inactive times with periods

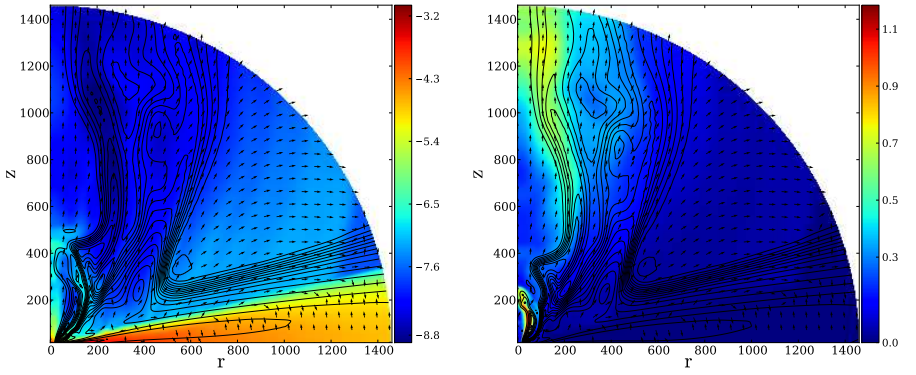

Figure 4. Jet launching from dynamo-active disks. Shown is the density (left) and outflow velocity (right) in code units (colors). The velocity is normalized to the Keplerian velocity at the inner disk radius, The dynamo model is time dependent with a period of about 100 orbital times. Superimposed are poloidal magnetic field lines (black), see also Stepanovs et al. 2014.

of about 100 disk rotations. During dynamo-active time periods new jet ejections happen close to the inner disk. In the figure two ejections periods are visible in the jet flow (more in velocity than in density), the latest one having reached $z = 200\,R_{\rm in}$, the earlier one currently at $z = 1200\,R_{\rm in}$.

4.3. 3D-launching simulations

Extending the launching setup to 3D, we have recently presented the first ever 3D simulations of the MHD accretion-ejection structure (Sheikhnezami & Fendt, 2015). We have implemented a 3D gravitational potential due to a companion star and run a variety of simulations with different binary separation. The simulations show typical 3D deviations from axial symmetry, such as jet bending outside the Roche lobe or spiral arms forming in the accretion disk. An exemplary parameter setup with a small binary separation of only $\simeq 200$ inner disk radii indicates the onset of jet precession - caused by the wobbling of the jet-launching disk. A final prove for precession can only be given by much longer simulations lasting several orbital time scales. In Fig. 5 we see the disk-realignment over time from the initial orientation towards the orbital plane. The secondary is located at $x = 200$ and $z = 60$ (outside the numerical grid).

5. Summary and outlook

So far we have discussed *global* models of jets launching in which the "micro-physics" of the disk is approximated by averaged quantities such as (mean)

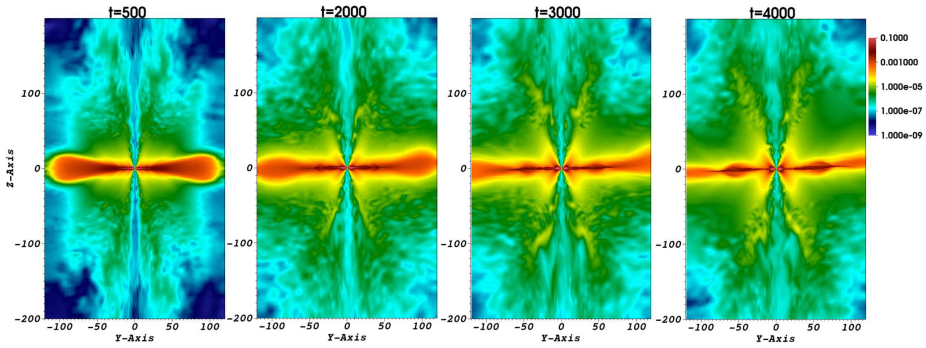

Figure 5. 3D jet launching from jet sources in binary systems. Shown is a time sequence of slices through the 3D simulation for the density structure. Taken from Sheikhnezami & Fendt (2015).

magnetic flux, plasma density, flow energy or angular momentum, and, in particular, mean turbulent diffusivity or a mean-field turbulent dynamo. This seems feasible and has so far provided promising results that are in nice agreement with analytical theory.

However, certain physical aspects that may play a role in reality have not yet been addressed in detail in global numerical launching models. Some are, however, currently investigated in (local and global) accretion disk simulations and will impact the future development of disk-jet launching modeling. Examples are e.g. (i) heating and cooling of the disk, (ii) a self-consistent description of the turbulent magnetic diffusivity, and similarly (iii) for the mean-field turbulent dynamo, then (iv) non-ideal MHD effects like ambipolar diffusion or Hall MHD, and the influence of (v) the stellar magnetic field, or (vi) the influence of radiation pressure.

While the main launching mechanism seems to be well understood from global launching simulations, a yet further, full understanding of jet launching will require a more complete understanding of the internal disk evolution that will require a high resolution and will be computed in a localized disk area.

Acknowledgements. This review is based on the collaboration with a few PhD students over the last years. The author is grateful to his former student collaborators Somayeh Sheikhnezami, Deniss Stepanovs, Bhargav Vaidya and Oliver Porth.

References

Bardou, A., von Rekowski, B., Dobler, W., Brandenburg, A., & Shukurov, A. 2001, *Astron. Astrophys.*, **370**, 635

Blandford, R. D. & Payne, D. G. 1982, *Mon. Not. R. Astron. Soc.*, **199**, 883

Carrasco-González, C., Rodríguez, L. F., Anglada, G., et al. 2010, *Science*, **330**, 1209

Casse, F. & Keppens, R. 2002, *Astrophys. J.*, **581**, 988

Edwards, S., Fischer, W., Hillenbrand, L., & Kwan, J. 2006, *Astrophys. J.*, **646**, 319

Edwards, S., Hartigan, P., Ghandour, L., & Andrulis, C. 1994, *Astron. J.*, **108**

Ferreira, J. 1997, *Astron. Astrophys.*, **319**, 340

Ferreira, J., Dougados, C., & Cabrit, S. 2006, *Astron. Astrophys.*, **453**, 785

Kuwabara, T., Shibata, K., Kudoh, T., & Matsumoto, R. 2005, *Astrophys. J.*, **621**, 921

Li, Z. 1995, *Astrophys. J.*, **444**, 848

Lynden-Bell, D. 1996, *Mon. Not. R. Astron. Soc.*, **279**, 389

Murphy, G. C., Ferreira, J., & Zanni, C. 2010, *Astron. Astrophys.*, **512**, A82

Ouyed, R. & Pudritz, R. E. 1997, *Astrophys. J.*, **482**, 712

Pudritz, R. E. & Norman, C. A. 1983, *Astrophys. J.*, **274**, 677

Pudritz, R. E., Ouyed, R., Fendt, C., & Brandenburg, A. 2007, *Protostars and Planets V*, 277

Romanova, M. M., Ustyugova, G. V., Koldoba, A. V., Chechetkin, V. M., & Lovelace, R. V. E. 1997, *Astrophys. J.*, **482**, 708

Sheikhnezami, S. & Fendt, C. 2015, *Astrophys. J.*, **814**, 113

Sheikhnezami, S., Fendt, C., Porth, O., Vaidya, B., & Ghanbari, J. 2012, *Astrophys. J.*, **757**, 65

Stepanovs, D. & Fendt, C. 2016, *Astrophys. J.*, **825**, 14

Stepanovs, D., Fendt, C., & Sheikhnezami, S. 2014, *Astrophys. J.*, **796**, 29

Tzeferacos, P., Ferrari, A., Mignone, A., et al. 2009, *Mon. Not. R. Astron. Soc.*, **400**, 820

Ustyugova, G. V., Koldoba, A. V., Romanova, M. M., Chechetkin, V. M., & Lovelace, R. V. E. 1995, *Astrophys. J., Lett.*, **439**, L39

von Rekowski, B., Brandenburg, A., Dobler, W., Dobler, W., & Shukurov, A. 2003, *Astron. Astrophys.*, **398**, 825

Zanni, C., Ferrari, A., Rosner, R., Bodo, G., & Massaglia, S. 2007, *Astron. Astrophys.*, **469**, 811

Contrib. Astron. Obs. Skalnaté Pleso **48**, 48 – 52, (2018)

The magnetic properties of Am stars

A. Blazère[1,2], P. Petit[3,4] and C. Neiner[2]

[1] *Institut d'Astrophysique et de Géophysique, Université de Liège, Quartier Agora (B5c), Allée du 6 août 19c, 4000 Sart Tilman, Liège, Belgium (E-mail: ablazere@ulg.ac.be)*

[2] *LESIA, Observatoire de Paris, PSL Research University, CNRS, Sorbonne Universités, UPMC Univ. Paris 06, Univ. Paris Diderot, Sorbonne Paris Cité, 5 place Jules Janssen, 92195 Meudon, France*

[3] *Université de Toulouse, UPS-OMP, Institut de Recherche en Astrophysique et Planétologie, Toulouse, France*

[4] *CNRS, Institut de Recherche en Astrophysique et Planétologie, 14 Avenue Edouard Belin, F-31400 Toulouse, France*

Received: November 17, 2017; Accepted: November 25, 2017

Abstract. We present the results of a spectropolarimetric study of three Am stars: β UMa, θ Leo and Alhena. Two of the three stars of this study showed peculiar magnetic signatures with prominent positive lobes, like the one of Sirius A, that are not expected in the standard theory of the Zeeman effect. Alhena, contrary to Sirius A, β UMa and θ Leo, exhibits normal signatures. The follow-up spectropolarimetric observations of Alhena allowed us to determine the magnetic properties of this star.

Key words: stars: magnetic fields – stars: early-type – stars: chemically peculiar

1. Introduction

Magnetic fields play an important role in the evolution of intermediate-mass stars. Until recently, among this kind of stars, the chemically peculiar Ap/Bp stars were the only known magnetic stars. The topology of the fields in these stars is quite simple (usually mostly a dipole) and the strength is above 300 G. This vision of the magnetic fields in intermediate-mass stars was disrupted by the discovery of an ultra-weak magnetic field (longitudinal magnetic field below 1 Gauss) at the surface of the fast rotating normal star Vega (Lignières et al., 2009; Petit et al., 2010) and raised the question of the existence of such kind of magnetic field in all intermediate-mass stars that do not host a strong magnetic field.

A first weak signature was discovered in the Stokes V profiles of the Am star (i.e. chemically peculiar stars showing metallic lines), Sirius A (Petit et al., 2011). However, the observed signature in circular polarization exhibits a prominent positive lobe. This signature shape is not expected in the normal Zeeman

theory. Therefore, the peculiar signature in the polarized profile remained a puzzle and required further investigation.

As a consequence, we observed three other Am stars with ultra-high precision spectropolarimetry: β UMa, θ Leo and Alhena. Detecting ultra-weak fields in Am stars is challenging due to the weakness of the expected signatures. The three objects are early A-type targets and have similar stellar parameters.

The targets were observed with the Narval spectropolarimeter, installed at the 2-meter Bernard Lyot Telescope (TBL) at the summit of Pic du Midi Observatory in the French Pyrénées. We used the polarimetry mode to measure circular polarization (Stokes V).

2. Magnetic analysis

To test whether the stars are magnetic, we applied the Least-Squares Deconvolution (LSD) technique (Donati et al., 1997) on each spectra using a line list adapted for each star.

For β UMa and θ Leo, we did not obtained a detection in the individual LSD profiles. To further improve the signal-to-noise ratio, we thus co-added all LSD profiles of each star, resulting in one single averaged LSD profile. The Stokes profiles of β UMa and θ Leo display peculiar signatures with a prominent positive lobe (see Fig. 1) similar to the signatures of Sirius A. This kind of signatures is not expected in the normal Zeeman theory, and required investigations to confirm or refute the magnetic origin of these signatures. For β UMa and θ Leo, we demonstrated thanks to several tests that the peculiar signatures are due to a magnetic field (see Blazère et al. 2016 for more details).

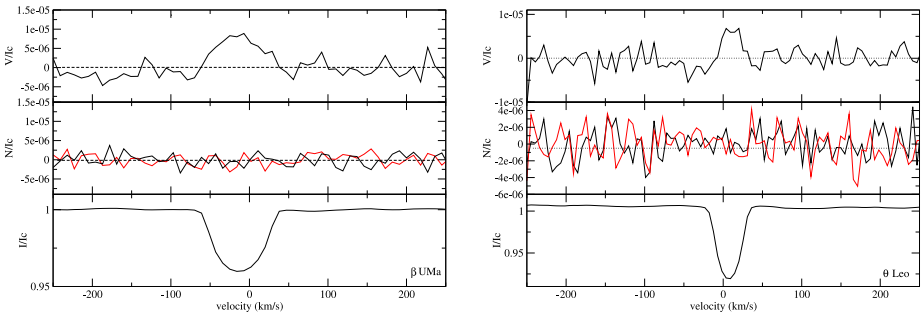

Figure 1. Co-added LSD profiles in Stokes I (bottom) and V (top). The two available "null" control parameters Null1 and Null2 are shown in the middle panel. *Left*: β UMa observations. *Right:* Same figure for θ Leo. Taken from Blazère et al. (2016)

For Alhena, contrary to β UMa and θ Leo, we obtain magnetic detections in the individual LSD profiles. The Stokes V profiles exhibit normal Zeeman

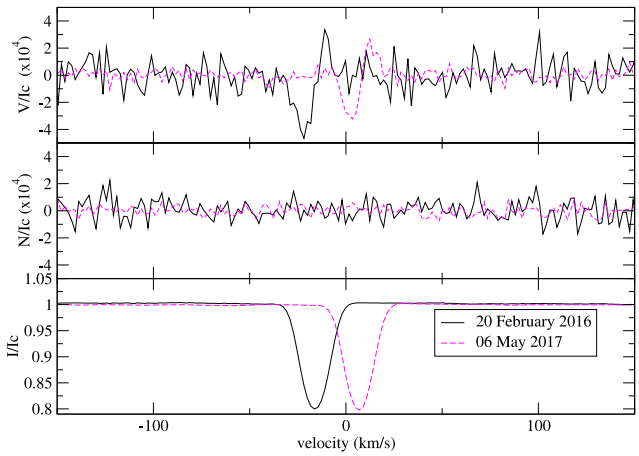

Figure 2. Example of LSD profiles in Stokes I (bottom), Stokes V (top), and "null" polarization (center) for two different nights of observations. All profiles are normalized to the intensity continuum level.

signatures for each night of observations. Examples of the LSD profiles are shown in Fig. 2. It is the first detection of normal signatures at the surface of an Am star.

The longitudinal field values (B_l) of Alhena were calculated thanks to the centre-of-gravity method (Rees & Semel, 1979). The longitudinal magnetic field is negative for each night of observations with values between -10 G and -3 G.

The Stokes V signatures were modelled using an oblique rotator model, assuming a dipole for the magnetic field of Alhena and a rotational period of 8.975 days (see Blazère et al. in prep. for more details). The best fit corresponds to an inclination of $22.8\pm4.1°$, an obliquity angle of $34.1\pm3.4°$, and a dipolar field strength of 32.4 ± 1.7 G.

Figure 3 shows the comparison between the observed and the best fit synthetic LSD V profiles for all observations. The model matches quite well the Stokes V profiles but it is not perfect. This difference between the model and the observations can be due to a more complex field than a dipole or due to non-rotational variations of the magnetic field or of the line profiles.

The magnetic map at the surface of Alhena was reconstructed thanks to the Zeeman-Doppler Imaging technique (ZDI, Donati & Brown 1997; see Fig. 4). The reconstructed field is compatible with a dipole. The surface differential rotation of Alhena was measured, following the method developed by Petit et al. (2002) that assumed a simplified solar rotation law. A differential rotation was detected at the surface of Alhena (Fig. 5).

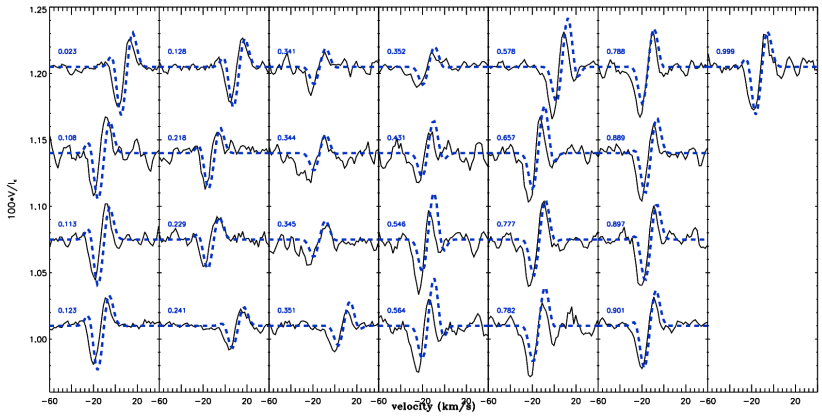

Figure 3. Best dipolar model fit (blue) of the observed Stokes V profiles (black) of Alhena. The blue numbers correspond to the rotational phase.

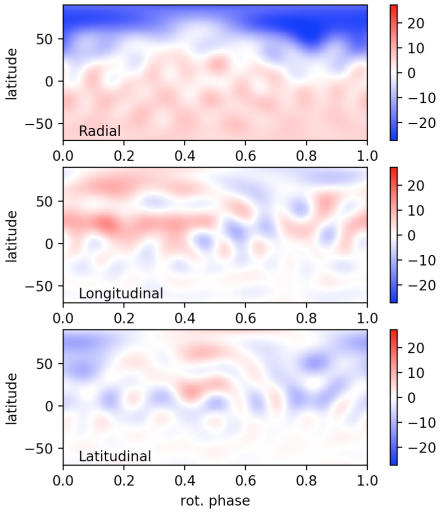

Figure 4. Magnetic map of Alhena. The three panels illustrate the field components in spherical coordinates (top: radial, center: azimuthal, and bottom: meridional). The magnetic field strength (colour scale) is expressed in Gauss.

3. Conclusion

Only four Am stars were observed with the required precision to detect ultra-weak magnetic fields, and all of them indeed host a weak magnetic field. Three of them (Sirius A, β UMa and θ Leo) show peculiar magnetic signatures with a prominent positive lobe and one star (Alhena) shows a normal Zeeman signature. The preliminary explanation for the peculiar signatures observed in most Am stars is a combination of a vertical gradient in velocity and in magnetic

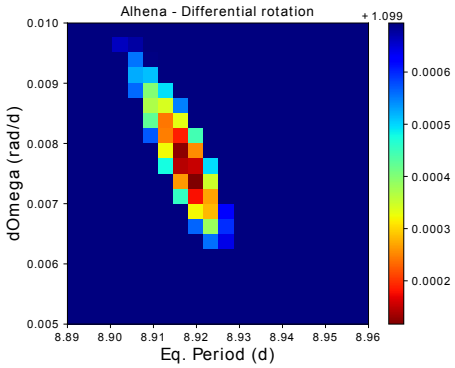

Figure 5. Surface differential rotation of Alhena.

field in the surface layers of the stars. This explanation is sustained by the fact that these Am stars have a high microturbulence and host a superficial layer of convection. The Am star that hosts a normal signature (Alhena) has a lower microturbulence compared to the other Am stars. Its microturbulence is close to the one of Vega, which also displays a normal signature. Alhena hosts a weak magnetic field with a dipolar strength of ~ 30 G. However this value is higher than the one of Vega. Finally, we discovered for the first time a differential rotation at the surface of a magnetic intermediate-mass star.

References

Blazère, A., Petit, P., Lignières, F., et al. 2016, *Astron. Astrophys.*, **586**, A97

Donati, J.-F. & Brown, S. F. 1997, *Astron. Astrophys.*, **326**, 1135

Donati, J.-F., Semel, M., Carter, B. D., Rees, D. E., & Collier Cameron, A. 1997, *Mon. Not. R. Astron. Soc.*, **291**, 658

Lignières, F., Petit, P., Böhm, T., & Aurière, M. 2009, *Astron. Astrophys.*, **500**, L41

Petit, P., Donati, J.-F., & Collier Cameron, A. 2002, *Mon. Not. R. Astron. Soc.*, **334**, 374

Petit, P., Lignières, F., Aurière, M., et al. 2011, *Astron. Astrophys.*, **532**, L13

Petit, P., Lignières, F., Wade, G. A., et al. 2010, *Astron. Astrophys.*, **523**, A41

Rees, D. E. & Semel, M. D. 1979, *Astron. Astrophys.*, **74**, 1

Contrib. Astron. Obs. Skalnaté Pleso **48**, 53 – 57, (2018)

Explaining the unusual Stokes V signatures of ultra-weak magnetic A stars

C. P. Folsom[1,2]

[1] *Université de Toulouse, UPS-OMP, IRAP, Toulouse, France (E-mail: colin.folsom@irap.omp.eu)*

[2] *CNRS, Institut de Recherche en Astrophysique et Planetologie, 14, avenue Edouard Belin, F-31400 Toulouse, France*

Received: December 31, 2017; Accepted: January 5, 2018

Abstract. Recently, extremely weak magnetic fields have been found in a small number of A-type stars. These magnetic fields are on the order of a few gauss or less, which is two to three orders of magnitude weaker than those found in magnetic Ap and Bp stars. The Stokes V (circularly polarized) line profiles of three out of five of these stars known (Sirius, beta UMa, and theta Leo) are highly unusual, consisting of a single positive lobe spanning most of the width of the line. While there is evidence that this signal is due to a magnetic field, the shape of the line profile cannot be explained by Zeeman splitting in a static atmosphere. Using synthetic spectra, we investigated introducing radial gradients in velocity and magnetic field strength, which can produce qualitatively similar model spectra. With some simple assumptions of geometry we produced disk integrated spectra that can match the observations. We propose this as a possible explanation for the unusual Stokes V signatures in these ultra-weak magnetic A stars.

Key words: stars: magnetic fields – stars: chemically peculiar

1. Introduction

A small fraction of A- and B-type stars (Ap and Bp stars) have strong magnetic fields, with strengths of hundreds to thousands of gauss. Recently, much weaker magnetic fields, on the order of a few gauss or less, have been detected in a few A stars, using extremely high signal-to-noise spectropolarimetric observations. These very weakly magnetic stars include Vega (Lignières et al., 2009), Sirius A (Petit et al., 2011), β Uma (Blazère et al., 2016b), θ Leo (Blazère et al., 2016b), and Alhena (Blazère et al., 2016a, see also Blazère et al. in these proceedings). These new detections suggest that very weak magnetic fields may be more common among A and B stars than the strong fields of Ap and Bp stars, and raises the question of the origin of these weak magnetic fields.

The spectropolarimetric observations used to detect these very weak magnetic fields exploit the Zeeman effect, as observed through circularly polarized (Stokes V) spectra. While the observations of Vega and Alhena have normal Zeeman signatures in their Stokes V line profiles, Sirius A, β Uma, and, θ Leo

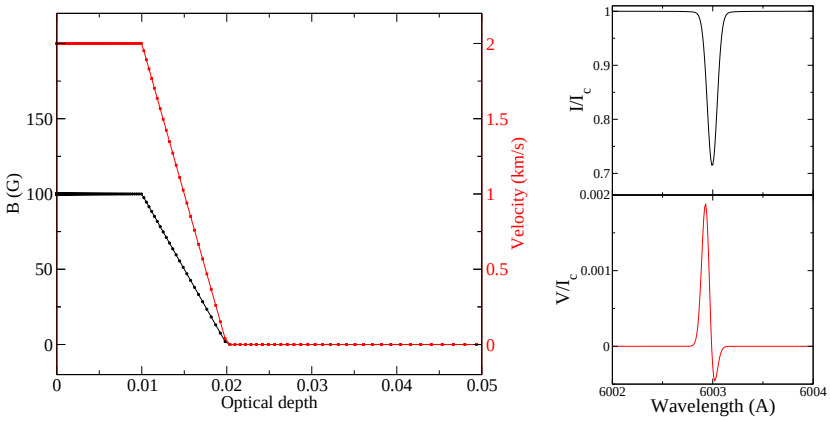

Figure 1. *Left:* magnetic field strength and velocity along the line of sight, as a function of optical depth. *Right:* model Stokes I and V profiles produced using this magnetic field and velocity distribution.

display unusual Stokes V line profiles, with a dominant positive lobe at the line center and little to no negative lobes. If V is integrated across the line, these unusual V profiles do not integrate to zero, and are referred to here as "asymmetric" line profiles (the profiles are approximately symmetric about the line center, but not symmetric in positive and negative V). Such a net circular polarization cannot be produced by the Zeeman effect in a static stellar atmosphere with an uniform magnetic field. This is essentially because the + and – σ components of a Zeeman split line have equal strengths and displacements from the line center.

Tests by Petit et al. (2011) and Blazère et al. (2016b) suggest that these asymmetric V signatures are due to the Zeeman effect, since the signatures are sensitive to the Landé factor and wavelength of the lines. The Zeeman effect can produce asymmetric V signatures if there are gradients in velocity and magnetic field strength in a stellar atmosphere. Here we investigate this possibility and apply it to the peculiar profiles of Sirius A.

2. Model line profiles

In order to investigate asymmetric V profiles numerically we used the Zeeman (Landstreet, 1988; Wade et al., 2001) spectrum synthesis code. This code performs polarized radiative transfer through a plane parallel model atmosphere using the "full" semi-analytic solution from Martin & Wickramasinghe (1979). The code was extensively tested against other polarized radiative transfer codes

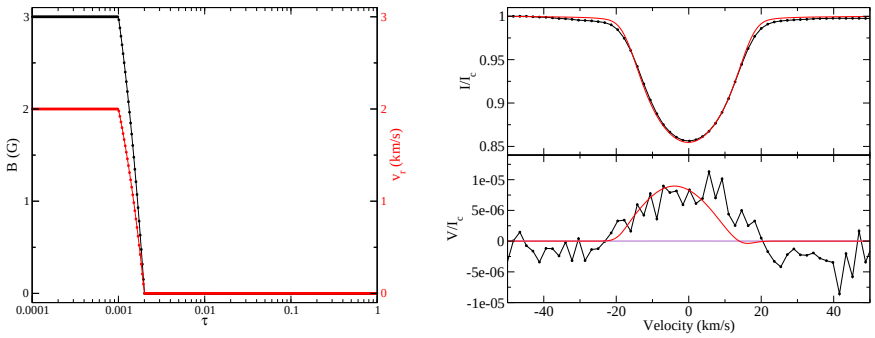

Figure 2. *Left:* Magnetic field and velocity distributions. *Right:* Resulting disk integrated model line profile, compared with an observed LSD profile of Sirius A.

by Wade et al. (2001). As input, an ATLAS9 model atmosphere with $T_{\rm eff} = 7000$ K, and $\log g = 4.5$ was used.

To begin with we looked at the spectrum emerging from just one point on the stellar surface. We assumed a linear transition of velocity and magnetic field strength with optical depth. Thus there was a region of constant magnetic field and velocity deeper in the atmosphere, a linear transition, and an region of constant magnetic field and velocity higher in the atmosphere. An illustration of one such configuration, which produces a strongly asymmetric profile, is shown in Fig. 1.

The general behavior of asymmetric V profiles with different magnetic and velocity distributions is complex. However, Sanchez Almeida et al. (1989) derived a convenient approximation for some of this behavior:

$$\int_0^\infty V(\lambda) d\lambda \propto \frac{dv}{d\tau}\frac{dB}{d\tau}. \tag{1}$$

The net V polarization, integrated over wavelength λ, is proportional to the gradients in magnetic field (B) and velocity (v) with optical depth (τ), when the velocities and Zeeman splitting are both small relative to the line width. Testing this behavior with the Zeeman code, we reproduce this linear relationship up to magnetic fields approaching $\sim$1 kG and velocities approaching $\sim$1 km s^{-1}. Beyond this point the increase net V polarization becomes slower than linear and eventually starts decreasing. This provides evidence that the Zeeman code is behaving as expected.

From these tests we can draw some guidelines for optimizing the asymmetry of the model line profiles. In order to have steep gradients in our model, having the transition over a small range of τ is helpful. In velocity, a maximum asymmetry is produced for a transition of around 2 km s^{-1}. In magnetic field, larger strengths produce a larger asymmetry, but also larger normal Zeeman signature

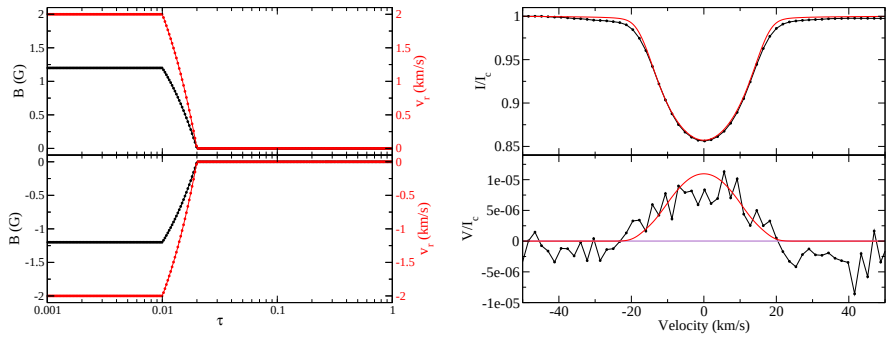

Figure 3. Same as for Fig. 2, but for a model evenly tiled with two regions across the surface of the star.

as well. Thus for a dominantly single lobed V profile, most of the line forming region of the atmosphere should have no or a very weak magnetic field. In our simple transition model, this favors sharp transitions very high or very low in the model atmosphere.

Moving to a disk integrated line profile introduces more potential model parameters and ambiguity. We first consider an uniform horizontal distribution of magnetic field and velocity, both oriented radially in the stellar coordinates. In this case the same general trends above still hold. However, if the line width is dominated by rotational broadening, this horizontal magnetic field distribution has an important impact on the shape of the line in V. For a horizontally uniform distribution, this produces a V profile that is nearly symmetric about the line center. For a dipolar magnetic field, the orientation of the dipole strongly impacts the rotationally broadened line profile. As the sign of the magnetic field changes, the sign of the gradient changes, and the sign of the asymmetry changes, as can be seen from Eq. 1.

The horizontally uniform model is almost certainly an oversimplification, however it is still instructive. We also consider a model where the surface is tiled with regions that have two different radial velocity and magnetic field distributions. In this case, if the regions have equal area, and opposite sign of only the magnetic field or the velocity, then the disk integrated profile has no asymmetry. However, if both velocity and magnetic field have opposite signs, a strongly asymmetric profile can be produced, centered on the line center.

In order to test whether these models can reasonably reproduce observed asymmetries, we attempted to fit the Least Squares Deconvolution (LSD) profile of Sirius A. For this model, we use the line parameters from the LSD profile, and the stellar $v \sin i$, $T_{\rm eff}$, and $\log g$. The fitting was only approximate and performed by hand. First we used a model that is horizontally uniform. The magnetic and velocity distributions, and resulting line profiles, are shown in

Fig. 2. This comes very close to matching the observed profiles, requiring only a very weak magnetic field, and the velocity transition of 2 $\mathrm{km\,s^{-1}}$ is within the microturbulence of the star. However the model V profile is marginally offset from the center of the observed profile. As a second case, we consider a model tiled with regions of positive and negative velocity and magnetic field. The two velocity and magnetic field distributions used are shown in Fig. 3, together with the resulting line profiles. This model reproduces the observed profiles well, although it includes more free parameters.

3. Conclusions

Gradients in velocity and magnetic field in a stellar atmosphere provide a plausible explanation for the unusual asymmetric V profiles of Sirius A, β Uma, θ Leo. The magnetic fields involved can be quite weak, and the velocity changes needed are compatible with the observed microturbulence in these Am stars. The right conditions can produce dominantly asymmetric V profiles from this mechanism, and some conditions can produce these asymmetric profiles centered on the line.

There are substantial degeneracies in these models, the observations do not seem to provide a unique constraint on the magnetic and velocity distributions needed for this mechanism. Further, while these tests show that this mechanism can explain the observations, it does not prove that this is the cause of the observed asymmetries. Nevertheless this provides an exciting avenue for exploring the perplexing Stokes V profiles of these stars.

References

Blazère, A., Neiner, C., & Petit, P. 2016a, *Mon. Not. R. Astron. Soc.*, **459**, L81

Blazère, A., Petit, P., Lignières, F., et al. 2016b, *Astron. Astrophys.*, **586**, A97

Landstreet, J. D. 1988, *Astrophys. J.*, **326**, 967

Lignières, F., Petit, P., Böhm, T., & Aurière, M. 2009, *Astron. Astrophys.*, **500**, L41

Martin, B. & Wickramasinghe, D. T. 1979, *Mon. Not. R. Astron. Soc.*, **189**, 883

Petit, P., Lignières, F., Aurière, M., et al. 2011, *Astron. Astrophys.*, **532**, L13

Sanchez Almeida, J., Collados, M., & del Toro Iniesta, J. C. 1989, *Astron. Astrophys.*, **222**, 311

Wade, G. A., Bagnulo, S., Kochukhov, O., et al. 2001, *Astron. Astrophys.*, **374**, 265

Contrib. Astron. Obs. Skalnaté Pleso **48**, 58 – 65, (2018)

Surface mapping of magnetic hot stars

Theories versus observations

O. Kochukhov

Department of Physics and Astronomy, Uppsala University, SE 75120, Uppsala, Sweden, (E-mail: oleg.kochukhov@physics.uu.se)

Received: November 8, 2017; Accepted: November 13, 2017

Abstract. This review summarises results of recent magnetic and chemical abundance surface mapping studies of early-type stars. We discuss main trends uncovered by observational investigations and consider reliability of spectropolarimetric inversion techniques used to infer these results. A critical assessment of theoretical attempts to interpret empirical magnetic and chemical maps in the framework of, respectively, the fossil field and atomic diffusion theories is also presented. This confrontation of theory and observations demonstrates that 3D MHD models of fossil field relaxation are successful in matching the observed range of surface magnetic field geometries. At the same time, even the most recent time-dependent atomic diffusion calculations fail to reproduce diverse horizontal abundance distributions found in real magnetic hot stars.

Key words: stars: atmospheres – stars: chemically peculiar – stars: magnetic fields – starspots

1. Introduction

The presence of strong, stable magnetic fields in the outer envelopes of early-type stars leads to formation of prominent horizontal and vertical chemical abundance inhomogeneities. These chemical structures can be mapped by applying Doppler imaging (DI) inversion procedures to high-resolution spectroscopic observations. Moreover, modern time-resolved spectropolarimetric data, in particular high-resolution spectra in all four Stokes parameters, provide sufficient information for reconstruction of detailed geometries of surface magnetic fields, relaxing the common assumption of oblique dipolar magnetic topologies.

This paper summarises results of recent observational magnetic and chemical abundance mapping studies of hot stars. We also touch upon the question of systematic errors of the surface mapping procedures and their intrinsic limitations. This review is concluded with a critical assessment of theoretical attempts to interpret empirical magnetic and chemical maps of stellar surfaces with the help of ab initio fossil field and atomic diffusion calculations.

2. Magnetic field mapping

2.1. Observational results

Most historic and many recent studies of the magnetic field topologies of hot stars were limited to fitting simple parametrised dipole or dipole plus quadrupole model topologies to the phase curves of integral magnetic observables. With the improvement of observational capabilities and, in particular, introduction of wide wavelength coverage, high-resolution full Stokes vector spectrometers (ESPaDOnS, Narval, HARPSpol) it became possible to reconstruct arbitrary surface magnetic field topologies directly from time-series polarisation profiles with the magnetic Doppler imaging (MDI) technique (Piskunov & Kochukhov, 2002; Kochukhov et al., 2014). These magnetic inversion studies, carried out for 16 A and B stars so far, demonstrate a key role of linear polarisation data (Stokes Q and U profiles) in detecting and characterising the small-scale field topologies (Kochukhov et al., 2004a; Kochukhov & Wade, 2010). Four Stokes parameter MDI analyses suggest that the typical surface magnetic geometry of an early-type star is represented by a superposition of (occasionally distorted) dipolar fields and local magnetic spots. Without the constraints provided by the Stokes QU data, spectropolarimetric inversions yield a smoother field distribution, almost entirely lacking small-scale details, and may suffer considerable ambiguity in rare cases of strongly non-dipolar field configurations (Kochukhov & Wade, 2016). Unfortunately, only 8 Ap/Bp stars have so far been analysed taking the linear spectropolarimetric data into account.

Figure 1 presents a summary of all MDI results obtained for early-type magnetic stars. The symbol sizes, shapes and colours encode the average field strength, contribution of the dipolar component and the fraction of toroidal field energy. Generally, the field topologies appear more diverse than thought previously. There are examples of very nearly dipolar fields, even for stars studied with high-quality full Stokes vector data (Rusomarov et al., 2015), clearly non-dipolar and non-axisymmetric field configurations (Kochukhov et al., 2011; Kochukhov & Wade, 2016), and field topologies with an unexpectedly large toroidal contribution (Oksala et al., 2017). However, no coherent pattern of the field geometry versus stellar mass or/and age emerges from Fig. 1, except for the tendency of finding the most complex non-dipolar fields in the more massive stars (τ Sco, HD 37776). At the same time, it must be acknowledged that most objects in this figure are field Ap/Bp stars for which the evolutionary status is constrained to no better than about half of the main sequence lifetime.

2.2. Comparison with theories

Few theoretical studies went beyond the dipolar approximation in studying the structure of surface magnetic fields in early-type stars. Among more general analyses, MHD simulations of the fossil field relaxation by Braithwaite & Nordlund (2006) and Braithwaite (2008) demonstrated formation of stable, mixed

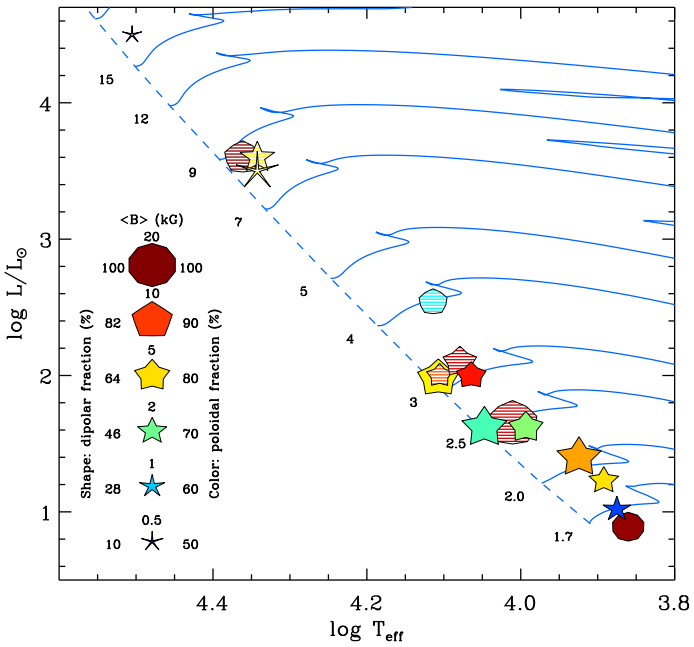

Figure 1. Positions of the hot-star MDI targets on the H-R diagram. The sizes of symbols correspond to the mean magnetic field strength, their shape to the dipolar magnetic energy fraction, and the colour to the ratio of poloidal and toroidal field components. The solid symbols indicate results based on the full Stokes vector inversions while the hatched symbols correspond to the MDI results based on circular polarisation alone.

poloidal-toroidal 3D magnetic configurations in stably stratified stellar interiors from initially random seed fields. We have analysed a number of models by Braithwaite (private communication) aiming to compare theoretical surface magnetic field configurations with observational MDI studies of early-type stars. This comparison shows that these theoretical calculations are remarkably successful in encompassing the entire range of the observed field geometries. Similar to empirical magnetic maps, Braithwaite's simulations sometimes produce almost perfect surface dipoles. But in other cases the surface field geometry is a dipole with significant distortions, such as small-scale local spots, or dipolar geometries with a significant toroidal contribution or even strongly non-dipolar fields. However, since these different outcomes of MHD modelling result from adopting different initial conditions in a highly idealised, non-rotating and non-evolving stellar interior model, it is not possible to relate theoretical predictions of different magnetic field geometries with physical properties of real stars or with some particular evolutionary stages.

3. Chemical abundance mapping

3.1. Observational results

A summary of 39 individual DI and MDI analyses of 36 magnetic Ap/Bp stars and 4 HgMn stars lacking global magnetic fields was complied by Kochukhov (2017). Five other abundance DI studies were published in 2017. Multi-element (5 or more species) abundance mapping results are available for 15 stars, with HD 3980 (Nesvacil et al., 2012), HD 24712 (Lüftinger et al., 2010b), HD 50773 (Lüftinger et al., 2010a), HD 83368 (Kochukhov et al., 2004b), ε UMa (Lüftinger et al., 2003), and α^2 CVn (Silvester et al., 2014) studied most comprehensively.

The published DI maps of early-type stars reveal a striking diversity of surface chemical spot morphologies, both in terms of distributions of different elements for the same star and in terms of behaviour of the same element for different stars with similar atmospheric parameters. It is very common to find elements showing an opposite relation to the magnetic field geometry for the same star. For instance, oxygen appears to be the only example of an element with a systematic enhancement at the equator of dipolar magnetic field (Rice et al., 1997; Kochukhov et al., 2004b), while Li, Cl and rare-earth elements tend to concentrate in the vicinity of one or both magnetic poles (see Fig. 2). But it is also not uncommon to find significant offsets of major element concentrations from the location of magnetic features (e.g. Pr in Fig. 2) or lack of any apparent relation to the field geometry.

Many recent abundance mapping studies have incorporated detailed treatment of magnetic field effects in polarised radiative transfer and often derived both magnetic field geometry and several chemical distributions with a self-consistent MDI inversion based on observations in several Stokes parameters. However, the bulk of historic Ap-star abundance mapping investigations neglected magnetic fields. Numerical experiments (Kochukhov, 2017) demonstrate that this leads to average errors of 0.2–0.3 dex in the inferred local abundances for typical dipolar field strength of a few kG. Similar systematic errors arise due to neglect of lateral variations of continuum brightness and model atmosphere structure. These errors are small compared to typical abundance contrasts of 2–5 dex derived with DI for Ap/Bp stars.

Photometric time-series studies provide an independent validation of the spectroscopic DI inversion results. Lüftinger et al. (2010a) found that the surface locations of main metal overabundance features in the Ap star HD 50773 coincide with positions of bright spots derived from the CoRoT light curve of this star. Several other studies (e.g. Krtička et al., 2015) compared light curves of Ap/Bp stars in multiple photometric bands with the synthetic SED models based directly on the local abundances inferred by independent DI analyses. These comparisons showed that the amplitudes, shapes and wavelength dependence of the observed photometric phase curves are satisfactorily or, in many

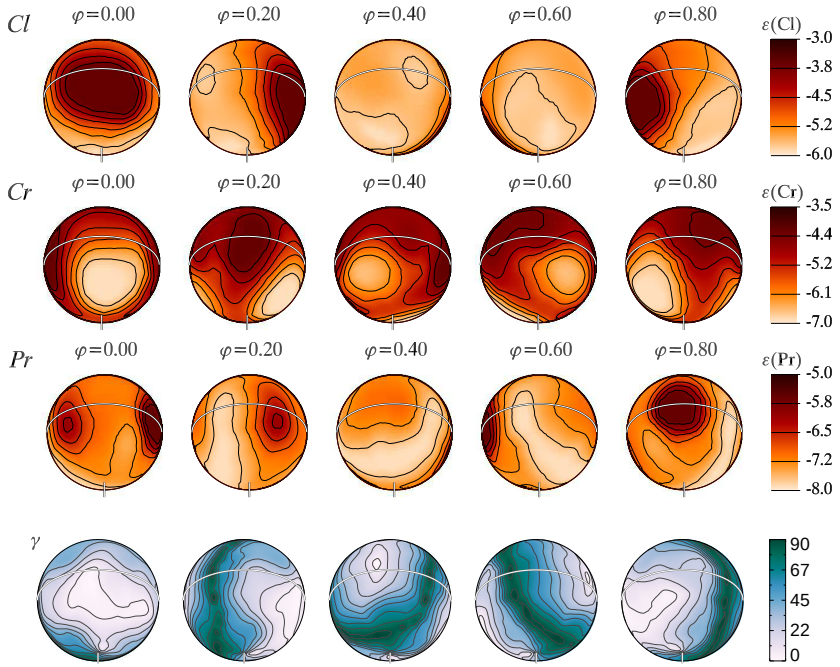

Figure 2. Surface distributions of Cl, Cr, and Pr (top three rows) derived for the magnetic Ap star α^2 CVn by Silvester et al. (2014) in comparison to the local field inclination (bottom row). The element abundances are given in the $\log N_{\rm el}/N_{\rm tot}$ scale. The field inclination is measured in degrees.

cases, very successfully reproduced by multi-element DI maps, confirming validity of abundance inversions over a wide stellar parameter range.

3.2. Comparison with theories

The origin of chemical spots in early-type stars is currently not understood. It is generally believed that anomalous surface chemistry of Ap/Bp stars is explained by the selective gravitational settling and radiative levitation of atoms, the process known as atomic diffusion (Michaud et al., 2015). Non-magnetic, spherically symmetric diffusion calculations in stellar interiors (Vick et al., 2010) and atmospheres (LeBlanc et al., 2009) are indeed reasonably successful in reproducing the observed temperature-dependent mean element abundances and mean vertical stratification of chemical elements (Ryabchikova et al., 2011).

In comparison, little progress is evident in the *ab initio* modelling of the horizontal chemical spots. Early, semi-qualitative studies attempting to link spot geometries with an underlying magnetic field structure (Michaud et al., 1981; Alecian & Vauclair, 1981; Babel & Michaud, 1991) have been superseded by de-

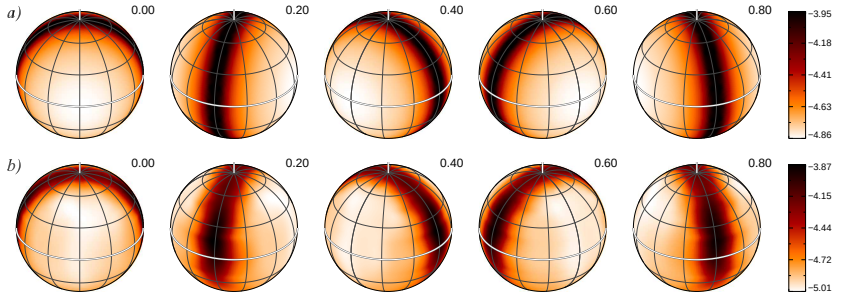

Figure 3. Horizontal distribution of Fe abundance at the optical depth $\log \tau_{5000} = -2$ from the theoretical 3D diffusion calculations by Stift & Alecian (2016) (a) compared to the 2D Doppler imaging reconstruction from simulated data for four Fe II lines (b).

tailed numerical models taking into account anisotropic diffusion in the presence of an arbitrary magnetic field and including a feedback of chemical stratification on the stellar atmospheric structure (Alecian & Stift, 2010; Alecian, 2015). This modelling has been also extended to a time-dependent treatment of diffusion (Alecian et al., 2011; Stift & Alecian, 2016), lifting the common arbitrary assumption of an equilibrium element stratification (zero net particle flux). At the same time, these diffusion calculations neglect several effects (ambipolar diffusion, weak stellar wind, electromagnetic particle drifts, realistic bottom boundary condition provided by the interior particle diffusion) already shown to be important by previous studies. None of the recent diffusion studies have considered stellar rotation and related global circulation and mixing effects.

Probably as a result of one or several of these simplifications, theoretical horizontal abundance distributions fail to achieve even a qualitative agreement with observations. Most importantly, both earlier equilibrium and more recent time-dependent calculations predict all chemical elements to be either homogeneously distributed or share the exact same distribution characterised by a preferential element concentration in (very nearly) horizontal field regions. As illustrated by Fig. 2 for α^2 CVn as well as by other recent DI results and many historic spectrum variability studies, this conjecture is clearly at odds with reality (with a possible exception of oxygen distributions in a couple of Ap stars).

A detailed analysis (Kochukhov & Ryabchikova, submitted) of the 3D Fe and Cr theoretical chemical profiles published by Stift & Alecian (2016) reveals that these time-dependent diffusion calculations underestimate the mean abundances of these elements by a factor of 100–1000, thus, paradoxically, leading to a far worse agreement with the observed mean abundances compared to, presumably less realistic, equilibrium diffusion models of previous generation.

Observational spectroscopic data simulated according to the diffusion model by Stift & Alecian (2016) can be used to test the impact of vertical chemical stratification (neglected by typical horizontal mapping studies) on the DI results,

thereby assessing another, potentially important, systematic error source. The outcome of this experiment, illustrated in Fig. 3, proves that neglect of vertical chemical stratification does not lead to a noticeable deterioration or a systematic bias in the DI maps. The usual 2D inversions are able to recover horizontal element distributions that closely match a representative cross-section of the input 3D abundance map. These results confirm that lateral cross-sections of the 3D diffusion model predictions can be meaningfully compared to the entire body of published 2D DI maps.

4. Conclusions and outlook

Modern spectral inversion techniques are able to provide detailed and reliable maps of chemical element and magnetic field vector distributions on the surfaces of Ap/Bp and related stars. Much of the recent progress in understanding magnetic field geometries of these objects is spurred by the extension of spectropolarimetric magnetic studies from the traditional circular polarisation diagnostic to a full Stokes vector analysis. However, the number of studies based on four Stokes parameter spectra needs to be increased in order to obtain an unbiased view of early-type star magnetism.

The evolutionary perspective has been almost entirely missing from the surface mapping studies owing to their focus on bright, easily accessible field stars. Systematic DI and MDI analyses of cluster Ap/Bp stars are necessary for putting surface structure information in a relevant evolutionary context.

The current theoretical atmospheric atomic diffusion calculations are fundamentally unable to account for the observed diversity of chemical spot distributions in Ap/Bp stars. The latest time-dependent diffusion calculations also fail to reproduce a large mean overabundance of Fe-peak elements, known to be a universal distinguishing feature of most of these objects. It is likely that one or several physical processes (e.g. weak mass loss, stellar rotation, electromagnetic particle drifts) ignored by the current diffusion calculations are playing important roles in shaping non-uniform element distributions in early-type stars.

Acknowledgements. This research is supported by the Knut and Alice Wallenberg Foundation, the Swedish Research Council, and the Swedish National Space Board. The author thanks Dr. J. Braithwaite for providing MHD models of fossil magnetic fields and Drs. G.A. Wade, J. Silvester and N. Rusomarov for many stimulating discussions and contributions to the studies described in this review.

References

Alecian, G. 2015, *Mon. Not. R. Astron. Soc.*, **454**, 3143

Alecian, G. & Stift, M. J. 2010, *Astron. Astrophys.*, **516**, A53

Alecian, G., Stift, M. J., & Dorfi, E. A. 2011, *Mon. Not. R. Astron. Soc.*, **418**, 986

Alecian, G. & Vauclair, S. 1981, *Astron. Astrophys.*, **101**, 16

Babel, J. & Michaud, G. 1991, *Astrophys. J.*, **366**, 560

Braithwaite, J. 2008, *Mon. Not. R. Astron. Soc.*, **386**, 1947

Braithwaite, J. & Nordlund, Å. 2006, *Astron. Astrophys.*, **450**, 1077

Kochukhov, O. 2017, *Astron. Astrophys.*, **597**, A58

Kochukhov, O., Bagnulo, S., Wade, G. A., et al. 2004a, *Astron. Astrophys.*, **414**, 613

Kochukhov, O., Drake, N. A., Piskunov, N., & de la Reza, R. 2004b, *Astron. Astrophys.*, **424**, 935

Kochukhov, O., Lüftinger, T., Neiner, C., Alecian, E., & MiMeS Collaboration. 2014, *Astron. Astrophys.*, **565**, A83

Kochukhov, O., Lundin, A., Romanyuk, I., & Kudryavtsev, D. 2011, *Astrophys. J.*, **726**, 24

Kochukhov, O. & Wade, G. A. 2010, *Astron. Astrophys.*, **513**, A13

Kochukhov, O. & Wade, G. A. 2016, *Astron. Astrophys.*, **586**, A30

Krtička, J., Mikulášek, Z., Lüftinger, T., & Jagelka, M. 2015, *Astron. Astrophys.*, **576**, A82

LeBlanc, F., Monin, D., Hui-Bon-Hoa, A., & Hauschildt, P. H. 2009, *Astron. Astrophys.*, **495**, 937

Lüftinger, T., Kuschnig, R., Piskunov, N. E., & Weiss, W. W. 2003, *Astron. Astrophys.*, **406**, 1033

Lüftinger, T., Fröhlich, H.-E., Weiss, W. W., et al. 2010a, *Astron. Astrophys.*, **509**, A43

Lüftinger, T., Kochukhov, O., Ryabchikova, T., et al. 2010b, *Astron. Astrophys.*, **509**, A71

Michaud, G., Alecian, G., & Richer, J. 2015, Atomic Diffusion in Stars (Springer)

Michaud, G., Charland, Y., & Megessier, C. 1981, *Astron. Astrophys.*, **103**, 244

Nesvacil, N., Lüftinger, T., Shulyak, D., et al. 2012, *Astron. Astrophys.*, **537**, A151

Oksala, M. E., Silvester, J., Kochukhov, O., et al. 2017, *Mon. Not. R. Astron. Soc.*, **473**, 3367

Piskunov, N. & Kochukhov, O. 2002, *Astron. Astrophys.*, **381**, 736

Rice, J. B., Wehlau, W. H., & Holmgren, D. E. 1997, *Astron. Astrophys.*, **326**, 988

Rusomarov, N., Kochukhov, O., Ryabchikova, T., & Piskunov, N. 2015, *Astron. Astrophys.*, **573**, A123

Ryabchikova, T., LeBlanc, F., & Shulyak, D. 2011, in Magnetic Stars, 69–80

Silvester, J., Kochukhov, O., & Wade, G. A. 2014, *Mon. Not. R. Astron. Soc.*, **444**, 1442

Stift, M. J. & Alecian, G. 2016, *Mon. Not. R. Astron. Soc.*, **457**, 74

Vick, M., Michaud, G., Richer, J., & Richard, O. 2010, *Astron. Astrophys.*, **521**, A62

Contrib. Astron. Obs. Skalnaté Pleso **48**, 66 – 72, (2018)

Stellar activity and stellar pulsations in ground- and space-based observations

E. Paunzen[1], K. Bernhard[2,3] and S. Hümmerich[2,3]

[1] *Department of Theoretical Physics and Astrophysics, Masaryk University, CZ-611 37 Brno, Czech Republic (E-mail: epaunzen@physics.muni.cz)*

[2] *American Association of Variable Star Observers (AAVSO), Cambridge, MA, 02138, USA*

[3] *Bundesdeutsche Arbeitsgemeinschaft für Veränderliche Sterne e.V. (BAV), D-12169 Berlin, Germany*

Received: November 12, 2017; Accepted: November 17, 2017

Abstract. The research on variable stars has significantly benefited from the availability of long-term photometric time series data from ground- and space-based surveys. Precise and long-term stable data allow the investigation of variable stars with small amplitudes and long periods, and the research on multi-periodic objects has profited greatly from the availability of quasi-uninterrupted time series data from space-based mission. To illustrate this situation, we have chosen to present our efforts to investigate the photometric variability of magnetic chemically peculiar stars using data from six different survey sources (ASAS-3, CoRoT, KELT, Kepler, Kepler-K2 and SuperWASP). Due to their range of periods (0.5 days to several years) and photometric amplitudes (sub-mmag range to about 0.1 mag), these objects constitute a challenge to observers. Long-term instrumental stability and a sufficient phase coverage are needed to detect and investigate this kind of variability.

Key words: stars: chemically peculiar – stars: variables: general – surveys – techniques: photometric

1. Introduction

The advent of ground- and space-based photometric surveys during the last two decades has led to the accumulation of a wealth of data that is mostly publicly available and constitutes a valuable resource for variable star research. The available surveys cover different time bases, observing cadences, magnitude ranges, wavelength ranges, and accuracies. Thus, a direct comparison of the available photometric data is often not straightforward.

For this paper, we haven chosen to present survey light curves of the group of α^2 Canum Venaticorum (ACV) variables. These objects are photometrically variable magnetic chemically peculiar (mCP) stars of the upper main sequence (spectral types early B to early F), whose spectra show abnormal line strengths indicating peculiar surface element abundances for elements such as Si, Cr, Sr, He or the rare-earth elements (Preston, 1974). As their name implies, mCP

stars exhibit strong, globally-organized magnetic fields reaching strengths of up to several tens of kiloGauss (Mathys, 2017). The observed chemical peculiarities are generally attributed to diffusion of chemical elements as a result of the competition between radiative pressure and gravitational settling (Richer et al., 2000; Turcotte, 2003). The photometric variations of ACV variables are explained in terms of the oblique rotator model (Stibbs, 1950); the observed photometric period is the rotational period of the star.

ACV variables exhibit periods ranging from about 0.5 days to several years and amplitudes from the sub-mmag range to about 0.1 mag, depending on the bandpasses of the employed photometric filters. The observed period and amplitude range of ACV variables presents a challenge because of the problem of daily aliasing and the need for long-term stable observations. Several investigations have been concerned with the study of the photometric variability of ACV variables in the recent past (Paunzen et al., 2016). In the following, we present typical light curves of several such objects from different survey sources which offer the possibility to directly compare the quality of these data.

2. Data sources

In this section, we shortly describe six photometric survey sources (ASAS-3, CoRoT, KELT, Kepler, Kepler-K2 and SuperWASP) that we have already employed for studying the variability of ACV stars. In addition, exemplary light curves are shown. This list is by no means complete, but the presented data are publicly available, which is why they have been chosen for this paper. Another important aspect to consider is the processing of the data, and the amount of effort involved. From our experience, almost all survey data need to be further reduced, or at least carefully inspected. Instrumental trends need to be identified, and the data have to be cleaned of outliers; sometimes time binning may be helpful. This data treatment has to be done with care in order to preserve the intrinsic variability of the star. When dealing with a new survey source, it has proven helpful to procure and analyze data for known variable stars with well-determined parameters before setting out on the search for new variable stars, as this will provide a good idea what can be expected from (and achieved with) the employed data source.

2.1. ASAS-3

The All Sky Automated Survey (ASAS) is a project that aims at continuous photometric monitoring of the whole sky, with the ultimate goal of detecting and investigating any kind of photometric variability. The typical exposure time for ASAS-3 V-filter observations is three minutes, which results in reasonable photometry for stars in the magnitude range $7 < V < 14$ mag (about 10^7 objects). In general, a field is observed each one, two, or three days (Pigulski, 2014). Using ASAS-3 data, Bernhard et al. (2015a) and Hümmerich et al. (2016) investigated

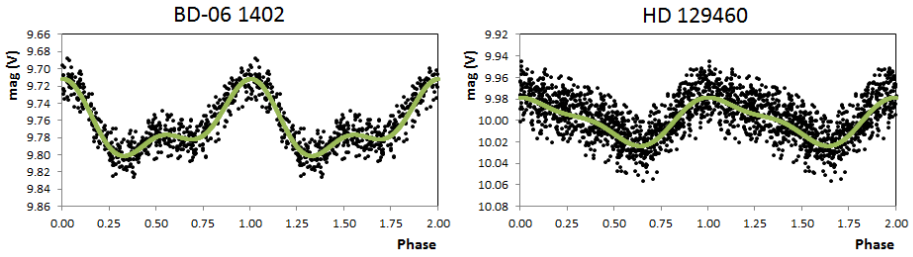

Figure 1. The ASAS-3 light curves of BD–06 1402 (period of 1.13063 days, left panel) and HD 129460 (1.76444 days, right panel), taken from Hümmerich et al. (2016).

the photometric variability of mCP stars and identified more than 650 new ACV variables. Two examples from the latter source are given in Fig. 1, which shows the light curves of BD–06 1402 ($V = 9.75$ mag, period of 1.13063 days, left panel) and HD 129460 ($V = 10.06$ mag, 1.76444 days, right panel).

2.2. CoRoT

The CoRoT (Convection, Rotation and planetary Transits) space mission (2006 – 2012) focused on high-precision photometry, taking advantage of the boons of space-bound photometry by observing given targets continuously for up to 150 days (De Medeiros et al., 2013). A set of light curves is available for about 170 000 stars. Observations have been performed in two modes optimized for targets with $6 < V < 9$ mag and $11 < V < 16$ mag, respectively. Paunzen et al. (2015) analyzed the high-quality CoRoT light curve of the CP2 star HD 49310 (Fig. 2) and photometrically modeled the star spots by applying a Bayesian technique. As can be seen in the available light curve, 'jumps' and linear trends are still visible in the data which have to be corrected for. However, the accuracy of the data is very high and comparable to data from the *Kepler* mission. Up to now, no statistical analysis of the ACV variables based on CoRoT data has been published.

2.3. KELT Transit Survey

The Kilodegree Extremely Little Telescope (KELT) is an all-sky survey boasting data for stars with $7 < V < 11$ mag in several filters and a time basis of up to 10 years (Pepper et al., 2008). Two combined dedicated telescopes observe over 70% of the entire sky with a 10 to 30 minute cadence. A detailed analysis of ACV variables using KELT data is in preparation but has not been published yet. In Fig. 3, we present the KELT light curves of two known CP stars, GSC 1773–00211 (HD 14522, $V = 8.79$ mag, period of 1.837182 days, left panel) and GSC 1875–00552 (HD 39865, $V = 8.62$ mag, 26.36 days, right panel). The scatter in the light curve is about 0.02 mag.

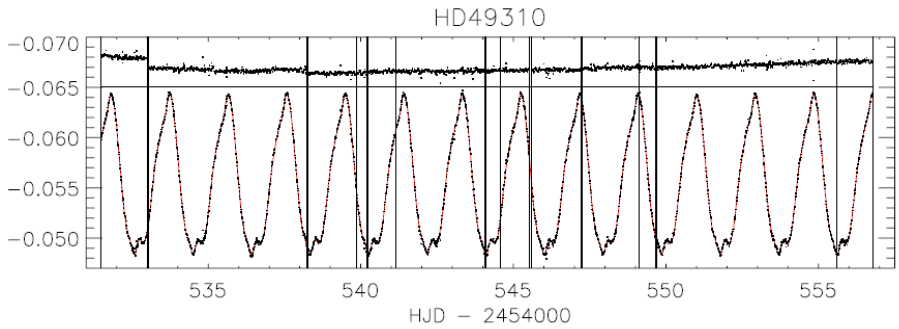

Figure 2. The CoRoT light curve of HD 49310 taken from Paunzen et al. (2015) and fitted by a six-spot model (red line). Residuals (arbitrary offset) are shown in the upper part of the figure. Jumps and linear trends have been accounted for automatically by using a likelihood function that integrates over all possible magnitude offsets and trends (lower part). The period of this star is 1.91909 days.

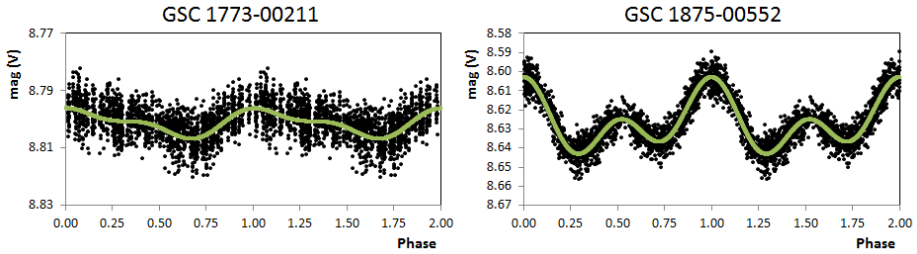

Figure 3. The KELT light curves of GSC 1773–00211 (period of 1.837182 days, left panel) and GSC 1875–00552 (26.36 days, right panel).

2.4. Kepler

During the first part of the *Kepler* space mission, the brightness of about 150 000 stars was continuously monitored for 4.5 yr in a 105-square-degree fixed field of view (Borucki, 2016). The mean top-of-the-noise level in the periodogram for a star of 10th magnitude is about 3 ppm for an observing run of 30 d, dropping to about 1 ppm after one year. For a star of 12th magnitude, the corresponding noise level is about 6 ppm for one month and 3 ppm after one year. This unprecedented level of precision allows the discovery of new CP stars and a detailed study of their photometric variability (Fig. 4).

The *Kepler* K2 mission became operational in mid-2014, after a severe malfunction had deprived the satellite of its ability to stay pointed at a target without drifting off course. Data from the K2 mission are generally of some-

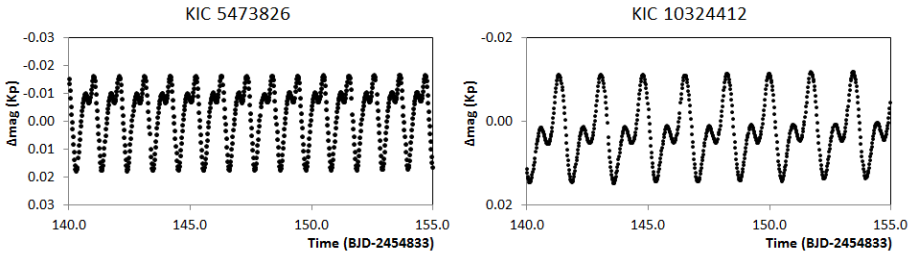

Figure 4. The Kepler light curves of KIC 5473826 (period of 1.05120 days, left panel) and KIC 10324412 (1.73150 days, right panel).

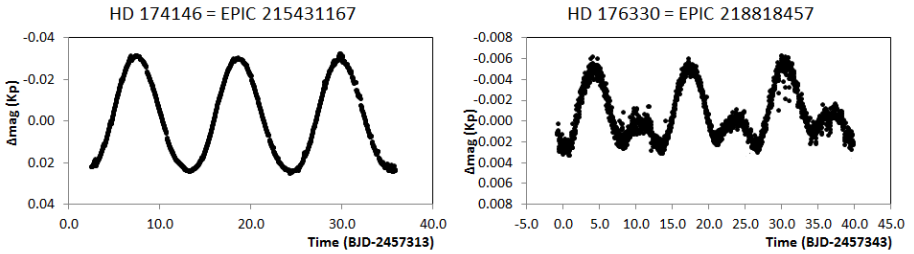

Figure 5. The Kepler–K2 light curves of HD 174146 (period of 11.185 days, left panel) and HD 176330 (13.16 days, right panel).

what lower quality but may approach a photometric precision similar to that obtained by the prime Kepler mission (Libralato et al., 2016). The K2 observing campaigns cover an approximate period of 80 days; target lists have been compiled from community solicitations for proposed targets. Fig. 5 illustrates the K2 light curves of two ACV variables. An investigation of ACV variables in K2 data is in progress.

2.5. SuperWASP

The SuperWASP survey started in 2004 and covers both hemispheres. It provides long-term photometric time series in a broadband filter (400–700 nm) with an accuracy better than 1% for objects in the magnitude range $8 < V < 11.5$ mag (Pollacco et al., 2006). Observations consist in general of two consecutive 30s integrations followed by a 10-minute gap. Bernhard et al. (2015b) analysed 3 850 000 individual photometric WASP measurements of 579 mCP stars and candidates. In total, 80 variables were found, from which 74 were reported for the first time (see Fig. 6 for exemplary light curves).

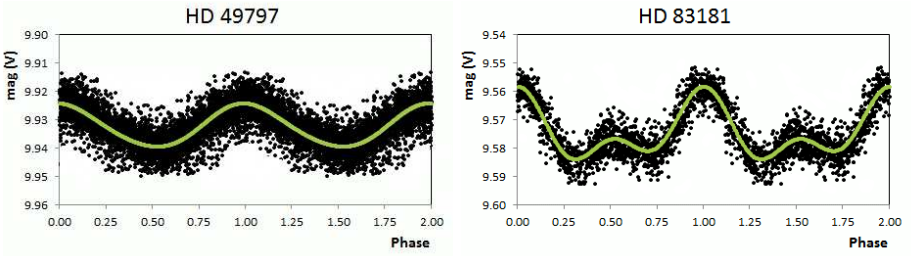

Figure 6. The SuperWASP light curves of HD 49797 (period of 1.2263 days, left panel) and HD 83181 (2.5241 days, right panel), taken from Bernhard et al. (2015b).

3. Conclusion

The present paper presents an overview over our recent efforts to investigate the photometric variability of ACV variables using data from diverse survey sources. Exemplary light curves are shown, which illustrate the capabilities of the employed surveys, which differ in parameters such as time base, observing cadence, accuracy and covered magnitude and wavelength range. After further processing (removal of outliers, instrumental trends etc.) and careful inspection, the survey data provide a wealth of information and constitute an important resource for variable star research. The research on variable stars with small amplitudes (such as ACV variables) and multiple periods (such as δ Scuti or γ Doradus stars), in particular, has benefited from the long-term and, in the case of space-based surveys, quasi-uninterrupted observations. New and exciting results are sure to come forth from the wealth of archival data that has been procured – and will be procured in future surveys.

References

Bernhard, K., Hümmerich, S., Otero, S., & Paunzen, E. 2015a, *Astron. Astrophys.*, **581**, A138

Bernhard, K., Hümmerich, S., & Paunzen, E. 2015b, *Astron. Nachr.*, **336**, 981

Borucki, W. J. 2016, *Reports on Progress in Physics*, **79**, 036901

De Medeiros, J. R., Ferreira Lopes, C. E., Leão, I. C., et al. 2013, *Astron. Astrophys.*, **555**, A63

Hümmerich, S., Paunzen, E., & Bernhard, K. 2016, *Astron. J.*, **152**, 104

Krtička, J., Janík, J., Marková, H., et al. 2013, *Astron. Astrophys.*, **556**, A18

Libralato, M., Bedin, L. R., Nardiello, D., & Piotto, G. 2016, *Mon. Not. R. Astron. Soc.*, **456**, 1137

Mathys, G. 2017, *Astron. Astrophys.*, **601**, A14

Paunzen, E., Fröhlich, H.-E., Netopil, M., Weiss, W. W., & Lüftinger, T. 2014, *Astron. Astrophys.*, **574**, A57

Paunzen, E., Netopil, M., Bernhard, K., & Hümmerich, S. 2016, *Bulgarian Astronomical Journal*, **24**, 97

Pepper, J., Stanek, K. Z., Pogge, R. W., et al. 2008, *Astron. J.*, **135**, 907

Pigulski, A. 2014, in IAU Symp., Vol. **301**, *Precision Asteroseismology*, ed. J. A. Guzik, W. J. Chaplin, G. Handler, & A. Pigulski, 31–38

Pollacco, D. L., Skillen, I., Collier Cameron, A., et al. 2006, *Publ. Astron. Soc. Pac.*, **118**, 1407

Preston, G. W. 1974, Ann. Rev. Astron. Astrophys., 12, 257

Richer, J., Michaud, G., & Turcotte, S. 2000, *Astrophys. J.*, **529**, 338

Stibbs, D. W. N. 1950, *Mon. Not. R. Astron. Soc.*, **110**, 395

Turcotte, S. 2003, in ASP Conf. Ser., Vol. **305**, *Magnetic Fields in O, B and A Stars: Origin and Connection to Pulsation, Rotation and Mass Loss*, ed. L. A. Balona, H. F. Henrichs, & R. Medupe, 199

Jan Janík, Ernst Paunzen, Zdeněk Mikulášek, Miloslav Zejda, Pavel Zieliński, Petr Kurfürst, Jakub Fišák and Lenka Matěchová

Contrib. Astron. Obs. Skalnaté Pleso **48**, 73 – 81, (2018)

Asteroseismology of magnetic stars

P. Walczak and J. Daszyńska-Daszkiewicz

Instytut Astronomiczny Uniwersytet Wrocławski, ul. Kopernika 11, 51-622 Wrocław, Poland

Received: November 13, 2017; Accepted: November 15, 2017

Abstract.

Precision asteroseismology requires a detailed modelling of stellar structure and pulsations. It means that even if some effects are small they must be taken into account for an accurate confrontation of theory and observations. Studies of the last decade have shown that magnetic field is quite ubiquitous among stellar objects. Thus, by studying pulsators with measurable magnetic filed one can derive seismic inferences about a distortion caused by the magnetic field inaccessible in other manner. Here we discuss the latest achievements of synergies between asteroseismic inferences and magnetic field measurements.

Key words: asteroseismology – magnetic field – stars: rotation – stars: oscillations

1. Introduction

The magnetic field and rotation are intrinsic features of stars. Their effects modify both stellar structure and oscillations. Besides the Sun, the surface magnetic field has been detected in various pulsating variables, including main sequence stars, giants, white dwarfs and neutron stars. Their asteroseismic analysis can yield an independent determination of many parameters connected with both stellar properties and magnetic field features. The most obvious example are rapidly oscillating chemically peculiar A type stars (roAp; Kurtz, 1982). The stars are interpreted as rapid rotators with rotation axis oblique to the pulsation axis which is aligned to magnetic field symmetry axis. The magnetic field splits the pulsational modes into multiple components. From the ratio of the different peak amplitudes, one can deduce the geometry of the system, determine the magnetic field configuration and the ratio of the Lorentz force to the Coriolis force (Shibahashi, 2001). In case of solar like oscillators, a combination of the photometric observations and asteroseismic analysis allows to calibrate age-rotation-magnetic activity relation. Another interesting application of asteroseismology is to discover the internal magnetic field confined into the stellar cores.

The paper is organized as follows. In Sect. 2, we give a short description of the theory of stellar pulsation under the influence of the magnetic field and rotation. In Sects. 3, 4, 5 we introduce the different types of pulsating stars that exhibit a presence of a magnetic field. The last section contains a summary.

2. Magnetic field - rotation - pulsation interaction

2.1. Basic properties

In general, an interaction between the magnetic field, rotation and stellar pulsations is a very complicated issue. To study the effects, we need to include into the pulsational equations additional factors associated with the Coriolis, centrifugal and Lorentz forces. A linearized equation for nonradial adiabatic pulsations under the influence of rotation and magnetic field can be written in the following form (Unno et al., 1989; Shibahashi & Takata, 1993):

$$\mathcal{L}(\boldsymbol{\xi}) - \omega^2 \boldsymbol{\xi} + \omega \mathbf{M}(\boldsymbol{\xi}) + \mathbf{N}(\boldsymbol{\xi}) + \mathbf{B}(\boldsymbol{\xi}) = 0, \tag{1}$$

where the operator $\mathcal{L}$ describes the linear, adiabatic oscillations of the non-rotating and non-magnetic star, $\boldsymbol{\xi}$ is the mass element displacement and ω is the angular pulsational frequency. First and second order effects of the rotational velocity field are described by the operators $\mathbf{M}$ and $\mathbf{N}$, respectively. The magnetic field effects are contained in the operator $\mathbf{B}$. The magnetic field perturbation is described by $\frac{\partial \mathbf{B}'}{\partial t} = \nabla \times (\mathbf{v} \times \mathbf{B}_0)$.

The effect of the magnetic field is measured by the ratio the Alfvén velocity to the sound velocity, c_A/c_s, which compares the Lorentz force with the pressure-gradient force. In most stellar models the values of c_A is comparable or larger than c_s only in the outer layers, e.g., in the case of roAp stars these are layers from the He II ionization zone. The frequency perturbation is proportional to the ratio of the total magnetic energy to the total gravitational energy of a star.

As in the case of higher order effects of rotation, the angular dependence of the eigenfunctions cannot be expressed by a single spherical harmonic. In the framework of the perturbation theory, the expansion in a sum of the spherical harmonics with $\ell = 2j - 1$ for odd modes and $\ell = 2(j - 1)$ for even modes $(j = 1, 2, 3, ...)$.

The magnetic field affects both the equilibrium structure and oscillations in the second order of magnitude. In contrast, the rotation affects the equilibrium structure in the second order, while their effects on the oscillations appear already in the first order. This means that in the first approximation we can discard the rotational effects when building equilibrium model and concentrate only on the pulsation-rotation interaction. In case of magnetic field, we need to take special care in preparing both the equilibrium and pulsation models.

2.2. The oblique pulsator model

The oblique pulsator model was developed to describe the frequency pattern found in roAp stars (see Sect. 3), but this model can also be used, e.g., to described pulsating magnetic B-type stars. In the simplest approach, we assume that the oscillation symmetric axis coincides with the magnetic axis which is inclined to the rotational axis (Stibbs, 1950; Kurtz, 1982). More advanced studies allow the magnetic axis to be inclined to both the pulsation and rotation

axes (Bigot & Dziembowski, 2002). The rotational modulation of the pulsational amplitude causes splitting of the single frequency peak into $2\ell + 5$ components. Their relative amplitudes depend on various properties of a star (i.e. Dziembowski & Goode, 1985; Shibahashi & Takata, 1993). It means that observations of the fine structure in the oscillation spectra can be used as a probe of the internal rotation and magnetic field. Such studies are very challenging but potentially highly rewarding because they can provide the information on the degrees of the pulsation modes, magnetic geometries and the strength of the magnetic field. For example, the radial mode ($\ell = 0$) distorted by the dipolar magnetic field gains an additional quadrupolar character ($\ell = 2$). Rotational modulation of the mode amplitude splits the frequency peak in the power spectrum into five components separated by the rotational frequency. The ratio of the amplitudes of the outer components to the inner components is given by (Shibahashi & Takata, 1993; Shibahashi, 2001):

$$\frac{A_2 + A_{-2}}{A_1 + A_{-1}} \simeq \frac{1}{4} |\tan\beta \tan i|, \tag{2}$$

where β is the angle between the rotation and magnetic axes and i is the inclination angle. In other words, detection of the five components of the distorted radial mode allow us to constrain the geometry of the magnetic field and rotation axis independently from polarimetric determinations.

The dipole axisymmetric mode influenced by the dipolar magnetic field is characterised by a superposition of the dipole axisymmetric mode, dipole non-axisymmetric modes and octupolar modes ($\ell = 3$) with azimuthal numbers $m = 0, \pm 1$. This leads to the occurrence of a triplet which can be used as a diagnostic tool. The relative amplitudes of its components depend strongly on the stellar magnetic field and rotation (Shibahashi & Takata, 1993):

$$\frac{A_1 + A_{-1}}{A_0} \simeq |\tan\beta \tan i|, \quad \frac{A_1 - A_{-1}}{A_1 + A_{-1}} \simeq \frac{C_{n\ell=1}\Omega}{\omega^{mag}_{|m|=0} - \omega^{mag}_{|m|=1}}, \tag{3}$$

where $\omega^{mag}_{|m|}$ is the perturbation of the pulsational frequency caused by magnetic field. $C_{n\ell}$ is a Ledoux constant (Ledoux, 1951), Ω is the rotational frequency and $mC_{n\ell}\Omega$ is the first effect of the Coriolis force. The right side of the second Eq. (3) is a measure of the ratio of the Coriolis force to the Lorentz force. In principle, it is possible to estimated the magnetic field strength of roAp stars, provided that the rotational velocity is known. Also, due to the rotational amplitude modulation every component of the triplet splits into seven components producing as many as 21 frequencies grouped in seven triplets. This structure is very characteristic and can be easily recognised in the power spectra.

3. Rapidly oscillating Ap star

The roAp stars were discovered by Kurtz (1982). A few dozen of roAp stars have been identified so far. The stars are main sequence object and can be

found near the classical instability strip. Their light variations are caused by pulsations in high-order acoustic modes (p modes) propagating in the presence of a strong magnetic field (so called magneto-acoustic modes). The roAp stars exhibit strong abundance anomalies, which are usually non-uniform on the stellar surface. The chemical peculiarities are regarded as a result of an atomic diffusion. It seems, that all A-type stars that are not chemically peculiar do not posses a surface magnetic field (Shorlin et al., 2002; Bagnulo et al., 2006). On the other hand, all Ap stars do posses a surface magnetic field of the order of several kG (Aurière et al., 2007). This clearly indicates that the Ap phenomenon is connected with the magnetic field (Wade et al., 2009).

An excellent example of a roAp star is HR 1217 which was one of the first discovered stars of this type (Kurtz, 1982). It is also one of the best studied roAp stars since it was a target of a lot of observations, (including multi-site campaigns; Kurtz et al., 2002, 2005). Kurtz et al. (2005) derived a series of six triplets with nearly equal spacing. Five triplets had alternating spacing of 33.4 μHz and 34.5 μHz. The sixth frequency triplet was separated by 50 μHz from fifth triplet. The highest triplet did not follow the asymptotic relation. This effect was explained by Cunha & Gough (2000); Cunha (2006), who found that at the frequencies of maximal magneto-acoustic coupling the influence of the magnetic field on the frequency value is much larger than in other cases. This should cause the decrease of the frequency spacing indicating a missing triplet separated by about 34.6 μHz from the fifth triplet. Indeed, the missing modes were found in the data gathered during world-wide observational campaign called Whole Earth Telescope (Kurtz et al., 2002), supporting the theory of Cunha and Gough.

From polarimetric measurements of the surface magnetic field of HR 1217 Bagnulo et al. (1995) found a polar field strength of 3.9 kG, an inclination $i = 137^\circ$ and a magnetic obliquity of $\beta = 150^\circ$. The rotation period is of the order $P_{\rm rot} = 12.46$ d (Kurtz et al., 2005; Ryabchikova et al., 2005) while Lüftinger et al. (2008) found that the magnetic field of the star can be quite well described as a simple dipole. The value of the left side of the first Eq. (3) is consistent with the inclination i and obliquity β derived by Bagnulo et al. (1995) strongly supporting the oblique pulsator model. Also, Ryabchikova et al. (2007) measured the radial velocities of pulsational modes as a function of a depth inside of the stellar atmosphere. The authors derived the phase shifts between the radial velocities and photometric light changes and constrained the pulsational velocity in the atmosphere which turned out to be slightly smaller that the sound speed.

4. Magnetic pulsating B-type stars

The majority of intermediate and massive main sequence stars show no evidence of surface magnetic fields. Detailed spectropolarimetric surveys like MiMes (Magnetism in Massive Stars; Alecian et al., 2014; Wade et al., 2016), BinaMIcS

(Binarity and Magnetic Interactions in various classes of stars; Alecian et al., 2015), BOB (B fields in OB stars; Hubrig et al., 2014) or BRITE spectropolarimetric survey (Neiner & Lèbre, 2014) brought however positive detection of magnetic field in a few B-type stars, including some β Cep variables.

The star β Cep itself pulsates in at least six frequencies (Aerts et al., 1994; Telting et al., 1997) and has a surface magnetic field that changes sinusoidally. This indicates that the magnetic axis is oblique to the rotation axis (Henrichs et al., 2013). The observed equidistant structures composed of five components in the frequency spectrum has been interpreted by Shibahashi & Aerts (2000) as a manifestation of magnetic perturbation of a radial mode. Since the star pulsates also in an independent quadrupole mode, the authors were able to determine the mass of the star, its evolutionary status and properties of the magnetic field. They derived that the star is on the main sequence and its mass is about $9\,\mathrm{M}_\odot$. The value of the inclination, i, was calculated from the rotational velocity $V \sin i \approx 25\,\mathrm{km\,s^{-1}}$ and the rotational period of the order of 6 days. This gave $i \approx 30^\circ$ and $\beta = 100^\circ$ (see Eq. 2). These results, although very interesting, may not be valid. Henrichs et al. (2013) derived a different value of the rotational period of β Cep. The new period is twice the value used by Shibahashi & Aerts (2000), i.e. 12 days. This gives a larger inclination $i \approx 60^\circ$. The angle between the magnetic field and the rotation axis does not change significantly, $\beta \approx 96^\circ$. This example shows that the analysis of magnetic pulsators gives large prospects but the results depends strongly on the observational constraints.

Another interesting example of a pulsating magnetic B-type star is HD 96446 (Neiner et al., 2012). This is a helium rich star that exhibits a strong large-scale magnetic field. Measuring of the magnetic field on the surface of a pulsating star is not an easy task. Between the subexposures there can be significant radial velocity shifts caused by the pulsational motion. To exclude the impact of the pulsation on the magnetic field measurements, the careful corrections of the individual spectra have to be taken into account. Otherwise, the magnetic field can be significantly underestimated. Such detailed studies were performed by Järvinen et al. (2017) who found the average value of the magnetic field of the order 4 kG and determined the inclination angle $i \approx 18^\circ$ and the magnetic field obliquity $\beta \approx 40^\circ$. The other interesting phenomenon connected with HD 96446 is that the magnetic field determined from different lines are shifted in phase. This indicates that the chemical elements are distributed inhomogeneously on the stellar surface. Although the star pulsates in p-modes, no detailed asteroseismic investigation has been performed, yet.

HD 43317 is a very interesting star because it is a magnetic hybrid β Cep/SPB pulsator. The surface magnetic filed is of the order of 1–1.5 kG and it seems to be in a dipolar configuration (Pápics et al., 2012; Buysschaert et al., 2017). The magnetic field can modify the internal structure of the star since the Lorentz force competes with the pressure gradient. The magnetic field stabilizes the differential rotation causing the uniform rotation and the overshooting from the convective core should be less efficient. These effects can be studied through an

asteroseismic analysis. The presence of both high-order g-modes (SPB-type) and low-order p- and g-modes (β Cep-type) gives an unique possibility of studying the entire star (the former modes penetrate the deep interior of the star, while the later the outer layers). As of HD 96446, no asteroseismic analysis has been performed.

5. Oscillating Red Giants

The oscillations of red giant stars are driven by turbulent motions in the outer convective envelope, similarly to the oscillations present in the Sun. Also, very similar are the oscillation power spectra (see for example Bedding et al., 2011).

The very interesting features of these kind of pulsations are constant relative amplitudes of modes with different mode degrees. Some stars, however, exhibit unexpectedly small amplitudes of the dipole modes (about 20% of oscillating red giants). Also, it was noticed that the higher the frequency at maximum power the lower the amplitudes of the dipole modes. No clear correlations with stellar parameters were found, although a lower limit on the mass seems to exist at about $1.1\,\mathrm{M}_{\odot}$ (García et al., 2014).

One of the most promising hypothesis explaining this phenomenon assumes that the dipole modes are effectively dumped in the radiative cores of red giants. Higher degree modes do not penetrate near core regions so they are not dumped. Fuller et al. (2015) and Cantiello et al. (2016) claimed that the strong internal magnetic field can be responsible for the dipole mode energy leakage. The wave that tunnels into the core gains a higher mode degree character (see Sect. 2.2). Such a modified mode can not leave the inner part of the star since it is effectively reflected back by the evanescence zone, which is thicker for higher mode degrees (the so-called magnetic greenhouse effect).

Assuming some reasonable model, it is possible to calculate the minimal value of the magnetic field strength in the vicinity of the hydrogen burning shell. In some particular cases, where the so-called transition frequency between the depressed and normal dipole modes can be identified, it is possible to estimate the value of the magnetic field in the hydrogen burning layers. This was the case of KIC8561221 for which Fuller et al. (2015) found a magnetic field strength of the order of 10^7 G.

Further theoretical studies by Lecoanet et al. (2017) showed, that the gravity dipole waves that tunnels into the core are effectively conversed into magnetosonic waves, which then are dissipated in the stellar interior.

It seems, that observations of solar-like oscillations in red giants with depressed dipole modes allow us to constrain the internal magnetic field strength. This hypothesis, although very promising, was questioned in the work by Mosser et al. (2017), who claimed, that the mechanism responsible for dumping modes can not significantly impact the stellar structure, as strong magnetic field would certainly do. Further studies are needed in order to resolve this issue.

6. Summary

Magnetic fields have been found in different types of stars. Some magnetic stars pulsate, which gives a possibility of deriving constrains inaccessible in other ways, i.e., the information on the magnetic field geometry and field strength, including the internal magnetic field confined into the red giant cores.

However, the pulsation-magnetic fields interaction is very complicated. To derived reliable constrain on stellar parameters the long term polarimetric and photometric observations are needed in order to characterize the stellar magnetic field and oscillations, respectively. Due to these requirements, a detailed magneto-asteroseismic analysis of many stars is still lacking.

Acknowledgements. This work was financially supported by the Polish National Science Centre grants no. DEC-2013/08/S/ST9/00583 and 2015/17/B/ST9/02082 and IA UWr grant no. 0420/2006/16.

References

Aerts, C., Mathias, P., Gillet, D., & Waelkens, C. 1994, *Astron. Astrophys.*, **286**, 109

Alecian, E., Kochukhov, O., Petit, V., et al. 2014, *Astron. Astrophys.*, **567**, A28

Alecian, E., Neiner, C., Wade, G. A., et al. 2015, in IAU Symp., Vol. **307**, *New Windows on Massive Stars*, ed. G. Meynet, C. Georgy, J. Groh, & P. Stee, 330–335

Aurière, M., Wade, G. A., Silvester, J., et al. 2007, *Astron. Astrophys.*, **475**, 1053

Bagnulo, S., Landi Degl'Innocenti, E., Landolfi, M., & Leroy, J. L. 1995, *Astron. Astrophys.*, **295**, 459

Bagnulo, S., Landstreet, J. D., Mason, E., et al. 2006, *Astron. Astrophys.*, **450**, 777

Bedding, T. R., Mosser, B., Huber, D., et al. 2011, *Nature*, **471**, 608

Bigot, L. & Dziembowski, W. A. 2002, *Astron. Astrophys.*, **391**, 235

Buysschaert, B., Neiner, C., Briquet, M., & Aerts, C. 2017, *Astron. Astrophys.*, **605**, A104

Cantiello, M., Fuller, J., & Bildsten, L. 2016, *Astrophys. J.*, **824**, 14

Cunha, M. S. 2006, *Mon. Not. R. Astron. Soc.*, **365**, 153

Cunha, M. S. & Gough, D. 2000, *Mon. Not. R. Astron. Soc.*, **319**, 1020

Dziembowski, W. & Goode, P. R. 1985, *Astrophys. J.*, **296**, L27

Fuller, J., Cantiello, M., Stello, D., Garcia, R. A., & Bildsten, L. 2015, *Science*, **350**, 423

García, R. A., Pérez Hernández, F., Benomar, O., et al. 2014, *Astron. Astrophys.*, **563**, A84

Henrichs, H. F., de Jong, J. A., Verdugo, E., et al. 2013, *Astron. Astrophys.*, **555**, A46

Hubrig, S., Fossati, L., Carroll, T. A., et al. 2014, *Astron. Astrophys.*, **564**, L10

Järvinen, S. P., Hubrig, S., Ilyin, I., Schöller, M., & Briquet, M. 2017, *Mon. Not. R. Astron. Soc.*, **464**, L85

Kurtz, D. W. 1982, *Mon. Not. R. Astron. Soc.*, **200**, 807

Kurtz, D. W., Cameron, C., Cunha, M. S., et al. 2005, *Mon. Not. R. Astron. Soc.*, **358**, 651

Kurtz, D. W., Kawaler, S. D., Riddle, R. L., et al. 2002, *Mon. Not. R. Astron. Soc.*, **330**, L57,

Lecoanet, D., Vasil, G. M., Fuller, J., Cantiello, M., & Burns, K. J. 2017, *Mon. Not. R. Astron. Soc.*, **466**, 2181

Ledoux, P. 1951, *Astrophys. J.*, **114**, 373

Lüftinger, T., Kochukhov, O., Ryabchikova, T., et al. 2008, *Contributions of the Astronomical Observatory Skalnate Pleso*, **38**, 335

Mosser, B., Belkacem, K., Pinçon, C., et al. 2017, *Astron. Astrophys.*, **598**, A62

Neiner, C., Landstreet, J. D., Alecian, E., et al. 2012, *Astron. Astrophys.*, **546**, A44

Neiner, C. & Lèbre, A. 2014, in *SF2A-2014: Proceedings of the Annual meeting of the French Society of Astronomy and Astrophysics*, ed. J. Ballet, F. Martins, F. Bournaud, R. Monier, & C. Reylé, 505–508

Pápics, P. I., Briquet, M., Baglin, A., et al. 2012, *Astron. Astrophys.*, **542**, A55

Ryabchikova, T., Sachkov, M., Weiss, W. W., et al. 2007, *Astron. Astrophys.*, **462**, 1103

Ryabchikova, T., Wade, G. A., Aurière, M., et al. 2005, *Astron. Astrophys.*, **429**, L55

Shibahashi, H., Asteroseismology of magnetic stars. 2001, in ESA Special Publication, Vol. **464**, *SOHO 10/GONG 2000 Workshop: Helio- and Asteroseismology at the Dawn of the Millennium*, ed. A. Wilson & P. L. Pallé, 457–460

Shibahashi, H. & Aerts, C. 2000, *Astrophys. J., Lett.*, **531**, L143

Shibahashi, H. & Takata, M. 1993, *Publ. Astron. Soc. Jap.*, **45**, 617

Shorlin, S. L. S., Wade, G. A., Donati, J.-F., et al. 2002, *Astron. Astrophys.*, **392**, 637

Stibbs, D. W. N. 1950, *Mon. Not. R. Astron. Soc.*, **110**, 395

Telting, J. H., Aerts, C., & Mathias, P. 1997, *Astron. Astrophys.*, **322**, 493

Unno, W., Osaki, Y., Ando, H., & Shibahashi, H. 1989, *Nonradial oscillations of stars*

Wade, G. A., Neiner, C., Alecian, E., et al. 2016, *Mon. Not. R. Astron. Soc.*, **456**, 2

Wade, G. A., Silvester, J., Bale, K., et al. 2009, in ASP Conf. Ser., Vol. **405**, *Solar Polarization 5: In Honor of Jan Stenflo*, ed. S. V. Berdyugina, K. N. Nagendra, & R. Ramelli, 499

Discussions during the welcome reception

Oleg Kochukhov

Contrib. Astron. Obs. Skalnaté Pleso **48**, 82 – 86, (2018)

Detecting magnetic fields in Ap/Bp stars observed with the K2 space mission

B. Buysschaert[1,2], C. Neiner[1], A. J. Martin[1], M. E. Oksala[1,3] and C. Aerts[2,4]

[1] *LESIA, Observatoire de Paris, PSL Research University, CNRS, Sorbonne Universités, UPMC Univ. Paris 06, Univ. Paris Diderot, Sorbonne Paris Cité, 5 place Jules Janssen, F-92195 Meudon, France (E-mail: bram.buysschaert@obspm.fr)*

[2] *Instituut voor Sterrenkunde, KU Leuven, Celestijnenlaan 200D, 3001 Leuven, Belgium*

[3] *Department of Physics, California Lutheran University, 60 West Olsen Road 3700, Thousand Oaks, CA, 91360, USA*

[4] *Dept. of Astrophysics, IMAPP, Radboud University Nijmegen, 6500 GL, Nijmegen, The Netherlands*

Received: December 11, 2017; Accepted: January 5, 2018

Abstract. To study the effect large-scale magnetic fields have on the interior of hot stars, we compiled a list of chemically peculiar Ap/Bp stars that were observed with K2 with the future goal of investigating their seismic properties employing space-based photometry. A sub-sample was observed with high-resolution spectropolarimetry to detect the anticipated large-scale magnetic field usually hosted by Ap/Bp stars. We confirm the presence of such a field for 75 % of the stars in the sample. Thus, not all stars in the sample host the expected large-scale magnetic field.

Key words: stars: magnetic field – stars: rotation – stars: early-type – stars: oscillations

1. Introduction

About 10 % of hot OBA-type stars host a large-scale magnetic field. These magnetic fields typically have a simple geometry (a dominantly dipolar structure), with strengths ranging from several 100 G up to a few 10 kG, and stability over long time scales. There seems to be no correlation between the magnetic field properties and other stellar parameters. Therefore, they are believed to be of a fossil origin, produced during earlier evolutionary phases (Neiner et al., 2015).

These large-scale magnetic fields influence the chemical composition of several elements, such as Si, Eu, Cr, Fe, or He, while also creating brighter surface abundance inhomogeneities. The latter produces typical rotational modulation signatures in photometry. Both rotational modulation and peculiar abundances are employed as indirect diagnostics for the presence of a large-scale magnetic

field in hot stars. As these magnetic fields extend to the stellar interior, they may have an impact on these regions. Theory and simulations suggest an enforced uniform rotation rate in the radiative envelope (e.g., Ferraro, 1937; Moss, 1992), leading to a smaller convective core overshooting region (e.g., Press, 1981; Browning et al., 2004). Yet, observations to confirm this scenario remain scarce.

Only asteroseismology, the study of non-radial oscillations inside stars, is able to probe the internal properties (Aerts et al., 2010). At present, these have only been successfully utilized for two magnetic hot stars, namely β Cep (Shibahashi & Aerts, 2000) and V2052 Oph (Neiner et al., 2012; Handler et al., 2012; Briquet et al., 2012). Briquet et al. (2012) confirmed the theoretical predictions for a smaller convective core overshooting layer for magnetic stars, but this remains the only such study to date. We intend to increase the number of known magnetic pulsating hot stars to have a larger sample to perform magneto-asteroseismology, the coherent and combined study of magnetometry and asteroseismology, to measure the effect of the large-scale magnetic field on the stellar interior.

We constructed our sample by cross-matching the Renson & Manfroid (2009) catalogue, containing known chemically peculiar stars, with the observing campaigns of the K2 space mission (Howell et al., 2014). More than 60 Ap/Bp stars or He weak/strong stars were observed with K2, resulting in $\sim$90 days of high-quality, high-cadence, space-based, white-light photometry for each star. We constructed a sub-sample out of these stars, by selecting the brightest and slowest rotating stars. This sub-sample was observed with high-resolution spectropolarimetry to confirm the presence of the anticipated large-scale magnetic field. We discuss these results here.

2. Magnetometry

2.1. Data

All stars were observed at least once with the high-resolution spectropolarimeter ESPaDOnS (Donati et al., 2006), mounted on CFHT at Mauna Kea in Hawaii in circular polarization mode. Standard settings were employed and each spectropolarimetric sequence consisted of four consecutive sub-exposures. The observations were reduced with the LIBRE-ESPRIT (Donati et al., 1997) and UPENA softwares available at CFHT, and span from 370 nm to 1050 nm. We normalized the spectropolarimetry by interactive spline fitting per spectral order (Martin et al., 2017, submitted).

2.2. Zeeman signature

For each star, we estimated stellar parameters by fitting synthetic spectra to the Balmer lines (Kurucz, 1993; Martin et al., 2017). From these estimates, we selected the closest VALD3 line mask (Ryabchikova et al., 2015) available in

Table 1. Details of the magnetometric analysis of the sample. Spectral types from the Renson & Manfroid (2009) catalogue are provided and known binary systems are indicated. For each observation, we provide the exposure time, $t_{\rm exp}$, the magnetic detection status, and the determined longitudinal magnetic field B_l.

Star	Spectral type	$t_{\rm exp}$ [s]	Detection	B_l [G]
HD 97859	B9 Si	4×1272	DD	653 ± 127
HD 107000	A2 Sr	4×338	DD	240 ± 10
		4×338	DD	168 ± 11
HD 134759	Bp Si + ...	4×37	DD	304 ± 28
		4×37	DD	369 ± 29
HD 139160	B7 He wk. + ...	8×22	ND	37 ± 48
HD 152366	B8 Si	4×599	DD	-112 ± 15
HD 152834	A0 Si	4×267	DD	229 ± 18
HD 155127	B9 Eu Cr Sr	4×676	DD	-402 ± 6
HD 158596	B9 Si + ...	4×1060	DD	532 ± 36
HD 164224	B9 Eu Cr	4×1089	DD	464 ± 24
HD 165972	B9 Si	4×517	DD	-281 ± 46
HD 166804	B9 Si	4×443	DD	-486 ± 47
		4×443	DD	-510 ± 47
		4×443	DD	-422 ± 63
HD 173406	B9 Si	4×214	ND	-23 ± 39
HD 173657	B9 Si Cr	4×226	ND	-113 ± 81
HD 177013	A2 Eu Cr Sr	4×310	DD	128 ± 34
HD 177562	B8 Si	4×262	ND	16 ± 17
HD 177765	A5 Eu Cr Sr	4×120	DD	1189 ± 20

our pre-calculated library, to construct an average line profile with the LSD technique (Donati et al., 1997). Absorption lines that blend with any Balmer line, telluric features, or known diffuse interstellar bands were discarded, and the line depth of the lines in the mask were adjusted to match the observations. Most of the observations show distortions in their LSD Stokes I profiles, caused by possible pulsations or rotational modulation. We show two examples of these LSD Stokes profiles in Fig. 1.

For each observation, we determined the False Alarm Probability (FAP; Donati et al., 1997) that a Zeeman signature is present in the LSD Stokes V profile. Definite detections (DD) have a FAP$< 10^{-3}$ %, non-detections (NDs) correspond to a FAP$> 10^{-1}$ %, and marginal detections (MDs) fall in between these limits. We indicate the detection states for each observation in Table 1. In the studied sample, 12 stars have a DD, while 4 stars have a ND. No obvious correlation was noted between the detection status and the estimated stellar parameters or binarity.

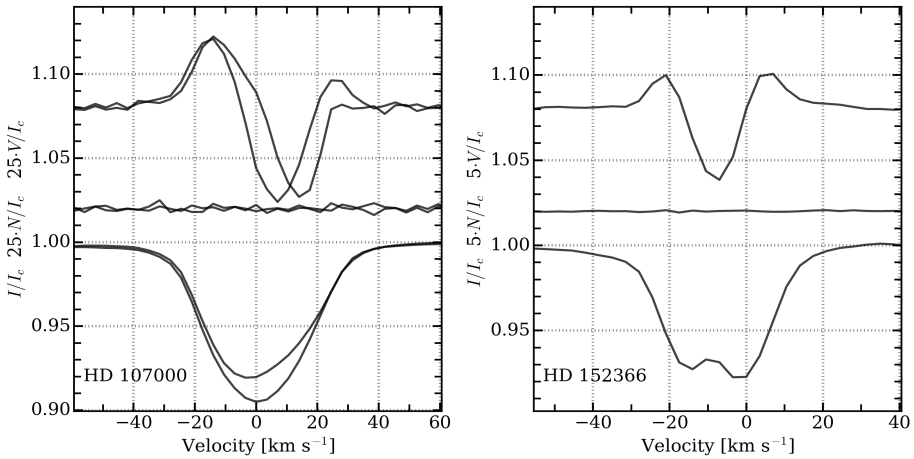

Figure 1. LSD Stokes profiles for two of the stars in the sub-sample. Each panel indicates the LSD Stokes I profile (*bottom*), the diagnostic null profile (*middle*), and the LSD Stokes V profile (*top*) with an arbitrary offset for increased visibility.

2.3. Longitudinal field measurements

In addition, we determined the longitudinal magnetic field (Rees & Semel, 1979) for each spectropolarimetric observation, and provide these values in Table 1. The strength of the field of the confirmed magnetic stars is consistent with what is anticipated for hot magnetic stars, ranging from about 100 G to more than 1 kG.

3. Conclusions and summary

We have compiled a sample of 60 candidate magnetic magnetic Ap/Bp stars that have been observed with K2 space-photometry to detect stellar pulsations. A sub-sample was observed with high-resolution spectropolarimetry to evaluate the presence or absence of large-scale magnetic fields. ESPaDOnS data confirms the presence of such a magnetic field for 75 % of the sub-sample. The K2 photometry might aid to confirm the presence of a magnetic field for the remaining 4 stars through indirect diagnostics. We conclude that some of the stars in the complete sample do not host a large-scale magnetic field in spectropolarimetry but might reveal magnetic signatures in the K2 photometry.

References

Aerts, C., Christensen-Dalsgaard, J., & Kurtz, D. W. 2010, *Asteroseismology* (Springer, Heidelberg)

Briquet, M., Neiner, C., Aerts, C., et al. 2012, *Mon. Not. R. Astron. Soc.*, **427**, 483

Browning, M. K., Brun, A. S., & Toomre, J. 2004, *Astrophys. J.*, **601**, 512

Donati, J.-F., Catala, C., Landstreet, J. D., & Petit, P. 2006, in ASP Conf. Ser., Vol. **358**, *Solar Polarization 4*, ed. R. Casini & B. W. Lites, 362

Donati, J.-F., Semel, M., Carter, B. D., Rees, D. E., & Collier Cameron, A. 1997, *Mon. Not. R. Astron. Soc.*, **291**, 658

Ferraro, V. C. A. 1937, *Mon. Not. R. Astron. Soc.*, **97**, 458

Handler, G., Shobbrook, R. R., Uytterhoeven, K., et al. 2012, *Mon. Not. R. Astron. Soc.*, **424**, 2380

Howell, S. B., Sobeck, C., Haas, M., et al. 2014, *Publ. Astron. Soc. Pac.*, **126**, 398

Kurucz, R. 1993, *Opacities for Stellar Atmospheres: [+0.0],[+0.5],[+1.0]* (Kurucz CD-ROM No. 2. Smithsonian Astrophysical Observatory, Cambridge, MA)

Martin, A. J., Stift, M. J., Fossati, L., et al. 2017, *Mon. Not. R. Astron. Soc.*, **466**, 613

Moss, D. 1992, *Mon. Not. R. Astron. Soc.*, **257**, 593

Neiner, C., Alecian, E., Briquet, M., et al. 2012, *Astron. Astrophys.*, **537**, A148

Neiner, C., Mathis, S., Alecian, E., et al. 2015, in IAU Symp., Vol. **305**, *Polarimetry*, ed. K. N. Nagendra, S. Bagnulo, R. Centeno, & M. Jesús Martínez González, 61–66

Press, W. H. 1981, *Astrophys. J.*, **245**, 286

Rees, D. E. & Semel, M. D. 1979, *Astron. Astrophys.*, **74**, 1

Renson, P. & Manfroid, J. 2009, *Astron. Astrophys.*, **498**, 961

Ryabchikova, T., Piskunov, N., Kurucz, R. L., et al. 2015, *Physica Scripta*, **90**, 054005

Shibahashi, H. & Aerts, C. 2000, *Astrophys. J., Lett.*, **531**, L143

Contrib. Astron. Obs. Skalnaté Pleso **48**, 87 – 92, (2018)

Understanding the fossil magnetic fields of Ap/Bp stars

Conclusions from a volume-limited survey

J. Sikora[1,2], G. A. Wade[2] and J. Power[1,2]

[1] *Dept. of Physics, Engineering Physics & Astronomy, Queen's University Kingston, ON, Canada, (E-mail: james.sikora@queensu.ca)*

[2] *Dept. of Physics and Space Science, Royal Military College of Canada Kingston, ON, Canada*

Received: December 7, 2017; Accepted: January 3, 2018

Abstract. Various observational properties of Ap/Bp stars have been well-established such as the often-cited 10 % incidence rate of strong, organized magnetic fields amongst all A- and B-type stars. However, these inferences have generally been drawn from surveys biased towards the strongest most easily detectable fields. A volume-limited spectropolarimetric survey of all intermediate-mass stars within 100 pc was initiated in 2007 in order to avoid the biases inherent in previous studies. This work yielded the magnetic properties of a large number of Ap/Bp stars in the sample; however, nearly half of the sample remained either unobserved or had relatively poor constraints on their field strengths and geometries. We have recently completed this survey using measurements obtained by ESPaDOnS and NARVAL. We discuss here some of the recent findings of this survey.

Key words: stars: magnetic – stars: chemically peculiar

1. Introduction

The generation and broader characteristics of magnetic fields of cool stars are reasonably well understood within the framework of stellar dynamo theory (e.g. Charbonneau, 2010). In contrast, the origin of the magnetic fields of main sequence stars (MS) more massive than about $1.5\,M_\odot$ remains a profound mystery. It is now reasonably well established that all chemically peculiar Ap/Bp stars, corresponding to roughly 10% of MS A- and B-type stars, host organized (primarily dipolar) magnetic fields with strengths $\lesssim 30$ kG (e.g. Wolff, 1968; Landstreet, 1982; Shorlin et al., 2002). However, these results have typically been derived from magnitude-limited surveys or from surveys with relatively high detection thresholds and thus, are inherently biased.

In 2007, Aurière et al. (2007) attempted to explore the weak field regime of Ap/Bp stars by obtaining high-precision longitudinal field measurements of 28 objects with reportedly weak or otherwise poorly constrained field strengths.

All of the observed Ap/Bp stars were found to exhibit dipolar field strengths of $B_{\rm d} \gtrsim 300\,{\rm G}$ with the two weakest fields found to have $B_{\rm d} = 100^{+392}_{-100}\,{\rm G}$ and $B_{\rm d} = 229^{+248}_{-76}\,{\rm G}$. Aurière et al. (2007) hypothesized that there exists a critical field strength ($B_{\rm c} \approx 300\,{\rm G}$), which corresponds to the minimum field strength that an Ap/Bp star must host in order to be invulnerable to a pinch-instability (Tayler, 1973; Spruit, 2002). More recently, a small number of A- and B-type stars hosting fields having $B_{\rm d}$ well below the proposed critical field strength have been identified in apparent contradiction to this explanation (e.g. Lignières et al., 2009; Petit et al., 2011; Alecian et al., 2016). While these recent discoveries call into question whether or not the so-called "magnetic desert" truly exists, the question remains why the vast majority of known Ap/Bp stars host fields with $B_{\rm d} \gtrsim 300\,{\rm G}$.

In the following article, we present several results from a volume-limited spectropolarimetric survey of Ap/Bp stars located within 100 pc. This survey has been carried out in order to constrain various fundamental and magnetic properties of this stellar population while attempting to minimize observational biases. This work was initiated by Power (2007), who obtained a large number of measurements using the now retired MuSiCoS instrument. These observations allowed for the magnetic parameters of approximately 50 % of the Ap/Bp stars in the sample to be derived. More recently, we have completed this survey primarily using Stokes V measurements obtained with ESPaDOnS along with a small number obtained with NARVAL. In Section 2, we briefly describe the sample and present the derived incidence rate of Ap/Bp stars with respect to stellar mass. In Section 3, we present several results from our analysis of the Ap/Bp magnetic properties and, in Section 4, we state our conclusions.

2. The Sample

The full sample of intermediate-mass stars (magnetic and non-magnetic early-F, A-, and B-type stars) was compiled by identifying all objects within the Hipparcos catalogue having parallax angles $> 10\,{\rm mas}$ ($d < 100\,{\rm pc}$) (van Leeuwen, 2007). This list was then cross-referenced with the Catalogue of Ap, HgMn and Am Stars (Renson & Manfroid, 2009) in order to identify both known and candidate Ap/Bp stars. This yielded a total of 139 stars, which were classified as being unlikely, probably, or definitely Ap/Bp stars based on whether they had reported (1) photometric variability, (2) chemical peculiarities consistent with Ap/Bp stars (identified either spectroscopically or through the use of photometric indices; i.e. Paunzen & Maitzen, 2005), or (3) magnetic detections. We obtained 327 Stokes V observations of 65 stars using MuSiCoS (185 measurements), ESPaDOnS (114 measurements), and NARVAL (28 measurements). Based on our magnetic measurements, archived magentic measurements, and on published magnetic measurements, we conclude that the sample of early-F, A-,

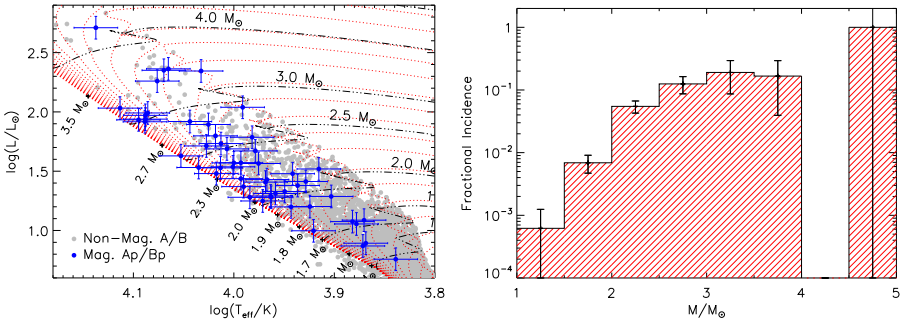

Figure 1. *Left*: The Hertzsprung-Russell diagram for the volume-limited sample. Grey points correspond to the presumably non-magnetic MS stars while the blue points correspond to the known magnetic (Ap/Bp) MS stars. *Right*: Incidence rate of Ap/Bp stars with respect to stellar mass. The large uncertainty and 100 % incidence rate associated with the highest mass bin ($4.5 \leq M/\mathrm{M}_{\odot} < 5$) is due to the fact that it contains only one star.

and B-type stars within a 100 pc volume contains 52 confirmed Ap/Bp stars and $\sim 3\,700$ non-magnetic stars.

We derived each of the (presumably) non-magnetic stars' effective temperatures and luminosities by applying various photometric calibrations to a wide range of archived photometric measurements (e.g. Mermilliod et al., 1997). A more detailed analysis of the fundamental parameters was performed on the 52 Ap/Bp stars. This involved fitting both the available photometry and spectroscopy (including Balmer lines, which are relatively sensitive to $\log g$, and multiple $25 - 100$ Å width spectral regions containing He and metallic lines) to synthetic models. The synthetic SEDs were generated using the LLMODELS code (Shulyak et al., 2004) while accounting for flux abnormalities caused by chemical peculiarities and, in the case of strongly magnetic stars ($B_{\mathrm{d}} \geq 5$ kG), the anomalous Zeeman effect. All of the stars' stellar masses and ages were then estimated through comparisons with the evolutionary models of Ekström et al. (2012). The total sample of MS stars is shown plotted on the Hertzsprung-Russell diagram in Fig. 1 (left). The incidence rate of Ap/Bp stars as a function of stellar mass is shown in Fig. 1 (right); it is evident that the incidence rate increases from $\lesssim 1$ % at $M \lesssim 2\,\mathrm{M}_{\odot}$ and plateaus at ≈ 10 % for $M > 2\,\mathrm{M}_{\odot}$.

3. Magnetic Properties

Both the dipole magnetic field strength and the obliquity angle β (i.e. the angle between the dipole field's axis of symmetry and the star's rotational axis) can be derived if the inclination angle i and the extrema of the longitudinal field (B_{z}) are known (Stibbs, 1950). We attempted to derive these properties by obtaining

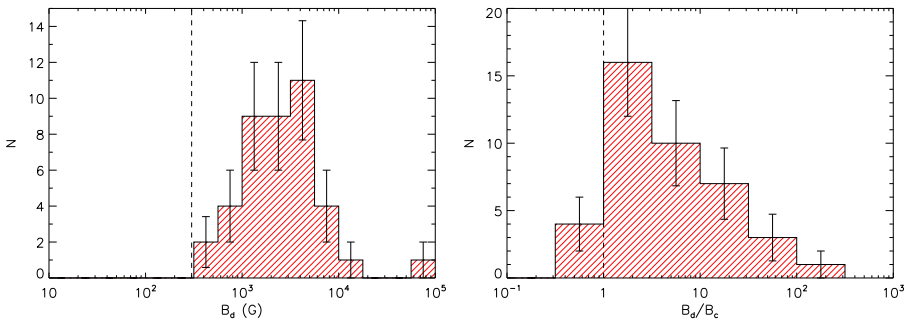

Figure 2. *Left*: The distribution of the derived dipole magnetic field strengths. The vertical dashed line indicates the critical field strength ($B_c = 300$ G) derived by Aurière et al. (2007) for a typical Ap star. *Right*: The ratio of each Ap/Bp star's dipole field strength to its critical field strength where B_c is calculated using Eqn. 8 of Aurière et al. (2007).

approximately five B_z measurements per star such that the rotational periods could be roughly sampled. We adopted a target precision of $15 \lesssim \delta B_z \lesssim 25$ G, which allowed for the detection of surface magnetic fields with $B_d \gtrsim 150$ G. The resulting distribution of B_d values is shown in Fig. 2 (left). The distribution peaks at approximately 2.5 kG and contains a minimum field strength of 340 G – slightly above the estimated critical field limit of $B_c = 300$ G calculated using Eqn. 8 of Aurière et al. (2007). B_c depends on each stars' $T_{\rm eff}$, rotational period, and radius; therefore, we derived the ratio, B_d/B_c, for each star yielding the distribution shown in Fig. 2 (right). We find that all but four of the Ap/Bp stars in our sample exhibit $B_d/B_c > 1$.

Our analysis also yielded the obliquity angles associated with the dipolar field component of each Ap/Bp stars' magnetic field; this distribution is shown in Fig. 3 (left) while the cumulative distribution functions for both the derived β and i values are shown in Fig. 3 (right). We find that, while the i distribution is consistent with a distribution of randomly oriented axes, the β distribution exhibits a slight excess of instances in which $\beta \lesssim 30°$. Given the relatively small sample size and the difficulty of accurately constraining β, this result may be considered to be insignificant. This is supported by the derived 3 sigma uncertainty in the Kolmogrov-Smirnoff test statistic of 0.16 obtained by employing bootstrap resampling.

4. Conclusions

We have completed a volume-limited spectropolarimetric survey of Ap/Bp stars located within a distance of 100 pc. We do not find any stars in our sample

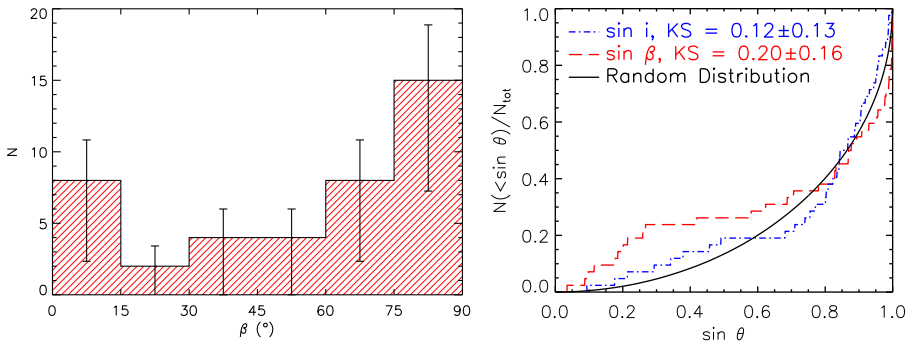

Figure 3. *Left*: Distribution of derived obliquity angles. *Right*: Cumulative distribution functions associated with the inclination angle (blue, dash-dotted) and obliquity angle (red, dashed). The solid black curve is generated from a distribution of randomly oriented axes. The $\sin i$ and $\sin \beta$ distributions are compared to the random distribution yielding Kolmogrov-Smirnov statistics of 0.12 ± 0.13 and 0.20 ± 0.16, respectively.

hosting magnetic fields with dipolar components less than 300 G, which supports the existence of the so-called "magnetic desert" first reported by Aurière et al. (2007). In the preceding article, we have summarized several results from this survey; additional findings, including those obtained from a chemical abundance analysis of the sample of Ap/Bp stars, will be presented in a forthcoming publication.

References

Alecian, E., Tkachenko, A., Neiner, C., Folsom, C. P., & Leroy, B. 2016, *Astron. Astrophys.*, **589**, 1

Aurière, M., Wade, G. A., Silvester, J., et al. 2007, *Astron. Astrophys.*, **475**, 1053

Charbonneau, P. 2010, *Living Rev. Sol. Phys.*, **7**

Ekström, S., Georgy, C., Eggenberger, P., et al. 2012, *Astron. Astrophys.*, **537**, 13

Jackson, R. J. & Jeffries, R. D. 2010, *Mon. Not. R. Astron. Soc.*, **402**, 1380

Landstreet, J. D. 1982, *Astrophys. J.*, **258**, 639

Lignières, F., Petit, P., Böhm, T., & Aurière, M. 2009, *Astron. Astrophys.*, **500**, L41

Mermilliod, J.-C., Mermilliod, M., & Hauck, B. 1997, *Astron. Astrophys., Suppl. Ser.*, **124**, 349

Paunzen, E. & Maitzen, H. M. 2005, *Astron. Astrophys.*, **441**, 631

Petit, P., Lignières, F., Aurière, M., et al. 2011, *Astron. Astrophys.*, **532**, 13

Power, J. 2007, Master's thesis, Queen's University, Canada

Renson, P. & Manfroid, J. 2009, *Astron. Astrophys.*, **498**, 961

Shorlin, S., Wade, G. A., Donati, J.-F., et al. 2002, *Astron. Astrophys.*, **392**, 637

Shulyak, D., Tsymbal, V., Ryabchikova, T., Stütz, C., & Weiss, W. 2004, *Astron. Astrophys.*, **428**, 993

Spruit, H. C. 2002, *Astron. Astrophys.*, **381**, 923

Stibbs, D. W. N. 1950, *Mon. Not. R. Astron. Soc.*, **110**, 395

Tayler, R. J. 1973, *Mon. Not. R. Astron. Soc.*, **161**, 365

van Leeuwen, F. 2007, *Astron. Astrophys.*, **474**, 653

Wolff, S. C. 1968, *Publ. Astron. Soc. Pac.*, **80**, 281

Audience in the lecture room

Contrib. Astron. Obs. Skalnaté Pleso **48**, 93 – 97, (2018)

The millimagnitude variability of the HgMn star φ Phe

M. Prvák[1], J. Krtička[1] and H. Korhonen[2]

[1] *Department of Theoretical Physics and Astrophysics, Masaryk University, Czech Republic*

[2] *Niels Bohr Institute, University of Copenhagen, Denmark*

Received: November 10, 2017; Accepted: January 2, 2018

Abstract. The horizontally inhomogeneous chemical composition of the atmospheres of the chemically peculiar stars causes wavelength redistribution of the spectral energy in areas with increased abundance of heavier elements. Due to the rotation of the star, this usually leads to strictly periodic photometric variability in some spectral regions. We used abundance maps of the HgMn star φ Phe (HD 11753), obtained by means of the Doppler imaging, to model its photometric variability. Comparing the light curves derived from abundance maps obtained at different times, we also study how the time evolution of the surface spots affects this variability.

Key words: stars: abundances – stars: chemically peculiar – stars: individual: HD 11753 – stars: variables: general

1. Introduction

Inhomogeneous distribution of heavier elements in the atmospheres of chemically peculiar (CP) stars, together with stellar rotation, commonly causes periodic photometric variability in some spectral regions. Spectral energy, absorbed by bound–free and bound–bound (line-blanketing) transitions, mainly in the far ultra-violet (far-UV) part of the spectrum, is typically re-transmitted in the near ultra-violet and the visible regions (backwarming effect). The physical processes involved are still not entirely understood.

Techniques such as the (magnetic) Doppler imaging have been used to derive the surface distribution of the heavier elements (e.g., Rice et al., 1989; Piskunov & Kochukhov, 2002; Lüftinger et al., 2010). Using these maps, we aim to model the photometric variability of CP stars (see Figure 1). Comparing the synthesised light curves with the observed variability of the stars (if available), we hope to provide verification of the correctness of the imaging method, the accuracy of the atomic data, and our understanding of the physical phenomena involved. This method has been used in the past to show that the variability of several CP stars is caused by bound–bound and bound-free transitions of various chemical elements (Krtička et al., 2009, 2012; Shulyak et al., 2010; Prvák et al., 2015).

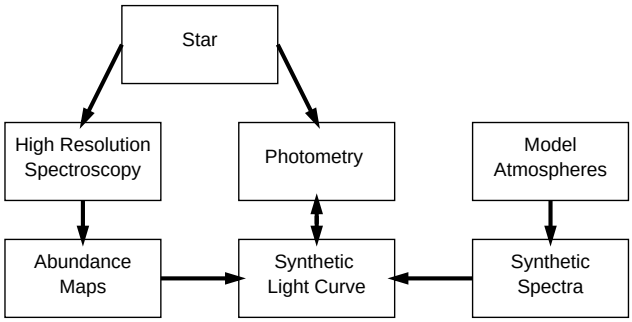

Figure 1. The workflow of synthetic light curve analysis.

Table 1. Abundances of the chemical elements with inhomogeneous surface distribution used in our calculations of the model atmospheres and the synthetic spectra.

Element	Abundances				
Cr	-6.1	-5.8			
Sr	-7.6	-7.1	-6.6		
Ti	-6.8	-6.3			
Y	-8.3	-7.8	-7.3	-6.8	-6.3

2. The star φ Phoenicis

The star φ Phe (HD 11753), an Am type (HgMn) CP star, is a primary component of a spectroscopic binary (Pourbaix et al., 2013). We adopted the following parameters: the effective temperature $T_{\rm eff} = 10\,600$ K, the surface gravity $\log g = 3.79$, the rotational period $P = 9.531$ d, and $v \sin i = 13.5\,{\rm km\,s^{-1}}$. Briquet et al. (2010) have shown that the abundance structures at the surface of the star evolve with time.

3. Methods

We used a set of abundance maps for chromium, titanium, strontium and yttrium, based on spectroscopy obtained using the CORALIE spectrograph at several distinct times (Korhonen et al., 2013). We generated a grid of Atlas12 LTE model atmospheres (Kurucz, 1996) and the corresponding synthetic spectra for various abundances of the chemical elements (See Tab. 1 for the complete list). Integrating the emergent flux over the visible surface of the star at several different wavelengths and at several different rotational phases, we get a light curve for the star.

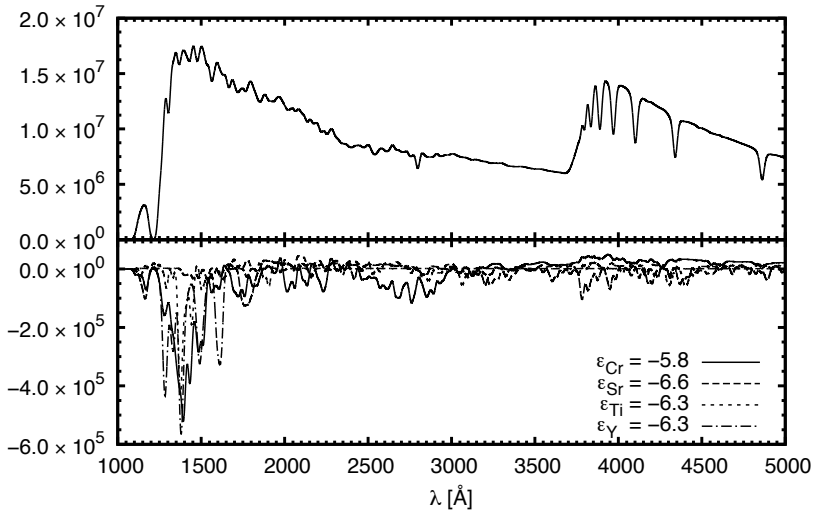

Figure 2. *Upper plot*: The emergent flux from a reference atmosphere with $\varepsilon_{\mathrm{Cr}} = -6.1$, $\varepsilon_{\mathrm{Sr}} = -7.6$, $\varepsilon_{\mathrm{Ti}} = -6.8$, $\varepsilon_{\mathrm{Y}} = -8.3$. *Lower plot*: The emergent flux from the model atmospheres with modified abundances minus the reference model. All curves were smoothed by a Gaussian function with a dispersion of 10 Å.

4. Results

The bound–bound transitions of heavier elements, especially titanium and yttrium, absorb a significant amount of radiation in the far-ultraviolet spectral region. The influence of chromium, titanium, strontium and yttrium on the spectral energy distribution is shown in Fig. 2. The areas of the stellar surface with higher abundance of these elements appear as dark spots at short wavelenghts, while the same spots are bright in the near-UV and in the visible (see Fig. 3).

As the star rotates, we observe millimagnitude variability in most parts of the spectrum. The synthetic light curves at several wavelengths are shown in Fig. 4. The amplitude and shape of the light curves depend on wavelength, and the light curves in the near-UV and in the visible are typically in anti-phase to the variability in the far-UV. Comparing light curves derived from data obtained in October and December 2000, August 2009, and January 2010 reveals noticable changes in the variability of the star.

5. Conclusions

We have shown that the presence of heavier elements causes millimagnitude variability of the star φ Phe. This variability also changes with time due to

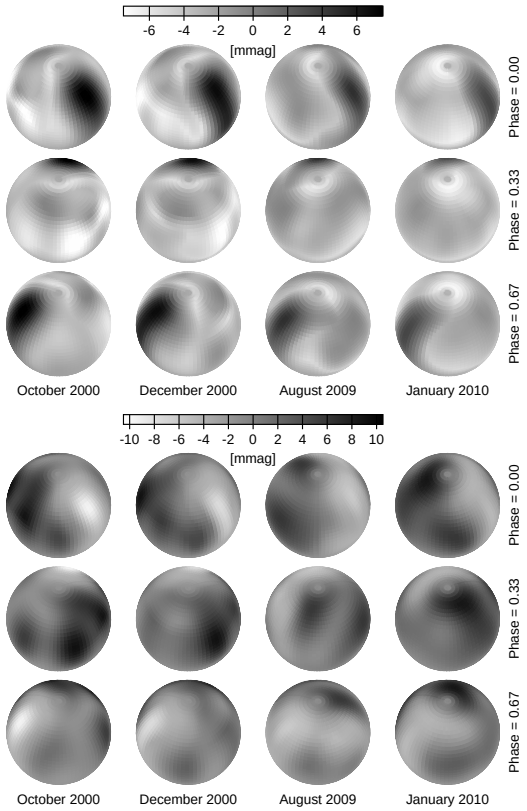

Figure 3. The emergent flux from the surface of φ Phe at 1700 Å (*upper plot*) and 3450 Å (*lower plot*) for different epochs as a function of rotational phase.

the changes of the surface abundance structure. Unfortunately, no observed photometry is available for comparison.

Acknowledgements. MP and JK were supported by grant GA ČR 16-01116S. HK acknowledges support from the Augustinus foundation.

References

Briquet, M., Korhonen, H., González, J. F., Hubrig, S., & Hackman, T. 2010, *Astron. Astrophys.*, **511**, A71

Korhonen, H., González, J. F., Briquet, M., et al. 2013, *Astron. Astrophys.*, **553**, A27

Krtička, J., Mikulášek, Z., Henry, G. W., et al. 2009, *Astron. Astrophys.*, **499**, 567

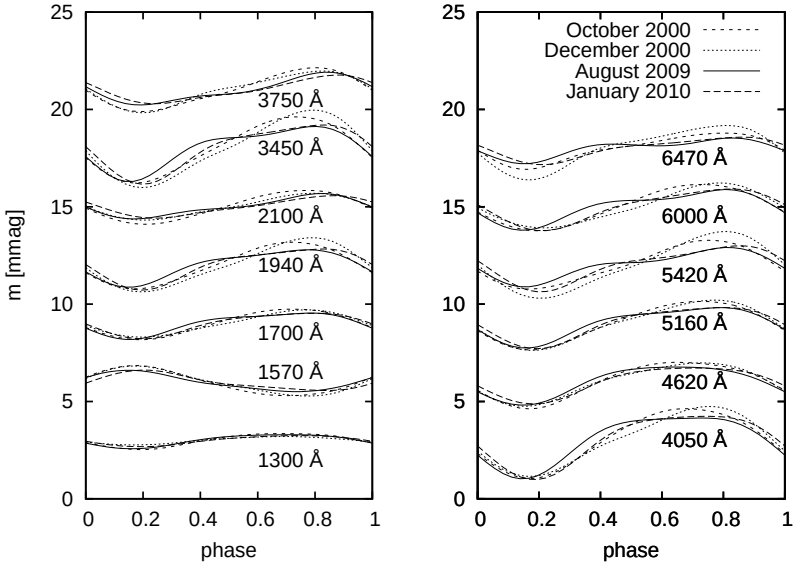

Figure 4. Synthesized light curves of φ Phe at various wavelengths at different observational epochs.

Krtička, J., Mikulášek, Z., Lüftinger, T., et al. 2012, *Astron. Astrophys.*, **537**, A14

Kurucz, R. L. 1996, in ASP Conf. Ser., Vol. **108**, *M.A.S.S., Model Atmospheres and Spectrum Synthesis*, ed. S. J. Adelman, F. Kupka, & W. W. Weiss, 160

Lüftinger, T., Kochukhov, O., Ryabchikova, T., et al. 2010, *Astron. Astrophys.*, **509**, A71

Piskunov, N. & Kochukhov, O. 2002, *Astron. Astrophys.*, **381**, 736

Pourbaix, D., Boffin, H. M. J., Chini, R., & Dembsky, T. 2013, *Astron. Astrophys.*, **556**, A45

Prvák, M., Liška, J., Krtička, J., Mikulášek, Z., & Lüftinger, T. 2015, *Astron. Astrophys.*, **584**, A17

Rice, J. B., Wehlau, W. H., & Khokhlova, V. L. 1989, *Astron. Astrophys.*, **208**, 179

Shulyak, D., Krtička, J., Mikulášek, Z., Kochukhov, O., & Lüftinger, T. 2010, *Astron. Astrophys.*, **524**, A66

Contrib. Astron. Obs. Skalnaté Pleso **48**, 98 – 105, (2018)

Magnetic fields in intermediate- and high-mass binary systems with short periods

Y. Nazé[1] **and E. Alecian**[2]

[1] *FNRS–Université de Liège, Belgium (E-mail: naze@astro.ulg.ac.be)*
[2] *IPAG, Toulouse, France*

Received: October 10, 2017; Accepted: November 2, 2017

Abstract. Most stars of the upper HRD live in multiple systems. When the separation is small, interactions may occur, affecting the stellar evolution and feedback. The presence of magnetic fields here opens the door to phenomena beyond the "usual" ones (mass transfer, wind collisions, tidal interactions,...) but it also put strong constraints on models of stellar evolution and magnetic field generation. This is why surveys of intermediate- and high-mass binaries with short periods have been undertaken. We will review results in this domain, including the properties of the (rare) detected cases such as Plaskett's star.

Key words: stars: magnetic field – stars: massive – binaries: general

1. Introduction

While a few detections were made in the 20th century, the magnetism of the most massive stars has only begun to be investigated in detail in the last decade, thanks to the advent of sensitive spectropolarimeters. Survey results indicate that magnetic stars share similar properties from spectral types A to O: the incidence rate is low (7% for OB, Fossati et al., 2015b; Grunhut et al., 2017, and 1–10% for Ap stars, depending on their masses, see Sikora et al. in these proceedings); the fields are generally strong (typically a few kG, though some very weak fields were also detected - see Blazère et al. (2015, 2016); Fossati et al. (2015a)), stable, and large-scale (with a strong dipolar component).

These magnetic fields are thought to be fossil. Indeed, the same magnetism incidence rate is found in HAeBe stars (Alecian et al., 2013; Hubrig et al., 2013) and the intermediate- and high-mass stars lack the convective envelopes responsible for the presence of magnetic fields in lower-mass stars. Three scenarios have then been invoked to explain the presence of such fields. First, the magnetism could be directly inherited from the primordial cloud. In this case, since strong magnetism is expected to inhibit cloud fragmentation, few magnetic binaries are expected; besides, in those rare cases, since close binaries are formed from the same material, both components would share the same magnetic properties (e.g., Moss, 2001). Second, the magnetism could relax from a convective dynamo taking place at a very early stage of the star formation. The reason why this process would only occur in some stars still needs to be ascertained. Finally,

the magnetism could arise from the strong shear associated to merging events (Ferrario et al., 2009; Schneider et al., 2016). This latter mechanism would naturally explain the low incidence rate since, from stellar evolution considerations, de Mink et al. (2014) predict that about 8% of massive stars are merger products (note that the field generation then needs to produce a stable field for every merging event, which is not ascertained). Such merging could occur in the PMS or MS stage but, since incidence rates are similar for PMS and MS stars, some decaying process is needed to avoid increasing rates. Theoretically, a MS merging leaves several signatures: rejuvenation (the magnetic stars should appear younger than surrounding cluster members), presence of ejecta (material ejected during the event should form a circumstellar nebula), rapid rotation and abundance anomalies (Schneider et al., 2016). Observationally, these properties are found, but are not universally shared, amongst magnetic intermediate- and high-mass stars: rejuvenation may have been detected for τ Sco and HR 2948, ejecta surround HD 148937, and rapid rotation or abundance anomalies have been found in some cases - but not all. Besides, if merging occurred, no close companion remains hence the resulting star should appear single or in a long-period binary (which could even form after the event by dynamical capture, for example).

The magnetic properties of intermediate- and high-mass binaries, especially the shortest-period ones, thus represent a crucial test for models of stellar evolution or of magnetism generation. Besides, such systems possess several advantages: the stellar properties can be derived with a high precision (masses, radii,...) and the age and composition should be the same for both stars. However, a good coverage of both the orbital and rotational periods is required, which represent a substantial investment of observing time. Finally, the presence of two stars opens the door to additional, interesting but still poorly known, phenomena, such as tidal interactions, magnetospheric interactions, or wind-wind collisions.

2. Results

Because multiplicity is widespread in massive stars, many of the magnetic detections actually occurred in binaries. For example, the first magnetic field detected in an O-star was found in θ^1 Ori C, which has a companion. However, the vast majority of these binaries have long periods, and cannot serve as a probing tool for the objectives previously mentioned. The first detection of magnetism in a close OBA binary occurred in 1958, for the intermediate-mass system HD 98088 (Babcock, 1958). The detailed study of Ap stars then revealed that their overall binary fraction was similar to, though maybe slightly smaller than, that of "normal" A stars (Abt & Snowden, 1973), and there seems to be an almost complete lack of binaries with periods shorter than 3d (Carrier et al., 2002). Recent surveys (general ones like MiMeS Grunhut et al. (2017) or BOB Schöller et al.

(2017), or ones specific to close binaries like BinaMIcS Alecian et al. (2015)) refined the picture and enlarged it to OB stars. They found few detections in close binaries composed of two hot stars, with an incidence rate limited to 2%. It is also important to underline that, in all but one case, only one of the two components is found to be magnetic.

Table 1 lists the dozen detections achieved up to now, with the main orbital/stellar/magnetic parameters. As a complement, we may note that (1) two other Ap+Am systems were proposed in the past but recently dismissed (Folsom et al., 2013b) and (2) HD 34736 was first thought to have $P_{orb} \sim 0.3$d (Semenko et al., 2014) but actually has $P_{orb} \sim 83$d (Semenko et al., in prep.) – the large excentricity of the system may lead to interactions at periastron, though. In addition, there are also two triple systems where a magnetic B star is associated to a close A+A binary: HD 35502 (Sikora et al., 2016) and HD 164492C (González et al., 2017; Wade et al., 2017). Those are not *per se* cases of magnetic objects in close binaries but these systems have an interesting configuration which may also sensitively test theoretical models.

2.1. Plaskett's star

This massive binary system harbours two late-type O-stars in a tight, 14.4 d orbit. It displays several peculiarities: the secondary is a fast rotator, there is a mismatch between dynamical and spectroscopic masses, as well as abundance anomalies (He enrichment of both stars, N depletion in the secondary, N enrichment and C depletion in the primary). This has led Bagnuolo et al. (1992) and Linder et al. (2008) to conclude that Plaskett's star actually is a post-mass transfer binary. In addition, the Doppler mapping of the Hα and He II 4686 emissions suggested a flattened wind region around the equator of the secondary (Linder et al., 2008). Grunhut et al. (2013) detected a magnetic signature in Stokes-V spanning the radial velocity interval covered by the fast-rotating secondary. The flattened wind region was then interpreted as magnetically confined winds. Since both stars have strong stellar winds, the interactions are complex in the system: preliminary MHD modelling suggests the simultaneous presence of a confined secondary wind and a wind-wind collision (ud-Doula, private communication). This may be reflected in the high-energy properties of the system, which is brighter at these wavelengths than other magnetic O-stars (Nazé et al., 2014). While X-ray variations are known from ROSAT, XMM, and Chandra data, their study could not definitely identify the recurrence timescale(s) (Linder et al., 2006, and Leutenegger et al., in prep.) and much remain to be done to characterize this unique wind interaction.

Plaskett's secondary is a fast rotator, and it is the sole fast-rotating magnetic O-star. This is puzzling since magnetic braking is supposed to play an important role in those stars. This led to question the origin of the field: could it be different from that of other magnetic massive stars? Because of its past interaction, Plaskett's secondary is obviously not a merging product (the companion being still

there!) but the shear generated by the mass-transfer event could here have been the magnetic trigger. In other words, could Plaskett's secondary be the prototype of a new category of magnetic massive stars, or is it simply amongst the 2% of magnetic stars in close massive binaries, its fast rotation being a coincidence? This was tested by observing with FORS2, ESPaDOnS or Narval a set of 15 short-period massive binaries known to undergo or to have undergone similar interactions (Nazé et al., 2017). The campaign resulted only in non-detections, with an overall limit of $B_d \sim 200$ G for the whole sample (considering all stars to share similar properties). In addition, the incidence rate after adding Plaskett's detection appears compatible with survey results. This finding strongly limits the putative role of binary interactions in the generation of magnetic fields in massive stars.

2.2. ϵ Lupi

This system comprises two B-type stars, both likely pulsating, in a short eccentric orbit ($P_{orb} = 4.6$ d, $e = 0.27$, Uytterhoeven et al., 2005). Magnetic signatures were detected in the system in the last decade (Hubrig et al., 2009; Shultz et al., 2012), and subsequent monitoring revealed that *both* components were actually magnetic. ϵ Lupi thus is the only known case of a doubly magnetic massive binary. This leads to an interesting phenomenon: because of the combination of strong fields and small separation, the two magnetospheres should interact – moreover, this interaction should vary with time, as the system is eccentric. The search for the signature of this unique interaction is ongoing, and will certainly unveil a wealth of new phenomena.

2.3. Others

Since we are dealing with close binaries, tidal interactions are supposed to take place. This may lead to alignment of orbital and rotational axes, synchronization of the orbital and rotational periods, and orbit circularization. In the sample of close magnetic binaries (Table 1), a few systems have achieved synchronization, about half of the systems have circularized, but nearly all have reached alignment (when the inclination information is known). This is in line with the timescale expectations of these phenomena. In this context, it is interesting to note that in BD–19°5044L, the synchronization is not complete (i.e. $P_{orb} \neq P_{rot}$) but the orbital and rotational angular velocities agree at periastron (Landstreet et al., 2017).

There are two interesting additional pieces of information: (1) the two components of HD 98088 have been found to display similar ages, an argument in favour of coevality; (2) the obliquity of the detected magnetic fields is generally large (the exceptions are the weaker fields of ϵ Lupi and HD 5550, and that of HD 36485).

3. Conclusion

Sensitive spectropolarimetric measurements have showed that magnetic stars do exist in close OBA binaries, and with field strengths similar to what is found in single stars or wide binaries of similar spectral types. Their mere existence seems incompatible with a merger scenario (even more so for the case of ϵ Lupi, the sole doubly magnetic massive binary). In this context, the non-detection of magnetism associated to blue stragglers (Grunhut et al., in prep.) is also a strong argument against the merger scenario. Furthermore, magnetism is even rarer in short-period binaries than in long-period systems or in single objects (2% vs. 7% for OB stars - the situation appears less clear-cut for Ap stars). This suggests that whatever generated magnetic fields in massive stars is somewhat inhibited when binaries form, placing strong constraints on their origin. This result could be compatible with the simulations showing that intense fields inhibit cloud fragmentation, if the fields are inherited from the primordial cloud. However, in all but one system, only one of the companions is detected to be magnetic, not both. Since both stars are formed from the same (piece of) cloud, one would rather expect to observe the contrary in case the stellar magnetic field originates from a field in the primordial, interstellar material.

A specific survey also demonstrated that interacting or post-interacting massive systems are not predominantly magnetic – there is only one case, the fast-rotating secondary in Plaskett's star. Therefore, binary interactions appear to play little role in the magnetic field generation. Plaskett's secondary is "just" one of the few examples of magnetic massive stars in binaries, not the prototype of a new class of magnetic objects.

Moreover, as expected for such close systems, some magnetic intermediate- and high-mass binaries are presenting signatures of tidal interactions, with stellar rotation synchronized and/or aligned with the orbital motion, and/or circularized orbits detected in more than half of the systems. In addition, two systems appear particularly exceptional: Plaskett's star combines magnetically confined winds and wind-wind collision, while ϵ Lupi should harbour (variable) magnetospheric interactions. These two systems therefore will continue to be monitored in detail, especially at high energies, to pinpoint the characteristics of these new phenomena.

Finally, the detected fields usually present a large obliquity, which is certainly linked to their origin. All these elements (incidence rate, obliquity,...) thus place strong constraints on the origin of the magnetism in intermediate- and high-mass stars but, while important results have already been achieved, much work remain to be done (notably refining models and enlarging observational samples) before fully understanding these "massive" magnetic phenomena.

Acknowledgements. YN acknowledges support from the FNRS (Belgium), the CFWB, the PRODEX XMM-Newton contract, and an ARC grant (Wallonia-Brussels Federation). ADS and CDS were used in preparing this document. The authors thank

C. Neiner, M. Shultz, E. Semenko, J. Grunhut, G. Wade, and T. Morel for interesting discussions and sharing of results before publication.

References

Abt, H. A. & Snowden, M. S. 1973, *Astrophys. J., Suppl. Ser.*, **25**, 137

Alecian, E., Kochukhov, O., Petit, V., et al. 2014, *Astron. Astrophys.*, **567**, A28

Alecian, E., Neiner, C., Wade, G. A., et al. 2015, in IAU Symposium, Vol. **307**, *New Windows on Massive Stars*, ed. G. Meynet, C. Georgy, J. Groh, & P. Stee, 330–335

Alecian, E., Tkachenko, A., Neiner, C., Folsom, C. P., & Leroy, B. 2016, *Astron. Astrophys.*, **589**, A47

Alecian, E., Wade, G. A., Catala, C., et al. 2013, *Mon. Not. R. Astron. Soc.*, **429**, 1001

Babcock, H. W. 1958, *Astrophys. J., Suppl. Ser.*, **3**, 141

Bagnulo, S., Fossati, L., Landstreet, J. D., & Izzo, C. 2015, *Astron. Astrophys.*, **583**, A115

Bagnuolo, Jr., W. G., Gies, D. R., & Wiggs, M. S. 1992, *Astrophys. J.*, **385**, 708

Blazère, A., Neiner, C., & Petit, P. 2016, *Mon. Not. R. Astron. Soc.*, **459**, L81

Blazère, A., Neiner, C., Tkachenko, A., Bouret, J.-C., & Rivinius, T. 2015, *Astron. Astrophys.*, **582**, A110

Borra, E. F. & Landstreet, J. D. 1979, *Astrophys. J.*, **228**, 809

Carrier, F., North, P., Udry, S., & Babel, J. 2002, *Astron. Astrophys.*, **394**, 151

de Mink, S. E., Sana, H., Langer, N., Izzard, R. G., & Schneider, F. R. N. 2014, *Astrophys. J.*, **782**, 7

Ferrario, L., Pringle, J. E., Tout, C. A., & Wickramasinghe, D. T. 2009, *Mon. Not. R. Astron. Soc.*, **400**, L71

Folsom, C. P., Likuski, K., Wade, G. A., et al. 2013a, *Mon. Not. R. Astron. Soc.*, **431**, 1513

Folsom, C. P., Wade, G. A., & Johnson, N. M. 2013b, *Mon. Not. R. Astron. Soc.*, **433**, 3336

Fossati, L., Castro, N., Morel, T., et al. 2015a, *Astron. Astrophys.*, **574**, A20

Fossati, L., Castro, N., Schöller, M., et al. 2015b, *Astron. Astrophys.*, **582**, A45

González, J. F., Hubrig, S., Przybilla, N., et al. 2017, *Mon. Not. R. Astron. Soc.*, **467**, 437

Grunhut, J. H., Wade, G. A., Leutenegger, M., et al. 2013, *Mon. Not. R. Astron. Soc.*, **428**, 1686

Grunhut, J. H., Wade, G. A., Neiner, C., et al. 2017, *Mon. Not. R. Astron. Soc.*, **465**, 2432

Hubrig, S., Briquet, M., De Cat, P., et al. 2009, *Astron. Nachr.*, **330**, 317

Hubrig, S., Carroll, T. A., González, J. F., et al. 2014, *Mon. Not. R. Astron. Soc.*, **440**, L6

Hubrig, S., Ilyin, I., Schöller, M., & Lo Curto, G. 2013, *Astron. Nachr.*, **334**, 1093

Landstreet, J. D., Kochukhov, O., Alecian, E., et al. 2017, *Astron. Astrophys.*, **601**, A129

Leone, F., Bohlender, D. A., Bolton, C. T., et al. 2010, *Mon. Not. R. Astron. Soc.*, **401**, 2739

Linder, N., Rauw, G., Martins, F., et al. 2008, *Astron. Astrophys.*, **489**, 713

Linder, N., Rauw, G., Pollock, A. M. T., & Stevens, I. R. 2006, *Mon. Not. R. Astron. Soc.*, **370**, 1623

Moss, D. 2001, in ASP Conf. Ser., Vol. **248**, *Magnetic Fields Across the Hertzsprung-Russell Diagram*, ed. G. Mathys, S. K. Solanki, & D. T. Wickramasinghe, 305

Nazé, Y., Neiner, C., Grunhut, J., et al. 2017, *Mon. Not. R. Astron. Soc.*, **467**, 501

Nazé, Y., Petit, V., Rinbrand, M., et al. 2014, *Astrophys. J., Suppl. Ser.*, **215**, 10, (+erratum in ApJS, 224, 13)

Neiner, C., Tkachenko, A., & MiMeS Collaboration. 2014, *Astron. Astrophys.*, **563**, L7

Petit, V., Wade, G. A., Drissen, L., Montmerle, T., & Alecian, E. 2008, *Mon. Not. R. Astron. Soc.*, **387**, L23

Schneider, F. R. N., Podsiadlowski, P., Langer, N., Castro, N., & Fossati, L. 2016, *Mon. Not. R. Astron. Soc.*, **457**, 2355

Schöller, M., Hubrig, S., Fossati, L., et al. 2017, *Astron. Astrophys.*, **599**, A66

Semenko, E. A., Romanyuk, I. I., Kudryavtsev, D. O., & Yakunin, I. A. 2014, *Astrophysical Bulletin*, **69**, 191

Shultz, M. 2016, The rotational evolution and magnetospheric emission of the magnetic early B-type stars, PhD thesis, Queen's University (Canada)

Shultz, M., Wade, G. A., Alecian, E., & BinaMIcS Collaboration. 2015, *Mon. Not. R. Astron. Soc.*, **454**, L1

Shultz, M., Wade, G. A., Grunhut, J., et al. 2012, *Astrophys. J.*, **750**, 2

Sikora, J., Wade, G. A., Bohlender, D. A., et al. 2016, *Mon. Not. R. Astron. Soc.*, **460**, 1811

Uytterhoeven, K., Harmanec, P., Telting, J. H., & Aerts, C. 2005, *Astron. Astrophys.*, **440**, 249

Wade, G. A., Shultz, M., Sikora, J., et al. 2017, *Mon. Not. R. Astron. Soc.*, **465**, 2517

Table 1. Properties of the detected magnetic stars in close (P < 30d) hot binaries (i.e. both objects being intermediate- or high-mass objects).

Name	sp. types	P_{orb}(d)	e	$P_{orb} = P_{rot}$?	$i_{orb} = i_{rot}$?	$\beta(^\circ)$	B_d(kG)	Ref.
Magnetic O-star in a close binary system								
Plaskett's star	O8III+O7.5III	14.4	0	no		>>	∼2.0	1, 2
Magnetic B-stars in close binary systems								
BD–19°5044L	Bp+Am	17.6	0.474	at peri.	yes	26	1.4	3
HD 1976	B5IVp+?+?	25-28	0.1-0.2					4
HD 36485	B3p+A	30.0	0.32	no	yes	<52	7–12	5
HD 37017	B2V+?	18.7	0.47	no	yes	63	6.5	6, 7
HD 149277	B2IV/V+?	11.5	0.24	no	yes	72	9.8	7, 8
HD 156324A	B2V+?+?	1.6	<0.03	yes	∼yes	69	12.3	7, 9
NU Ori	B0.5V+?+?	14.3	<0.07	no	∼yes	56	1.8	7, 10
ϵ Lupi	B2V+B3V	4.6	0.27	no	∼yes	36	0.8	7, 11
						5	0.5	
Magnetic A-stars in close binary systems								
HD 161701	B9+Ap	12.5	0.004	∼yes		>>		12
HD 5550	Ap+Am	6.8	0.006	yes		–24	0.065	13
HD 98088	Ap+Am	5.9	0.18	yes	yes	75	3.85	14

References: 1: Grunhut et al. (2013), 2: Grunhut et al., in prep., 3: Landstreet et al. (2017), 4: Neiner et al. (2014), 5: Leone et al. (2010), 6: Borra & Landstreet (1979), 7: Shultz (2016), 8: Bagnulo et al. (2015), 9: Alecian et al. (2014), 10: Petit et al. (2008), 11: Shultz et al. (2015), 12: Hubrig et al. (2014), 13: Alecian et al. (2016), 14: Folsom et al. (2013a)

Contrib. Astron. Obs. Skalnaté Pleso **48**, 106 – 115, (2018)

Magnetism of hot stars

G. A. Wade[1] **and C. Neiner**[2]

[1] *Department of Physics & Space Science, Royal Military College of Canada, P.O. Box 17000, Station Forces, Kingston, Ontario, Canada, K7K 7B4*

[2] *LESIA, Observatoire de Paris, PSL Research University, CNRS, Sorbonne Universités, UPMC Univ. Paris 06, Univ. Paris Diderot, Sorbonne Paris Cité, 5 place Jules Janssen, 92195 Meudon, France*

Received: December 28, 2017; Accepted: January 9, 2018

Abstract. Strong, stable, and organised magnetic fields are present at the surfaces of a small fraction of OBA stars. These "fossil fields" exhibit uniform characteristics in stars over a tremendous range of stellar mass, age, temperature, and rotation rate. In hot O- and B-type stars, these magnetic fields couple efficiently to the stellar radiatively driven winds, strongly influencing stellar mass loss and rotation. In this article we review the characteristics of the known magnetic hot stars, discuss recent discoveries and insights, and describe recent theoretical progress toward understanding basic field properties and the influence of magnetic fields on hot star evolution.

Key words: stars: magnetic fields – stars: evolution – stars: winds, outflows – stars: rotation

1. Introduction

Recent large surveys (Wade et al., 2016a; Grunhut et al., 2017; Fossati et al., 2015; Schöller et al., 2017) have investigated the properties of surface magnetism of stars having radiative envelopes, i.e. stars of spectral types A, B and O ranging in effective temperature from roughly 7 000–50 000 K. The largest of these surveys - the Magnetism in Massive Stars (or MiMeS) project (Wade et al., 2016a) - obtained magnetic measurements of over 550 bright stars of spectral types B and O. Based on these data, they reported that organized magnetic fields stronger than a few hundred gauss are present at the surfaces of approximately 7% of such stars (e.g. Grunhut et al., 2017). Their surface dipolar field components range in strength from less than 100 G to well over 10 kG (e.g. Briquet et al., 2016; Wade et al., 2012; Petit et al., 2013; Shultz, 2016). Like their lower-mass A-type cousins, their magnetic fields are not symmetric about the stellar rotation axis, leading to rotational modulation of the measured line-of-sight magnetic field and other photospheric and wind diagnostics, phenomena explained by the Oblique Rotator Model (Stibbs, 1950).

The essential characteristics of these magnetic fields (their organized topologies, their large range of strengths, their stability on timescales of at least decades, and their lack of correlation with basic stellar parameters such as mass

and rotation rate) are identical to those of cooler, lower-mass A-type stars, but stand in strong contrast to those of the dynamo-generated fields of cool stars. On the other hand, they bear a number of similarities to the fields of white dwarfs and neutrons stars. These fields are thought to be "fossils", i.e. the slowly-evolving remnants of magnetic fields generated or accumulated during an earlier phase of stellar evolution. That the properties of these fields remain essentially unchanged in stars ranging in mass from 1.5 to about 60 times that of the Sun (Wade et al., 2014; Wade & MiMeS Collaboration, 2015), notwithstanding the important differences in stellar structure that occur over this enormous range of mass, suggests a basic underlying commonality of the formation or evolution of their magnetic fields. Understanding this remarkable observational fact is a key challenge of modern stellar astrophysics.

1.1. The physics of fossil magnetism

A major breakthrough of the first decades of the 21st century has been to establish that stochastic initial seed magnetic fields in stellar radiative zones relax naturally to long-lived stable configurations with mixed poloidal/toroidal configurations organized on large scales. Numerical and semi-analytic calculations (Braithwaite & Spruit, 2004; Duez & Mathis, 2010; Duez et al., 2010) have shown that the characteristics of the fields predicted at the stellar surface by these models are in good qualitative agreement with those observed in real magnetic O, B and A-type stars (also see Kochukhov, these proceedings). In the stellar interior, the toroidal fields are predicted to be very strong, and they may have important consequences for chemical and angular momentum transport throughout the radiative envelope.

This breakthrough has provided the first quantitative physical model for the interpretation and study of fossil stellar magnetism, with the consequence that there now exists a theoretical context for the interpretation of the magnetic fields observed at the surfaces of main sequence (MS) and evolved A, B and O stars, in white dwarfs (Braithwaite & Spruit, 2004), and in neutron stars (Braithwaite & Spruit, 2006). It has even spawned the first theoretical speculations aimed at understanding why only a minority (about 10%) of MS stars exhibit detectable surface magnetism, and to explain the puzzling "magnetic field desert" phenomenon (Aurière et al., 2007; Braithwaite & Cantiello, 2013).

Notwithstanding this important progress, the origins of the seed fields that give rise to the observed fossil fields remain unknown and poorly constrained (Neiner et al., 2015). Currently, there exist three principal hypotheses: conservation of magnetic flux from the interstellar medium (ISM) during star formation, convective dynamos operating during protostellar or pre-MS phases that could enhance the ISM field (e.g. Hussain & Alecian, 2014), and stellar mergers early in the formative history (e.g. Ferrario et al., 2009; Langer, 2014).

2. Observed properties of magnetic B- and O-type stars

To date, about 70 early-type magnetic stars with spectral types earlier than B5 or effective temperatures above 15 000 K have been confidently identified. Most are relatively bright stars. Petit et al. (2013), Wade & MiMeS Collaboration (2015), and Shultz (2016) provide summaries.

2.1. Fundamental characteristics

Fossil magnetic fields are observed without any significant change in their general characteristics in stars ranging in spectral type from mid-F to early O. The earliest magnetic stars have spectral types of about O4, although their spectral classification changes somewhat due to the periodic variability of their spectra (Walborn, 1972; Howarth et al., 2007). These most massive magnetic stars have inferred masses of 40–60 $M_{\odot}$. However, because the field characteristics of magnetic O stars are poorly sampled (only about one dozen are known), this does not represent a confident upper limit and higher-mass magnetic stars could exist.

The HR diagram of the known magnetic hot stars (Shultz, 2016) shows that the lion's share of the known magnetic A, B and O stars are MS objects. A small number of pre-MS magnetic B-type stars (see e.g. Alecian et al., 2013) and post-MS magnetic O, B and high-mass A stars (see Martin, these proceedings, Neiner et al., 2017; Martin et al., 2017) are also known.

2.2. Spectral properties

The properties of stellar spectra at visible wavelengths change significantly from the early B stars to the mid-O stars. While some of this change is attributable to the evolving radiation field, changing ionization balance and the importance of non-LTE effects, it is also in large part due to the growing influence of the stellar wind.

As is discussed later in Sect. 3, a key impact of a magnetic field at the surface of a hot star is the channeling of its outflowing wind. This phenomenon results in the presence of a large quantity of relatively dense magnetically-confined plasma typically located within a few stellar radii of the stellar surface. The presence of this plasma weakly modifies the optical spectra of magnetic B stars, but can fundamentally alter the spectra of magnetic O stars (see e.g. Petit et al., 2013; Wade & MiMeS Collaboration, 2015) by introducing many periodically-variable emission lines. At radio wavelengths, magnetic B and O stars exhibit non-thermal emission, likely due to the gyrosynchrotron mechanism (e.g. Trigilio et al., 2004; Kurapati et al., 2017). At shorter wavelengths, X-ray emission diagnoses the hot plasma produced as a consequence of the large-scale shocks caused by channelling of the supersonic wind (ud-Doula & Nazé, 2016).

In addition to wind channeling effects, the magnetic field may also influence transport processes in the photosphere, producing large-scale chemical abundance inhomogeneities (e.g. Oksala et al., 2015). This chemical spots, which are prevalent for magnetic stars cooler than about 25 000 K, are responsible for periodic modulation of the profiles of many photospheric spectral lines.

2.3. Magnetic field strengths and topologies

Shultz (2016) (see also Shultz et al., these proceedings) performed a homogeneous study of the physical, rotational, magnetic and magnetospheric properties of the known magnetic B-type stars. The properties of the known magnetic O stars are summarized by Wade & MiMeS Collaboration (2015). Apart from a small number of well-known exceptions (e.g. the B stars τ Sco and HD 37776), the magnetic field toplogies of hot stars appear to be qualitatively identical to those of their lower-mass Ap star cousins: they contain most of their magnetic energy in the dipole mode, their dipole axes are inclined significantly relative to their rotation axes, and their magnetic configurations are stable on long timescales (years to decades, corresponding to hundreds or even thousands of stellar rotations). The distributions of surface dipole magnetic field strengths are very similar for O, B and A stars: they range from a few times 10^1 to a few times 10^4 G, and peak at a few times 10^3 G.

A key characteristics of the distribution of magnetic fields strengths of Ap stars is the so-called "magnetic desert", characterized by a "critical dipole field strength" of about 300 G below which essentially no magnetic stars are detected (Aurière et al., 2007). The characteristics of this 'desert' for more massive stars remains to be established, as several clear examples of stars with field strengths below 300 G have already been discovered (e.g. Briquet et al., 2016).

While the magnetic properties of the hot pre-MS magnetic stars are similar to those of the MS population, the evolved post-MS magnetic stars generally have much weaker fields (Neiner et al., 2017), as would be expected from magnetic flux conservation (e.g. Keszthelyi et al., 2017). Those evolved stars thus often appear in the magnetic desert, and explain, at least to some extent, the hot stars that reside there.

2.4. Rotation

Magnetic hot stars generally exhibit rotation rates below those of "normal", non-magnetic stars of similar spectral types. The magnetic field impacts the stellar rotation by coupling to the outflowing wind, enhancing angular momentum loss and rapidly braking the star. Nevertheless, several examples of magnetic hot stars exhibiting rapid rotation have been discovered (e.g. Oksala et al., 2010; Grunhut et al., 2012).

Classical Be stars exhibit the most rapid rotation of any class of B-type stars. As of today, no magnetic field has been directly detected in any classical

Be star, notwithstanding extensive searches (Wade et al., 2016a,b). However, indirect evidence of the presence of a magnetic field, i.e. rotationally modulated observables, seems to be have been found in the classical Be star ω Ori (Neiner et al., 2003, 2012).

2.5. Binarity

Magnetic fields in binary systems may be strongly affected by, and may also strongly affect, the transfer of energy, mass and angular momentum between the components.

Although binary systems containing hot stars are extremely common, binaries with orbital periods shorter than $\sim$ 60 days containing magnetic hot stars are very rare. At the conclusion of the MiMeS survey, less than one dozen SB2 systems containing magnetic A, B or O stars were known. Of these, less than one-half contained a hot primary star. The Binarity and Magnetic Interactions in various classes of Stars (BinaMIcS, e.g. Neiner et al., 2015) project has studied this issue further in short-period spectroscpic binaries and indeed confirms that the occurence of magnetic fields in hot stars in those binaries is lower than in single hot stars. A possible explanation for this dearth of magnetic fields in hot binary systems may lie in stellar formation processes. For example, Commerçon et al. (2011) showed in their simulations that fragmentation of dense stellar cores is inhibited when the medium is magnetic. This could make binary system more difficult to form in the presence of a seed field.

Similar discrepancies between incidence rates of strong magnetic fields in cataclysmic variables (CV) vs. single white dwarfs led Tout et al. (2008) to conclude that the formation of white dwarf magnetic fields was initimately tied to the physics of CV formation, in particular the mass transfer and merger processes. Others (e.g. Langer, 2014) have speculated about a similar connection between binarity and the origin of the fossil magnetic fields of non-degenerate hot stars. The binarity of magnetic hot stars is discussed in greater detail by Nazé and Alecian (these proceedings).

3. Stellar wind-magnetic field interactions

Magnetic stars of spectral types A to moderately early B (often called Ap and Bp stars) exhibit strong, characteristic spectral line strength anomalies and variability. These phenomena - diagnostic of complex, large-scale distributions of abundance enhancement and depletion of various chemical elements - result from the interaction of the magnetic field with photospheric atoms diffusing under the competitive effects of gravity and radiative levitation (e.g. Alecian & Stift, 2017). These structures are able to form and subsist because, at the effective temperatures of these stars, the radiative and gravitational forces on some ions are of similar orders of magnitude. At earlier spectral types, the strong growth of the UV radiation field leads to radiative accelerations that

rapidly overwhelm gravity, leading to the appearance of radiatively driven stellar winds. (The disappearance of evidence of systematic photospheric chemical peculiarities and abundance structures at about the temperature at which winds become significant is thereby naturally explained.)

Systematic MHD studies of the interaction of these outflowing winds with dipolar magnetic fields have been carried out during the past 15 years (e.g. ud-Doula & Owocki, 2002; Ud-Doula et al., 2008, 2009; Petit et al., 2013). A basic conclusion of these investigations is that two physical quantities are capable of describing the general behaviour of the wind of a hot star under the influence of a magnetic field and stellar rotation (Petit et al., 2013): the *wind magnetic confinement parameter* (ud-Doula & Owocki, 2002), which determines the *Alfvén radius* $R_{\rm A}$, and the *rotation parameter* (Ud-Doula et al., 2008), which determined the Kepler co-rotation radius $R_{\rm K}$.

In the case of a rapidly-rotating star, the Kepler radius is located relatively close to the stellar surface, and for sufficiently strong magnetic fields is located inside the Alfvén radius. In this scenario, plasma in the region between $R_{\rm K}$ and $R_{\rm A}$ is forced (by the magnetic field) to orbit at greater than the local Keplerian speed, and hence experiences an unbalanced (outward) net force. In such a "centrifugal magnetosphere" (CM), wind plasma is trapped in this region by the combined effects of magnetic field and rotation. In the case of a slowly-rotating star, the Kepler radius is located far from the stellar surface. The net gravitational + centrifugal force is always directed toward the star. In such a "dynamical magnetosphere" (DM) scenario, plasma driven up the field lines ultimately cools and falls back to the stellar surface. The material in the DM is thus frequently renewed (i.e. on the dynamical timescale).

Centrifugal and dynamical magnetospheres can be observationally distinguished in several ways. First, broad emission features, often found at high velocities, are observed in optical spectra of stars hosting a CM, while stars with DMs show narrower emission if any (see, e.g. Grunhut & Neiner, 2015). DM emission is mostly observed for O stars, since the winds of B stars are too weak to feed the magnetosphere at a sufficient rate to produce significant emission. Rotationally-modulated variability of the magnetospheric emission can be used to reconstruct the circumstellar plasma distribution, especially for stars with CMs (e.g. Grunhut et al., 2013). The magnetospheres of hot stars can be comparatively classified using the *rotation-confinement diagram* (Petit et al., 2013).

4. The influence of magnetic fields on stellar evolution

Current 2D and 3D MHD models can effectively compute the short-term evolution of the wind under such conditions, and have provided a sound theoretical basis for understanding the general observational behaviour of hot magnetic stars. In particular, they demonstrate that the surface field interaction with the

wind results in two effects that are predicted to significantly influence the evolution of hot stars. *Mass-loss quenching* (e.g. ud-Doula & Owocki, 2002) refers to the net reduction in the mass loss rate of a star through the top of its magnetosphere as a consequence of magnetic wind trapping. *Magnetic braking* (e.g. Ud-Doula et al., 2009) refers to the enhanced loss of angular momentum through the wind resulting principally from Maxwell stresses imparted by the magnetic field. Recent efforts have sought to incorporate the effects of these two important phenomena into models of stellar evolution. Meynet et al. (2011) performed first calculations that showed the potential evolutionary impact of magnetic braking. Keszthelyi et al. (these proceedings) have developed more complete and realistic models, and demonstrate that mass-loss quenching also yields an important evolutionary impact. Petit et al. (2017) and Georgy et al. (2017) have recently exploited these new modeling capabilities to provide potential explanations of the appearance of high-mass stellar black holes and pair-instability supernovae in high (∼Galactic) metallicity environments. Moreover, recent identification of candidate magnetic stars in the Magellanic Clouds (e.g. Nazé et al., 2015; Walborn et al., 2015) provides the potential to explore the properties and evolution of magnetic stars in environments very different from those occurring in the Milky Way.

In addition to these predicted (and observed) large scale poloidal surface fields, models of relaxed fossil fields predict very strong, predominantly toroidal fields throughout the stellar radiative zone. The extent to which these fields are modified or modify internal circulation currents and differential rotation, including coupling of the rotation of the core to the envelope, is of great current interest (Langer, 2014) and is beginning to become amenable to observational verification (Briquet et al., 2012).

5. Transformation of fields on evolutionary timescales

As magnetic fields influence stellar evolution, so are magnetic fields expected to transform in response to changes in the structure of the stars in which they are embedded. The evolution of surface magnetic fields of MS stars has been investigated by e.g. Landstreet et al. (2007), and more recently by Fossati et al. (2016). These studies suggest that magnetic flux conservation - a basic assumption in models attempting to connect fossil magnetism through different phases of stellar evolution - is poorly supported by observations of main sequence stars.

Extensive surveys of magnetic fields in cool giants and supergiants (the evolutionary descendants of hot MS stars) show that these stars exhibit magnetic fields powered by dynamos (e.g. Grunhut et al., 2010; Aurière et al., 2015). Although a small population of red giants show evidence of surviving fossil fields from the MS (and the unique interactions between the post-MS dynamo and the pre-existing fossil field; e.g. Aurière et al., 2008), the growth of the deep convective envelope generally appears to erase evidence of their earlier magnetic

characteristics. However, because hot OBA supergiants retain the radiative envelopes they had on the MS, these stars provide a capability to directly extend the studies of MS objects to more advanced evolutionary phases and a much greater range of stellar structural changes (e.g. Blazère et al., 2015; Neiner et al., 2017). The Large Impact of magnetic Fields on the Evolution of hot stars (LIFE) project aims at detecting and characterizing magnetic evolved hot stars at various phases of the post-MS evolution. This project and magnetic fields of evolved stars are discussed in more detail by Martin (these proceedings).

References

Alecian, E., Wade, G. A., Catala, C., et al. 2013, *Mon. Not. R. Astron. Soc.*, **429**, 1001

Alecian, G. & Stift, M. J. 2017, *Mon. Not. R. Astron. Soc.*, **468**, 1023

Aurière, M., Konstantinova-Antova, R., Charbonnel, C., et al. 2015, *Astron. Astrophys.*, **574**, A90

Aurière, M., Konstantinova-Antova, R., Petit, P., et al. 2008, *Astron. Astrophys.*, **491**, 499

Aurière, M., Wade, G. A., Silvester, J., et al. 2007, *Astron. Astrophys.*, **475**, 1053

Blazère, A., Neiner, C., Tkachenko, A., Bouret, J.-C., & Rivinius, T. 2015, *Astron. Astrophys.*, **582**, A110

Braithwaite, J. & Cantiello, M. 2013, *Mon. Not. R. Astron. Soc.*, **428**, 2789

Braithwaite, J. & Spruit, H. C. 2004, *Nature*, **431**, 819

Braithwaite, J. & Spruit, H. C. 2006, *Astron. Astrophys.*, **450**, 1097

Briquet, M., Neiner, C., Aerts, C., et al. 2012, *Mon. Not. R. Astron. Soc.*, **427**, 483

Briquet, M., Neiner, C., Petit, P., Leroy, B., & de Batz, B. 2016, *Astron. Astrophys.*, **587**, A126

Commerçon, B., Hennebelle, P., & Henning, T. 2011, *Astrophys. J., Lett.*, **742**, L9

Duez, V., Braithwaite, J., & Mathis, S. 2010, *Astrophys. J., Lett.*, **724**, L34

Duez, V. & Mathis, S. 2010, *Astron. Astrophys.*, **517**, A58

Ferrario, L., Pringle, J. E., Tout, C. A., & Wickramasinghe, D. T. 2009, *Mon. Not. R. Astron. Soc.*, **400**, L71

Fossati, L., Castro, N., Schöller, M., et al. 2015, *Astron. Astrophys.*, **582**, A45

Fossati, L., Schneider, F. R. N., Castro, N., et al. 2016, *Astron. Astrophys.*, **592**, A84

Georgy, C., Meynet, G., Ekström, S., et al. 2017, *Astron. Astrophys.*, **599**, L5

Grunhut, J., Townsend, R., & Wade, G. 2013, in Massive Stars: From alpha to Omega, 69

Grunhut, J. H. & Neiner, C. 2015, in IAU Symp., Vol. **305**, *Polarimetry*, ed. K. N. Nagendra, S. Bagnulo, R. Centeno, & M. Jesús Martínez González, 53–60

Grunhut, J. H., Rivinius, T., Wade, G. A., et al. 2012, *Mon. Not. R. Astron. Soc.*, **419**, 1610

Grunhut, J. H., Wade, G. A., Hanes, D. A., & Alecian, E. 2010, *Mon. Not. R. Astron. Soc.*, **408**, 2290

Grunhut, J. H., Wade, G. A., Neiner, C., et al. 2017, *Mon. Not. R. Astron. Soc.*, **465**, 2432

Howarth, I. D., Walborn, N. R., Lennon, D. J., et al. 2007, *Mon. Not. R. Astron. Soc.*, **381**, 433

Hussain, G. A. J. & Alecian, E. 2014, in IAU Symp., Vol. **302**, *Magnetic Fields throughout Stellar Evolution*, ed. P. Petit, M. Jardine, & H. C. Spruit, 25–37

Keszthelyi, Z., Wade, G. A., & Petit, V. 2017, in IAU Symp., Vol. **329**, *The Lives and Death-Throes of Massive Stars*, ed. J. J. Eldridge, J. C. Bray, L. A. S. McClelland, & L. Xiao, 250–254

Kurapati, S., Chandra, P., Wade, G., et al. 2017, *Mon. Not. R. Astron. Soc.*, **465**, 2160

Landstreet, J. D., Bagnulo, S., Andretta, V., et al. 2007, *Astron. Astrophys.*, **470**, 685

Langer, N. 2014, in IAU Symp., Vol. **302**, *Magnetic Fields throughout Stellar Evolution*, ed. P. Petit, M. Jardine, & H. C. Spruit, 1–9

Martin, A. J., Neiner, C., Oksala, M. E., et al. 2017, *ArXiv e-prints* [arXiv:1712.07403]

Meynet, G., Eggenberger, P., & Maeder, A. 2011, *Astron. Astrophys.*, **525**, L11

Nazé, Y., Walborn, N. R., Morrell, N., Wade, G. A., & Szymański, M. K. 2015, *Astron. Astrophys.*, **577**, A107

Neiner, C., Grunhut, J. H., Petit, V., et al. 2012, *Mon. Not. R. Astron. Soc.*, **426**, 2738

Neiner, C., Hubert, A.-M., Frémat, Y., et al. 2003, *Astron. Astrophys.*, **409**, 275

Neiner, C., Morin, J., & Alecian, E. 2015, in SF2A-2015: Proceedings of the Annual meeting of the French Society of Astronomy and Astrophysics, ed. F. Martins, S. Boissier, V. Buat, L. Cambrésy, & P. Petit, 213–216

Neiner, C., Oksala, M. E., Georgy, C., et al. 2017, *Mon. Not. R. Astron. Soc.*, **471**, 1926

Oksala, M. E., Kochukhov, O., Krtička, J., et al. 2015, *Mon. Not. R. Astron. Soc.*, **451**, 2015

Oksala, M. E., Wade, G. A., Marcolino, W. L. F., et al. 2010, *Mon. Not. R. Astron. Soc.*, **405**, L51

Petit, V., Keszthelyi, Z., MacInnis, R., et al. 2017, *Mon. Not. R. Astron. Soc.*, **466**, 1052

Petit, V., Owocki, S. P., Wade, G. A., et al. 2013, *Mon. Not. R. Astron. Soc.*, **429**, 398

Schöller, M., Hubrig, S., Fossati, L., et al. 2017, *Astron. Astrophys.*, **599**, A66

Shultz, M. 2016, PhD thesis, Queen's University (Canada)

Stibbs, D. W. N. 1950, *Mon. Not. R. Astron. Soc.*, **110**, 395

Tout, C. A., Wickramasinghe, D. T., Liebert, J., Ferrario, L., & Pringle, J. E. 2008, *Mon. Not. R. Astron. Soc.*, **387**, 897

Trigilio, C., Leto, P., Umana, G., Leone, F., & Buemi, C. S. 2004, *Astron. Astrophys.*, **418**, 593

ud-Doula, A. & Nazé, Y. 2016, *Adv. Space Res.*, **58**, 680

ud-Doula, A. & Owocki, S. P. 2002, *Astrophys. J.*, **576**, 413

Ud-Doula, A., Owocki, S. P., & Townsend, R. H. D. 2008, *Mon. Not. R. Astron. Soc.*, **385**, 97

Ud-Doula, A., Owocki, S. P., & Townsend, R. H. D. 2009, *Mon. Not. R. Astron. Soc.*, **392**, 1022

Wade, G. A., Grunhut, J., Alecian, E., et al. 2014, in IAU Symp., Vol. **302**, *Magnetic Fields throughout Stellar Evolution*, ed. P. Petit, M. Jardine, & H. C. Spruit, 265–269

Wade, G. A., Maíz Apellániz, J., Martins, F., et al. 2012, *Mon. Not. R. Astron. Soc.*, **425**, 1278

Wade, G. A. & MiMeS Collaboration. 2015, in ASP Conf. Ser., Vol. **494**, *Physics and Evolution of Magnetic and Related Stars*, ed. Y. Y. Balega, I. I. Romanyuk, & D. O. Kudryavtsev, 30

Wade, G. A., Neiner, C., Alecian, E., et al. 2016a, *Mon. Not. R. Astron. Soc.*, **456**, 2

Wade, G. A., Petit, V., Grunhut, J. H., Neiner, C., & MiMeS Collaboration. 2016b, in ASP Conf. Ser., Vol. **506**, *Bright Emissaries: Be Stars as Messengers of Star-Disk Physics*, ed. T. A. A. Sigut & C. E. Jones, 207

Walborn, N. R. 1972, *Astron. J.*, **77**, 312

Walborn, N. R., Morrell, N. I., Nazé, Y., et al. 2015, *Astron. J.*, **150**, 99

Contrib. Astron. Obs. Skalnaté Pleso **48**, 116 – 123, (2018)

Modelling complex magnetic fields in stars with radiative envelopes

J. Silvester

Department of Astronomy and Space Physics, Uppsala Universitet, Uppsala, Sweden, (E-mail: james.silvester@physics.uu.se)

Received: December 10, 2017; Accepted: January 4, 2018

Abstract. Magnetic chemically peculiar A and B type stars (Ap/Bp) exhibit strong globally organised magnetic fields, this is combined with strong chemical abundance non-uniformities within the atmosphere. The presence of the magnetic field influences energy and mass transport within the atmosphere of a star, this is thought to cause these observed chemical non-uniformities. These stars offer the ideal laboratory for understanding the interplay between magnetic field structure, atmospheric transport processes and other stellar parameters. With the recent increase in the availability of spectropolarimetric data and by using magnetic Doppler imaging (MDI) techniques, the number of detailed maps of the magnetic structure of Ap/Bp stars is growing. It is now possible to begin to investigate correlations between the magnetic field structure, chemical abundance structures in the photospheres of Ap/Bp stars and other stellar parameters, the first steps in understanding the evolution of such magnetic fields.

Key words: stars: magnetic fields – stars: chemically peculiar

1. Introduction

The magnetic fields of stars with radiative envelopes have quite different characteristics than those of late-type stars. In the radiative envelope stars, the large-scale surface magnetic field is static on timescales of at least many decades and appears to be frozen into a rigidly rotating atmosphere. The magnetic field is globally organised, permeating the entire stellar surface, with a high field strength (typically of a few hundred up to a few tens of thousands of Gauss). The presence of a such a magnetic field can strongly influence energy and mass transport within the atmosphere of the star and results in the presence of strong chemical abundance non-uniformities in the atmosphere, the so-called chemically peculiar stars (the Ap and Bp stars). Because the atmospheric mixing processes are weak in the atmospheres of Ap/Bp stars (due in part to the magnetic field), these stars offer a unique insight into the internal processes, via the impression these processes leave on the surface of a star.

Historically, the magnetic field geometries of chemically peculiar Ap/Bp stars were modelled in the context of a simple dipole field. However, with the acquisition of increasingly sophisticated diagnostic data, it has become clear that

the large-scale field topologies exhibit important departures from this simple model. High-resolution circular and linear polarisation spectroscopy have shown the presence of strong, small-scale field structures, which were completely unexpected based on earlier modelling.

Recent advances in tomographic imaging techniques and improvements in instrumentation offer the opportunity to improve our understanding of the magnetic field structure and the effect it has on atmospheric transport mechanisms. By mapping the magnetic field and chemical surface structure of Ap stars simultaneously, it is possible to directly investigate the relationship between the local magnetic field, the local surface chemistry and also to look for correlations between the magnetic field and other stellar properties.

1.1. Spectropolarimetric Observations and MDI

There has been a large increase in the availability of sophisticated spectropolarmetric data obtained for Ap/Bp stars in Stokes IQUV observations using instruments such as the ESPaDOnS, HARPSpol and NARVAL spectropolarimeters. These new spectropolarimeters have overcome the limitations of the previous generations of instrumentation, such as limited resolving power and sensitivity. The ESPaDOnS spectropolarimeter is installed on the Canada France Hawaii Telescope (CFHT) located on Mauna Kea, Hawaii, HARPSpol is installed on the ESO 3.6m telescope at ESO La Silla Observatory, Chile and the NARVAL spectropolarimeter on the 2m TBL telescope at l'Observatoire du Pic du Midi (France). ESPaDOnS and NARVAL are in fact identical instruments, with high spectral resolving power ($R = \lambda/\Delta\lambda = 65000$) and HARPSpol has an even higher spectral resolving power ($R = \lambda/\Delta\lambda = 110000$).

These three instruments have proven to be stable over long time-scales and have been shown to provide high-quality data suitable for the basis of long time-series observations which is a requirement for reliable MDI mapping (e.g. Silvester et al., 2012). With the vastly improved data available from these instruments and by using MDI techniques, we are able to reliably characterise the magnetic field geometry of the target stars. The reproducibility and reliableness of the maps extracted using the INVERS MDI codes have been clearly demonstrated (e.g. Kochukhov, 2017).

An example of such test which verified both that the newer instrumentation and INVERS codes can produce consistent results is given by the mapping of α^2 CVn (Silvester et al., 2014). It was shown that the derived magnetic field structure was consistent with the magnetic structure map previously derived for α^2 CVn using MuSiCoS data (illustrated in Fig. 1) and that maps reconstructed using differing spectral lines sets resulted in similar magnetic field structures.

With the reliability of the instrumentation and mapping techniques shown, it has been possible to concentrate on studying individual stars in detail, looking for correlations between magnetic structure and other stellar parameters.

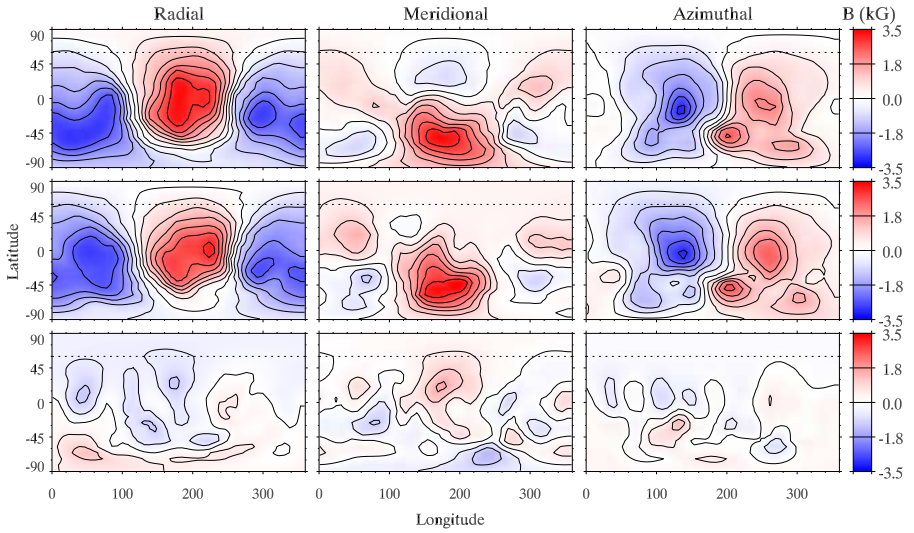

Figure 1. Comparison between magnetic field maps derived for α^2 CVn. The map based on ESPaDOnS / Narval data is shown in top row, MuSiCoS map middle row and the difference given in the bottom row. Taken from Silvester et al. (2014).

2. Recent Mapping Results

In recent years the number of Ap/Bp stars mapped has increased quite measurably, a full list of Ap/Bp stars mapped using imaging techniques is given in Kochukhov (2017). Below we summarize some of the most recent results/maps for Ap/Bp stars.

2.1. HD 32633

The star HD 32633 has an effective temperature of 12,000–13,000 K and is of the peculiar subclass SiCr (Renson & Manfroid, 2009). Observations were obtained with ESPaDOnS and Narval and mapping was performed using individual Stokes $IQUV$ lines. As described in detail in Silvester et al. (2015), the resulting magnetic maps of HD 32633 revealed a largely axisymmetric field topology (field shown in Fig. 2). Within the harmonic modes $\ell = 1$ dominates, with around 75% of the energy in that mode; 9% is contained in the poloidal quadrupolar $\ell = 2$ mode. In total 16% of the energy in toroidal components. Importantly it was shown that the Stokes parameter profiles of HD 32633 cannot be reproduced by assuming a pure dipole or dipole + quadrupole magnetic field geometry. This indicates that the field is definitely more complex than can expressed by such low-order multipolar parametrisation. The plot of the final derived harmonic energies for HD 32633 are shown as part of Fig. 5.

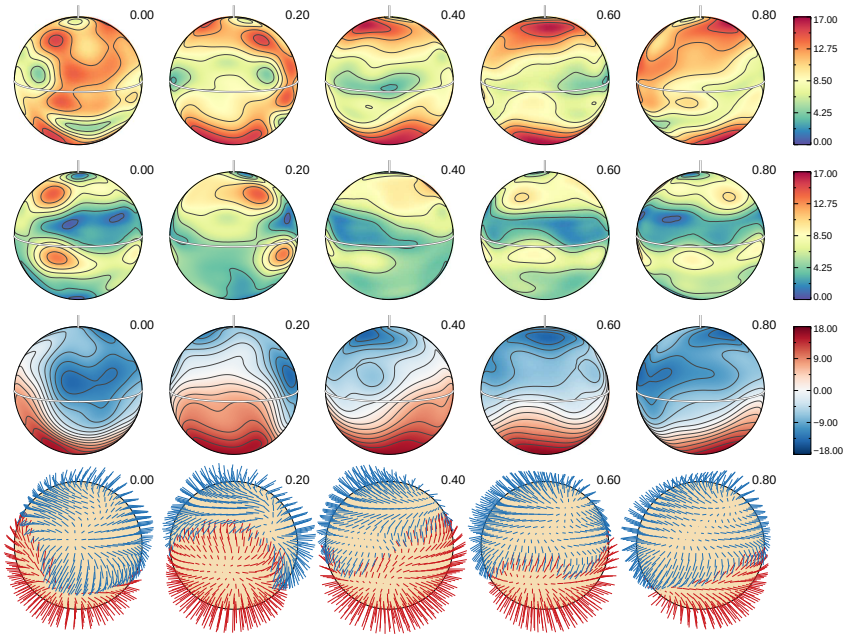

Figure 2. The spherical plots of the magnetic field map of the magnetic field map of HD 32633 taken from Silvester et al. (2015). Showing distributions of: the field modulus, horizontal field, the radial field, and the field orientation. Each column corresponds to a different phase of rotation (0.0, 0.2, 0.4, 0.6, and 0.8).

2.2. 49 Cam

49 Cam is a cool Ap star with classification as F0p (SrEu) by Cowley (1968) and later as A8p (SrEu) by Leone et al. (2000). Mapping was performed using Stokes $IQUV$ individual lines from ESPaDOnS and Narval observations (Silvester et al., 2017). A complex magnetic field structure for 49 Cam (shown in Fig. 3) was found, with a relatively large contribution in the $\ell = 3$ mode. The magnetic field of 49 Cam contradicts an earlier trend seen where cooler Ap stars showed simpler magnetic configurations and only hotter stars showing complex field structure. This gives a strong suggestion that the temperature of an Ap/Bp star is not a clear indicator of the expected magnetic field complexity.

2.3. 36 Lyn

36 Lyn (HD 79158, HR 3652) is a well known magnetic Bp star, classified as B8 IIImnp by the Bright Star Catalog (Hoffleit & Warren, 1995). Unlike the previous two stars, mapping (as described in Oksala et al., 2018) was performed using averaged Stokes IV profiles. Whilst the resulting magnetic map shows

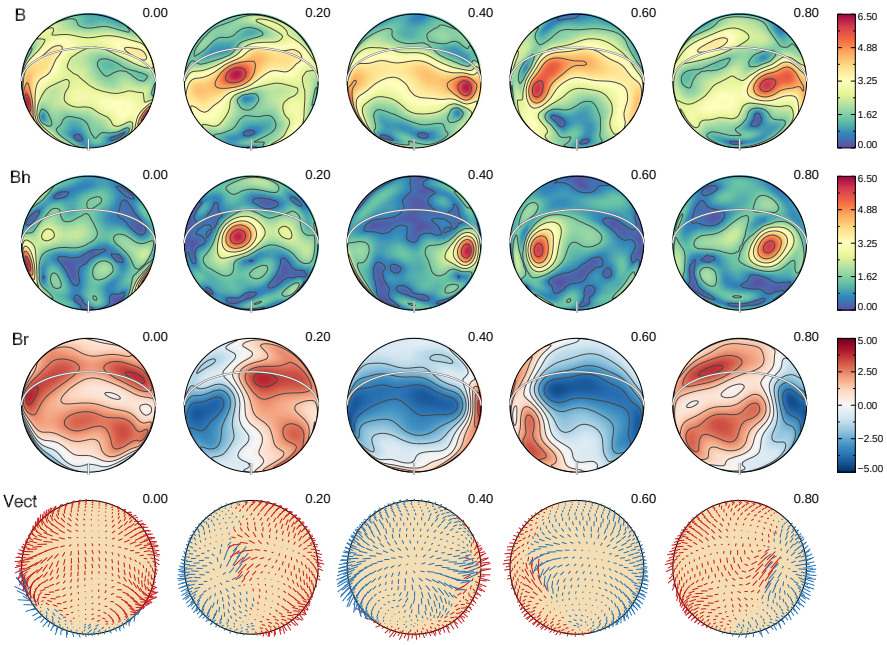

Figure 3. The spherical plots of the magnetic field map of 49 Cam taken from Silvester et al. (2017). Showing distributions of: the field modulus, horizontal field, the radial field, and the field orientation. Each column corresponds to a different phase of rotation (0.0, 0.2, 0.4, 0.6, and 0.8).

a very simple global structure, 36 Lyn does contains a large toroidal component ($\approx 36\%$), which has not been seen at this level in any other Ap/Bp stars mapped thus far. It was shown that this large toroidal component is required to successfully fit the observed Stokes V profiles. The resulting map is shown in Fig. 4 and the final derived harmonic energies are shown as part of Fig. 5.

2.4. Summary of Recent Harmonic Energies

Whilst the spherical magnetic field maps provide a useful illustration of the derived magnetic surface structure of the star, for direct comparison with other Ap stars using the spherical surface maps is not trivial. It is far more useful to describe the resulting magnetic field of a star in terms of spherical harmonics, something which is done as standard in the majority of the current inversion codes. It was thought that stellar mass or stellar temperature could correlate with magnetic field complexity. To look for any links between magnetic field complexity and for example temperature (and ultimately mass), the resulting spherical harmonic energies are plotted for a selection of Ap stars in different

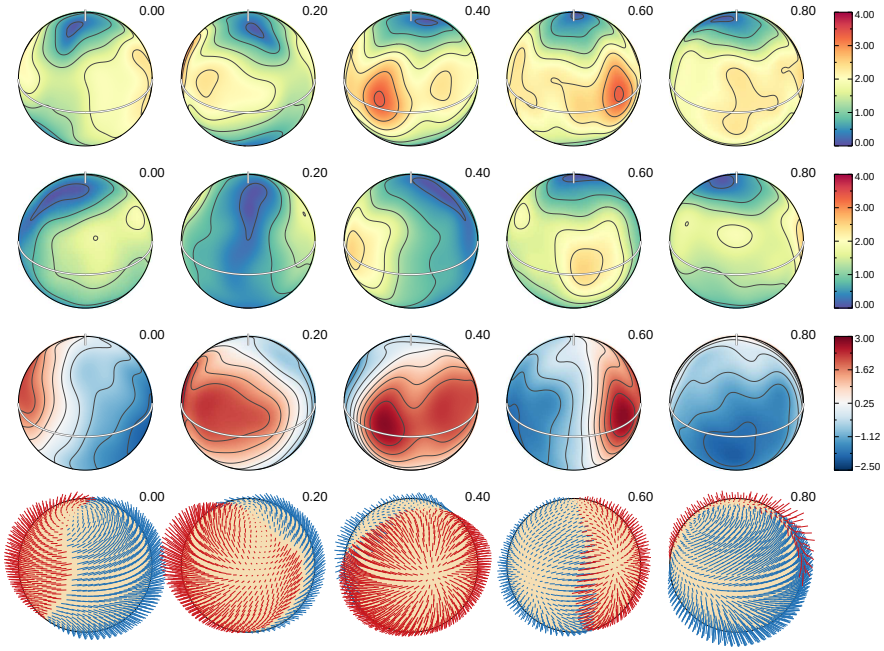

Figure 4. The spherical plots of the magnetic field map of 36 Lyncis taken from Oksala et al. (2018). Showing distributions of: the field modulus, horizontal field, the radial field, and the field orientation. Each column corresponds to a different phase of rotation (0.0, 0.2, 0.4, 0.6, and 0.8).

temperature bins. As illustrated in Fig. 5, it appears that there is little correlation between temperature and field complexity, with various levels of complexity being seen in all of the temperate bins. The most important parameter which is thought to correlate with magnetic field complexity is stellar age.

3. Conclusion

Both the current generation of spectropolarimeters and the current inversion codes have been shown to be for reliable and suitable for performing MDI mapping (e.g. Silvester et al., 2012; Kochukhov, 2017).

Magnetic Doppler imaging has now been performed for an increasingly large sample of Ap/Bp stars. With this recent surge in mapping, it has been shown that Ap/Bp stars exhibit a wide variety of magnetic field substructure, with complexity differing between each star. For many of the stars mapped, which showed complex structures, the requirement for such a complexity due was illustrated clearly the fact that the observed Stokes $IQUV$ profiles cannot be reproduced by using a simpler field geometry.

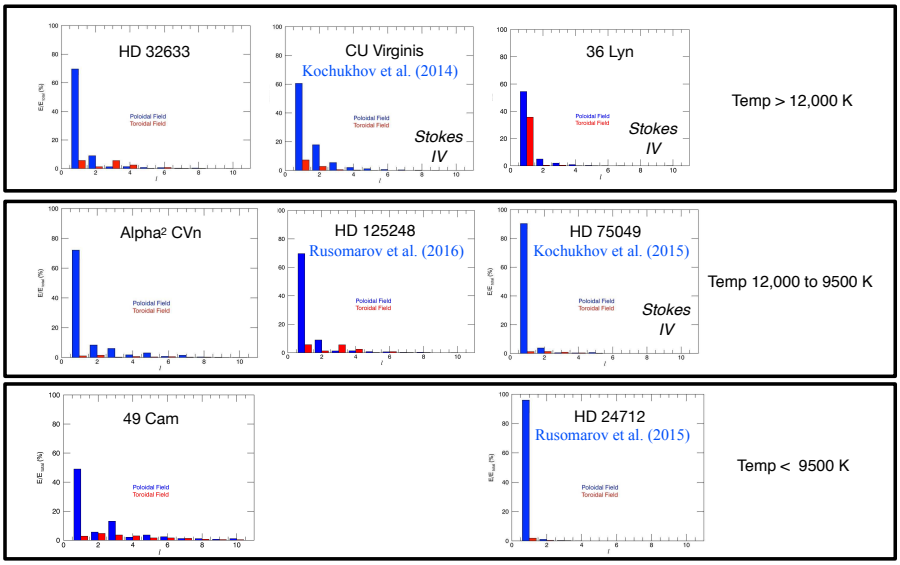

Figure 5. Harmonic Energies of Ap Stars Recently Mapped using MDI classified into temperature range bins. Additional stars shown with harmonic energies for HD 24712 (Rusomarov et al., 2015), HD 125248 (Rusomarov et al., 2016), HD 75049 (Kochukhov et al., 2015), and CU Vir (Kochukhov et al., 2014).

With the harmonic energy comparison shown between some of the most recently mapped stars (as shown in Fig. 5) it can be seen that temperature and magnetic field complexity show no direct correlation. It is still possible that field complexity correlates with the stellar age. However, because all of the current MDI targets have been field stars for which age determination is notoriously uncertain (Landstreet et al., 2007) they are not suitable for such investigations. To correctly investigate if correlations between field complexity and age exist requires the study of cluster stars for which reliable ages can be obtained.

Also, the observed diversity in the field structures between stars highlights the fact that the comparison of observed abundance structures to theoretical abundance models which use simplified magnetic field descriptions is not suitable, as stars show varying levels of magnetic field complexity even within the same spectral subclass. So any theoretical modelling of abundance structures should be performed ideally on a star by star basis taking into account this field diversity.

References

Cowley, A. P. 1968, *Publ. Astron. Soc. Pac.*, **80**, 453

Hoffleit, D. & Warren, Jr., W. H. 1995, *VizieR Online Data Catalog*, **5050**

Kochukhov, O. 2017, *Astron. Astrophys.*, **597**, A58

Kochukhov, O., Lüftinger, T., Neiner, C., Alecian, E., & MiMeS Collaboration. 2014, *Astron. Astrophys.*, **565**, A83

Kochukhov, O., Rusomarov, N., Valenti, J. A., et al. 2015, *Astron. Astrophys.*, **574**, A79

Landstreet, J. D., Bagnulo, S., Andretta, V., et al. 2007, *Astron. Astrophys.*, **470**, 685

Leone, F., Catanzaro, G., & Catalano, S. 2000, *Astron. Astrophys.*, **355**, 315

Oksala, M. E., Silvester, J., Kochukhov, O., et al. 2018, *Mon. Not. R. Astron. Soc.*, **473**, 3367

Renson, P. & Manfroid, J. 2009, *Astron. Astrophys.*, **498**, 961

Rusomarov, N., Kochukhov, O., Ryabchikova, T., & Ilyin, I. 2016, *Astron. Astrophys.*, **588**, A138

Rusomarov, N., Kochukhov, O., Ryabchikova, T., & Piskunov, N. 2015, *Astron. Astrophys.*, **573**, A123

Silvester, J., Kochukhov, O., Rusomarov, N., & Wade, G. A. 2017, *Mon. Not. R. Astron. Soc.*, **471**, 962

Silvester, J., Kochukhov, O., & Wade, G. A. 2014, *Mon. Not. R. Astron. Soc.*, **440**, 182

Silvester, J., Kochukhov, O., & Wade, G. A. 2015, *Mon. Not. R. Astron. Soc.*, **453**, 2163

Silvester, J., Wade, G. A., Kochukhov, O., et al. 2012, *Mon. Not. R. Astron. Soc.*, **426**, 1003

Contrib. Astron. Obs. Skalnaté Pleso **48**, 124 – 128, (2018)

The impact and evolution of magnetic confinement in hot stars

Z. Keszthelyi[1,2], G. A. Wade[1], V. Petit[3], G. Meynet[4] and C. Georgy[4]

[1] *Department of Physics and Space Science, Royal Military College, Kingston, ON, K7K 0C6, Canada, (E-mail: zsolt.keszthelyi@rmc.ca)*

[2] *Department of Physics, Engineering Physics and Astronomy, Queen's University, Kingston, ON, K7L 3N6, Canada*

[3] *Department of Physics and Astronomy, University of Delaware, Newark, DE 19716, USA*

[4] *Geneva Observatory, University of Geneva, 1290 Sauverny, Switzerland*

Received: November 17, 2017; Accepted: November 23, 2017

Abstract. Magnetic confinement of the winds of hot, massive stars has far-reaching consequences on timescales ranging from hours to Myr. Understanding the long-term effects of this interplay has already led to the identification of two new evolutionary pathways to form 'heavy' stellar mass black holes and pair-instability supernova even at galactic metallicity. We are performing 1D stellar evolution model calculations that, for the first time, account for the surface effects and the time evolution of fossil magnetic fields. These models will be thoroughly confronted with observations and will potentially lead to a significant revision of the derived parameters of observed magnetic massive stars.

Key words: stars: massive – stars: magnetic field

1. Introduction

Massive stars are key objects in the Universe, shaping their local environment via chemical enrichment and energy deposition. Therefore it is crucial to understand the physical processes governing the structure and evolution of these stars. A distinct subsample ($\sim 7\%$) of massive OB stars shows evidence for large scale magnetic fields at their surfaces (e.g. Petit et al., 2013; Wade et al., 2016). These fields have been characterised: they are stable on long time scales, and the measured variations in the line-of-sight field strength are well understood under the oblique rotator model. In this article we elaborate on a developing consensus how surface magnetic fields can be accounted for in state-of-the-art stellar evolution models.

2. Methods

2.1. Analytical prescription of surface magnetic fields

Our understanding of the interactions of the winds of hot star with surface magnetic fields has have greatly benefited from multidimensional magnetohydrodynamic (MHD) simulations performed by ud-Doula & Owocki (2002) and subsequently by ud-Doula et al. (2009). These simulations have successfully established – in accord with observational evidence – that surface magnetic fields have two major 'surface effects'.

The magnetic field lines channel and confine the wind plasma, an interaction that is fundamentally described by the ratio of magnetic energy density and wind kinetic energy density, that is the *equatorial magnetic confinement parameter*,

$$\eta_\star = \frac{B_p^2 R_\star^2}{4\dot{M}_{B=0} v_\infty}\,, \tag{1}$$

introduced by ud-Doula & Owocki (2002). Here B_p is the polar magnetic field strength, $R_\star$ is the stellar radius, $\dot{M}_{B=0}$ is the mass-loss rate the star would have in absence of a magnetic field, and v_∞ is the terminal wind velocity. *Mass-loss quenching* refers to the phenomenon by which wind plasma is trapped inside the magnetosphere by this channeling, hence the effective mass-loss rate is less than it would be in absence of a magnetosphere. This can be described by a scaling factor, f_B, that is,

$$f_B = 1 - \sqrt{1 - \frac{R_\star}{R_c}}\,, \tag{2}$$

where R_c is the closure radius. As a consequence, the effective mass-loss rate will be

$$\dot{M}_{\rm effective} = f_B \cdot \dot{M}_{B=0}\,. \tag{3}$$

Magnetic braking accounts for surface angular momentum removal due to Maxwell stresses and the magnetic field's capability to transport energy and momentum. The additional angular momentum removed on a dynamical timescale is calculated as,

$$\frac{{\rm d}J}{{\rm d}t} = \frac{2}{3}\Omega R_\star^2 R_A^2 \dot{M}_{B=0}\,, \tag{4}$$

where Ω is the surface angular velocity and R_A is the Alfvén radius. The magnetic field strength scales with $R_\star^{-2}$, assuming magnetic flux is conserved at the stellar surface during the evolution of the star.

2.2. Stellar evolution codes

Currently there are two hydrodynamic stellar evolution codes that have incorporated the analytical expressions above in order to account for the effects and the evolution of a surface magnetic field.

Modules for Experiments in Stellar Astrophysics (MESA, Paxton et al., 2013) is a versatile, open-source stellar evolution code. MESA is very rapidly developing and the code capabilities have greatly increased over recent years. MESA models including surface magnetic fields were recently described by Petit et al. (2017) and Keszthelyi et al. (2017). The Geneva stellar evolution code (GENEC, Eggenberger et al., 2008) has been actively used for over three decades. GENEC models incorporate magnetic braking (Meynet et al., 2011), as well as the quenching and field evolution components (Georgy et al., 2017).

3. Results & Discussion

A key result from previous studies has been that mass-loss quenching can alter massive star evolution by retaining a significant fraction of the star's mass. As a consequence, magnetic progenitors can explain the existence of 'heavy' stellar mass black holes (Petit et al., 2017) and pair instability supernova (Georgy et al., 2017) even at solar metallicity.

However, it has became evident that the surface spin-down due to magnetic fields is very sensitive to the model details. To this extent, we computed rotating models at solar metallicity ($Z = 0.014$) with the MESA code. These models include a strong internal coupling between the core and the envelope, which leads to solid body rotation in every model. In Fig. 1 we show main sequence models with initial masses of 16, 18, and $20\,M_\odot$ including the effects of mass-loss quenching, magnetic braking, and magnetic field evolution. These models do require several Myrs to completely brake their surface rotation. This depends on the strength of their stellar winds, which is tightly tied to their initial mass.

In contrast, Fig. 2 shows two models with the same input parameters but the only difference is that one model (green line) is computed with the inclusion of magnetic braking and the other (blue line) is computed without magnetic braking. Mass-loss quenching and field evolution is included in both models. The rotating model with mass-loss quenching but without magnetic braking evolves 'blueward', that is, chemically homogeneously. It is indeed expected that models including core-envelope coupling are very efficiently mixed by meridional currents. In the other model, the inclusion of magnetic braking does brake the whole star (it is nearly solid body rotating). This rapidly decreases the meridional currents and thus the mixing of the elements is less efficient. The star evolves 'redwards' once the rotational velocity approaches zero. Models computed with a core-envelope coupling and an initial rotation of $300\,\mathrm{km\,s^{-1}}$ evolve homogeneously. With the same conditions, the models evolve redward when magnetic braking is accounted for. This result would mean that in case of a coupled core-envelope configuration, a star evolving redwards either should begin with an initial rotation smaller than the one considered here, or its surface rotation should be braked by magnetic braking. These two scenarios have different predictions for the changes of the surface abundances.

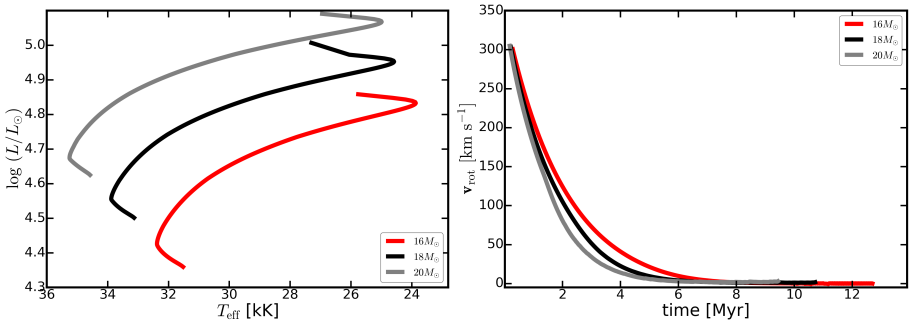

Figure 1. MESA models with $v_{\rm rot}(initial) = 300\,{\rm km\,s^{-1}}$, assuming solid body rotation. These models include the effects of mass-loss quenching, magnetic braking, and magnetic field evolution. *Left:* The HRD shows that an initial blueward evolution on the main sequence is followed by a redward turn when the rotational velocity approaches zero. *Right:* The time evolution of the surface rotational velocity shows that magnetic braking may take several Myr, and it depends on the initial mass of the star.

4. Conclusions

The incorporation of surface magnetic fields in stellar evolution models has resulted in identifying two new evolutionary pathways of massive stars. Additional channels may also be discovered, however, this will require new and extensive grids of models extending the parameter space of previous studies. Currently, the model dependence of the inclusion of magnetic braking needs to be thoroughly investigated.

Forthcoming works will focus on how state-of-the-art stellar evolution models will allow the improved derivation of stellar parameters of observed magnetic stars, how the observables (e.g., surface nitrogen abundance, rotational velocity) evolve in these models, and for how long the magnetic confinement can be maintained during the evolution.

Acknowledgements. We appreciate fruitful discussions with Rich Townsend and Alexandre David-Uraz. GAW acknowledges support in the form of a Discovery Grant from the Natural Science and Engineering Research Council (NSERC) of Canada. VP acknowledges support provided by the NASA through Chandra Award Number GO3-14017A issued by the Chandra X-ray Observatory Center, which is operated by the Smithsonian Astrophysical Observatory for and on behalf of the NASA under contract NAS8-03060.

References

Eggenberger, P., Meynet, G., Maeder, A., et al. 2008, *Astrophys. Space Sci.*, **316**, 43

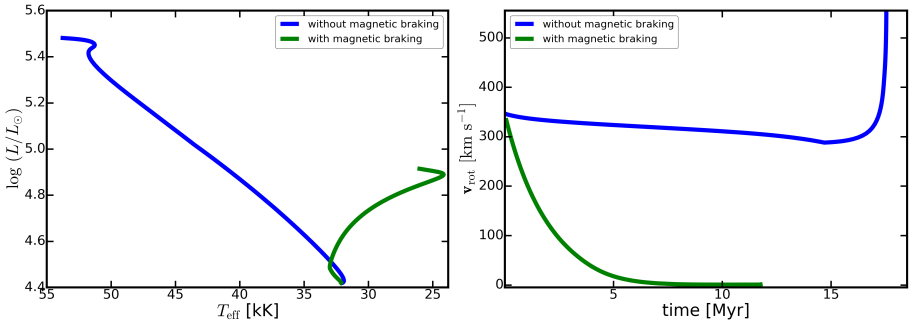

Figure 2. Two 17 $M_\odot$ MESA models with solar metallicity. Both models include mass-loss quenching and magnetic field evolution, but one model (green line) includes magnetic braking, the other (blue line) neglects magnetic braking. *Left:* The HRD shows large differences between the two models, which originate from their rotational properties. *Right:* The surface rotational velocity vs time plot shows that with solid body rotation, the model maintains a constant rotational velocity on the main sequence if magnetic braking is not accounted for.

Georgy, C., Meynet, G., Ekström, S., et al. 2017, *Astron. Astrophys.*, **599**, L5

Keszthelyi, Z., Wade, G. A., & Petit, V. 2017, in *IAU Symposium*, ed. J. J. Eldridge, J. C. Bray, L. A. S. McClelland, & L. Xiao, Vol. **329**, 250–254

Meynet, G., Eggenberger, P., & Maeder, A. 2011, *Astron. Astrophys.*, **525**, L11

Paxton, B., Cantiello, M., Arras, P., et al. 2013, *Astrophys. J., Suppl. Ser.*, **208**, 4

Petit, V., Keszthelyi, Z., MacInnis, R., et al. 2017, *Mon. Not. R. Astron. Soc.*, **466**, 1052

Petit, V., Owocki, S. P., Wade, G. A., et al. 2013, *Mon. Not. R. Astron. Soc.*, **429**, 398

ud-Doula, A. & Owocki, S. P. 2002, *Astrophys. J.*, **576**, 413

ud-Doula, A., Owocki, S. P., & Townsend, R. H. D. 2009, *Mon. Not. R. Astron. Soc.*, **392**, 1022

Wade, G. A., Neiner, C., Alecian, E., et al. 2016, *Mon. Not. R. Astron. Soc.*, **456**, 2

Contrib. Astron. Obs. Skalnaté Pleso **48**, 129 – 133, (2018)

Winds of Massive Magnetic Stars: Interacting Fields and Flow

S. Daley-Yates and I. R. Stevens

School of Physics and Astronomy, University of Birmingham, Edgbaston, Birmingham, B15 2TT, U.K., (E-mail: sdaley@star.sr.bham.ac.uk)

Received: November 9, 2017; Accepted: January 5, 2018

Abstract. We present results of 3D numerical simulations of magnetically confined, radiatively driven stellar winds of massive stars, conducted using the astrophysical MHD code Pluto, with a focus on understanding the rotational variability of radio and sub-mm emission. Radiative driving is implemented according to the Castor, Abbott and Klein theory of radiatively driven winds. Many magnetic massive stars posses a magnetic axis which is inclined with respect to the rotational axis. This misalignment leads to a complex wind structure as magnetic confinement, centrifugal acceleration and radiative driving act to channel the circumstellar plasma into a warped disk whose observable properties should be apparent in multiple wavelengths. This structure is analysed to calculate free-free thermal radio emission and determine the characteristic intensity maps and radio light curves.

Key words: stars: magnetic field – stars: massive

1. Introduction

Radio emission from massive stars has historically been the subject of considerable interest (Braes et al., 1972; Wright et al., 1974; Wright & Barlow, 1975; Cohen & Barlow, 1975). This is, in part, due to the deviation from the expected results from Plank curve calculations of their millimetre and radio fluxes, which are substantially higher than expected. The additional emission is thought to be due to free-free interactions between charged species in the stellar wind. The spectral index of the continuum radio flux of a massive star is an indirect measure of its wind mass-loss (Wright & Barlow, 1975; Daley-Yates et al., 2016). An accurate model for calculating stellar wind mass-loss needs to take account of any factor which can influence this spectral index. Perturbations that leads to non-spherical symmetry such as binary interactions (Pittard, 2010) or stellar magnetic fields, the subject of this proceeding, can affect this. The magnetic confinement of massive star winds has also been proposed as an explanation for time dependant Hα emission (Townsend et al., 2005) as well as confined wind shocks which result in X-ray emission (ud-Doula & Nazé, 2016).

ud-Doula et al. (2013) presented the first 3D MHD simulations of a massive star wind, studying a highly symmetric configuration, with stellar rotational and magnetic field axes aligned with the z-axis. The magnetic field results in

a disk structure in the equatorial region of the star. They also concluded that 2D time averaged simulation agree well with 3D spacially averaged results. Papers focusing on inclined magnetic fields of massive stars are absent from the literature. Inclined fields lead to the breaking of both symmetry and the disk like structure which develops in the magnetosphere of the star. This symmetry breaking is investigated here. The following section describes the parameters of the simulated star.

2. Simulations

The simulated star is based on model *S3* from Daley-Yates et al. (2016), which is summarised in Table 1. Parameters were chosen to provide a typical massive star wind, with a dipolar magnetic field centred at the origin.

Table 1. Parameters of the simulated star.

Parameter	Symbol	Value
Stellar radius	R_*	9 $\mathrm{R}_\odot$
Stellar mass	M_*	27 $\mathrm{M}_\odot$
Equatorial magnetic field strength	B_{eq}	300 G
Mass-loss rate	$\dot{M}_{B=0}$	3.2×10^{-8} $\mathrm{M}_\odot$ yr^{-1}
Wind terminal velocity	V_∞	3000 $\mathrm{km\,s^{-1}}$
Escape velocity	V_{esc}	1000 $\mathrm{km\,s^{-1}}$
Rotational rate as fraction of critical	ω	0.2 ω_{crit}
CAK force multiplier	α	0.6
Velocity law exponent	β	0.8

The public code PLUTO (version 4.2) was used to solve the MHD equations (Mignone et al., 2007). Our simulations were conducted in spherical polar coordinates and covered an extent of $r \in [1R_*, 40R_*]$ in 300 cells, $\theta \in [0, \pi]$ in 120 cells and $\phi \in [0, 2\pi]$ in 120 cells. This region was divided into a mesh with resolution in the r direction increasing from $\Delta r_1 \approx 0.00024 R_*$ to $\Delta r_{300} \approx 1.0\ R_*$. Both the θ and ϕ directions had the same resolution of $\Delta\theta_j \approx 0.026$ radians and $\Delta\phi_k \approx 0.026$ radians respectively.

Winds of massive stars are driven by absorption in emission lines, as described by (Castor et al., 1975, CAK theory hereafter). According to CAK theory, wind material accelerates as

$$g_{\mathrm{L}} \propto \left(\frac{dr/dv}{\rho} \right)^{\alpha}, \tag{1}$$

where dr/dv is the radial velocity gradient. g_{L} is incorporated into the simulations as a source term in the momentum component of the MHD equations.

Thermal radio emission was calculated accurding to Daley-Yates et al. (2016) with the spectral flux density given by

$$S_\nu = \int_0^\infty \frac{I(\nu, T)}{D^2} \mathrm{d}V. \tag{2}$$

$I(\nu, T)$ is the intensity of radio emission at frequency ν, T is the temperature, D is the distance from the star to the observer and V is the computational volume.

3. Results and Conclusions

The simulations were evolved for a total of 1 Ms in order to reach quasi-steady state. Figure 1 shows the resulting density structure. The star is at the centre with a disk structure extending into the equatorial region. The inclination of the dipole magnetic field, clockwise by 30°, warps the disk until roughly 10 R_* where it breaks up into diffuse clumps, which expand as they move radially outwards. Clumping behaviour is common in massive star winds, however the mechanism responsible is due to the intricacies of radiative line driving, which is not captured in these simulations. The interested reader is directed towards Owocki & Puls (1999) for an in-depth analysis.

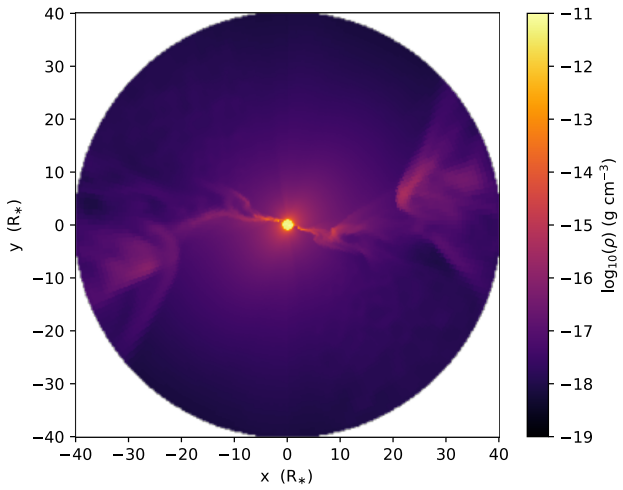

Figure 1. Density structure with the simulated star at the centre and disk structure extending to roughly 10 R_* before breaking up into diffuse clumps which expand as they move radially outwards.

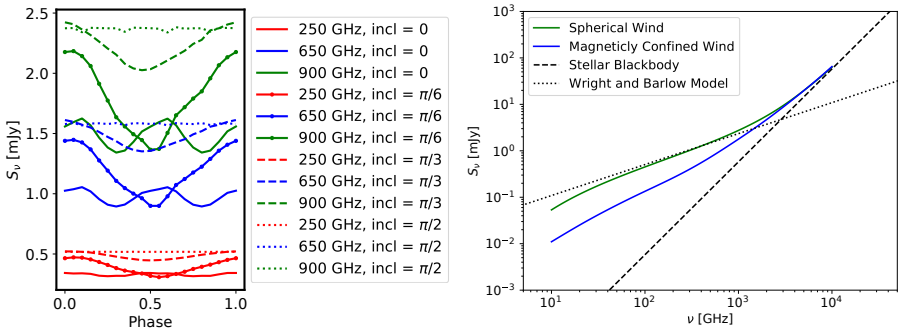

Figure 2. *Left*: rotational modulation of the radio emission at discrete frequencies and observer inclination angles. *Right*: radio continuum spectrum for the three models described in the text. The black dashed line is the stellar Planck curve the other lines are described in the text.

Synthetic radio spectra for three models are presented on the left hand image of Fig. 2. These models are used to compare spherically symmetric (both analytic (Wright & Barlow, 1975) and numerical) and the magnetically confined wind results from Fig. 1. Both spherically symmetric calculations result in good agreement, only deviating at low frequencies, due to the finite size of the computational box, as low frequency emission originates at larger radii. The spectrum of the magnetically confined wind exhibits strong deviation at all radii except at frequencies close to the Planck curve, where emission is dominated by the stellar surface. This reduction in emission is due to the confinement of the wind material into a dense structured disk in a significant departure from spherically symmetry. The free-free optical depth is proportional to the density squared, $\tau_{\rm ff} \propto \rho^2$. Material otherwise observable is obscured and increases the spectral index of the emission, leading to a decrease in emission at frequencies below the Planck curve.

Time dependent emission is illustrated in the right hand side of Fig. 2. Four angles of inclination between 0 and $\pi/2$ are explored for 250 GHz, 650 GHz and 900 GHz. Both higher frequencies and observing inclination angles lead to greater emission. This is explained by considering that emission from the far side of the disk is obstructed when viewed side on. When viewed top down, much less obstruction takes place and a greater flux reaches the observer.

Both the radio spectrum and light curves show deviations from the behaviour of spherical emission. This demonstrates that it is insufficient to simply know the emission at a given time. A full light curve, at numerous frequencies, is needed to fully understand the thermal emission from magnetically confined massive star winds.

References

Braes, L. L. E., Habing, H. J., & Schoenmaker, A. A., 1972, *Nature*, **240**, 230

Castor, J. I., Abbott, D. C. D., & Klein, 1975, *Astrophys. J.*, **195**, 157

Cohen, M. & Barlow, M. J., 1975, *Astrophys.Lett.*, **16**, 165

Daley-Yates, S., Stevens, I. R., & Crossland, T. D., 2016, *Mon. Not. R. Astron. Soc.*, **463**, 2735

Mignone, A., Bodo, G., Massaglia, S., et al., 2007, *Astrophys. J., Suppl.*, **170**, 228

Owocki, S. P. & Puls, J., 1999, *Astrophys. J.*, **510**, 355

Pittard, J. M., 2010, *Mon. Not. R. Astron. Soc.*, **403**, 1633

Townsend, R. H. D., Owocki, S. P., & Groote, D., 2005, *Astrophys. J.*, **630**, L81

ud-Doula, A. & Nazé, Y., 2016, *Adv. Space Res.*, **58**, 680

ud-Doula, A., Sundqvist, J. O., Owocki, S. P., Petit, V., & Townsend, R. H. D., 2013, *Mon. Not. R. Astron. Soc.*, **428**, 2723

Wright, A. E. & Barlow, M. J., 1975, *Mon. Not. R. Astron. Soc.*, **170**, 41

Wright, A. E., Fourikis, N., Purton, C. R., & Feldman, P. A., 1974, *Nature*, **250**, 715

Lisa Lehmann, Gaitee Hussain and Heidi Korhonen

Contrib. Astron. Obs. Skalnaté Pleso **48**, 134 – 138, (2018)

Massive star winds interacting with magnetic fields on various scales

A. David-Uraz[1], V. Petit[1], C. Erba[1], A. Fullerton[2], N. Walborn[2] and R. MacInnis[1]

[1] *Department of Physics & Astronomy, University of Delaware Newark, DE 19716, USA, (E-mail: adu@udel.edu)*

[2] *Space Telescope Science Institute Baltimore, MD 21218, USA*

Received: January 17, 2018; Accepted: January 18, 2018

Abstract. One of the defining processes which govern massive star evolution is their continuous mass loss via dense, supersonic line-driven winds. In the case of those OB stars which also host a surface magnetic field, the interaction between that field and the ionized outflow leads to complex circumstellar structures known as magnetospheres. In this contribution, we review recent developments in the field of massive star magnetospheres, including current efforts to characterize the largest magnetosphere surrounding an O star: that of NGC 1624-2. We also discuss the potential of the "analytic dynamical magnetosphere" (ADM) model to interpret multi-wavelength observations. Finally, we examine the possible effects of – heretofore undetected – small-scale magnetic fields on massive star winds and compare their hypothetical consequences to existing, unexplained observations.

Key words: stars: massive – magnetic fields – stars: mass loss

1. Introduction

One of the dominant processes driving massive star evolution is their continuous mass loss via stellar winds. These outflows are line-driven; despite having small abundances, metals possess numerous transitions (especially in the ultraviolet range of the electromagnetic spectrum) which can then lead to efficient driving in an expanding atmosphere since the associated Doppler shift counteracts the effects of saturation (for a concise review, see, e.g., Owocki 2011). Thus, ultraviolet (UV) resonance lines constitute one of the most reliable observational diagnostics of massive star winds (e.g., Pauldrach et al. 1994). This wind-launching mechanism is well described using a power-law distribution of lines, leading to well-known scalings which allow us to derive relevant wind parameters (Castor et al., 1975); theoretical mass-loss rates and terminal velocities can easily be calculated for a given star given its stellar parameters (Vink et al., 2001).

However, the picture becomes a bit more complicated when we account for the effect of surface magnetic fields. About 7% of OB stars possess detectable,

globally organized, surface magnetic fields (e.g., Morel et al. 2015; Grunhut et al. 2017). These fields are found to be mostly dipolar and stable over large periods of time (Silvester et al., 2014).

2. Magnetospheres

Surface magnetic fields redirect and confine the stellar wind, as evidenced by a number of magnetohydrodynamic (MHD) simulations (e.g., Ud-Doula et al. 2008, 2009), to form a circumstellar *magnetosphere*. Material trapped in closed field loops is forced to co-rotate with the stellar surface, leading to various observational signatures.

2.1. General structure and effects

The structure of a magnetosphere is determined by the competition between the magnetic field and the wind momentum. Within closed field loops, wind material launched from both magnetic hemispheres accumulates around the magnetic equator, forming X-ray emitting shocks. Once cooled, it falls along the field lines back onto the surface. This corresponds to a *dynamical magnetosphere*, or DM. However, around rapidly rotating stars, there is an added component as some material is centrifugally supported, preventing it from falling, thus forming dense co-rotating clouds, a so-called *centrifugal magnetosphere*, or CM (Ud-Doula et al., 2008).

While MHD simulations can provide a detailed description of magnetospheres, analytical models can help predict their behavior at a much smaller computational cost. For instance, the *Rigidly Rotating Magnetosphere* model (Townsend & Owocki, 2005) provides a useful description of CMs and successfully reproduces various observations. Likewise, the *Analytic Dynamical Magnetosphere* model (Owocki et al., 2016) was developed to describe the time-averaged structure of DMs.

On top of confining and redirecting winds, magnetic fields also lead to mass loss quenching (Ud-Doula et al., 2008) and can brake surface rotation very efficiently (Ud-Doula et al., 2009), leading to important evolutionary consequences (see Keszthelyi et al., these proceedings).

2.2. Observable consequences

According to the *Oblique Rotator Model* (Stibbs, 1950), the obliquity between the rotational and magnetic axes leads to periodic variations in the magnetospheric viewing angle. This can be seen for instance in Hα profile variations, which can be modelled with the ADM model (Owocki et al., 2016). This model can also explain the X-ray luminosity of magnetic massive stars due to magnetically confined wind shocks (Nazé et al., 2014). Early attempts (Munoz et al., these proceedings) are being made to apply the ADM model to reproduce

optical photometric variations, such as those seen in HD 191612 (Wade et al., 2011)[1]. However, as mentioned previously, the most useful observational diagnostic to probe massive star winds is UV spectroscopy. The periodic variation of UV resonance line profiles has been detected in a number of magnetic O stars, and most recently in NGC 1624-2, the most strongly magnetized O-type star known to this day (Wade et al., 2012). Figure 1 shows two resonance lines from the UV spectra of NGC 1624-2 (obtained with *HST/COS*) at high (nearly magnetic pole-on) and low (nearly magnetic equator-on) states. Their profiles show dramatic variations, as well as peculiarities that are not seen in non-magnetic stars.

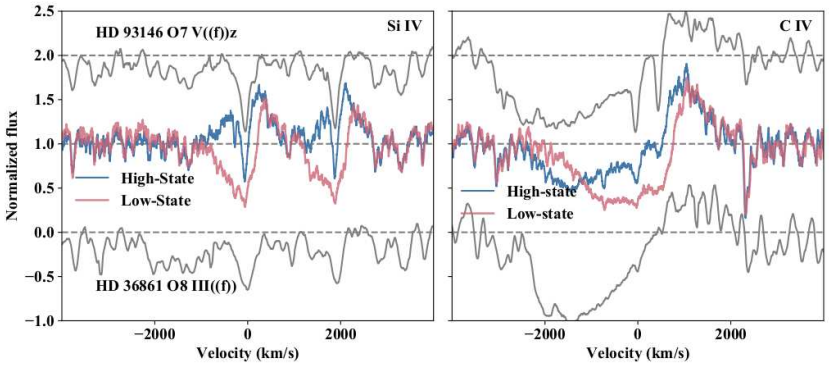

Figure 1. Comparison between the UV resonance lines of NGC 1624-2 (middle, at high and low state) and that of non-magnetic stars of similar spectral type. We can see that the magnetic star's line profiles show very different characteristics, and in particular, the CIV line is desaturated at high velocity, which might lead to an underestimation of the mass-loss rate using spherically symmetric wind models.

While synthetic line profiles computed using spherically symmetric wind models have been compared to high state observations of magnetic O stars to yield wind parameters (e.g., Marcolino et al. 2013), ongoing efforts using the ADM model suggest that this technique leads to inaccurate mass-loss rate determinations.

2.3. Complex fields

The ADM formalism accounts for a large scale dipolar field, but can also be generalized for different magnetic topologies. Though rare, some massive stars

[1]Another proposed explanation for photometric variations in O stars involves wind blanketing and the latitudinal dependence of the mass flux (Krtička 2016, and these proceedings)

exhibit complex magnetic fields, notably τ Sco (Donati et al., 2006). The ADM model can be expanded to explain the observations of such stars (Fletcher et al., these proceedings).

3. Small-scale magnetic fields

While they have not yet been detected, small-scale magnetic fields (or magnetic spots) might arise as a consequence of the subsurface convection zone due to the iron opacity bump, and are expected to cause photospheric brightness variations (Cantiello & Braithwaite, 2011). Such bright spots have been detected in ξ Per (Ramiaramanantsoa et al., 2014) and ζ Pup (Ramiaramanantsoa et al., 2018). Hydrodynamical models (Cranmer & Owocki, 1996; David-Uraz et al., 2017) show that bright spots might be the cause of the puzzling *discrete absorption components* (DACs; e.g., Kaper et al. 1996).

4. Conclusions and future work

Magnetic fields profoundly influence the density and velocity structure of massive star winds. This means that spherically symmetric wind models cannot lead to proper determinations of wind parameters. Future studies will test the ADM model and use it to determine the wind properties of magnetic massive stars.

While magnetic spots offer an attractive explanation of phenomena such as DACs, they have yet to be detected. Such an undertaking will require very deep magnetometry (Kochukhov & Sudnik, 2013) and requires a significant observational effort.

Acknowledgements. ADU gratefully acknowledges support from the *Fonds québécois de la recherche en nature et technologies*. This research is based on observations made with the NASA/ESA *Hubble Space Telescope*, which is operated by the Association of Universities for Research in Astronomy, Inc., under NASA contract NAGS 5-26555. Support for HST General Observer Program number GO-13734 was provided by NASA through a grant from the Space Telescope Science Institute, which is operated by the Association of Universities for Research in Astronomy, Incorporated, under NASA contract NAS5-26555.

References

Cantiello, M. & Braithwaite, J. 2011, *Astron. Astrophys.*, **534**, A140

Castor, J. I., Abbott, D. C., & Klein, R. I. 1975, *Astrophys. J.*, **195**, 157

Cranmer, S. R. & Owocki, S. P. 1996, *Astrophys. J.*, **462**, 469

David-Uraz, A., Owocki, S. P., Wade, G. A., Sundqvist, J. O., & Kee, N. D. 2017, *Mon. Not. R. Astron. Soc.*, **470**, 3672

Donati, J.-F., Howarth, I. D., Jardine, M. M., et al. 2006, *Mon. Not. R. Astron. Soc.*, **370**, 629

Grunhut, J. H., Wade, G. A., Neiner, C., et al. 2017, *Mon. Not. R. Astron. Soc.*, **465**, 2432

Kaper, L., Henrichs, H. F., Nichols, J. S., et al. 1996, *Astron. Astrophys., Suppl.*, **116**, 257

Kochukhov, O. & Sudnik, N. 2013, *Astron. Astrophys.*, **554**, A93

Krtička, J. 2016, *Astron. Astrophys.*, **594**, A75

Marcolino, W. L. F., Bouret, J.-C., Sundqvist, J. O., et al. 2013, *Mon. Not. R. Astron. Soc.*, **431**, 2253

Morel, T., Castro, N., Fossati, L., et al. 2015, in IAU Symposium, Vol. **307**, *New Windows on Massive Stars*, ed. G. Meynet, C. Georgy, J. Groh, & P. Stee, 342–347

Nazé, Y., Petit, V., Rinbrand, M., et al. 2014, *Astrophys. J., Suppl.*, **215**, 10

Owocki, S., Theory of Winds from Hot, Luminous Massive Stars. 2011, *Bulletin de la Societe Royale des Sciences de Liege*, **80**, 16

Owocki, S. P., ud-Doula, A., Sundqvist, J. O., et al. 2016, *Mon. Not. R. Astron. Soc.*, **462**, 3830

Pauldrach, A. W. A., Kudritzki, R. P., Puls, J., Butler, K., & Hunsinger, J. 1994, *Astron. Astrophys.*, **283**, 525

Ramiaramanantsoa, T., Moffat, A. F. J., Chené, A.-N., et al. 2014, *Mon. Not. R. Astron. Soc.*, **441**, 910

Ramiaramanantsoa, T., Moffat, A. F. J., Harmon, R., et al. 2018, *Mon. Not. R. Astron. Soc.*, **473**, 5532

Silvester, J., Kochukhov, O., & Wade, G. A. 2014, *Mon. Not. R. Astron. Soc.*, **440**, 182

Stibbs, D. W. N., 1950, *Mon. Not. R. Astron. Soc.*, **110**, 395

Townsend, R. H. D. & Owocki, S. P. 2005, *Mon. Not. R. Astron. Soc.*, **357**, 251

Ud-Doula, A., Owocki, S. P., & Townsend, R. H. D. 2008, *Mon. Not. R. Astron. Soc.*, **385**, 97

Ud-Doula, A., Owocki, S. P., & Townsend, R. H. D. 2009, *Mon. Not. R. Astron. Soc.*, **392**, 1022

Vink, J. S., de Koter, A., & Lamers, H. J. G. L. M. 2001, *Astron. Astrophys.*, **369**, 574

Wade, G. A., Howarth, I. D., Townsend, R. H. D., et al. 2011, *Mon. Not. R. Astron. Soc.*, **416**, 3160

Wade, G. A., Maíz Apellániz, J., Martins, F., et al. 2012, *Mon. Not. R. Astron. Soc.*, **425**, 1278

Contrib. Astron. Obs. Skalnaté Pleso **48**, 139 – 143, (2018)

Constraining the weak-wind problem: an XMM-HST campaign for the magnetic O9.7 V star HD 54879

T. Shenar[1], L. M. Oskinova[1], S. P. Järvinen[2], P. Luckas[3], R. Hainich[1], H. Todt[1], S. Hubrig[2], A. A. C. Sander[1], I. Ilyin[2] and W.-R. Hamann[1]

[1] *University of Potsdam, Potsdam, Germany*
(E-mail: shtomer@astro.physik.uni-potsdam.de)
[2] *Leibniz-Institute for Astrophysics, Potsdam, Germany*
[3] *The University of Western Australia, Crawley WA 6009, Australia*

Received: September 25, 2017; Accepted: October 10, 2017

Abstract. Mass-loss rates of massive, late type main sequence stars are much weaker than currently predicted, but their true values are very difficult to measure. We suggest that confined stellar winds of magnetic stars can be exploited to constrain the true mass-loss rates $\dot{M}$ of massive main sequence stars. We acquired UV, X-ray, and optical amateur data of HD 54879 (O9.7 V), one of a few O-type stars with a detected atmospheric magnetic field ($B_\mathrm{d} \gtrsim 2\,\mathrm{kG}$). We analyze these data with the Potsdam Wolf-Rayet (PoWR) and XSPEC codes. We can roughly estimate the mass-loss rate the star would have in the absence of a magnetic field as $\log \dot{M}_{B=0} \approx -9.0\,\mathrm{M_\odot\,yr^{-1}}$. Since the wind is partially trapped within the Alfvén radius $r_\mathrm{A} \gtrsim 12\,R_*$, the true mass-loss rate of HD 54879 is $\log \dot{M} \lesssim -10.2\,\mathrm{M_\odot\,yr^{-1}}$. Moreover, we find that the microturbulent, macroturbulent, and projected rotational velocities are lower than previously suggested ($< 4\,\mathrm{km\,s^{-1}}$). An initial mass of $16\,\mathrm{M_\odot}$ and an age of 5 Myr are inferred. We derive a mean X-ray emitting temperature of $\log T_\mathrm{X} = 6.7\,\mathrm{K}$ and an X-ray luminosity of $\log L_\mathrm{X} = 32\,\mathrm{erg\,s^{-1}}$. The latter implies a significant X-ray excess ($\log L_\mathrm{X}/L_\mathrm{Bol} \approx -6.0$), most likely stemming from collisions at the magnetic equator. A tentative period of $P \approx 5\,\mathrm{yr}$ is derived from variability of the Hα line. Our study confirms that strongly magnetized stars lose little or no mass, and supplies important constraints on the weak-wind problem of massive main sequence stars.

Key words: stars: massive – stars: magnetic field – stars: mass-loss

1. Introduction

Massive, late-type main sequence stars are generally known to exhibit mass-loss rates that are orders of magnitude lower than predicted by theory, often referred to as the *weak wind problem* (e.g., Martins et al., 2005; Oskinova et al., 2006). As a consequence of this, typical spectral diagnostics of mass-loss are void of stellar-wind signatures and cannot be used to measure $\dot{M}$ for such stars. However, in the presence of global magnetic fields, stellar winds are confined

to stream along to field lines (e.g., ud-Doula & Owocki, 2002), leading to a significant density enhancement that leaves a spectroscopic signature. In our study, we analyze the magnetic O-type star HD 54879. For details, we refer the reader to our recently published study (Shenar et al., 2017, S2017 hereafter).

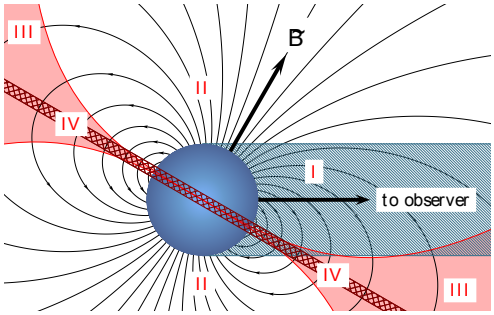

Figure 1. A schematic sketch of a star with a global dipole magnetic field, illustrating the formation regions of different features in the spectrum of HD 54879. See S2017 for details.

The subject of our study, HD 54879, was classified as O9.7 V. Castro et al. (2015) measured a longitudinal magnetic field reaching a maximum of $|B_z| \approx 600$ G for HD 54879, from which they estimated a dipole field of $B_d \gtrsim 2$ kG. The star is believed to reside in the CMa OB1 association, with an estimated distance of $d \approx 1$ kpc (Gregorio-Hetem, 2008). To study HD 54879, we perform a multiwavelength spectral analysis of UV and X-ray spectra acquired by us simultaneously with the *Hubble Space Telescope* (*HST*), and the *XMM-Newton* satellite, complemented by optical HARPS and amateur spectra (see S2017). For the analysis of the UV and optical spectra, we utilize the Potsdam Wolf-Rayet (PoWR) code (Hamann et al., 2006), while the X-ray analysis is performed with the XSPEC software. The combination of X-ray, UV, and optical data is essential, as these spectral ranges probe different regions of the magnetosphere and stellar wind (see Fig. 1).

2. Results

The PoWR code is an established tool for the spectroscopy of massive stars, but relies on the assumption of spherical symmetry, which breaks in the case of magnetic stars. Nevertheless, as we show below, we can derive the photospheric parameters and constrain the wind properties of HD 54879.

2.1. The photosphere

While variability observed in the Hα line is suggestive of a period of $P \approx 5$ yr (Fig. 15 in S2017), no notable variability is observed in photospheric features of HD 54879 along ≈ 6 yr of observing time. We conclude that the impact of the magnetic field on the photosphere is negligible. This is supported by our success to reproduce the majority of the observed photospheric features with our models. The effective temperature $T_{\rm eff}$ is derived from the ratios between lines from different ionization stages (e.g., He I, II, see Fig. 5 in S2017), while the surface gravity g_* is derived from the profiles and strengths of Balmer and

He II lines (see Fig. 4 in S2017). The luminosity and extinction are derived by fitting the observed spectral energy distribution (Fig. 2 in S2017). Overall, the physical parameters are found to be very typical for an O9.7 V star (see S2017 for their full compilation). Two peculiar results involving the photosphere are, however, striking.

Firstly, the macroturbulent ($v_{\rm mac}$), microturbulent (ξ), and projected rotational ($v \sin i$) velocities are found to be much smaller than values reported for other massive stars. In fact, only an upper limit of $4\,{\rm km\,s^{-1}}$ can be derived for all three velocities, since the line widths are dominated by thermal broadening (Fig. 6 in S2017). The low value of $v \sin i$ may very well be due to angular momentum loss via magnetic breaking, but the strength of the magnetic field does not seem to be sufficient to suppress convective motions in sub-photospheric layers of HD 54879 (cf. Sundqvist & Owocki, 2013). The low values of ξ and $v_{\rm mac}$ may therefore be related to the relatively late-type of HD 54879, as late-type massive stars seem to systematically show weaker turbulence (cf. Simón-Díaz et al., 2017).

Secondly, the derived carbon and nitrogen abundances are found to be subsolar by about a factor of three (see Table 2 in S2017), a result also reported by Castro et al. (2015). This stands in contrast to reports of nitrogen enhancements in magnetic B-type stars (Morel et al., 2008). While this result may be explained by a non-homogeneous distribution of the different chemical species over the stellar surface, the lack of photospheric variability does not support this hypothesis.

2.2. The magnetosphere

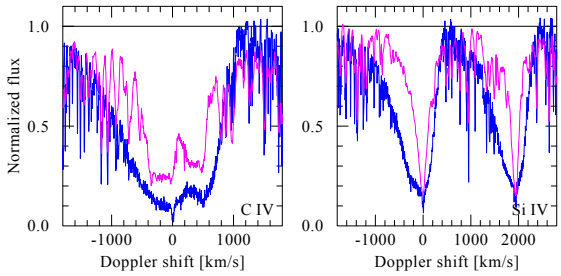

Figure 2. Comparison of normalized *HST* observations of the O9.7 V star HD 36512 (ID: 13346, PI: Ayres, pink solid line) and of HD 54879 (blue solid line)

A comparison of *HST* UV data of the prototypical O9.7 V star υ Ori (HD 36512) with the *HST* data collected for our target, HD 54879, is shown in Fig. 2, where we focus on the two most prominent wind features, the resonance lines C IV $\lambda\lambda 1548, 1551$ and Si IV $\lambda\lambda 1394, 1403$. It is evident that υ Ori shows no,

or very little, evidence for a stellar wind, allowing only for an upper-limit of $\dot{M}$ to be derived. In contrast to υ Ori, our target shows a clear asymmetry that is suggestive of absorption stemming from matter surrounding the star. The profiles of HD 54879 have unusually shallow blueshifted edges, suggesting the presence of a large velocity dispersion, reaching a maximum speed of $\approx 1\,000\,\mathrm{km\,s^{-1}}$. Similar line profiles were reported in other studies of magnetic stars (e.g., Nazé et al., 2015).

Solving the full non-LTE radiative transfer in the presence of a magnetic field in 3D is currently not feasible and beyond the scope of this study. Instead, we simulate the motion of the matter along the field lines by a turbulent velocity which is strongly enhanced close above the stellar surface, at $r \approx 1.1\,R_*$. We find the best fit for the combination of $\upsilon_{\infty,\mathrm{sph}} = 300\,\mathrm{km\,s^{-1}}$, $\xi_{\mathrm{wind,sph}} = 500\,\mathrm{km\,s^{-1}}$, and $\log \dot{M}_{\mathrm{sph}} = -8.8\,\mathrm{M_\odot\,yr^{-1}}$. X-ray ionization is approximately accounted for in a spherically-symmetric fashion based on our X-ray analysis (see Sects. 3.4 and 5 in S2017). The resulting fit for key diagnostics is shown in Fig. 3. However, because of the false assumption of spherical symmetry, these parameters cannot be assumed to correspond to actual physical parameters. Rather, these parameters serve to reproduce the conditions in the formation region of the resonance lines.

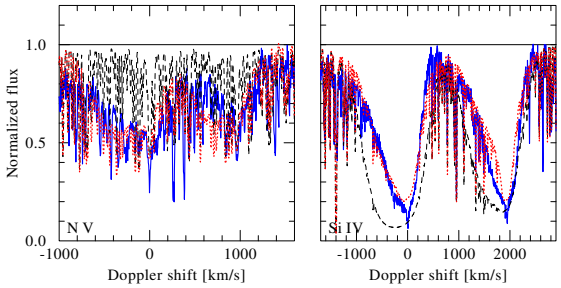

Figure 3. Normalized *HST* observations of HD 54879 (blue solid line) compared to our best-fitting model (red dotted line) and to the same model without the inclusion of X-rays (black dashed line)

By comparing the derived densities to predictions by an analytical model derived for stars with a constant outflow and a global dipole magnetic field (Owocki et al., 2016), we can provide a rough estimate of the mass-loss rate that HD 54879 would have in the absence of a magnetic field, $\dot{M}_{B=0}$. Doing so, we find $\log \dot{M}_{B=0} \approx -9.0\,\mathrm{M_\odot\,yr^{-1}}$. This value, which is expected to represent the mass-loss rate of a *non-magnetic* O9.7 V star, is more than an order of magnitude lower than predicted by theory (Vink et al., 2000), but in line with values reported for other stars of similar spectral type (e.g., Marcolino et al., 2009). From this, we can constrain the Alfvén radius to $r_{\mathrm{A}} \gtrsim 12\,R_*$. The true

mass-loss from the star is then estimated to be $\log \dot{M} \lesssim -10.2\,\mathrm{M}_\odot\,\mathrm{yr}^{-1}$ (see equations 1-3 of Petit et al., 2017).

3. Summary

We performed a multiwavelength (X-ray to optical) spectral analysis of the object HD 54879, one of about a dozen O-type stars for which a magnetic field was reported. Furthermore, spectroscopic variability of the Hα line was studied. A detailed account of our analysis and results can be found in S2017. Most importantly, we took advantage of the density enhancement caused by the magnetic confinement of the stellar wind to estimate $\dot{M}_{B=0} \approx -9.0\,\mathrm{M}_\odot\,\mathrm{yr}^{-1}$. This value should represent the mass-loss rate of non-magnetic stars of similar spectral types, but is very difficult to measure in non-magnetic stars. We therefore encourage future studies to further exploit magnetically-confined winds to quantify the poorly-known mass-loss rates of massive main sequence stars.

References

Castro, N., Fossati, L., Hubrig, S., et al. 2015, *Astron. Astrophys.*, **581**, A81

Gregorio-Hetem, J. 2008, in *Handbook of Star Forming Regions: Vol. II, The Southern Sky*, ed. B. Reipurth (San Francisco, CA: ASP), 1

Hamann, W.-R., Gräfener, G., & Liermann, A. 2006, *Astron. Astrophys.*, **457**, 1015

Marcolino, W. L. F., Bouret, J.-C., Martins, F., et al. 2009, *Astron. Astrophys.*, **498**, 837

Martins, F., Schaerer, D., Hillier, D. J., et al. 2005, *Astron. Astrophys.*, **441**, 735

Morel, T., Hubrig, S., & Briquet, M. 2008, *Astron. Astrophys.*, **481**, 453

Nazé, Y., Sundqvist, J. O., Fullerton, A. W., et al. 2015, *Mon. Not. R. Astron. Soc.*, **452**, 2641

Oskinova, L. M., Feldmeier, A., & Hamann, W.-R. 2006, *Mon. Not. R. Astron. Soc.*, **372**, 313

Owocki, S. P., ud-Doula, A., Sundqvist, J. O., et al. 2016, *Mon. Not. R. Astron. Soc.*, **462**, 3830

Petit, V., Keszthelyi, Z., MacInnis, R., et al. 2017, *Mon. Not. R. Astron. Soc.*, **466**, 1052

Shenar, T., Oskinova, L. M., Järvinen, S. P., et al. 2017, *Astron. Astrophys.*, **606**, A91

Simón-Díaz, S., Godart, M., Castro, N., et al. 2017, *Astron. Astrophys.*, **597**, A22

Sundqvist, J. O. & Owocki, S. P. 2013, *Mon. Not. R. Astron. Soc.*, **428**, 1837

ud-Doula, A. & Owocki, S. P. 2002, *Astrophys. J.*, **576**, 413

Vink, J. S., de Koter, A., & Lamers, H. J. G. L. M. 2000, *Astron. Astrophys.*, **362**, 295

Contrib. Astron. Obs. Skalnaté Pleso **48**, 144 – 148, (2018)

Detailed ADM-based Modeling of Shock Retreat and X-ray Emission of τ Sco

C. L. Fletcher[1], V. Petit[2], D. H. Cohen[3], R. H. Townsend[4] and G. A Wade[5]

[1] *Department of Physics and Space Sciences, Florida Institute of Technology, Melbourne, FL 32901, USA, (E-mail: cfletcher2013@my.fit.edu)*

[2] *Department of Physics and Astronomy, University of Delaware, Newark, DE 19716, USA*

[3] *Department of Physics and Astronomy, Swarthmore College, Swarthmore, PA 19081, USA*

[4] *Department of Astronomy, University of Wisconsin-Madison, Madison, WI 53706, USA*

[5] *Department of Physics and Space Science, Royal Military College of Canada, Kingston, ON, Canada K7K 0C6*

Received: November 10, 2017; Accepted: November 15, 2017

Abstract. Leveraging the improvement of spectropolarimeters over the past few decades, surveys have found that about 10% of OB-type stars host strong ($\sim$ kG) and mostly dipolar surface magnetic fields. One B-type star, τ Sco, has a more complex surface magnetic field than the general population of OB stars. Interestingly, its X-ray luminosity is an order of magnitude higher than predicted from analytical models of magnetized winds. Previous studies of τ Sco's magnetosphere have predicted that the region of closed field loops should be located close to the stellar surface. However, the lack of X-ray variability and the location of the shock-heated plasma measured from forbidden-to-intercombination X-ray line ratios suggest that the hot plasma, and hence the closed magnetic loops, extend considerably farther from the stellar surface, implying a significantly lower mass loss rate than initially assumed. We present an adaptation of the Analytic Dynamical Magnetosphere model, describing the magnetic confinement of the stellar wind, for an arbitrary field loop configuration. This model is used to predict the shock-heated plasma temperatures for individual field loops, which are then compared to high resolution grating spectra from the Chandra X-ray Observatory. This comparison shows that larger closed magnetic loops are needed.

Key words: magnetic fields – stars: massive – x-rays: general – stars: winds, outflows

1. Introduction

With recent spectropolarimetric advancements, the number of magnetic OB stars has grown rapidly (Wade et al., 2016; Schöller et al., 2017). These stars

host strong ($\sim$ kG), mostly dipolar magnetic fields. The magnetically confined wind shock (MCWS) paradigm, first developed by Babel & Montmerle (1997) and refined by ud-Doula & Owocki (2002), explains the formation of a circumstellar magnetosphere by the competition of the magnetic field with the stellar wind. For regions close to the photosphere, the magnetic field energy density is larger than the stellar wind kinetic energy density, resulting in closed magnetic loops. In these regions, the stellar wind is forced to flow along the magnetic loop from the surface footpoints until it collides with the corresponding flow from the opposite hemisphere. Since the velocity of the stellar wind is supersonic, the collision will result in a shock. As the shocked material cools radiatively, it will emit photons in the X-ray waveband.

The Analytic Dynamical Magnetosphere (ADM) model was developed by Owocki et al. (2016) to provide an analytical scaling for the MCWS model that could reproduce time-averaged results from MHD simulations and be used to quickly calculate observable diagnostics at many wavelengths. A key parameter of the ADM model is the wind magnetic confinement parameter (η_*), relating the stellar kinetic energy density to the magnetic field energy density near the stellar surface, and providing a simple way to find the apex heights of the last closed field loops for a dipolar magnetic field (ud-Doula & Owocki, 2002).

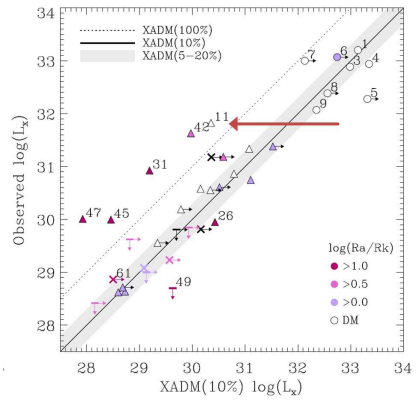

Figure 1. A comparison of the observed and XADM-predicted X-ray luminosity for all the magnetic OB stars with modern X-ray observations (Nazé et al., 2014). τ Sco is #11 in the small group of overluminous stars shown with the red arrow.

For typical O-type stars, the stellar wind is dense and cools efficiently once shocked. The post-shock material will cool quickly as it expands from the shock front to the loop apex, resulting in a narrow post shock region. However, for B-type stars with low-density stellar winds that do not cool as efficiently, the post shock region will be larger pushing the shock front down the field loop closer to

the stellar radius. Since the velocity of the stellar wind increases monotonically with radial distance from the stellar surface, a retreat of the shock front towards the stellar surface will result in lower shock jump velocities and lower post-shock temperatures. This phenomenon is called "shock retreat" and is addressed by the X-ray ADM (XADM, ud-Doula et al., 2014) model. The XADM model uses a similar analytical scaling as presented by the ADM model but focuses on determining the X-ray properties.

Nazé et al. (2014) performed a study of all of the known magnetic OB-type stars with existing modern X-ray observations. The observed X-ray luminosity was then compared to that predicted by the XADM model. This study identified a small group of X-ray "overluminous" stars shown in Fig. 1. The majority of these overluminous stars are rapid rotators, except for τ Sco (#11 in Fig. 1). One hypothesis proposed to explain why τ Sco appears overluminous is that it has a more complex magnetic field than the dipolar approximation made by the XADM model.

2. An ADM Model for an Arbitrary Field Topology

Donati et al. (2006) observed that the magnetic field of τ Sco was significantly more complex than a dipole. Using Zeeman-Doppler imaging surface field topology maps, the magnetic field loops can be extrapolated to give a three dimensional model using the assumption that the field can be expressed as the gradient of a scalar potential (Jardine et al., 1999). An important parameter in extrapolating the magnetic field is the so-called "source radius", corresponding to the radius of the last closed field loop.

The last closed field loop depends directly on η_* and therefore the mass loss rate. Mass loss rates for main sequence B-type stars are uncertain, especially for magnetic stars. Donati et al. (2006) used a source radius of $2R_*$ corresponding to a mass loss rate of $\dot{M} = 2\times10^{-8}\mathrm{M}_\odot\,\mathrm{yr}^{-1}$ with a polar magnetic field strength of 100G.

As the ADM model was previously developed for dipolar field configurations, we adapted the ADM scaling relations for arbitrary field loops to determine the temperatures and velocities of the confined wind plasma. We then applied this model to the field extrapolation of τ Sco's surface field maps (Fig. 3) and compared with the observed time variability, f/i-inferred radii and modeled APEC plasma temperatures.

The high resolution grating spectrum from the Chandra X-ray Observatory of τ Sco (Cohen et al., 2003) was modeled with APEC plasma temperature models using XSPEC to determine the temperatures needed to reproduce features present in the spectrum (Fig. 2). Comparing the modeled temperatures to the shock temperatures determined by the arbitrary ADM model (Fig. 3), it is shown that compact closed field loops, as implied by the $2R_*$ source radius, do not produce strong enough shocks to create the observed short wavelength line

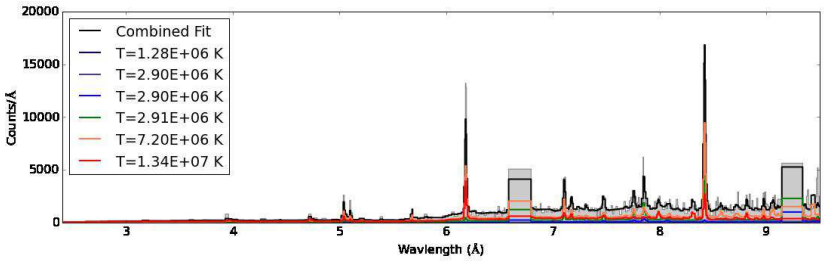

Figure 2. Part of the Chandra high resolution grating spectrum for τ Sco modeled with APEC plasma models (V. Petit et al. in prep.). The modeled temperatures are compared to the post-shock temperatures produced in the arbitrary XADM model.

emission.

With the compact field loops of the $2R_*$ source radius model, we should also expect to see periodic variations in the X-rays produced as the star rotates. However, from Suzaku observations obtained at various phases, Ignace et al. (2010) reported that there appears to be no periodic variations in the X-ray counts, suggesting a larger source radius, and therefore a smaller mass loss rate, is needed. Our calculations seem to agree with this hypothesis.

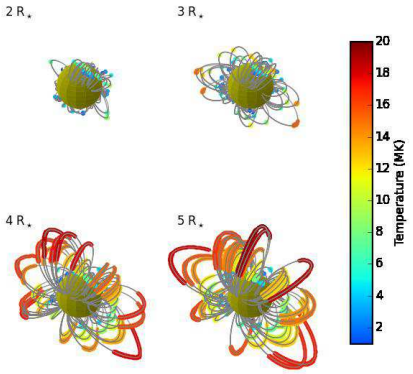

Figure 3. 3-dimensional magnetic field plots of τ Sco for some source radii. The immediate post-shock temperature for each loop and the extent of the shock region along the loop are displayed with the color scheme. As the field loops get larger, the shock temperatures increase (V. Petit et al. in prep.).

By analyzing the ratio of the forbidden line to the intercombination line (f/i ratio) found in helium-like ions such as magnesium, or silicon, we can predict the location of the X-ray emitting plasma. For τ Sco, the f/i ratios from the

high resolution Chandra spectrum determined for magnesium indicate the X-rays to be emitted around $2.65R_*$ above the photosphere and the silicon f/i ratios provide a lower limit of $2.44R_*$ above the photosphere (V. Petit et al. in prep.). These results further support the need for a source radius larger than $2R_*$. Therefore, a field extrapolation for source radii of $3R_*$, $4R_*$, and $5R_*$ was performed (Fig. 3). The largest source radius requires a reduction of the Donati et al. (2006) mass loss rate by a factor of 42, which we adjust accordingly when determining the shock retreat. The mass loss rate for $5R_*$ is on the low end of predicted values, but comparable to those determined by Oskinova et al. (2011).

Applying the arbitrary ADM model to the 3-dimensional magnetic field loops for the other three source radii shows that the post-shock temperatures will increase for a larger source radius. Although the shock retreat for the larger loops extends further toward the stellar surface, it is not enough to quench the higher post-shock temperatures needed to reproduce the observed spectral features seen in Fig.2. The bulk of the X-rays are well above the surface, resulting in less variability than observed due to the star producing less occultation. Constraining the source radius would help to constrain the mass loss rate for τ Sco, however, more work is needed to directly recover the X-ray luminosity from the arbitrary ADM model.

References

Babel, J. & Montmerle, T. 1997, *Astron. Astrophys.*, **323**, 121

Cohen, D. H., de Messières, G. E., MacFarlane, J. J., et al. 2003, *Astrophys. J.*, **586**, 495

Donati, J.-F., Howarth, I. D., Jardine, M. M., et al. 2006, *Mon. Not. R. Astron. Soc.*, **370**, 629

Ignace, R., Oskinova, L. M., Jardine, M., et al. 2010, *Astrophys. J.*, **721**, 1412

Jardine, M., Barnes, J. R., Donati, J.-F., & Collier Cameron, A. 1999, *Mon. Not. R. Astron. Soc.*, **305**, L35

Nazé, Y., Petit, V., Rinbrand, M., et al. 2014, *Astrophys. J., Suppl. Ser.*, **215**, 10

Oskinova, L. M., Todt, H., Ignace, R., et al. 2011, *Mon. Not. R. Astron. Soc.*, **416**, 1456

Owocki, S. P., ud-Doula, A., Sundqvist, J. O., et al. 2016, *Mon. Not. R. Astron. Soc.*, **462**, 3830

Schöller, M., Hubrig, S., Fossati, L., et al. 2017, *Astron. Astrophys.*, **599**, A66

ud-Doula, A., Owocki, S., Townsend, R., Petit, V., & Cohen, D. 2014, *Mon. Not. R. Astron. Soc.*, **441**, 3600

ud-Doula, A. & Owocki, S. P. 2002, *Astrophys. J.*, **576**, 413

Wade, G. A., Neiner, C., Alecian, E., et al. 2016, *Mon. Not. R. Astron. Soc.*, **456**, 2

Contrib. Astron. Obs. Skalnaté Pleso **48**, 149 – 153, (2018)

The Of?p stars of the Magellanic Clouds: Are they strongly magnetic?

M. Munoz[1], G. A. Wade[2], Y. Nazé[3], S. Bagnulo[4] and J. Puls[5]

[1] *Queen's University, Kingston, Ontario, Canada*
(E-mail: 16msm5@queensu.ca)
[2] *Royal Military College, Kingston, Ontario, Canada*
[3] *Université de Liège, 4000 Liège, Belgium*
[4] *Armagh Observatory, Armagh BT61 9DG, Northern Ireland, UK*
[5] *Universitätssternwarte, D-81679 München, Germany*

Received: November 11, 2017; Accepted: November 15, 2017

Abstract. All known Galactic Of?p stars have been shown to host strong, organized, magnetic fields. Recently, five Of?p stars have been discovered in the Magellanic Clouds. They posses photometric (Nazé et al., 2015) and spectroscopic (Walborn et al., 2015) variability compatible with the Oblique Rotator Model (ORM). However, their magnetic fields have yet to be directly detected. We have developed an algorithm allowing for the synthesis of photometric observables based on the Analytic Dynamical Magnetosphere (ADM) model by Owocki et al. (2016). We apply our model to OGLE photometry in order to constrain their magnetic geometries and surface dipole strengths. We predict that the field strengths for some of theses candidate extra-Galactic magnetic stars may be within the detection limits of the FORS2 instrument

Key words: stars: massive – stars: magnetic fields – stars: rotation – stars: chemically peculiar

1. Introduction

Of?p stars are a rare class of chemically peculiar O-type stars. They are characterized by the presence of strong NIII λ4634-41 and CIII λ4686 emission lines. In Nazé et al. (2008), the Galactic sample of Of?p stars were shown to display phase-locked spectroscopic and photometric variability that is reminiscent of a magnetic oblique rotator model. Searching for Magnetism in Massive Stars (MiMeS), the MiMeS survey confirmed magnetic detections in all Galactic Of?p stars (Grunhut et al., 2017), thus linking their anomalous surface abundances to the presence of magnetic fields.

Recently, a small sample of extra-Galactic Of?p stars have been detected in the Small and Large Magellanic Clouds (Walborn et al., 2015). Similar to the Galactic sample of Of?p stars, the Magellanic Of?p stars also possess phase dependent spectroscopic and photometric variability (Nazé et al., 2015). It is therefore highly suspected that the Magellanic Of?p stars host magnetic fields

as well. Despite a first attempt to detect these proposed magnetic fields using the FORS2 instrument at VLT, none were detected due to poor weather conditions and non-optimal observing times (Bagnulo et al., 2017).

Therefore, we propose an indirect method to infer the magnetic field properties of magnetic massive stars via modeling of the photometric variations caused by the rotation-phase-dependent scattering of their photospheric light by their magnetospheres. Since stars residing in the Magellanic Clouds have intrinsically lower metallicities than those from the Milky way, this investigation may provide useful insight on the impact of metallicity on the ORM paradigm.

In Sect.
refsec:model, we will describe the numerical method allowing for the light curve synthesis and consider the effect of metallicity on some sample light curves. In Sect. 3, we will first apply our algorithm to archival Hipparcos photometry of the thoroughly-studied Galactic Of?p star HD 191612 (Wade et al., 2011) as a proof of concept, and then on the recent OGLE photometry of the Magellanic Of?p stars (Nazé et al., 2015). Finally, we will summarize our results in the last section.

2. The model light curves

2.1. The algorithm

For a wind dominated by electron scattering (which is appropriate for hot massive stars), the photometric variability will be modulated by the amount of plasma occulting the star's surface along the line-of-sight of an observer. This is parametrized via the α angle corresponding to the inclination of the magnetic equator with respect to the observer's line-of-sight. The projection of such an angle is

$$\cos\alpha = \cos\phi \sin\beta + \cos\beta \cos i, \tag{1}$$

where i is the inclination angle (angle between the observer's line-of-sight and the rotation axis), β is the magnetic obliquity (angle between the magnetic axis and the rotation axis) and ϕ is the rotational phase.

At each rotational phase, the differential magnitude due to an optically thin single electron scattering wind is given by

$$\Delta m = \Delta m_0 + (2.5 \log e)\tau, \tag{2}$$

where Δm_0 is a constant magnitude shift and τ is the Thompson scattering optical depth. For an observer arbitrarily placed on the z axis, the line-of-sight optical depth will be related to the magnetosphere density, ρ, as follows

$$\tau = \frac{\alpha \sigma_e}{m_p} \int \rho dz, \tag{3}$$

where σ_e is the Thompson cross section, α is the free electron baryon mass and m_p is the mass of a proton. For a completely ionized gas composed of helium, that is suitable for hot massive stars, $\alpha = 0.5$.

The density structure surrounding the star is provided by the Analytic Dynamical Magnetosphere (ADM) model from Owocki et al. (2016). The ADM model is capable of characterizing the density, temperature and wind flow structures via analytical prescriptions. For simplicity, it assumes a dipolar field geometry which is observationally consistent with the well-known Galactic Of?p stars (Grunhut et al., 2017). Traditionally, magnetosphere models were obtained using computationally expensive MHD simulations. As the ADM model is vastly more computationally efficient and was shown to be in good agreement with more sophisticated MHD simulations (Owocki et al., 2016), we have chosen to implement the ADM formalism.

2.2. The effect of metallicity

Studying stars outside the Milky Way presents a unique opportunity to investigate the effect of varying metallicity (Z). To anticipate this effect, we will synthesize and compare model light curves at three different metallicities: solar ($Z_\odot$), $0.5\,Z_\odot$ for the Large Magellanic Cloud (LMC) and $0.2\,Z_\odot$ for the Small Magellanic Cloud (SMC). Using stellar and magnetic parameters from Wade et al. (2011), the original light curve, at solar metallicity, will be based upon the prototypical Galactic Of?p star, HD 191612. The subsequent light curves will be computed with adjusted mass-loss rates and wind terminal velocities that are scaled according to Z using Vink et al. (2001) prescriptions.

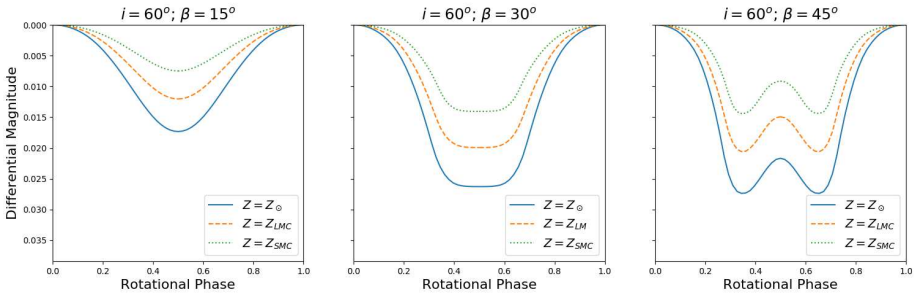

Figure 1. Model light curves with constant inclination. The different panels show curves of increasing obliquity: 15° (left), 30°(middle) and 45° (right). Over-plotted on each panel are curves of decreasing metallicity: $Z_\odot$ (solid), $0.5\,Z_\odot$ (dashed) and $0.2\,Z_\odot$ (dotted).

Figure 1 illustrates the effect of decreasing Z for a selection of $i + \beta$ angles. Panels from left to right, show increasing angles of $i + \beta$. Overplotted on each

panel are curves of decreasing Z. We notice that curves with $i+\beta = 90°$ are flat bottomed and mark the transition from single peaked curves ($i + \beta < 90°$) to double peaked curves ($i + \beta > 90°$). This is because at high $i + \beta$, the magnetic equator, corresponding to the densest region of the magnetosphere, crosses the observer's line-of-sight twice during one rotational cycle. Furthermore, we can see that curves with lower metallicities have linearly scaled down occultation depths. This is to be expected as lowering the metallicity will lower the star's mass-loss rate and thus the magnetosphere density as well. As a decrease in density effectively yields a decrease in opacity, the overall light curve depth will diminish. Therefore, a change in metallicity can only account for linear scalings. In contrast, the increase of $i + \beta$ can morphologically change the light curve shape that is essentially related to the double peak separation.

3. Applications

3.1. HD 191612

HD 191612 is a well-known Galactic Of?p star with observationally constrained magnetic field strength and field geometry. From longitudinal magnetic field measurements, a dipolar field strength of $B_d = 2\,450 \pm 400\,\mathrm{G}$ was obtained satisfying the general set of solutions characterized by $i + \beta = 95 \pm 10\,°$. While tentative Monte Carlo radiative transfer light curve models have been computed for this star, no genuine fit has ever been performed to its light curve. Using the same stellar parameters from Wade et al. (2011), we attempt to fit a light curve to the Hipparcos photometry. The fitting procedure is accomplished via a Python implementation of Markov chain Monte Carlo (MCMC) method using the `emcee` package from Foreman-Mackey et al. (2013). We obtained $B_d = 3.8^{+0.9}_{-1.8}\,\mathrm{kG}$ and $i + \beta = 92^{+5}_{-5}\,°$. It is reassuring to see that, within uncertainty, the best-fitted parameters are compatible with the previous findings obtained from direct measurements of the magnetic fields.

3.2. LMC and SMC Of?p stars

Among the five recently reported Of?p stars from the Magellanic Clouds, only four stars have accurately determined photometric periods. We first utilized published prescriptions in order to deduce their wind parameters (Vink et al., 2001). The remaining stellar parameters were determined via spectroscopic modeling using FASTWIND. The best-fit parameters are listed in Table 1. We notice that the dipole field strengths are unusually high in comparison to the Galactic sample of Of?p stars. This is because the light curve depths from Magellanic Of?p stars are comparable to those of the Galactic Of?p stars, while the former have inherently lower mass-loss rates due their the sub-solar metallicities. It is therefore required for the dipole field strength to be increased in order to compensate for the reduced density in the magnetosphere.

Table 1. Best-fit i, β couple and B_d for the Magellanic Of?p stars.

	SMC 159-2	LMC 164-2	2dFS 936	BI 57
$i + \beta$ [°]	88^{+4}_{-3}	100^{+5}_{-5}	86^{+3}_{-3}	66^{+3}_{-4}
$i - \beta$ [°]	42^{+18}_{-24}	50^{+23}_{-13}	44^{+23}_{-16}	22^{+15}_{-24}
B_d [kG]	7^{+2}_{-2}	6^{+1}_{-2}	13^{+4}_{-5}	$3.1^{+0.8}_{-0.9}$

4. Discussion and conclusion

To summarize, we described a simple prescription allowing for the light curve synthesis of magnetic massive stars. We apply this model to the OGLE photometry of the first-candidate Of?p stars from the Magellanic clouds and predict the magnitude and geometry of their suspected magnetic fields. We note that these stars have already previously been observed with FORS2 (Bagnulo et al., 2017). However, due to unfavorable weather conditions and non-optimal observing times, no surface fields could be confirmed with certainty. We suspect that SMC 159-2, in particular, will be detectable with the FORS2 instrument and is scheduled to be re-observed in the coming year.

References

Bagnulo, S., Nazé, Y., Howarth, I. D., et al. 2017, *Astron. Astrophys.*, **601**, A136

Foreman-Mackey, D., Conley, A., Meierjurgen Farr, W., et al. 2013, emcee: The MCMC Hammer, Astrophysics Source Code Library

Grunhut, J. H., Wade, G. A., Neiner, C., et al. 2017, *Mon. Not. R. Astron. Soc.*, **465**, 2432

Nazé, Y., Walborn, N. R., & Martins, F. 2008, *Rev. Mex. Astron. Astrofis.*, **44**, 331

Nazé, Y., Walborn, N. R., Morrell, N., Wade, G. A., & Szymański, M. K. 2015, *Astron. Astrophys.*, **577**, A107

Owocki, S. P., ud-Doula, A., Sundqvist, J. O., et al. 2016, *Mon. Not. R. Astron. Soc.*, **462**, 3830

Vink, J. S., de Koter, A., & Lamers, H. J. G. L. M. 2001, *Astron. Astrophys.*, **369**, 574

Wade, G. A., Howarth, I. D., Townsend, R. H. D., et al. 2011, *Mon. Not. R. Astron. Soc.*, **416**, 3160

Walborn, N. R., Morrell, N. I., Nazé, Y., et al. 2015, *Astron. J.*, **150**, 99

Contrib. Astron. Obs. Skalnaté Pleso **48**, 154 – 161, (2018)

The stability of magnetic fields in massive stars

A. Bonanno

Osservatorio Astrofisico di Catania, Via S.Sofia 78, 95123, Catania, Italy
(E-mail: alfio.bonanno@inaf.it)

Received: November 17, 2017; Accepted: November 28, 2017

Abstract. The stability of magnetic fields in massive stars is a topic of great interest for its astrophysical implications. The combined role of rotation, stable stratification and heat transport in determining the stability of a predominant toroidal field in radiation zones is briefly reviewed. It is shown that, depending on the basic state, rotation can suppress the instability. Moreover stable stratification strongly inhibit the occurrence of instabilities produced by the toroidal field, thus rendering the possibility of dynamo action in radiative zones rather remote. On the other hand, if thermal conductivity is considered, no stable toroidal field configurations are possible, although the growth time of the instability is comparable with the star evolutionary time-scale.

Key words: magnetohydrodynamics (MHD) – magnetic fields – stars: evolution

1. Introduction

Magnetic fields are ubiquitous along the Hertzsprung-Russell (HR) diagram where, depending on the stellar mass, they play an important role in several astrophysical transport phenomena such as mixing and angular momentum transport. From the observational point of view the magnetic fields of hot stars are topologically much simpler and generally much stronger than the fields of cool stars (Donati & Landstreet, 2009). Moreover, unlike cool stars, their characteristics show no clear correlations with fundamental stellar parameters and for this reason the origin of these fields has been longly debated.

It is difficult to imagine that a dynamo action can operate in stellar radiation zones as plasma flows with $\mathrm{Re}_m \gg 1$ (Re_m is the magnetic Reynolds number) are not available in internal radiation zones. The viability of the mechanism proposed in Spruit (2002), and further investigated in Braithwaite (2006) has never been proved (Zahn et al., 2007). For these reasons the prevalent opinion is that these fields have fossil origin, although recent analysis of the available observational data have seriously questioned this possibility (Ferrario et al., 2015). It is therefore essential to progress in the analytical study of magnetic field instabilities, in spite of the mathematical complexity of the problem. In fact, numerical simulations alone can fail to detect resonant instabilities with very short azimuthal wavenumber (Bonanno & Urpin, 2011).

Under the action of differential rotation even a weak fossil field with non-vanishing poloidal component will quickly wrap up into a predominantly toroidal

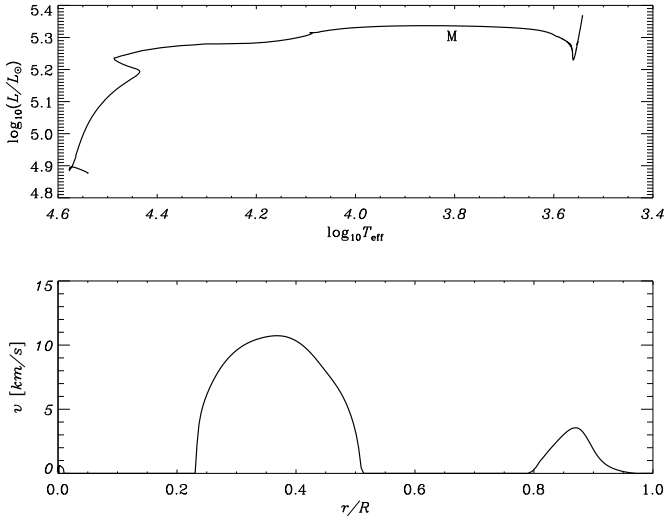

Figure 1. Upper panel: evolutionary track of a $M = 25\,\mathrm{M}_\odot$. Lower panel: convective velocities of model M in the upper panel as a function of the radius.

configuration. Such configuration can be generated if Re_m of differential rotation is greater than 1, or $|\nabla\Omega| > \eta_m/r^3$ where Ω and η_m are the angular velocity and magnetic diffusivity, respectively. Estimating $|\nabla\Omega| \sim \Delta\Omega/r$ where $\Delta\Omega$ is a departure from the rigid rotation and assuming that the conductivity of plasma is $\sim 10^{16}$ s^{-1}, one obtains that this condition is satisfied if $\Delta\Omega/\Omega > 10^{-18}\Omega_{sec}^{-1}$ where Ω_{sec} is the angular velocity in inverse seconds. Therefore, even very weak departures from the rigid rotation lead to a generation of a strong toroidal field in stellar radiative interiors. On the other hand, during its evolution a massive star develops multiple convective regions as it can be seen in Fig. 1 for an $M = 20\,\mathrm{M}_\odot$ stellar mass (see Costa et al. (2006) for further details). Therefore a dynamo-generated field produced in these regions can in general penetrate the neighboring radiative zones and alter the transport properties of the local plasma.

The stability of toroidal field in stellar radiation zone has been discussed by Tayler in his seminal work (Tayler, 1973). The important conclusions of his investigations can be summarized in the following necessary and sufficient conditions for instability

$$\frac{d\ln B_\phi}{d\ln s} < 1, \quad m = 0, \qquad \frac{d\ln B_\phi}{d\ln s} < -\frac{1}{2}, \quad m \pm 1 \tag{1}$$

where s is the cylindrical radius and m is the azimuthal wavenumber. On the other hand, in spherical geometry the situation is much more involved and there are no clearly established sufficient conditions for instability in this case.

The purpose of this contribution is to briefly summarize recent results obtained in this direction by means of the analytical and numerical analysis of the stability problem.

2. Basic formalism

Following the approach presented in Bonanno & Urpin (2013), one can consider the stability of an axisymmetric toroidal magnetic field neglecting viscosity and magnetic diffusivity. In spherical coordinates (r, θ, φ) the unit vectors are ($\boldsymbol{e}_r$, $\boldsymbol{e}_\theta$, $\boldsymbol{e}_\varphi$). It is assumed that the radiation zone rigidly rotates with angular velocity $\boldsymbol{\Omega}$ and that the toroidal field depends on r and θ, $B_\varphi = B_\varphi(r, \theta)$. The gas pressure is supposed to be much greater than the magnetic pressure so that the fluid can be considered incompressible.

In this limit, the MHD equations read

$$\frac{\partial \boldsymbol{v}}{\partial t} + (\boldsymbol{v} \cdot \nabla)\boldsymbol{v} = -\frac{\nabla p}{\rho} + \boldsymbol{g} + \frac{1}{4\pi\rho}(\nabla \times \boldsymbol{B}) \times \boldsymbol{B}, \tag{2}$$

$$\frac{\partial \boldsymbol{B}}{\partial t} - \nabla \times (\boldsymbol{v} \times \boldsymbol{B}) = 0, \tag{3}$$

$$\nabla \cdot \boldsymbol{v} = 0, \quad \nabla \cdot \boldsymbol{B} = 0, \tag{4}$$

where $\boldsymbol{g}$ is gravity. The equation of thermal balance, in Boussinesq approximation, reads

$$\frac{\partial T}{\partial t} + \boldsymbol{v} \cdot (\nabla T - \nabla_{ad} T) = \nabla \cdot (\kappa \nabla T), \tag{5}$$

where κ is the thermal diffusivity and $\nabla_{ad} T$ is the adiabatic temperature gradient.

In the basic (unperturbed) state, the gas is assumed to be in hydrostatic equilibrium, thus

$$\frac{\nabla p}{\rho} = \boldsymbol{g} + \frac{1}{4\pi\rho}(\nabla \times \boldsymbol{B}) \times \boldsymbol{B} + \boldsymbol{e}_s \, \Omega^2 \, r \sin\theta, \tag{6}$$

where $\boldsymbol{e}_s$ is the unit vector in the cylindrical radial direction. The rotational energy is assumed to be much smaller than the gravitational one, $g \gg r\Omega^2$. Since the magnetic energy is subthermal, $\boldsymbol{g}$ is approximately radial in the basic state.

When linearizing Eqs. (2 – 5) it is important to recall that small perturbations of the density and temperature are related by $\rho_1/\rho = -\beta(T_1/T)$ where β is the thermal expansion coefficient. For small perturbations, a local approximation in the θ-direction is assumed and θ is proportional to $\exp(-il\theta) = \exp(-k_\theta r\theta)$, where $l \gg 1$ and $k_\theta = l/r$ are the longitudinal wavenumber and wavevector, respectively. The perturbations can be assumed to be proportional

to $\exp(\sigma t - il\theta - im\varphi)$ where m is the azimuthal wavenumber. The dependence on r should thus be determined from Eqs. (2 – 5).

For the sake of simplicity, unperturbed ρ and T are assumed to be approximately homogeneous in the radiation zone. This assumption does not change the main conclusions qualitatively but substantially simplifies calculations. Eliminating all variables in the linearized (2-5) in favor of the perturbations of the radial velocity v_{1r} and temperature T_1, to lowest order in $(k_\theta r)^{-1}$ the following two coupled equations are obtained

$$\begin{aligned}
&(\sigma_1^2 + \omega_A^2 + D\Omega_i^2)\, v_{1r}'' \qquad (7)\\
&+\left(\frac{4}{r}\sigma_1^2 + \frac{2}{H}\omega_A^2\right) v_{1r}' + \left[\frac{2}{r^2}\sigma_1^2 - k_\perp^2(\sigma_1^2+\omega_A^2) - D\Omega_e^2 k_\theta^2\right.\\
&\left.+\frac{2}{r}\omega_A^2\left(\frac{1}{H}\frac{k_\perp^2}{k_\varphi^2} - \frac{2}{r}\frac{k_\theta^2}{k_\varphi^2}D\right) - i\sigma_1\Omega_e\left(\frac{k_\varphi}{r} + 4D\frac{k_\theta^2}{rk_\varphi}\frac{\omega_A^2}{\sigma_1^2}\right)\right] v_{1r} = -k_\perp^2\beta g\sigma_1\frac{T_1}{T}\\
&\frac{\kappa}{r^2}\frac{\partial}{\partial r}\left[r^2\frac{\partial}{\partial r}\left(\frac{T_1}{T}\right)\right] - (\sigma_1 + \kappa k_\perp^2)\frac{T_1}{T} = \frac{\omega_{BV}^2}{\beta g}v_{1r} \qquad (8)
\end{aligned}$$

where $1/H = \frac{\partial}{\partial r}\ln(rB_\varphi)$, the prime denotes a derivative with respect to r and

$$\begin{aligned}
&\sigma_1 = \sigma - im\Omega, \quad \omega_A^2 = \frac{k_\varphi^2 B_\varphi^2}{4\pi\rho}, \quad \omega_{BV}^2 = -\frac{g\beta}{T}(\nabla_{ad}T - \nabla T)_r,\\
&D = \frac{\sigma_1^2}{\sigma_1^2+\omega_A^2} \quad \Omega_i = 2\Omega\cos\theta, \quad \Omega_e = 2\Omega\sin\theta, \quad k_\perp^2 = k_\theta^2 + k_\varphi^2,\\
&k_\varphi = \frac{m}{r\sin\theta} \qquad (9)
\end{aligned}$$

Some general stability properties can be derived directly from Eqs. (7 and 8). Let us consider perturbations with a very short radial wavelength for which one can use a local approximation in the radial direction, such as $v_{1r} \propto \exp(-ik_r r)$, where k_r is the radial wavevector. If $k_r \gg \max(k_\theta, k_\varphi)$, then Eqs. (2 – 5) read, in lowest order in $(k_r r)^{-1}$,

$$-(\sigma_1 + \kappa k^2)\frac{T_1}{T} = \frac{\omega_{BV}^2}{\beta g}v_{1r}, \qquad k_r^2(\sigma_1^2 + \omega_A^2 + D\Omega_i^2)v_{1r} = k_\perp^2\beta g\sigma\frac{T_1}{T}, \qquad (10)$$

where $k^2 = k_r^2 + k_\perp^2$. From the above set of algebraic equations the corresponding dispersion relation can be obtained

$$\begin{aligned}
&\sigma_1^5 + \kappa k^2\sigma_1^4 + \left(2\omega_A^2 + \Omega_i^2 + \frac{k_\perp^2}{k^2}\omega_{BV}^2\right)\sigma_1^3\\
&+\kappa k^2(2\omega_A^2 + \Omega_i^2)\sigma_1^2 + \omega_A^2\left(\omega_A^2 + \frac{k_\perp^2}{k^2}\omega_{BV}^2\right)\sigma_1 + \kappa k^2\omega_A^4 = 0 \qquad (11)
\end{aligned}$$

The conditions that at least one of the roots has a positive real part (unstable mode) are determined by the Routh criterion (Aleksandrov et al., 1963). These

criteria yield the only non-trivial condition of instability $\omega_{BV}^2 < 0$ that is not satisfied in the radiation zone by definition. Therefore, modes with short radial wavelength are always stable to the current-driven instability.

2.1. Influence of rotation

Let us assume that the radiation zone is located at $R_i \leq r \leq R$ so that introducing the dimensionless radius $x = r/R$, at $x_i \leq x \leq 1$ where $x_i = R_i/R$ the toroidal field can be conveniently represented as

$$B_\varphi = B_0(x/x_i)^\alpha \sin\theta, \tag{12}$$

where B_0 is the field strength at $x = x_i$ at the equator and α an exponent which models the radial profile dependence. It is useful to introduce the following quantities

$$\Gamma = \frac{\sigma_0}{\omega_{A0}}, \quad \eta = \frac{2\Omega}{\omega_{A0}}, \tag{13}$$

where $\omega_{A0} = B_0/R\sqrt{4\pi\rho}$.

In Fig. 2 the growth rate and frequency for the toroidal field with $\alpha = 1$ are plotted. Like the previous cases, the instability is most efficient at the equator and its growth rate decreases if θ decreases. Generally, the instability at $\alpha = 1$ is suppressed more strongly than in the cases $\alpha = 3$ and $\alpha = 2$: in particular, in these latter cases, there are always unstable modes at high latitudes which cannot be stabilized. On the contrary the instability for $\alpha = 1$ is characterized by the threshold, η_{cr}, which is latitude dependent. The threshold is lower for smaller θ. The field near the magnetic axis turns out to be stable. The instability does not occur at any η in the region with $\theta < \theta_{cr} \approx 30°$. (see Fig. 2).

The condition of stability $\eta > \eta_{cr}$ can easily be reformulated in terms of the angular velocity and magnetic field. Rotation completely suppresses the Tayler instability if the star rotates with the angular velocity

$$\Omega > \frac{\eta_{cr} B_0}{2R\sqrt{4\pi\rho}}. \tag{14}$$

We can also rewrite this inequality as the condition for the magnetic field,

$$B_0 < \frac{2\Omega R}{\eta_{cr}}\sqrt{4\pi\rho}. \tag{15}$$

The Tayler modes become oscillatory (Im $\Gamma = 0$) if conditions (14) or (15) are satisfied. Note that such behavior was also seen in numerical simulations of the Tayler instability (Braithwaite, 2006). The frequency of marginally stable waves is of the order of $\omega_{A0}(\omega_{A0}/\Omega)$ at $\eta > 1$ and it decreases as $\propto 1/\eta$ at large η. The dispersion relation for these waves can easily be obtained from Eq. (11) which in our case becomes

$$\sigma_1^4 + \sigma_1^2(2\omega_A^2 + \Omega_i^2) + \omega_A^4 = 0. \tag{16}$$

The solution of this equation is

$$\sigma_1^2 = -\frac{1}{2}(\Omega_i^2 + 2\omega_A^2) \pm \frac{1}{2}\Omega_i^2\sqrt{1 + \frac{4\omega_A^2}{\Omega_i^2}}. \tag{17}$$

If $\Omega_i \gg \omega_A$ then we can expand a square root in a power series of $(\omega_A/\Omega_i)^2$. Then, choosing the upper sign with accuracy in the lowest order in $(\omega_A/\Omega_i)^2$, we obtain

$$\sigma_1^2 \approx -\omega_A^2(\omega_A/\Omega_i)^2. \tag{18}$$

This dispersion relation describes new types of oscillatory modes that can exist in rapidly rotating stars. These modes can be called the "magneto-inertial" waves because they can exist only in a magnetized and rotating plasma. For

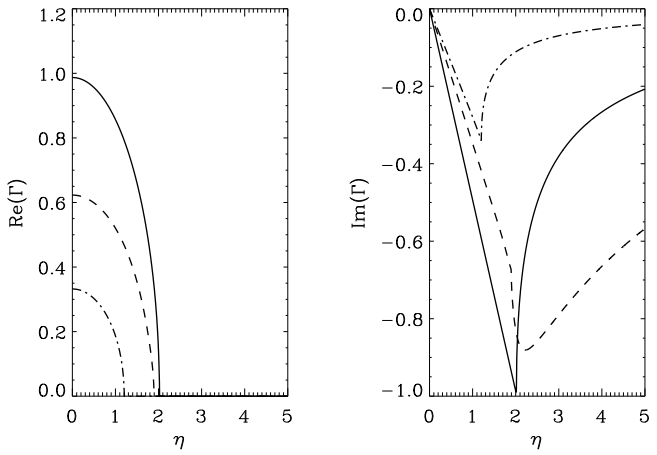

Figure 2. The growth rate (left panel) and frequency (right panel) for $\alpha = 1$ as a function of the rotational parameter η (see the text). The curves correspond to $\theta = 90^\circ$ (solid), 45° (dashed), and 37° (dash-and-dotted).

$\alpha = -0.4$ the instability is strongly suppressed. Basically it can occur only in a narrow region around the equator, $90^\circ \geq \theta > \theta_{cr} \approx 65^\circ$, and does not occur in the extended region around the rotation axis, $\theta < \theta_{cr} \approx 65^\circ$. The threshold value of η at the equator is ≈ 2. Therefore, the Tayler instability is entirely suppressed everywhere in the radiation zone with $\alpha = -0.4$ if $\eta > 2$, or $\Omega > \omega_{A0}$. However, stable oscillating modes can exist even at much higher η. Extended numerical investigation does not show the presence of instability in the spherical geometry if $\alpha < -1/2$.

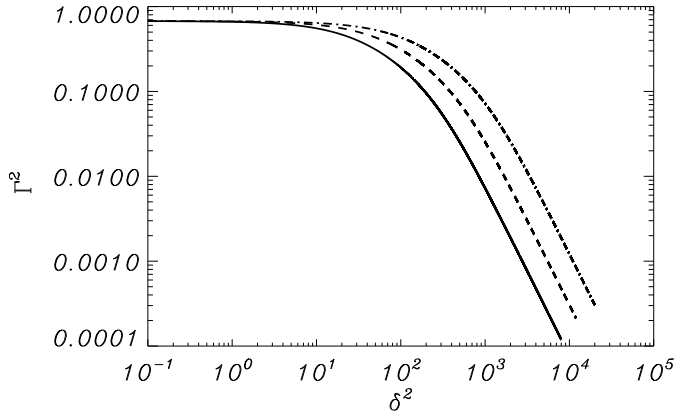

Figure 3. The dimensionless growth rate at the equator as a function of δ^2 for the fundamental eigenmode with $m = 1$, $l = 20$, $d = 0.1$, and three values of ε: 10^{-2} (solid line), 2×10^{-2} (dashed), and 4×10^{-2} (dot-dashed).

2.2. Influence of gravity and heat transport

In order to characterize the effect of stratification and thermal conductivity let us introduce the following quantities

$$\delta^2 = \frac{\omega_{BV}^2}{\omega_{A0}^2}, \quad \varepsilon = \frac{\omega_T}{\omega_{A0}}, \tag{19}$$

The effect of thermal conductivity significantly changes the properties of the current-driven instability. In Fig. 3 we plot the dependence of the growth rate at the equator ($\theta = \pi/2$) on the parameter stratification δ^2 for three different values of the thermal conductivity, corresponding to $\varepsilon = 10^{-2}$, 2×10^{-2}, and 4×10^{-2}. The behaviour of all curves is qualitatively similar: the growth rate is ≈ 1 at small δ and it tends to zero as $\Gamma \propto \delta^{-2}$ for large δ or, in the dimensional form,

$$\sigma \propto \omega_{A0}(\omega_{A0}/\omega_{BV})^2. \tag{20}$$

3. Conclusions

The effect of a finite thermal diffusivity, summarized in Eq. (20) has striking implications: it implies that even in the presence of an extremely strong stable stratification the instability can never be completely suppressed. The growth rate turns out to be non-vanishing even for large δ. In particular, if the field is

weak enough its evolution can be comparable with the life-time of the star. On the other hand, stable stratification can suppress the current-driven instability of the toroidal field if perturbations are not influenced by the thermal conductivity (very small ε). In this case the instability does not arise if the Brunt-Väisälä frequency is greater than $\sim 9\,\omega_{A0}$. Since ω_{BV} is typically high in radiative zones ($\sim 10^{-3} - 10^{-4}$ s^{-1}) the instability sets in only if the field is very strong ($\geq 10^6 - 10^7$ G). Higher eigenmodes are suppressed more strongly than the fundamental one and perturbations with short radial wavelength are always stable (see Bonanno & Urpin (2012) for further details).

In conclusion, a possible explanation for the origin of the magnetic field in massive stars is the presence of the Tayler instability operating on secular time scale: from this point of view the apparent stationarity of the observed field is only a consequence of a very small thermal conductivity in the radiative interior (compared to the Alfven time scale). The numerical simulation of Szklarski & Arlt (2013) support this picture although further investigations in this direction, including a more realistic description of the stellar plasma, are certainly needed.

Acknowledgements. The author is grateful to the organizers of the Brno conference on magnetic field in stars for having created such an important occasion of meeting and discussions. The author would also like to acknowledge Luigia Santagati for careful reading of the manuscript.

References

Aleksandrov, A. D., Kolmogorov, A. N., & Lavrent'ev, M. A. 1963, *Mathematics, its content, methods, and meaning* (Cambridge, MA: M.I.T. Press)

Bonanno, A. & Urpin, V. 2011, *Phys.Rev.E*, **84**, 056310

Bonanno, A. & Urpin, V. 2012, *Astrophys. J.*, **747**, 137

Bonanno, A. & Urpin, V. 2013, *Astrophys. J.*, **766**, 52

Braithwaite, J. 2006, *Astron. Astrophys.*, **449**, 451

Costa, V., Pumo, M. L., Bonanno, A., & Zappalà, R. A. 2006, *Astron. Astrophys.*, **447**, 641

Donati, J.-F. & Landstreet, J. D. 2009, *Ann. Rev. Astron. Astrophys.*, **47**, 333

Ferrario, L., Melatos, A., & Zrake, J. 2015, *Space Sci. Rev.*, **191**, 77

Spruit, H. C. 2002, *Astron. Astrophys.*, **381**, 923

Szklarski, J. & Arlt, R. 2013, *Astron. Astrophys.*, **550**, A94

Tayler, R. J. 1973, *Mon. Not. R. Astron. Soc.*, **161**, 365

Zahn, J.-P., Brun, A. S., & Mathis, S. 2007, *Astron. Astrophys.*, **474**, 145

Contrib. Astron. Obs. Skalnaté Pleso **48**, 162 – 169, (2018)

The evolution of magnetic fields from the main-sequence to very late stages

A. J. Martin

LESIA, Observatoire de Paris, PSL Research University, CNRS, Sorbonne Universités, UPMC Univ. Paris 06, Univ. Paris Diderot, Sorbonne Paris Cité, 5 place Jules Janssen, F-92195 Meudon, France
(E-mail: alexander.martin@obspm.fr)

Received: November 8, 2017; Accepted: November 24, 2017

Abstract. Magnetic fields have been detected in most if not all types of stars across the Hertzsprung-Russell diagram. Where present, these fields have the potential to significantly impact the evolution of their host stars. Furthermore, they themselves are affected by the various structural changes which occur in a star during its life. For example, the significant radius expansion during the post-main-sequence phase, due to flux conservation, may lead to a decrease in surface magnetic field strength, to a point where the magnetic field may no longer be detectable. As a result, it is a challenge to link the magnetic fields observed in main sequence (MS) stars with those observed in very late stage stars and even to those in post-MS stars. In this review, I present what we know, from observations, about magnetic stars at various stages of stellar evolution.
Key words: stars: magnetic field – stars: evolution

1. Introduction

The magnetic fields present in stars are shown to affect their host star in a variety of ways, both at the stellar surface and in the interior. For example, they modify the mixing and diffusion of chemical elements (Stift & Alecian, 2016) and the surface wind (ud-Doula & Owocki, 2002; ud-Doula et al., 2008, 2009). Thus, a good understanding of the structure of the magnetic field is important for the study of the evolution of magnetic stars. However, the magnetic fields present in stars are themselves affected by the changing physical properties of the star as it undergoes the sometimes extreme structural changes during its life. In this review, I explore what we infer from observations about the magnetic field evolution for stars at different stages of their lives, from the MS to the very late stages.

2. Dynamo and fossil fields

In general, we infer two main mechanisms for the presence of magnetic fields in stars. Those of "dynamo origin" (e.g., Charbonneau, 2014) are magnetic fields

generated as the result of a dynamo process in the inner layers of a star. Those of "fossil field origin" (e.g., Braithwaite & Spruit, 2004) are magnetic fields inherited and possibly amplified in the earlier stages of a star's life. Since the mechanism by which these fields form is different, different processes can affect their evolution.

2.1. Ohmic decay

In the absence of any additional degenerative or regenerative force, a magnetic field will decay over a time-scale called the Ohmic decay time, $t_{\rm ohm}$. This is given by

$$t_{\rm ohm} = \frac{4\pi\sigma L^2}{c^2}, \tag{1}$$

where L is the magnetic field length scale, c is the speed of light and σ is the electrical conductivity. In the context of this review, Ohmic decay is only relevant for fossil fields, since dynamo fields are constantly regenerated. The Ohmic decay timescale gives a baseline for the time over which we could expect a field to decay. This means we can investigate whether the field is decaying faster and so by a different means.

2.2. Magnetic flux conservation

If there is no change in magnetic field flux then, as a star evolves and its radius expands or contracts, by the laws of flux conservation the surface magnetic field strength is expected to decrease or increase respectively. The current dipole magnetic field strength ($B_{\rm d,current}$) after a change in radius is calculated as

$$B_{\rm d,current} = B_{\rm d,previous}\left(\frac{R_{\rm previous}}{R_{\rm current}}\right)^2, \tag{2}$$

where $B_{\rm d,previous}$ is the previous dipole magnetic field strength, $R_{\rm previous}$ is the previous radius of the star and $R_{\rm current}$ is the current radius of the star.

3. Magnetic field evolution during the main sequence

During the evolution of stars along the MS, two key properties change. First the rotation period of the star increases as a result of angular momentum loss and second in all but the smallest of stars the radius increases. In stars of approximately one solar mass, this is rather modest and between the zero-age main-sequence (ZAMS) and terminal-age main-sequence (TAMS) we would expect a radius increase of a factor of ~ 1.4 based on the evolutionary models of Ekström et al. (2012). In contrast, for stars with $M = 50\,{\rm M}_\odot$ we would expect a radius increase of a factor of ~ 6 based on the evolutionary models of Ekström et al. (2012). In addition, we expect that the time that a star spends on the MS decreases with increasing ZAMS mass.

3.1. Low-mass stars

Stars with masses below $\sim 1.5\,M_\odot$ have been shown to host dynamo magnetic fields (e.g., Donati, 2011). Vidotto et al. (2014) investigated the prediction of Skumanich (1972) that a dynamo magnetic field will decay as the inverse square of stellar age. Their sample has a mass range of 0.1–2.0 $M_\odot$ and an age range of 1 Myr–$\sim$10 Gyr. They find a power law fit $\langle |B_V| \rangle \propto t^{-0.655 \pm 0.045}$, which supports the prediction of Skumanich (1972). In addition, they find a similar relationship between the unsigned surface flux and stellar age: $\Phi_V \propto t^{-0.622 \pm 0.042}$.

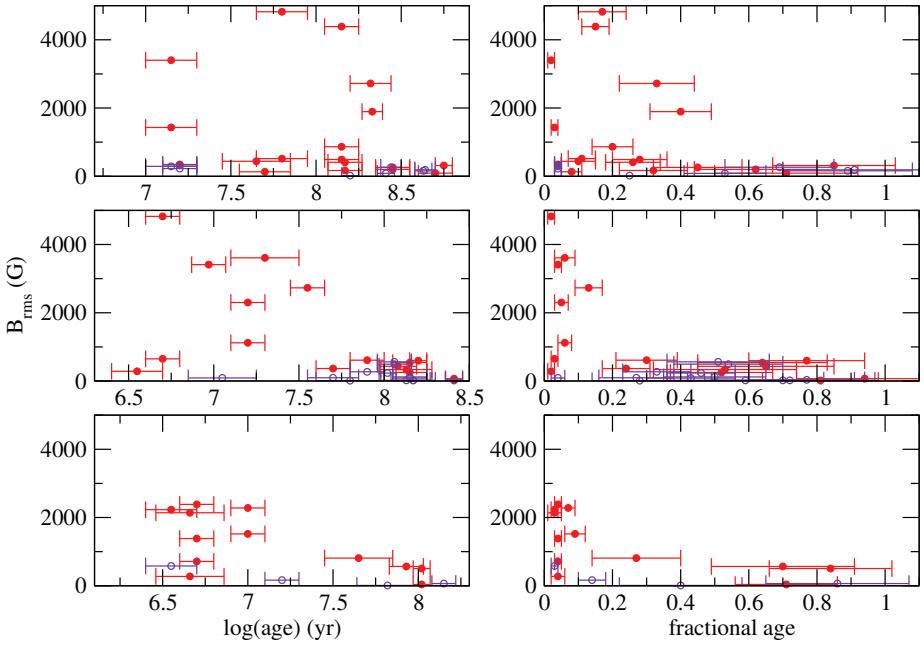

Figure 1. $B_{\rm rms}$ as a function of logarithmic stellar age (left) and as a function of fractional MS age (right) for the sample of stars given in Landstreet et al. (2008). Filled symbols = stars with definite field detections, open symbols = probable Ap stars for which a magnetic field has not yet been detected. From top to bottom, the panels indicate three mass bins, 2–3$M_\odot$, 3–4$M_\odot$, and 4–5$M_\odot$. Credit: Landstreet et al. (2008) reproduced with permission © ESO.

3.2. Intermediate-mass stars

Stars with masses larger than $\sim$1.5 $M_\odot$ host fossil magnetic fields. The incidence rate of magnetic fields in Ap/Bp stars is $\sim$10% and they host large-scale

magnetic fields with strengths ranging from 300 G to 30 kG (Power et al., 2008; Aurière et al., 2007). Landstreet et al. (2008) studied the magnetic fields of 23 late B- and early A-type stars and their results are shown in Fig. 1 and their Fig. 5. They find that the magnetic field of stars with masses between 2 and 3 $M_\odot$ declines after about 2.5×10^8 yr, for 3-4 $M_\odot$ the field declines after about 4×10^7 yr and for 4-5 $M_\odot$ the field declines after about 1.5×10^7 yr as shown in Fig. 1. In addition, as shown by their Fig. 5, Landstreet et al. (2008) find that magnetic flux decays with stellar age for all of their sample. They conclude that either magnetic flux declines in all Ap/Bp stars during the MS lifetime or that magnetic flux in the more strongly magnetic stars found at young fractional ages is somehow reduced.

3.3. Massive stars

Like the intermediate-mass stars, there is convincing evidence that $\sim$10 % of massive stars host a fossil magnetic field (Grunhut & Neiner, 2015; Fossati et al., 2015; Wade et al., 2016; Grunhut et al., 2017). The study by Fossati et al. (2016) investigated the incidence of magnetic field as a function of fractional MS age (τ). Their results are shown in Fig. 2. They find that the incident rate of magnetic fields in massive stars sharply decreases above $\tau \sim 0.6$, with this effect being significantly more pronounced for stars above 14 $M_\odot$. Fossati et al. (2016) investigated the possible causes of this, and conclude that binary rejuvenation and suppression of core convection cannot explain the observed distributions. In addition, while flux conservation is likely a contributing factor, if it were the sole explanation for this, at least a third of the stars which have a detectable magnetic field on the ZAMS, would still be detectable as magnetic on the TAMS. As a result, they conclude that there is likely a mass dependant field decay mechanism operating.

4. Post-main sequence stars

The post-main sequence of most stars is characterised by significant inflation of the stellar radius and the end of H-burning. Therefore, for stars with fossil magnetic fields, it is predicted that as a result of flux conservation the surface magnetic field strength will be significantly reduced.

4.1. Post-MS FGK-type stars

The study by Grunhut et al. (2010) determined that a third of their sample of $\sim$30 massive late-type stars host dynamo magnetic fields. To explain such a high incidence rate in comparision to other stars, they conclude that a mechanism may exist to excite magnetic fields in cool supergiants. The work by Aurière et al. (2015) investigated the magnetic fields of active G-K giants. They found that most of the stars in their sample were either in the first dredge-up phase or

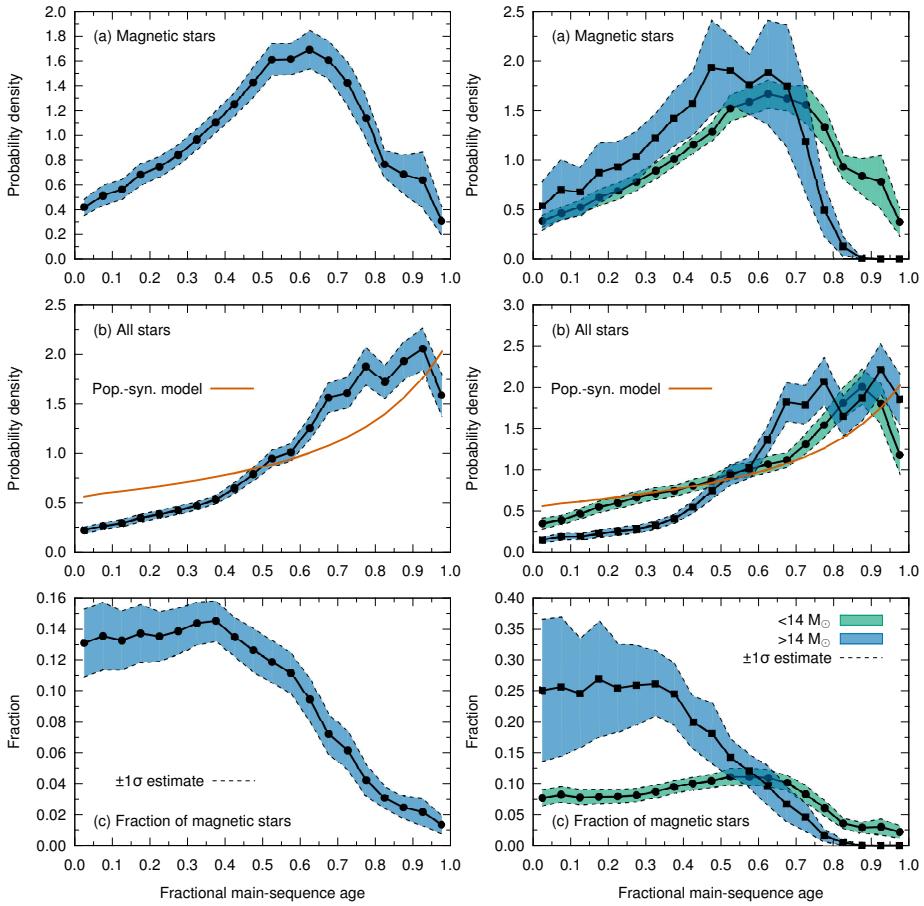

Figure 2. "Fractional MS τ-distributions of (a) the magnetic stars and (b) all stars in the sample from Fossati et al. (2016). Panel (c) shows the fraction of magnetic stars as a function of fractional MS age (τ), normalised such that the incidence of magnetic stars is 7% (Wade et al. 2014; Fossati et al. 2015b). The shaded regions indicate bootstrapped 1σ estimates to give an indication of the statistical significance of the variability in the τ-distributions. The solid line in the middle panel shows the τ-distribution of a synthetic population of a magnitude-limited sample of massive stars (see the text of Fossati et al., 2016)." Figure and caption (adapted) credit: Fossati et al. (2016), reproduced with permission © ESO.

core helium-burning phase. As a result they conclude that this could be evidence for a magnetic strip of the most active stars.

4.2. Post-MS OBA stars and the LIFE project

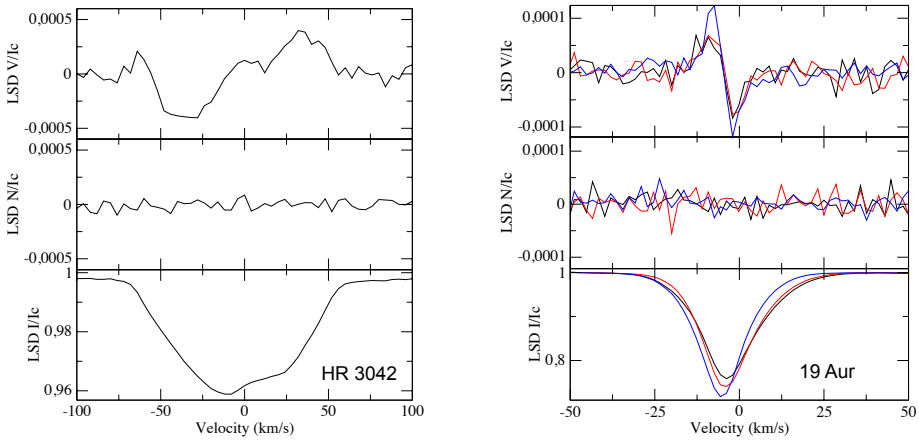

Figure 3. LSD Stokes V (top panels), Null (middle panels) and Stokes I (bottom panels) profiles of the B8III star HR 3042 with $B_\ell = -230 \pm 10$ G (left) and the A5Ib-II star 19 Aur with $B_\ell = 1.0 \pm 0.2$ G (right; 3 observations superposed) obtained by the ESPaDOnS instrument of the CFHT in semester 2016B, showing that these 2 stars are magnetic (Martin et al., submitted).

Until recently there were no known, clearly evolved, magnetic hot stars. However, as part of the BRIght Target Explorer spectropolarimetric survey (BRITEpol; Neiner et al., 2016), Neiner et al. (2017) identified two magnetic A7 supergiants: ι Car and HR 3890. To systematically study the magnetic fields of hot giants and supergiants, the Large Impact of magnetic Fields on the Evolution of hot stars (LIFE) project (Martin et al., submitted) was started. These stars provide an important link between magnetic stars on the MS and the late stages of a star's life. So far, 15 stars have been observed as part of this project. Out of these, two have been found to be magnetic: HR 3042 and 19 Aur (see Fig. 3). The current strength of the magnetic fields detected in these stars is compatible with what we would expect if conservation of magnetic flux was the main driver for magnetic field evolution, however, it does not exclude the possibility of other magnetic field decay processes affecting the field evolution.

5. Late stages of stellar evolution

The late stages of stellar evolution are characterised by arguably the most extreme changes to occur in the stellar structure since the birth of the star. As a result, it is challenging to link the magnetic field observed in these stars with those observed in MS stars.

5.1. White dwarfs

White dwarfs (WDs) are the final evolutionary stage of most stars: those stars with masses less than $\sim 8\,M_\odot$. They are found to have a broad range of magnetic field strengths from $\sim 10^3$ G to 10^9 G (e.g., Ferrario et al., 2015). The lower limit of $\sim 10^3$ G may, however, be the result of instrument limitations rather than a true lower limit, in which case, the range in field strengths could be even greater. The mechanism responsible for the presence of magnetic fields in WDs remains unclear, however, possible explanations include: they are fossil fields preserved from the MS; they are fossils of the strong convective core fields of red giants, revealed as the outer layers of the star are stripped off; or they are fossils of dynamo fields generated in common envelope evolution of close binaries. Furthermore, It is interesting to note that currently the incidence rate of magnetic fields in WDs appears to be $\sim$10% (Ferrario et al., 2015), which is consistent with the incidence rate seen for the hot stars mentioned earlier in this review. A comprehensive review by Ferrario et al. (2015) shows the results of the magnetic field measurement of a large sample of WDs in their Fig. 3. This figure shows that there is no evidence for magnetic field evolution with age, which is consistent with the long ohmic decay timescale (2-6 $\times$ 10^{11} yr) for WDs.

5.2. Neutron Stars

The final evolutionary stage of more massive stars from $\sim 8\,M_\odot$ to $\sim 25-30\,M_\odot$ is the neutron star, formed as the result of a supernova. Neutron stars are found to have magnetic field strengths of $\sim$ 10^8-10^{14} G (e.g., Harding & Lai, 2006), where the strongest magnetic fields of $\sim 10^{14}$ G are above the quantum critical field strength. The study by Harding & Lai (2006) shows that the magnetic fields of these stars decrease in strength with stellar age in their Fig. 1. However, connecting the magnetic fields observed in neutron stars with those observed on the MS is a challenge, because of the extreme physics acting during their birth. The continued analysis of magnetic fields of stars at various evolutionary stages is therefore necessary to connect the fields we observe on the MS with those at the very late stages of stellar life.

Acknowledgements. I am very grateful to John Landstreet, Stefano Bagnulo, Coralie Neiner and Luca Fossati for their help collating the information necessary for this review.

References

Aurière, M., Konstantinova-Antova, R., Charbonnel, C., et al. 2015, *Astron. Astrophys.*, **574**, A90

Aurière, M., Wade, G. A., Silvester, J., et al. 2007, *Astron. Astrophys.*, **475**, 1053

Braithwaite, J. & Spruit, H. C. 2004, *Nature*, **431**, 819

Charbonneau, P. 2014, *Ann. Rev. Astron. Astrophys.*, **52**, 251

Donati, J.-F. 2011, in IAU Symp., Vol. **271**, *Astrophysical Dynamics: From Stars to Galaxies*, ed. N. H. Brummell, A. S. Brun, M. S. Miesch, & Y. Ponty, 23–31

Ekström, S., Georgy, C., Eggenberger, P., et al. 2012, *Astron. Astrophys.*, **537**, A146

Ferrario, L., de Martino, D., & Gänsicke, B. T. 2015, *Space Sci. Rev.*, **191**, 111

Fossati, L., Castro, N., Schöller, M., et al. 2015, *Astron. Astrophys.*, **582**, A45

Fossati, L., Schneider, F. R. N., Castro, N., et al. 2016, *Astron. Astrophys.*, **592**, A84

Grunhut, J. H. & Neiner, C. 2015, in IAU Symp., Vol. **305**, *Polarimetry*, ed. K. N. Nagendra, S. Bagnulo, R. Centeno, & M. Jesús Martínez González, 53–60

Grunhut, J. H., Wade, G. A., Hanes, D. A., & Alecian, E. 2010, *Mon. Not. R. Astron. Soc.*, **408**, 2290

Grunhut, J. H., Wade, G. A., Neiner, C., et al. 2017, *Mon. Not. R. Astron. Soc.*, **465**, 2432

Harding, A. K. & Lai, D. 2006, *Rep. Prog. Phys.*, **69**, 2631

Landstreet, J. D., Silaj, J., Andretta, V., et al. 2008, *Astron. Astrophys.*, **481**, 465

Neiner, C., Oksala, M. E., Georgy, C., et al. 2017, *Mon. Not. R. Astron. Soc.*, **471**, 1926

Neiner, C., Wade, G., Marsden, S., & Blazère, A. 2016, *ArXiv e-prints* [arXiv:1611.03285]

Power, J., Wade, G. A., Aurière, M., Silvester, J., & Hanes, D. 2008, *Contributions of the Astronomical Observatory Skalnate Pleso*, **38**, 443

Skumanich, A. 1972, *Astrophys. J.*, **171**, 565

Stift, M. J. & Alecian, G. 2016, *Mon. Not. R. Astron. Soc.*, **457**, 74

ud-Doula, A. & Owocki, S. P. 2002, *Astrophys. J.*, **576**, 413

ud-Doula, A., Owocki, S. P., & Townsend, R. H. D. 2008, *Mon. Not. R. Astron. Soc.*, **385**, 97

ud-Doula, A., Owocki, S. P., & Townsend, R. H. D. 2009, *Mon. Not. R. Astron. Soc.*, **392**, 1022

Vidotto, A. A., Gregory, S. G., Jardine, M., et al. 2014, *Mon. Not. R. Astron. Soc.*, **441**, 2361

Wade, G. A., Neiner, C., Alecian, E., et al. 2016, *Mon. Not. R. Astron. Soc.*, **456**, 2

Contrib. Astron. Obs. Skalnaté Pleso **48**, 170 – 174, (2018)

The nature of light variations in magnetic hot stars

J. Krtička[1], L. Huang[2], M. Jagelka[1], T. Lüftinger[3], Z. Mikulášek[1], E. Niemczura[4], M. Prvák[1], J. Silvester[5] and G. Wade[2]

[1] *Department of Theoretical Physics and Astrophysics, Masaryk University, CZ-611 37 Brno, Czech Republic*

[2] *Department of Physics, Royal Military College of Canada, P.O. Box 17000, Station Forces, Kingston, Ontario K7K 7B4, Canada*

[3] *Institut für Astronomie, Universität Wien, 1180 Wien, Austria*

[4] *Astronomical Institute, Wrocław University, 51-622 Wrocław, Poland*

[5] *Department of Astronomy and Space Physics, Uppsala University, SE-751 20 Uppsala, Sweden*

Received: October 31, 2017; Accepted: November 5, 2017

Abstract. Magnetic stars show several types of light variability which is modulated by the stellar rotation. In chemically peculiar stars, the redistribution of the flux in the surface regions with peculiar chemical composition leads to the light variability with a typical amplitude of the order of hundredths of magnitude. The most efficient processes that cause the flux redistribution are bound-bound (line) transitions of iron and bound-free (ionization) transitions of silicon. This type of light variability typically leads to a complex dependence of the amplitude on the wavelength and shows antiphase light curves in the far ultraviolet and visual regions. In hot magnetic stars, the modulation of the stellar wind by the magnetic field and the wind blanketing cause the light variability with a typical amplitude of the order of millimagnitudes. We predict the light variations in selected magnetic hot stars and compare the simulated light curves with light variations derived from observations.

Key words: stars: chemically peculiar – stars: early type – stars: variables – stars: winds, outflows – stars: mass-loss

1. Introduction

Rotational light variability of magnetic chemically peculiar stars is caused by inhomogeneous surface distribution of individual elements. The abundance inhomogeneities lead to the spatial variations of opacity due to bound-free (Peterson, 1970; Lanz et al., 1996) and bound-bound (Wolff & Wolff, 1971) transitions. Because the opacities depend on wavelength, the surface abundance variations cause the flux redistribution and the light variability. Detailed abundance maps combined with advanced model atmospheres enable us to predict the flux variability and to understand the mechanism of the light variability in detail (Krtička et al., 2007, 2015; Prvák et al., 2015).

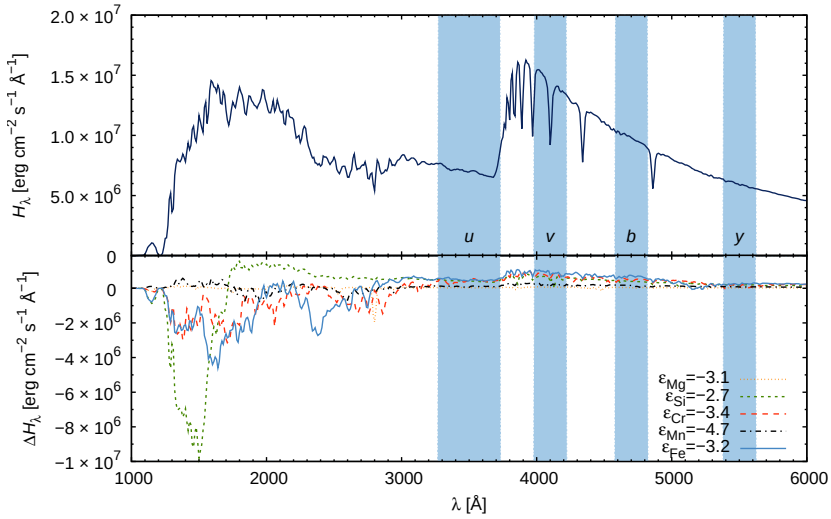

Figure 1. Influence of abundance variations on emergent flux. *Upper panel:* Emergent flux for the solar chemical comparison. *Lower panel:* Difference between the fluxes calculated for higher elemental abundances and the solar flux. The regions corresponding to the filters *uvby* of Strömgren photometric system are denoted in the graph.

2. Modelling of the flux variability

We assume constant effective temperature and surface gravity for the modelling of the flux. The abundance of individual elements $\{\epsilon_{\rm el}\}$ is taken from the Doppler maps. We calculate TLUSTY (Lanz & Hubeny, 2007) or ATLAS (Kurucz, 2005) model atmospheres with chemical composition from the maps and using the SYNSPEC code predict the specific intensities $I(\lambda, \theta, \{\epsilon_{\rm el}\})$. With the maps we therefore obtain the emergent intensities $I(\lambda, \theta, \Omega)$ as a function of the location on the stellar surface (with coordinates Ω). The specific intensities are integrated over the stellar surface to give the total phase-dependent emergent flux and magnitudes in individual photometric filters.

3. Chemically peculiar star θ Aur

For the modelling of chemically peculiar star θ Aur we used surface abundance maps of He, Si, Cr, and Fe derived from spectroscopy by Kuschnig (1998).

In the models with enhanced abundance, the flux is redistributed typically from far-UV region to the near-UV region and to the optical domain (Fig. 1). Consequently, the surface regions with enhanced abundance of heavier elements

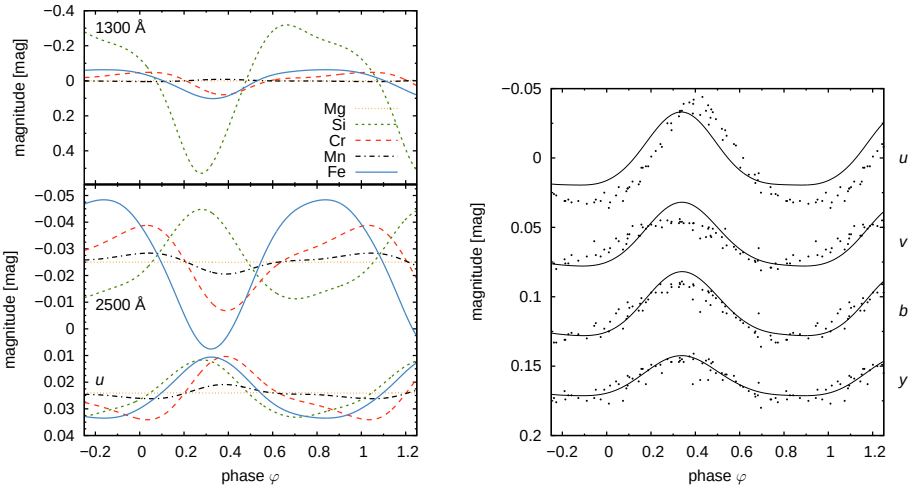

Figure 2. *Left*: Light variations of θ Aur in different wavelength regions calculated from the surface distribution of one element only. *Right:* Comparison of predicted light variations in the pass-bands of Strömgren photometric systems with observed variations (Adelman & Kaewkornmaung, 2005).

should be relatively bright in the optical region and relatively dark in the far-UV. This leads to the antiphase light curves in far-UV and in optical (see Fig. 2).

The predicted light variations due to individual elements (Fig. 2) show that mostly Si, Cr, and Fe contribute to the light variations of θ Aur (Krtička et al., 2015). Predicted and observed light variations nicely agree (Fig. 2). The remaining difference is likely caused by some missing element(s).

4. Chemically peculiar star a Cen

Modelling of the light variations of chemically peculiar star a Cen is based on He, N, O, Si, and Fe surface abundance maps derived from spectroscopy.

The modelling of the emergent flux and its variations nicely reproduces the UV flux and its variations observed by the IUE satellite (Fig. 3). Also the optical light curve observed by the BRITE satellite is nicely reproduced (Fig. 4).

5. Light variations due to wind blanketing in magnetic stars

Galactic O stars have strong winds that prevent the formation of surface layers with peculiar chemical composition. Therefore, we do not expect any rotationally modulated light variability in these stars. Despite this, Nazé (2004) found periodic light variations in magnetic O8fpe star HD 191612, which was

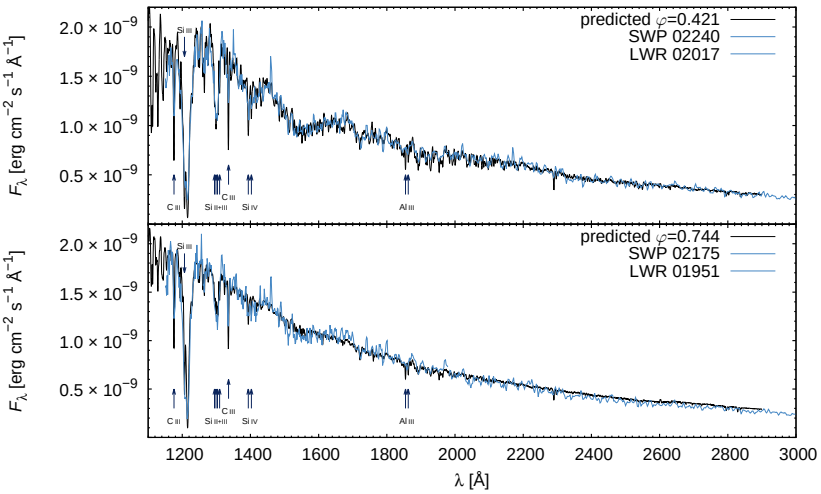

Figure 3. Comparison of predicted UV flux distribution of a Cen (black lines) with observed UV spectra (IUE, blue lines) for two rotational phases.

attributed to the light absorption in circumstellar magnetosphere (Wade et al., 2011).

In magnetic stars, the stellar wind is modulated by the magnetic field leading to the dependence of the wind mass-loss rate on the magnetic field tilt (Owocki & ud-Doula, 2004). This may cause additional light variability due to the wind blanketing, which scales with the wind mass-loss rate (Krtička, 2016). This effect explains part of the light variability of HD 191612 in Fig. 4.

6. Conclusions

Magnetic hot stars show several types of the light variability due to blanketing effects. In chemically peculiar stars, the rotational variability is caused by flux redistribution in the abundance spots due to bound-free (continuum, mainly He and Si) and bound-bound (lines, mainly Fe and Cr) transitions. In magnetic stars with winds, part of the light variability is caused by the wind blanketing modulated by the magnetic field.

Acknowledgements. MJ, JK, ZM, and MP were supported by grants GA ČR 16-01116S and 7AMB17AT030 (MŠMT). EN acknowledges the Polish National Science Center grant no. 2014/13/B/ST9/00902.

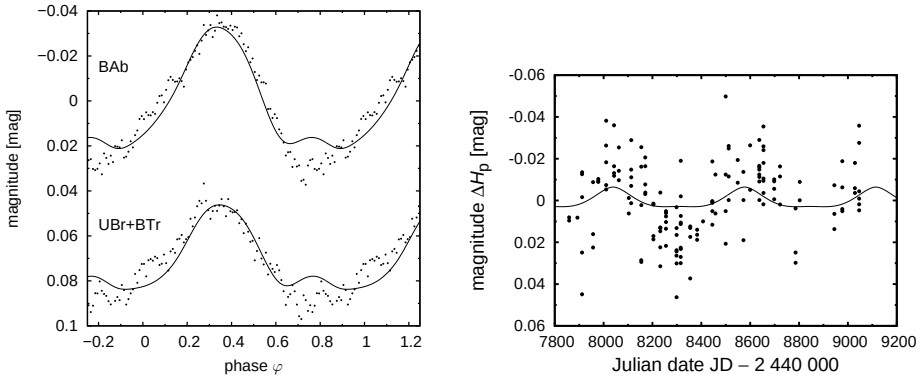

Figure 4. *Left*: Comparison of predicted optical light curve of a Cen with observations from BRITE satellite in the blue and red domains. *Right:* Light curve of HD 191612 due to wind blanketing in comparison with Hipparcos observations.

References

Adelman, S. J. & Kaewkornmaung, P. 2005, *Astron. Astrophys.*, **435**, 1099

Krtička, J. 2016, *Astron. Astrophys.*, **594**, A75

Krtička, J., Mikulášek, Z., Lüftinger, T., & Jagelka, M. 2015, *Astron. Astrophys.*, **576**, A82

Krtička, J., Mikulášek, Z., Zverko, J., & Žižňovský, J. 2007, *Astron. Astrophys.*, **470**, 1089

Kurucz, R. L. 2005, *Mem. Soc. Astron. Ital. Suppl.*, **8**, 14

Kuschnig, R. 1998, PhD thesis, University of Vienna

Lanz, T., Artru, M.-C., Le Dourneuf, M., & Hubeny, I. 1996, *Astron. Astrophys.*, **309**, 218

Lanz, T. & Hubeny, I. 2007, *Astrophys. J., Suppl. Ser.*, **169**, 83

Nazé, Y. 2004, PhD thesis, Institut d'Astrophysique et de Géophysique, Université de Liège

Owocki, S. P. & ud-Doula, A. 2004, *Astrophys. J.*, **600**, 1004

Peterson, D. M. 1970, *Astrophys. J.*, **161**, 685

Prvák, M., Liška, J., Krtička, J., Mikulášek, Z., & Lüftinger, T. 2015, *Astron. Astrophys.*, **584**, A17

Wade, G. A., Howarth, I. D., Townsend, R. H. D., et al. 2011, *Mon. Not. R. Astron. Soc.*, **416**, 3160

Wolff, S. C. & Wolff, R. J. 1971, *Astron. J.*, **76**, 422

Contrib. Astron. Obs. Skalnaté Pleso **48**, 175 – 179, (2018)

Rotation, Emission, & Evolution of the Magnetic Early B-type Stars

M. Shultz[1], G.A. Wade[2], Th. Rivinius[3], C. Neiner[4], O. Kochukhov[1] and E. Alecian[5]

[1] *Department of Physics and Astronomy, Uppsala University, Box 516, Uppsala 75120, (E-mail: matt.shultz@gmail.com)*

[2] *Department of Physics, Royal Military College of Canada, Kingston, Ontario K7K 7B4, Canada*

[3] *European Southern Observatory, Casilla 19001, Santiago 19, Chile*

[4] *LESIA, Observatoire de Paris, PSL Research University, CNRS, Sorbonne Universits, UPMC Univ. Paris 06, Univ. Paris Diderot, Sorbonne Paris Cit, 5 place Jules Janssen, 92195 Meudon, France*

[5] *Univ. Grenoble Alpes, CNRS, IPAG, F-38000 Grenoble, France*

Received: November 8, 2017; Accepted: January 5, 2018

Abstract. We report the results of the first population study of 51 magnetic early B-type stars, based upon a large database of high-resolution spectropolarimetry assembled by the MiMeS and BinaMIcS collaborations. Utilizing these data, rotational periods were determined for all but 5 of the sample stars. This enabled us to determine dipole oblique rotator model parameters, rotational parameters, and magnetospheric parameters. We find that the ratio of the Alfvén radius to the Kepler corotation radius is highly predictive of whether or not a star displays Hα emission from a Centrifugal Magnetosphere (CM), as expected from theoretical considerations. We also find that CM host stars are systematically younger than the general population, as expected given that CM emission requires rapid rotation and a strong magnetic field, and a strong magnetic field will lead to rapid magnetic braking. We conclude that emission-line magnetic early B-type stars are, almost without exception, strongly magnetized, rapidly rotating, and young.

Key words: stars: magnetic field – stars: rotation – stars: early-type – stars: evolution – stars: massive

1. Introduction

Thanks to extensive spectropolarimetric surveys, in particular the Magnetism in Massive Stars (MiMeS) survey, the number of early-type stars with detected magnetic fields has increased dramatically during the past decade (Wade et al., 2016). Approximately 10% of early-type stars are magnetic (Wade et al., 2016; Grunhut et al., 2017), a fraction that is approximately constant for stars with radiative envelopes. Magnetic stars earlier than about type B5 sometimes possess Hα emission originating in their corotating magnetospheres. Petit et al.

(2013) showed that emission-line magnetic hot stars can be classified as possessing either Dynamical Magnetospheres (DMs) or Centrifugal Magnetospheres (CMs), depending on whether the centrifugal force arising from corotation of the magnetically confined plasma with the stellar surface is strong enough to prevent gravitational infall. While this division was approximately succesful in separating stars with and without detectable Hα emission, when first proposed there was significant uncertainty regarding the combination of magnetic, rotational, and stellar parameters necessary for a star's magnetosphere to become detectable. In addition, the presence or absence of Hα emission had not been determined for many of the stars examined by Petit et al. (2013).

In order to more precisely explore the boundaries between stars with and without emission, we assembled a sample of 51 magnetic stars with spectral types between B5 and B0, i.e. essentially all known such objects. The study is based upon a large database of high-resolution ESPaDOnS, Narval, and HARPSpol spectropolarimetry, principally obtained by the MiMeS Large Programs (LPs), but also including data obtained by the Binarity and Magnetic Interactions in various classes of Stars (BinaMIcS) and BRITE spectropolarimetric survey (BRITEpol) LPs (Alecian et al., 2015; Neiner et al., 2016), as well as various individual observing programs. In total 1159 spectropolarimetric sequences were obtained, yielding 792 magnetic measurements after removal of bad data and, when appropriate and necessary, temporal binning. Longitudinal magnetic field $\langle B_z \rangle$ measurements (Mathys, 1989) were obtained from Least-Squares Deconvolution (LSD) profiles (Donati et al., 1997; Kochukhov et al., 2010) and H lines. The $\langle B_z \rangle$ measurements, supplemented in some cases by spectroscopic or archival Hipparcos photometric data, were used to obtain rotational periods $P_{\rm rot}$. The empirical analysis of these data were presented by Shultz et al. (2018). These data also enabled us to evaluate the Hα emission status of all stars. Here, we discuss some of the principle conclusions that can be drawn about the differences between magnetic early B-type stars with and without optical emission lines.

2. Results

Basic stellar parameters (radius R_*, mass M_*, age t, and fractional main sequence age $\tau_{\rm TAMS}$) were determined from the effective temperatures $T_{\rm eff}$ (determined spectroscopically either via spectral modelling, where this was available, or via EW ratios, where it was not), log luminosities $\log(L_*/{\rm L}_\odot)$ (determined photometrically), and log surface gravities $\log g$ (determined via spectral modelling of Hβ and Hγ). For each star, overlapping positions on the Hertzsprung-Russell Diagram and $T_{\rm eff}$-$\log g$ diagrams were determined, and stellar parameters then obtained via interpolation within the rotating evolutionary tracks and isochrones calculated by Ekström et al. (2012). For stars belonging to clusters or OB associations (about half the sample), stellar parameters were further

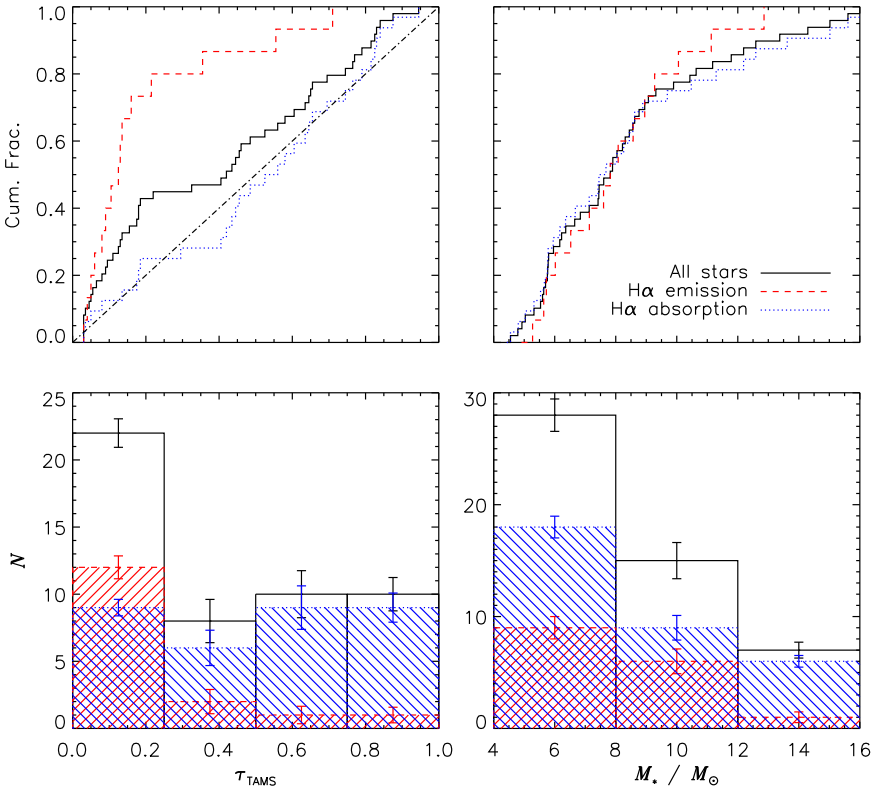

Figure 1. Cumulative distributions (top) and histograms (bottom) of fractional main sequence age $\tau_{\rm TAMS}$ (left) and mass M_* (right) for stars with (dashed red) and without (dotted blue) Hα emission. Emission-line stars are systematically younger than absorption-line stars. The dot-dashed line indicates a flat age distribution, with which the absorption-line stars are consistent. No such dichotomy is apparent for stellar mass.

required to be consistent with the cluster ages determined via main-sequence turnoffs, thus improving the precision of age determination.

Figure 1 shows cumulative distributions and histograms of $\tau_{\rm TAMS}$ and M_* for stars with and without emission. While Hα emission-line stars comprise only about 25% of the overall sample, they are a majority (57%) of stars with $\tau_{\rm TAMS} < 0.25$. The two-sample K-S test probability that the emission- and absorption-line stars belong to the same age distribution is 0.002. By way of contrast, there is no difference in the mass distributions (K-S test probability of 0.95 to belong to the same distribution). From this we conclude that emission-line stars are systematically younger than stars without emission.

Stellar magnetospheres are characterized by two length scales: the Alfvén

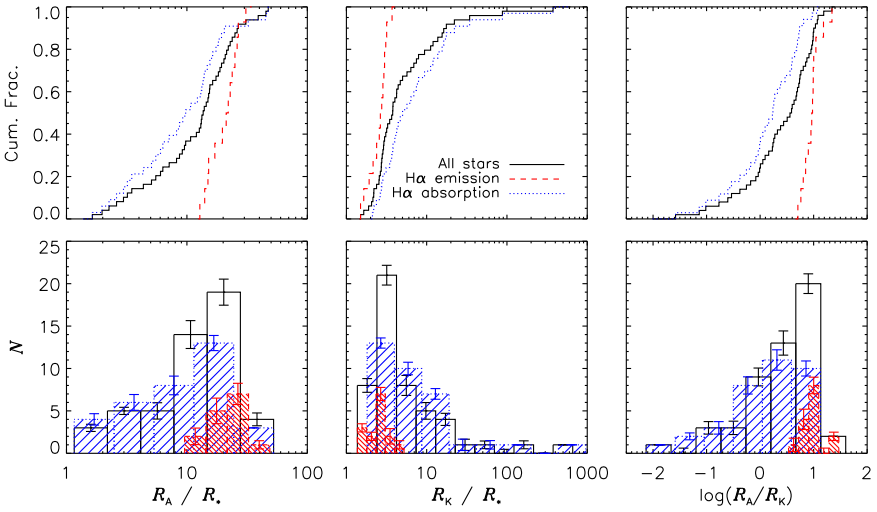

Figure 2. Cumulative distributions (top) and histograms (bottom) of Alfvén radius $R_{\rm A}$ (left), Kepler corotation radius $R_{\rm K}$ (middle), and $\log(R_{\rm A}/R_{\rm K})$ (right), for stars with (dashed red) and without (dotted blue) Hα emission. While there are clear differences in the distributions of $R_{\rm A}$ and $R_{\rm K}$ between emission and absorption-line stars, $\log(R_{\rm A}/R_{\rm K})$ provides a superior separation of the two populations.

radius $R_{\rm A}$, giving the distance to which the stellar wind remains magnetically confined; and the Kepler corotation radius $R_{\rm K}$, giving the distance at which centrifugal and gravitational forces balance. Only stars with $R_{\rm A} > R_{\rm K}$ possess CMs. $R_{\rm K}$ is calculated from $P_{\rm rot}$, M_*, and R_* (Townsend & Owocki, 2005). $R_{\rm A}$ is calculated from the surface magnetic dipole strength $B_{\rm d}$, R_*, the mass-loss rate $\log \dot{M}$, and the wind terminal velocity v_∞ (ud-Doula & Owocki, 2002), where we obtained $B_{\rm d}$ from dipole oblique rotator models based upon $\langle B_z \rangle$ curves, and wind parameters were calculated using the theoretical predictions of Vink et al. (2001).

Petit et al. (2013) suggested that $\log(R_{\rm A}/R_{\rm K}) > 0.8$ may be a minimum condition for Hα to go into emission. Figure 2 shows cumulative distributions and histograms for $R_{\rm A}$, $R_{\rm K}$, and $\log(R_{\rm A}/R_{\rm K})$, for stars with and without Hα emission. Emission-line stars possess systematically higher $R_{\rm A}$ and lower $R_{\rm K}$ than absorption-line stars: the median value of $R_{\rm A}$ for emission-line stars is 22 R_* vs. 9 R_* for absorption-line stars, and for $R_{\rm K}$ the respective medians are 2.7 R_* vs. 4.8 R_*. However, there is substantial overlap in both cases, with 9% of absorption line stars having $R_{\rm A}$ above the median value for emission-line stars, and 13% having $R_{\rm K}$ below the emission-line median. $\log(R_{\rm A}/R_{\rm K})$ provides a superior separation, with emission- and absorption-line medians of 0.97 and 0.23, and only 6% of absorption-line stars being above the emission-line median. The

two-sample K-S test probabilities for $R_{\rm A}$, $R_{\rm K}$, and $\log(R_{\rm A}/R_{\rm K})$ are respectively 10^{-3}, 10^{-5}, and 10^{-7}.

3. Conclusions

Magnetic B-type stars hosting detectable CMs are without exception rapidly rotating and strongly magnetized, and almost invariably young. The youth of Hα-bright stars makes sense given that strong magnetic fields should lead to rapid magnetic braking. This suggests that young stellar clusters should be the best places to look for more CM hosts, and that any such object will have a magnetic field of at least several kG, and $P_{\rm rot}$ below about 1.5 d.

References

Alecian, E., Neiner, C., Wade, G. A., et al. 2015, in IAU Symp., Vol. **307**, *New Windows on Massive Stars*, ed. G. Meynet, C. Georgy, J. Groh, & P. Stee, 330–335

Donati, J.-F., Semel, M., Carter, B. D., Rees, D. E., & Collier Cameron, A. 1997, *Mon. Not. R. Astron. Soc.*, **291**, 658

Ekström, S., Georgy, C., Eggenberger, P., et al. 2012, *Astron. Astrophys.*, **537**, A146

Grunhut, J. H., Wade, G. A., Neiner, C., et al. 2017, *Mon. Not. R. Astron. Soc.*, **465**, 2432

Kochukhov, O., Makaganiuk, V., & Piskunov, N. 2010, *Astron. Astrophys.*, **524**, A5

Mathys, G. 1989, *Fundamentals of Cosmic Physics*, **13**, 143

Neiner, C., Wade, G., Marsden, S., & Blazère, A. 2016, *ArXiv e-prints* [arXiv:1611.03285]

Petit, V., Owocki, S. P., Wade, G. A., et al. 2013, *Mon. Not. R. Astron. Soc.*, **429**, 398

Shultz, M. E., Wade, G. A., Rivinius, T., et al. 2018, *Mon. Not. R. Astron. Soc.*, accepted, *ArXiv e-prints* [arXiv:1801.02924]

Townsend, R. H. D. & Owocki, S. P. 2005, *Mon. Not. R. Astron. Soc.*, **357**, 251

ud-Doula, A. & Owocki, S. P. 2002, *ApJ*, **576**, 413

Vink, J. S., de Koter, A., & Lamers, H. J. G. L. M. 2001, *Astron. Astrophys.*, **369**, 574

Wade, G. A., Neiner, C., Alecian, E., et al. 2016, *Mon. Not. R. Astron. Soc.*, **456**, 2

Contrib. Astron. Obs. Skalnaté Pleso **48**, 180 – 186, (2018)

Magnetic fields of cool giant and supergiant stars: models versus observations

H. Korhonen

Dark Cosmology Centre, Niels Bohr Institute, University of Copenhagen
DK-2100 Copenhagen, Denmark

Received: December 13, 2017; Accepted: January 6, 2018

Abstract. The recent years have brought great advances in our knowledge of magnetic fields in cool giant and supergiant stars. For example, starspots have been directly imaged on the surface of an active giant star using optical interferometry, and magnetic fields have been detected in numerous slowly rotating giants and even on supergiants. Here, I review what is currently known of the magnetism in cool giant and supergiant stars, and discuss the origin of these fields and what is theoretically known about them.

Key words: stars: atmospheres – stars: evolution – stars: late-type – stars: magnetic field

1. Introduction

Korhonen (2014) presented a review of the magnetism in cool giant and supergiant stars. The current review concentrates on the advances that have been made since then. The emphasis of this review is on actual magnetic field measurements, but also some discussion is included on imaging starspots and other interesting developments in the field.

2. Imaging starspots

Over the years starspot locations have been imaged from photometry and high resolution spectroscopy. The modelling of the photometric light-curves gives only accurate information on the longitudinal location of the spots (see, e.g., Vida et al., 2010). Using high resolution, high signal-to-noise spectroscopic observations and inversion techniques (Doppler imaging; see, e.g., Vogt & Penrod, 1983) gives information on both the spot longitude and latitude (e.g., Korhonen et al., 2007). In the following two recent advances on imaging surfaces of giant stars are discussed.

2.1. Interferometric imaging

During the last decade significant advances have been made in using long-baseline interferometric imaging. Nowadays, there are facilities that can combine

the light from six telescopes and produce high fidelity images. The latest breakthrough in interferometric imaging comes from imaging starspots on the surface of RS CVn-type active K giant ζ Andromedae (Roettenbacher et al., 2016).

Roettenbacher et al. (2016) imaged ζ And using the Michigan Infrared Combiner (MIRC) at Centre for High Angular Resolution Astronomy (CHARA) on Mt. Wilson. MIRC combines the light from all the six telescopes in the CHARA-array allowing for high fidelity imaging. The images obtained by Roettenbacher et al. (2016) at two different epochs, 2011 and 2013, show persistent polar spot and changing spots at lower latitudes. The images also revealed, for the first time, reliable starspot hemispheres (north vs south). In a very recent paper Roettenbacher et al. (2017) also critically discusses the pros and cons of different techniques for imaging stellar surface structures: light-curve inversions, Doppler imaging, and interferometric imaging.

2.2. Magnetic field maps from all four Stokes parameters

In another recent development, Rosén et al. (2015) used full four Stokes parameters in the magnetic field mapping of a RS CVn-type binary star II Peg. Typically only circular polarisation (Stokes V) is used in magnetic field mapping. The linear polarisation (Stokes Q and U) signals from starspot are weak, and linear polarisation also requires sophisticated radiative transfer modelling for interpreting the results.

Rosén et al. (2015) show the difference between maps obtained only from circular polarisation (Stokes I and V) and using full four Stokes parameters (Stokes I, V, Q, and U). Their results clearly show that the strength of some of the surface features increases significantly (doubles or even quadrupled) when linear polarization is taken into account. At the same time, the total magnetic energy of the reconstructed field becomes significantly higher, and the over-all field complexity increases. This is well illustrated in Fig. 1, which shows the magnetic field energy in different spherical harmonic modes for IV and IVQU maps.

The study of Rosén et al. (2015) underlines the importance of using all the four Stokes parameters, if possible, when doing Zeeman Doppler imaging. This result has been shown before for the hot stars (e.g., Wade et al., 2000), but is now also convincingly expanded to cool stars.

3. Magnetic field measurements in cool giant stars

The following sections discuss the recent measurements of magnetic fields in stars when they evolve away from the main sequence towards the asymptotic giant branch (AGB). AGB stars are not in the scope of this review, as they were discussed in another review talk (Vlemmings 2018, these proceedings).

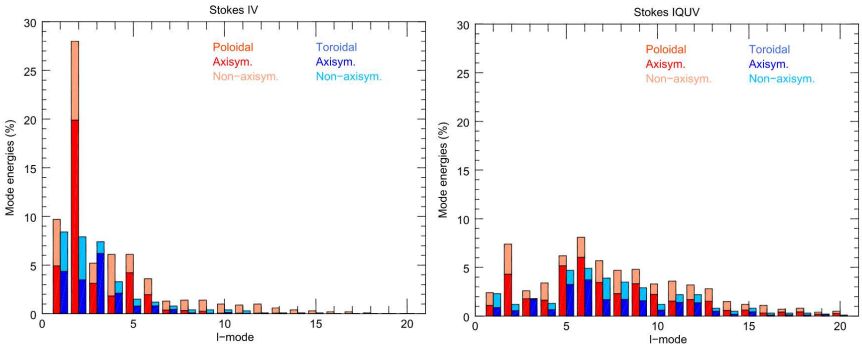

Figure 1. Distribution of the magnetic energy in different harmonic modes for the map obtained only from circular polarisation (Stokes IV) and also taking into account linear polarisation (Stokes IVQU). (From Rosén et al., 2015)

3.1. Hertzsprung gap stars

When a star leaves the main sequence, it will first cross the so-called Hertzsprung gap; an area where there are only a few stars due to the fast evolution in this phase.

Magnetic field measurements, and also surface magnetic field maps, have been obtained of few stars in the Hertzsprung gap. For example, Tsvetkova et al. (2017) looked at 37 Com, a 6.5 $M_\odot$ Hertzsprung gap star, and recover magnetic field configuration that has mainly poloidal geometry. Borisova et al. (2016) compared the behaviour of two Hertzsprung gap giants, OU And and 31 Com, which have very similar masses but different rotation period. OU And has rotation period of 24.2 days and mass of 2.7 $M_\odot$, whereas 31 Com has rotation period of 6.8 days and mass of 2.85 $M_\odot$. Magnetic fields are detected in both stars. Surprisingly, the faster rotating 31 Com has a weaker field with complex topology, and the slower rotating OU And has a stronger field and largely dipolar topology. Borisova et al. (2016) concluded that the field in 31 Com was most likely dynamo created, and that OU And was possibly a descendant of a magnetic Ap star.

3.2. Red giant stars

In the recent years magnetic field measurements in numerous red giant stars have been obtained. Aurière et al. (2015) studied magnetic fields in a sample of 48 evolved cool stars. From the target stars 24 were known to show signs of magnetic activity. The study found definite detection of magnetic field in 29 targets, and Zeeman signatures were found in all but one of the 24 active red giants. The additional six stars showing magnetic fields were bright red giants. When comparing the activity index S to the magnetic field detection, one can

see that the sample of Aurière et al. (2015) has detections mostly on stars with higher activity levels.

However, also really slowly rotating red giants can exhibit weak, but detectable, magnetic fields. Weak, sub-Gauss, magnetic fields have been detected for example in Pollux (K0 III, period ∼100-500 d, Aurière et al., 2015), and Arcturus (K1.5 III, ∼730 d, Sennhauser & Berdyugina, 2011). Aurière et al. (2015) detect weak fields also on Aldebaran, Alphard, and η Psc. Aurière et al. (2015) suggested that a solar-like $\alpha\Omega$-dynamo driven by convection and differential rotation is operating in these stars.

Theoretical calculations by Charbonnel et al. (2017) show that Dynamo processes might be favoured in the stellar convective envelope at two specific moments at the later stages of stellar evolution: during the first dredge-up, and during central helium burning in the helium-burning phase and early-AGB. This is nicely supported by the results of Aurière et al. (2015).

3.3. The special case of EK Eri

EK Eridani is a special case among magnetic cool giants. Its highest measured longitudinal magnetic field is ∼100 G (Aurière et al., 2015), but its rotation period is surprisingly long, ∼300 days (Strassmeier et al., 1999).

Stars with dynamo created magnetic fields tend to scatter around a line, if one plots their Rosby number (rotation period divided by the convective turnover time) against the longitudinal magnetic field strength. In Fig. 2 stars in Aurière et al. (2015) sample are plotted. The location of EK Eri this diagram implies that its magnetic field is most likely not dynamo created. Therefore, it is most likely a descendant of a strongly magnetic Ap star (Aurière et al., 2015).

However, the formation of the convective outer layer during the transition from main sequence to red giant phase would initiate dynamo-created field. This should destroy the earlier fossil field with very short time scales (Arlt & Bonnano, private communication). The location of EK Eri at the base of the red giant branch would imply that the possible fossil field should have already been destroyed. Another star that is an outlier in Fig. 2 is OU And. But, as discussed earlier, this star is still in the Hertzsprung gap, and therefore could have still maintained its fossil field.

Also, β Cet has been proposed to be a descendant of Ap stars (Tsvetkova et al., 2013), but its location on the Rosby number vs magnetic field strength diagram, as seen in Fig. 2, implies that the magnetic field is most likely dynamo created.

4. Cool supergiants

Grunhut et al. (2010) carried out an extensive study of magnetic fields in supergiants. Their sample of 33 supergiants spanned the spectral types M1.5Iab to

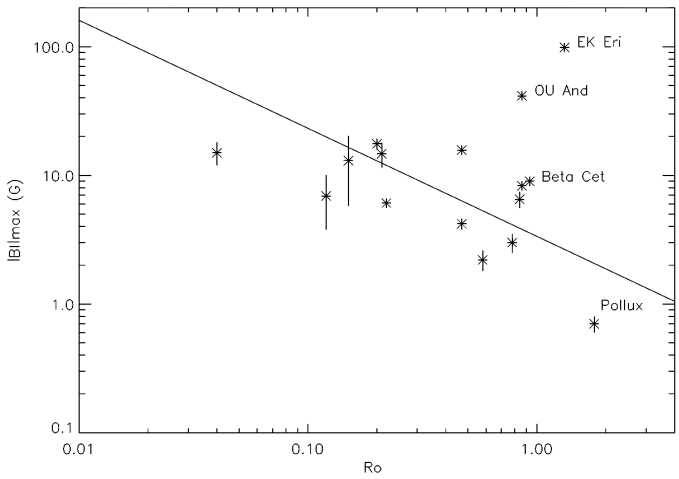

Figure 2. Correlating Rosby number and longitudinal magnetic field strength. (From Aurière et al., 2015)

A0Ib. They detected fields in nine of the sample stars, spanning spectral types F–K.

The first M supergiant star with detected magnetic fields was Betelgeuse (Aurière et al., 2010), and the fields have been proposed to concentrate in the sinking components of the convective flows (Petit et al., 2013). Recently, weak magnetic fields have also been detected in two other red supergiants: CE Tau and μ Cep (Tessore et al., 2017). It has been postulated that the fields in supergiants can be created by local dynamo operating in the giant convective cells (Dorch, 2004).

5. Other interesting developments

For this last section I have selected two interesting ideas from recent papers dealing with magnetic fields in evolved stars.

5.1. Dynamo enhancement due to engulfment of planets?

If a star engulf planets during the later stages of its evolution, it will also acquire the angular momentum of those planets. This, on the other hand, increases the rotation rate of the star and enhances dynamo operation

Privitera et al. (2016) show that the engulfment of a 15 M_J planet produces a dynamo triggered magnetic field stronger than 10 G for gravities between 2.5 and 1.9. They also show that for reasonable magnetic braking laws, the high

rotation rate induced by a planet engulfment may be maintained sufficiently long to be observable.

5.2. The mysterious case of red giant oscillations

20% of red giants have suppressed $l = 1$ modes. Fuller et al. (2015) show that the suppression can be explained if waves entering the stellar core are prevented from returning to the envelope. Stello et al. (2016) saw no suppression in red giants below 1.1 $M_\odot$, and the incidence of magnetic suppression increases with mass, with red giants above 1.6 $M_\odot$ showing a suppression rate of 50% to 60%. Interestingly, this is the mass range where main sequence stars have convective cores. These results could imply magentic field creation in the convective cores, as predicted by, e.g., Augustson et al. (2016).

6. Conclusions

As is evident from this review, recent years have shown many new developments in observing magnetic fields in cool giant and supergiant stars. Our observations show that magnetic fields are indeed present in basically all the stellar evolutionary stages – at least weak fields.

The origin of these magnetic fields are roughly from two different origins: $\alpha\Omega$-type dynamo process operating in the convective envelope, and fossil fields. It has also been postulated that dynamos can operate in giant convective shells of super giant stars. And there is also increasing evidence that higher mass stars can have dynamos operating also in their convective cores.

Acknowledgements. HK acknowledges financial support from the conference organisers and the Danish Augustinus foundation which made her participation in this interesting conference possible.

References

Augustson, K. C., Brun, A. S., & Toomre, J. 2016, *Astrophys. J.*, **829**, 92

Aurière, M., Donati, J.-F., Konstantinova-Antova, R., et al. 2010, *Astron. Astrophys.*, **516**, L2

Aurière, M., Konstantinova-Antova, R., Charbonnel, C., et al. 2015, *Astron. Astrophys.*, **574**, A90

Borisova, A., Aurière, M., Petit, P., et al. 2016, *Astron. Astrophys.*, **591**, A57

Charbonnel, C., Decressin, T., Lagarde, N., et al. 2017, *Astron. Astrophys.*, **605**, A102

Dorch, S. B. F. 2004, *Astron. Astrophys.*, **423**, 1101

Fuller, J., Cantiello, M., Stello, D., Garcia, R. A., & Bildsten, L. 2015, *Science*, **350**, 423

Grunhut, J. H., Wade, G. A., Hanes, D. A., & Alecian, E. 2010, *Mon. Not. R. Astron. Soc.*, **408**, 2290

Korhonen, H. 2014, in IAU Symp., Vol. **302**, *Magnetic Fields throughout Stellar Evolution*, ed. P. Petit, M. Jardine, & H. C. Spruit, 350–358

Korhonen, H., Berdyugina, S. V., Hackman, T., et al. 2007, *Astron. Astrophys.*, **476**, 881

Petit, P., Aurière, M., Konstantinova-Antova, R., et al. 2013, in Lecture Notes in Physics, Berlin Springer Verlag, Vol. **857**, *The Environments of the Sun and the Stars*, ed. J.-P. Rozelot & C. Neiner, 231

Privitera, G., Meynet, G., Eggenberger, P., et al. 2016, *Astron. Astrophys.*, **593**, L15

Roettenbacher, R. M., Monnier, J. D., Korhonen, H., et al. 2016, *Nature*, **533**, 217

Roettenbacher, R. M., Monnier, J. D., Korhonen, H., et al. 2017, *Astrophys. J.*, **849**, 120

Rosén, L., Kochukhov, O., & Wade, G. A. 2015, *Astrophys. J.*, **805**, 169

Sennhauser, C. & Berdyugina, S. V. 2011, *Astron. Astrophys.*, **529**, A100

Stello, D., Cantiello, M., Fuller, J., et al. 2016, *Nature*, **529**, 364

Strassmeier, K. G., Stępień , K., Henry, G. W., & Hall, D. S. 1999, *Astron. Astrophys.*, **343**, 175

Tessore, B., Lèbre, A., Morin, J., et al. 2017, *Astron. Astrophys.*, **603**, A129

Tsvetkova, S., Petit, P., Aurière, M., et al. 2013, *Astron. Astrophys.*, **556**, A43

Tsvetkova, S., Petit, P., Konstantinova-Antova, R., et al. 2017, *Astron. Astrophys.*, **599**, A72

Vida, K., Oláh, K., Kovári, Z., et al. 2010, *Astron. Nachr.*, **331**, 250

Vogt, S. S. & Penrod, G. D. 1983, *Publ. Astron. Soc. Pac.*, **95**, 565

Wade, G. A., Donati, J.-F., Landstreet, J. D., & Shorlin, S. L. S. 2000, *Mon. Not. R. Astron. Soc.*, **313**, 851

Contrib. Astron. Obs. Skalnaté Pleso **48**, 187 – 193, (2018)

Magnetic fields around evolved stars

W. H. T. Vlemmings

Department of Space, Earth and Environment, Chalmers University of Technology, Onsala Space Observatory, 439 92 Onsala, Sweden (E-mail: wouter.vlemmings@chalmers.se)

Received: December 19, 2017; Accepted: December 28, 2017

Abstract. There has long been evidence of magnetic fields in the extended envelopes of asymptotic giant branch (AGB) and red supergiant (RSG) stars. These stars are important contributors to the enrichment of the interstellar medium by dust and heavy elements. Magnetic fields might play a role in the mass loss process responsible. Additionally, magnetic fields, typically in combination with binary companions, have often be suggested to be involved in shaping strongly a-spherical planetary nebulae (PNe). New telescopes and instruments are increasing our knowledge about magnetic fields around these evolved, mass losing, stars and their descendants.

Key words: supergiants – stars: AGB and post-AGB – stars: mass-loss – planetary nebulae: general magnetic fields – polarization – masers

1. Introduction

The role of magnetic fields around AGB stars is not clear. In principle, they could help levitate material off the stellar surface of AGB stars, through Alfvén waves (e.g. Falceta-Gonçalves & Jatenco-Pereira, 2002), or through the creation of cool spots on the surface above with dust can form easier (Soker, 1998). After the AGB phase, the stellar envelopes undergo a major modification as they evolve to PNe. The formation mechanism of in particular bipolar PNe is still a matter of fierce debate. Current theories to explain the PNe shapes include binaries, disks, magnetic fields or a combination of these. A promising mechanism could be a binary companion or massive planet that helps maintain a strong magnetic field capable of shaping the outflow (Nordhaus et al., 2007). The mechanisms that drive mass loss from more massive evolved stars are also not well understood. The formation of dust grains that are non-transparent to stellar radiation, thought to drive the winds for several types of AGB stars, is inhibited close to evolved massive stars due to their extreme luminosity (e.g Norris et al., 2012). It is thus puzzling how the material is transported from the surface of the star to the radius where non-transparent dust species form. The distribution of material in the CSE of RSG stars is also highly a-spherical (e.g. Humphreys et al., 2007; O'Gorman et al., 2015). Models invoking e.g. convection, pulsations, scattering and magnetic waves have been proposed to explain the (anisotropic) mass loss in evolve massive stars, but it remains unclear which of these mechanisms plays the dominant role.

A previous review on AGB and (P-)PNe magnetic fields(e.g. Vlemmings, 2014) provides much of the background. Here I specifically focus on the most recent observational developments. I also predominantly focus on the observations of magnetic fields in the CSEs, although will present new observations that could indicate magnetic activity at the surface. This review concerns the magnetic field in RSG stars, AGB stars, and beyond. The earlier phases of cool giant stars are discussed in another review (Korhonen 2018, these proceedings).

2. Observational Techniques of CSE magnetic fields

2.1. Circular Polarization

The predominant source of magnetic field strength information during the late stages of stellar evolution comes from maser Zeeman splitting observations, and particularly the common SiO, H_2O and OH masers. These can show circular polarization fractions ranging from $\sim 0.1\%$ (H_2O) up to $\sim 100\%$ (OH) and are, because of their compactness and strength, excellent sources to be observed with high angular resolution (for a review, see Vlemmings, 2012). More recently, Zeeman splitting has also been detected in circumstellar CN (Duthu et al., 2017).

2.2. Linear Polarization

Linear polarization can be observed both in the dust (through aligned grains) and molecular lines (through radiation anisotropy - the Goldreich-Kylafis (GK) effect). The GK effect on CO has only recently been mapped for the first time in the envelope of evolved stars (Vlemmings et al., 2012) and allows for a systematic study of magnetic fields using ALMA. Typical percentages of linear polarization range from up to a few percent (e.g. dust, CO, H_2O masers) to several tens of percent (OH and SiO masers). Recent ALMA observations have confirmed that the linear polarization of OH masers probes the same large scale fields as observed in non-masing molecular lines (Tafoya & Vlemmings in prep.).

3. Observational status

3.1. AGB stars

Generally, AGB magnetic field measurements come from maser polarization observations (SiO, H_2O and OH). These have revealed a strong magnetic field throughout the circumstellar envelope. Figure 1, the magnetic field strength in the regions of the envelope traced by the maser measurements throughout AGB envelopes. The field appears to vary between $B \propto R^{-2}$ (solar-type) and $B \propto R^{-1}$ (toroidal). Although the maser observations trace only oxygen-rich AGB stars, recent CN Zeeman splitting observations (Duthu et al., 2017) indicate that similar strength fields are found around carbon-rich stars.

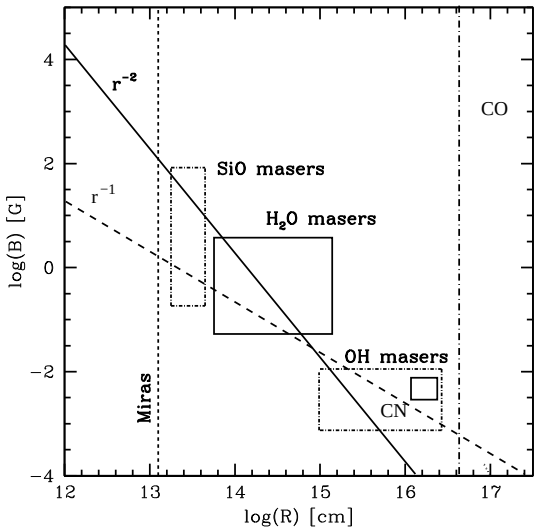

Figure 1. Magnetic field strength vs. radius relation as indicated by current maser polarization observation of a number of Mira stars. The boxes show the range of observed magnetic field strengths derived from the observations of SiO masers (Kemball et al., 2009; Herpin et al., 2006)), H_2O masers (Vlemmings et al., 2002, 2005; Leal-Ferreira et al., 2013), OH masers (Rudnitski et al., 2010; Gonidakis et al., 2014) and CN (Duthu et al., 2017). The thick solid and dashed lines indicate an r^{-2} solar-type and r^{-1} toroidal magnetic field configuration. The vertical dashed line indicates the stellar surface. CO polarization observations (e.g. Vlemmings et al., 2012) will uniquely probe the outer edge of the envelope (vertical dashed dotted line).

The exact structure of the magnetic fields is more difficult to determine. Even though OH observations indicate a systematic field structure (e.g. Bains et al., 2003), it has often been suggested that there might not be a large scale component to the field that would be necessary to shape the outflow (Soker, 2002). Observations of the linear polarization of CO (and other molecular lines) caused by the Goldreich-Kylafis effect (e.g. Vlemmings et al., 2012) allows for a much more detailed study of the magnetic field morphology. In the case of IK Tau, the observations indicate a more or less uniform field from close to the star out to a few thousand AU. Recent ALMA observations of CO polarization around the post-AGB star OH17.7-2.0 further indicate that the magnetic field probed by the CO molecule is that same as that probed by the OH masers (Tafoya & Vlemmings, in prep.).

The envelope magnetic fields are also consistent with thus far the only direct measurement of the Zeeman effect on the surface of an AGB star, the Mira

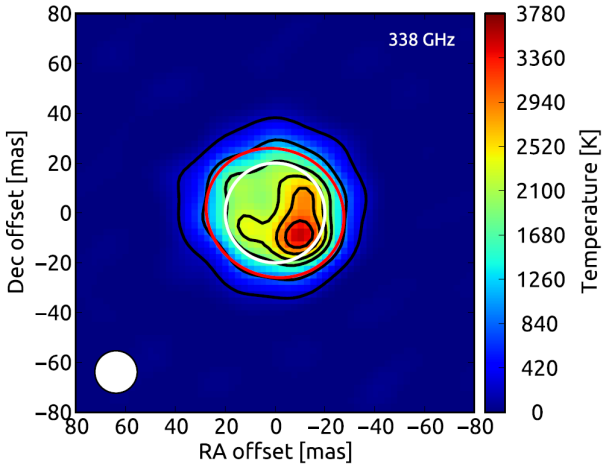

Figure 2. Brightness temperature map of the AGB star W Hya observed with ALMA at 338 GHz (Vlemmings et al., 2017a). The red ellipse indicates the size of the stellar disk at 338 GHz while the white circles indicates the size of the optical photosphere. The clear hotspot is unresolved and it brightness temperature in the map is a lower limit. From size measurements we can constrain the true brightness temperature to be $> 50\,000$ K, which could be a sign of shock interaction or magnetic activity.

variable star χ Cyg (Lèbre et al., 2014). Interestingly, recently observations were made with ALMA of the surface activity of the AGB star W Hya (Vlemmings et al., 2017a, Fig. 2). The activity could be related to magnetic fields. In Table 1 an overview is given of the energy densities throughout the AGB envelopes.

3.2. post-AGB stars and (P-)PNe

Similar to the AGB stars, masers are the main source of magnetic field information of post-AGB and P-PNe and even for some PNe. OH maser observations indicate magnetic field strengths similar to those of AGB stars (few mG) and a clear large scale magnetic field structure (Bains et al., 2003; Gómez et al., 2016). Also dust polarization observations indicate a large scale magnetic field (e.g. Sabin et al., 2015a).

Magnetic fields have also been detected around the so-called 'water-fountain' sources. These sources exhibit fast and highly collimated H_2O maser jets that often extend beyond even the regular OH maser shell. With the dynamical age of the jet of order 100 years, they potentially are the progenitors of the bipolar (P-)PNe. Observations of the arch-type of the water-fountains, W43A, have revealed a strong toroidal magnetic field that is collimating the jet (Vlemmings et al., 2006). For another water-fountain source, IRAS 15445-5449, a synchrotron

Table 1. Energy densities in AGB envelopes

		Photosphere	SiO	H_2O	OH
B	[G]	$\sim 1-10$?	~ 3.5	~ 0.3	~ 0.003
R	[AU]	-	~ 3	~ 25	~ 50
$V_{\rm exp}$	[km s^{-1}]	~ 20	~ 5	~ 8	~ 10
$n_{\rm H_2}$	[cm^{-3}]	$\sim 10^{11}$	$\sim 10^{10}$	$\sim 10^{8}$	$\sim 10^{6}$
T	[K]	~ 2500	~ 1300	~ 500	~ 300
$B^2/8\pi$	[dyne cm^{-2}]	$\mathbf{10^{-1.4,+0.6}}$?	$\mathbf{10^{+0.1}}$	$\mathbf{10^{-2.4}}$	$10^{-6.4}$
nKT	[dyne cm^{-2}]	$10^{-1.5}$	$10^{-2.7}$	$10^{-5.2}$	$10^{-7.4}$
$\rho V_{\rm exp}^2$	[dyne cm^{-2}]	$10^{-0.3}$	$10^{-2.5}$	$10^{-4.1}$	$\mathbf{10^{-5.9}}$
V_A	[km s^{-1}]	~ 20	~ 100	~ 300	~ 8

jet related to strong magnetic fields has been detected (Pérez-Sánchez et al., 2013). Similar, synchrotron emission has been found from what could be one of the youngest PNe (Suárez et al., 2015).

Finally, recently also surface fields have been measured for two post-AGB stars (Sabin et al., 2015b). These fields are consistent with the fields inferred from the envelope measurements

3.3. RSG stars

Maser observations have also long indicated strong magnetic fields in the envelopes of RSG stars (e.g. Vlemmings et al., 2002; Herpin et al., 2006). Most of the points that are relevant for AGB stars, such as the questions about local or large scale fields, are the same. The supergiant VX Sgr is one of the first stars where a large scale magnetic field, with a structure consistent throughout the envelope, was found (e.g. Vlemmings et al., 2005). With ALMA it is now possible to simultaneously study the polarization of regular molecular lines, maser lines, and circumstellar dust. Recent observations of VY CMa indicate magnetically aligned dust and consistent structures between the maser and non-maser molecular lines (Vlemmings et al., 2017b, Fig. 3). The observations indicate the magnetic processes might be involved in the mass loss of these massive stars.

4. Conclusions

Many observations have now shown that ordered magnetic fields are present throughout the envelopes of AGB, post-AGB, (P-)PNe and RSG stars. The question on their origin and influence however, has not yet conclusively been answered. In the near future, it will finally be possible to relate dust and gas

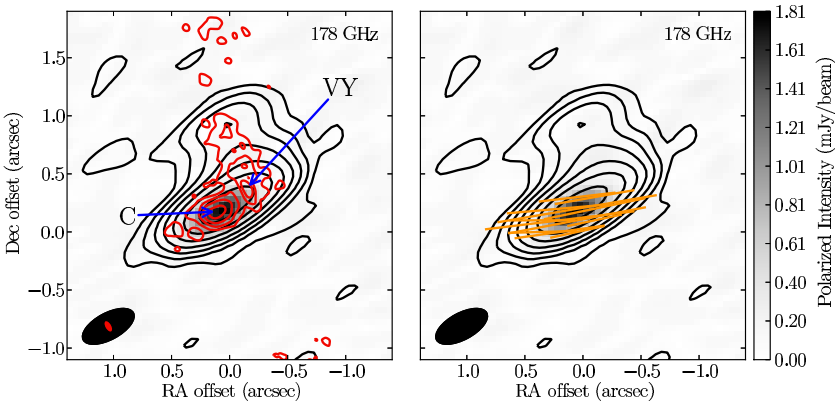

Figure 3. ALMA observations of the dust around the RSG VY CMa at 178 GHz (Vlemmings et al., 2017b). Arrows indicate dust clump C and the star (VY) identified in previous ALMA observations (O'Gorman et al., 2015). The grey scale image is the linearly polarized intensity, which is seen to peak at the bright dust component Clump C in the South-East. The similarly spaced red contours (left) indicate the ALMA 658 GHz continuum from O'Gorman et al. (2015). The vectors (right) indicate the direction of polarization rotated by 90° to indicate the magnetic field direction traced by magnetically aligned dust grains.

structures and kinematics, to the strength and morphology of the magnetic field for significant samples of stars.

Acknowledgements. WV acknowledges support from the European Research Council (ERC) through the ERC consolidator grant nr. 614264 and from the Swedish Research Council.

References

Bains, I., Gledhill, T. M., Yates, J. A., & Richards, A. M. S. 2003, *Mon. Not. R. Astron. Soc.*, **338**, 287

Duthu, A., Herpin, F., Wiesemeyer, H., et al. 2017, *Astron. Astrophys.*, **604**, A12

Falceta-Gonçalves, D. & Jatenco-Pereira, V. 2002, *Astrophys. J.*, **576**, 976

Gómez, J. F., Uscanga, L., Green, J. A., et al. 2016, *Mon. Not. R. Astron. Soc.*, **461**, 3259

Gonidakis, I., Chapman, J. M., Deacon, R. M., & Green, A. J. 2014, *Mon. Not. R. Astron. Soc.*, **443**, 3819

Herpin, F., Baudry, A., Thum, C., Morris, D., & Wiesemeyer, H. 2006, *Astron. Astrophys.*, **450**, 667

Humphreys, R. M., Helton, L. A., & Jones, T. J. 2007, *Astron. J.*, **133**, 2716

Kemball, A. J., Diamond, P. J., Gonidakis, I., et al. 2009, *Astrophys. J.*, **698**, 1721

Leal-Ferreira, M. L., Vlemmings, W. H. T., Kemball, A., & Amiri, N. 2013, *Astron. Astrophys.*, **554**, A134

Lèbre, A., Aurière, M., Fabas, N., et al. 2014, *Astron. Astrophys.*, **561**, A85

Nordhaus, J., Blackman, E. G., & Frank, A. 2007, *Mon. Not. R. Astron. Soc.*, **376**, 599

Norris, B. R. M., Tuthill, P. G., Ireland, M. J., et al. 2012, *Nature*, **484**, 220

O'Gorman, E., Vlemmings, W., Richards, A. M. S., et al. 2015, *Astron. Astrophys.*, **573**, L1

Pérez-Sánchez, A. F., Vlemmings, W. H. T., Tafoya, D., & Chapman, J. M. 2013, *Mon. Not. R. Astron. Soc.*, **436**, L79

Rudnitski, G. M., Pashchenko, M. I., & Colom, P. 2010, *Astron. Rep.*, **54**, 400

Sabin, L., Hull, C. L. H., Plambeck, R. L., et al. 2015a, *Mon. Not. R. Astron. Soc.*, **449**, 2368

Sabin, L., Wade, G. A., & Lèbre, A. 2015b, *Mon. Not. R. Astron. Soc.*, **446**, 1988

Soker, N. 1998, *Mon. Not. R. Astron. Soc.*, **299**, 1242

Soker, N. 2002, *Mon. Not. R. Astron. Soc.*, **336**, 826

Suárez, O., Gómez, J. F., Bendjoya, P., et al. 2015, *Astrophys. J.*, **806**, 105

Vlemmings, W., Khouri, T., O'Gorman, E., et al. 2017a, *Nature Astronomy*, **1**, 848

Vlemmings, W. H. T. 2012, in IAU Symp., Vol. **287**, *Cosmic Masers - from OH to H0*, ed. R. S. Booth, W. H. T. Vlemmings, & E. M. L. Humphreys, 31–40

Vlemmings, W. H. T. 2014, in IAU Symp., Vol. **302**, *Magnetic Fields throughout Stellar Evolution*, ed. P. Petit, M. Jardine, & H. C. Spruit, 389–397

Vlemmings, W. H. T., Diamond, P. J., & Imai, H. 2006, *Nature*, **440**, 58

Vlemmings, W. H. T., Diamond, P. J., & van Langevelde, H. J. 2002, *Astron. Astrophys.*, **394**, 589

Vlemmings, W. H. T., Khouri, T., Martí-Vidal, I., et al. 2017b, *Astron. Astrophys.*, **603**, A92

Vlemmings, W. H. T., Ramstedt, S., Rao, R., & Maercker, M. 2012, *Astron. Astrophys.*, **540**, L3

Vlemmings, W. H. T., van Langevelde, H. J., & Diamond, P. J. 2005, *Astron. Astrophys.*, **434**, 1029

Contrib. Astron. Obs. Skalnaté Pleso **48**, 194 – 202, (2018)

Rotational properties of magnetic chemically peculiar stars

M. Netopil[1,2], E. Paunzen[2], S. Hümmerich[3] and K. Bernhard[3]

[1] *Institute for Astrophysics, University of Vienna, Türkenschanzstraße 17, 1180 Vienna, Austria, (E-mail: mn.netopil@gmail.com)*

[2] *Department of Theoretical Physics and Astrophysics, Masaryk University, Kotlárská 2, 611 37 Brno, Czech Republic*

[3] *Bundesdeutsche Arbeitsgemeinschaft für Veränderliche Sterne e.V. (BAV), Berlin, Germany*

Received: October 15, 2017; Accepted: October 25, 2017

Abstract. The magnetic chemically peculiar (mCP) stars of the upper main sequence exhibit strong and globally organized magnetic fields that are inclined to the rotational axis and facilitate the development of surface abundance inhomogeneities resulting in photometric and spectroscopic variability. Photometric time series data are much easier to obtain than spectroscopic/polarimetric data or are available from large surveys, thus the number of known rotational periods increased significantly during the last years. Furthermore, Gaia data allow us to place an unprecedentedly large sample of mCP stars in the Hertzsprung-Russell diagram and to investigate evolutionary effects. In this paper we review the rotational properties of mCP stars and discuss open issues of stellar rotation in the presence of strong magnetic fields.

Key words: stars: chemically peculiar – stars: magnetic field – stars: rotation – stars: evolution

1. Introduction

Stellar rotation is an important physical property that can have a significant influence on stellar evolution. For example, the main-sequence lifetime of a $3\,M_\odot$ star is extended by about 30 percent when comparing the evolutionary tracks by Ekström et al. (2012) for non-rotating models and for a rotation rate of $v_{ini}/v_{crit} = 0.4$, the peak of the observed velocity distribution of young B-type stars according to Huang et al. (2010). For most stars, rotation can only be inferred by spectroscopic data and the spectral line broadening, which is used to estimate the projected surface velocity on the line of sight ($v \sin i$). However, for some star groups photometry is a very powerful tool to obtain a direct estimate of the rotation period. Many active stars show large star spots that may cause brightness variations observable even with smaller ground-based telescopes, but high-precision satellite data by Kepler, for example, also allows to study rotation based on star spots with much lower contrast levels (e.g. Reinhold & Gizon, 2015).

Photometry is also a very well suited tool for deriving the rotational period for a group of hotter stars. Chemically peculiar (CP) stars are upper main sequence objects (spectral types early B to early F) with spectra that are characterized by abnormally strong (or weak) absorption lines that indicate peculiar surface elemental abundances. The observed chemical peculiarities are thought to arise from the diffusion of chemical elements due to the competition between radiative pressure and gravitational settling. CP stars constitute about 10% of upper main sequence stars and are commonly subdivided into four classes according to Preston (1974): metallic line (or Am) stars (CP1), magnetic Ap stars (CP2), HgMn stars (CP3), and He-weak stars (CP4). The CP2 and the CP4 objects (also known as Bp/Ap or mCP stars) are notorious for exhibiting strong, globally organized magnetic fields of up to several tens of kiloGauss. Their atmospheres are enriched by various elements such as Si, Cr, Sr, or Eu and usually present surface abundance patches or spots. These lead to photometric variability, which is considered to be caused by rotational modulation and is explained in terms of the oblique rotator model (Stibbs, 1950). As a result, the observed photometric period is the rotational period of the star. mCP stars that exhibit this phenomenon are normally classified as $\alpha 2$ Canum Venaticorum (ACV) variables.

Besides the Galactic mCP stars, representatives in the Large Magellanic Cloud have been discovered (Paunzen et al., 2006, 2011b). However, these stars show no or only weak evidence of variability (Paunzen et al., 2013). This can be either due to the accuracy of the available photometric data or caused by different conditions during star formation that result in the absence of photometric spots of overabundant optically active chemical elements.

2. Knowledge of rotational periods

For a long time the knowledge of mCP star periods increased only at a moderate level, but with the availability of Hipparcos epoch photometry we noticed a huge improvement. This resulted in a list of about 360 stars with known periods in the latest compilation by Renson & Catalano (2001). The onset of large photometric surveys during the last years provided the basis for another boost of knowledge. A first attempt was made by Wraight et al. (2012) using lightcurves obtained with the STEREO spacecraft. They were able to derive reliable periods for 82 mCP stars. However, a significant enlargement of the sample was provided by a series of papers using data from the The All Sky Automated Survey (ASAS) or the SuperWASP survey (Bernhard et al., 2015a,b; Hümmerich et al., 2016). These authors derived rotational periods for more than 750 mCP stars including a large fraction of hitherto unstudied objects. We also refer to the summary paper by Hümmerich et al. (2018, these proceedings). Furthermore, numerous additional stars are classified as ACV in variable star catalogues, for example in the International Variable Star Index of the AAVSO (VSX, Watson et al., 2006).

The above listed sources were merged by Netopil et al. (2017) to construct a list that includes period values for more than 1300 objects, covering almost four times more stars than the previous catalogue by Renson & Catalano (2001). Certainly, some more objects were studied on an individual basis, thus a careful evaluation of the literature published during the last one and a half decades is still an essential task to obtain a complete census of our knowledge of mCP star periods. Nonetheless, the compilation by Netopil et al. (2017) provides an unprecedented basis for detailed investigations of rotational properties.

3. Previous studies of rotational properties

In the course of time it became clear that mCP stars rotate less rapidly than chemically-normal type objects of the same spectral type and that they are not rapid rotators seen pole-on (e.g. Wolff, 1967). Later, based on some cluster stars, Hartoog (1977) concluded that there is no magnetic braking on a time scale up to one Gyr. He also proposed that most of the angular momentum (AM) is probably lost in the pre-main-sequence phase. Furthermore, comparisons of the velocity distributions suggest that mCP stars rotate about three to four times slower than normal type objects (Abt & Morrell, 1995). Thanks to Hipparcos parallax data and spectroscopic surface gravities, North (1998) was then able to investigate evolutionary effects in more detail. Based on a sample of about 100 field stars with known periods he concluded that the observations are entirely compatible with conservation of angular momentum. This finding was also confirmed by more recent studies (e.g. Kochukhov & Bagnulo, 2006; Hubrig et al., 2007), although the first reference notes that for lower mass mCP stars an additional AM loss on the main sequence cannot be ruled out.

Calculations by Stępień & Landstreet (2002) showed that it is fairly clear that mCP stars achieve their unusually low AM prior to the main sequence stage, which was already postulated by Hartoog (1977), as mentioned above. An observational confirmation was then presented by Alecian et al. (2013), who investigated a sample of Herbig Ae/Be stars with and without magnetic fields. It was shown that the magnetic stars have already lost most of their angular momentum, despite their young ages. Although the sample was still based on only a small number of magnetic objects, the conclusion can be considered as a confident one.

4. A rejuvenation study of rotational properties

The large number of available rotation periods and the first data release of the Gaia satellite mission allow a detailed reinvestigation of some rotational properties. Therefore, Netopil et al. (2017) compiled photometric data to estimate effective temperatures using the calibrations by Netopil et al. (2008) and to place a substantial sample of mCP stars in the Hertzsprung-Russell diagram

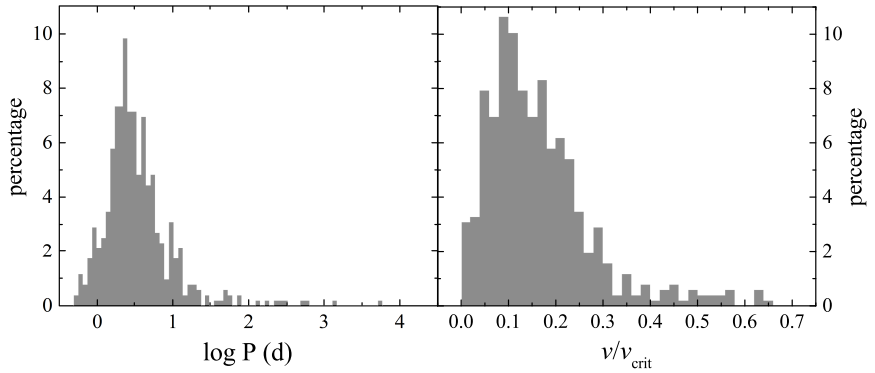

Figure 1. Distribution of periods and rotation rates $v/v_{\rm crit}$ based on the working sample of 518 mCP stars by Netopil et al. (2017). We adopted a binning so that both distributions show a comparable percentage at the maximum peaks.

(HRD). Although ACV characteristics already provide a reasonable hint at the mCP nature, they also used spectral types, photometric peculiarity indices, and magnetic field measurements to define a final working sample of 518 objects. Figure 1 shows the distribution of the adopted periods. The long-period tail of the distribution was recognized already for example by Wolff (1975), suggesting that a powerful deceleration mechanism has operated in these stars. This might be a result of the inclination of the magnetic and rotation axes, which are fairly closely aligned in stars with longer periods (Landstreet & Mathys, 2000). However, the distribution of the ratio of equatorial velocity ($V_{\rm eq}$) to the mass and time dependent critical velocity ($v/v_{\rm crit}$) shows also a tail of fast rotators (right panel of Fig. 1). This provides a stringent constraint for models of mCP stars, the efficiency of diffusion and its interplay with mixing processes. For only a few of the fast rotators the magnetic field has yet been measured, but all of these display field strengths of the order of 1.5 kG. Moreover, the fast rotators all have comparable masses of about $3\,{\rm M}_{\odot}$. However, this might not be an intrinsic property, because the mass distribution of all mCP stars peaks at this mass (see Fig. 3 by Netopil et al., 2017).

The comprehensive sample by Netopil et al. (2017) allowed an investigation of the rotational periods as a function of gravity by adopting narrower mass groups ($0.5\,{\rm M}_{\odot}$) than in previous studies. For all mass ranges they found excellent agreement with the evolutionary models by Georgy et al. (2013). This suggests conservation of angular momentum during the main sequence evolution without evidence of additional magnetic braking, which confirms previous conclusions. However, the very slow and very fast rotators cannot be explained by the increase of period during main sequence evolution alone. The period data were also transformed to $V_{\rm eq}$ and to the velocity ratio $v/v_{\rm crit}$. The latter

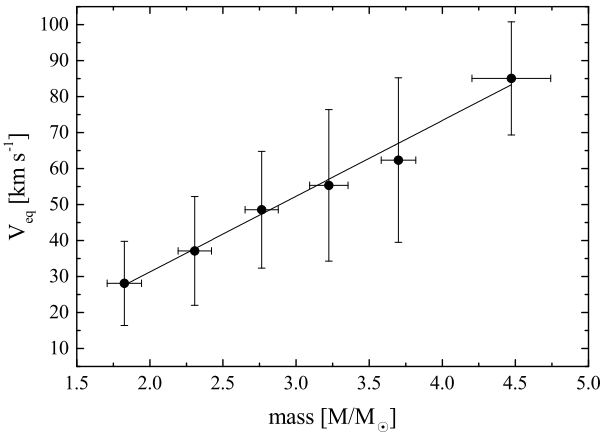

Figure 2. Median equatorial velocities of mCP stars as a function of mass based on the data by Netopil et al. (2017). The solid line represents the linear fit $V_{\rm eq}= -11(3) + 21(1)M/{\rm M}_{\odot}$.

represents a value that shows little dependence on evolutionary effects (Zorec & Royer, 2012). Netopil et al. (2017) investigated its dependence on mass, and Fig. 2 explores this in terms of $V_{\rm eq}$. Thus, consideration of the mass dependence is of importance in studies requiring the inclusion of stars with quite different masses. Based on 180 objects with available $v \sin i$ data the authors also investigated the inclination of the rotational axes. As expected, they found that these are randomly distributed, which confirms the previous conclusion by Abt (2001) using data for 102 stars. The increase of the number of objects is mostly based on the fact that more period data has become available, but we still notice a lack of spectroscopic studies.

Most of the results mentioned above are confirmations of previous studies, but the important link between rotation and magnetic field strength has not been considered yet. Usually, previous studies evaluated this relation only in the period domain. Kochukhov & Bagnulo (2006) concluded that their results indicate that the surface field is more intense in slowly rotating stars. On the other hand, Hubrig et al. (2007) note that stronger magnetic fields tend to be found in hotter, younger and more massive stars, as well as in stars with shorter rotation periods. Recently, Mathys (2017) significantly improved our knowledge by additional measurements of the mean magnetic field modulus, the most reliable measure of the actual field strength. He concluded that very strong magnetic fields ($\gtrsim 7.5$ kG) are found only in stars with rotation periods shorter than ~ 150 days. Furthermore, he notes that there are some atypical mCP stars which should not be considered for a generalised conclusion. One of these objects is HD 215441 (Babcock's star), the strongest magnetic mCP star.

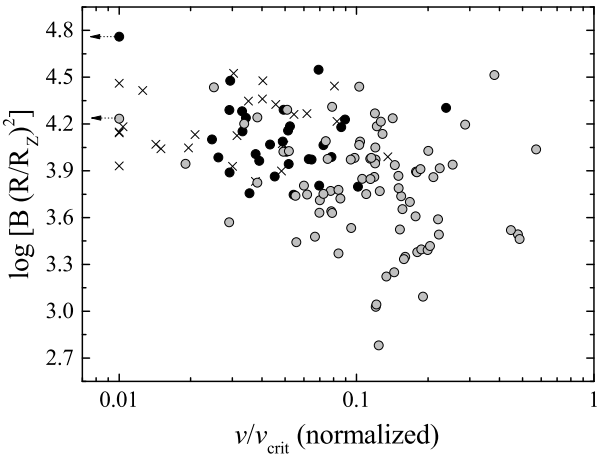

Figure 3. Magnetic fluxes as a function of normalized rotation rates. Black circles represent single stars from the sample of Mathys (2017), crosses SB systems in the last reference, and grey circles the data of Netopil et al. (2017) for stars with phase covered longitudinal field measurements. For the sake of a better representation we adopt a rotation rate of 0.01 for the slowest rotating stars, which represent approximately the error of this parameter for the slow rotators. The symbol at the very top left side represents Babcock's star.

Netopil et al. (2017) used the velocity ratio $v/v_{\rm crit}$ and the derived mass dependency of rotation to normalize their data sample. By adopting conservation of magnetic flux, they were able to show that the slowest rotating stars indeed show the strongest magnetic field. Thus, Babcock's star does not seem to be atypical at least in respect to rotation. Babcock's star is more massive than the very long-period objects, and its rotation rate, corrected for mass, is therefore actually lower, and it was braked more efficiently owing to its very strong magnetic field. However, the sample by Netopil et al. (2017) only includes a fraction of the stars listed by Mathys (2017). Figure 3 follows their investigation and shows an update by including about two third of the stars with a measured mean magnetic field modulus. A large fraction represents binary stars, and their inclusion certainly does not support the conclusion by Netopil et al. (2017). However, rotation might be influenced by both, the magnetic field and tidal braking by the companion. Thus, binary stars should be excluded from such an analysis. Furthermore, the position in the HRD clearly suffers from larger errors when the mass ratio is not very well known. We also note that the rotation period is still unknown for several objects in the list by Mathys (2017). An investigation of these objects will be of importance to obtain an even more profound picture between rotation and magnetic field strength. In addition, the possible binary nature of many little-studied objects requires more attention.

5. Conclusions

We reviewed some rotational properties of mCP stars. These cover the distribution of periods and their evolution on the main sequence, which suggests conservation of angular momentum, or the linear mass dependency of rotation. We also show a possible link between rotation and magnetic field strength. Although we notice a significant increase in the knowledge of rotation periods, we unfortunately still lack sufficient additional spectroscopic data. Beside the somewhat over-represented number of long-period stars, the distribution also shows a tail of very fast rotators. These are not yet fully explored, but they may also be in part the result of erroneous period data. Aliasing might be a problem for stars with sparse sampling or objects with very small amplitudes, for example. An additional influence might result from not correctly identified double-wave ACVs. These factors still has to be taken into account, but also the use of evolutionary models shows some open issues (see discussion by Netopil et al., 2017). We still do not know which metallicity is the proper choice for mCP stars. In addition, the width of the main sequence differs from model to model, mostly as a result of the adopted overshooting parameter. Also, evolutionary models appropriate for mCP objects do not yet take into account the magnetic field, which in turn offers another free parameter in the fitting procedure to obtain reliable parameters such as the mass. However, stellar age in particular is the most uncertain parameter for field stars. The investigation of more open cluster stars in respect to mCP nature or rotation period such as done by Paunzen et al. (2011a,c, 2014) would be imperative to further improve our knowledge.

References

Abt, H. A. 2001, *Astron. J.*, **122**, 2008

Abt, H. A. & Morrell, N. I. 1995, *Astrophys. J., Suppl. Ser.*, **99**, 135

Alecian, E., Wade, G. A., Catala, C., et al. 2013, *Mon. Not. R. Astron. Soc.*, **429**, 1027

Bernhard, K., Hümmerich, S., Otero, S., & Paunzen, E. 2015a, *Astron. Astrophys.*, **581**, A138

Bernhard, K., Hümmerich, S., & Paunzen, E. 2015b, *Astron. Nachr.*, **336**, 981

Ekström, S., Georgy, C., Eggenberger, P., et al. 2012, *Astron. Astrophys.*, **537**, A146

Georgy, C., Ekström, S., Granada, A., et al. 2013, *Astron. Astrophys.*, **553**, A24

Hartoog, M. R. 1977, *Astrophys. J.*, **212**, 723

Huang, W., Gies, D. R., & McSwain, M. V. 2010, *Astrophys. J.*, **722**, 605

Hubrig, S., North, P., & Schöller, M. 2007, *Astron. Nachr.*, **328**, 475

Hümmerich, S., Paunzen, E., & Bernhard, K. 2016, *Astron. J.*, **152**, 104

Kochukhov, O. & Bagnulo, S. 2006, *Astron. Astrophys.*, **450**, 763

Landstreet, J. D. & Mathys, G. 2000, *Astron. Astrophys.*, **359**, 213

Mathys, G. 2017, *Astron. Astrophys.*, **601**, A14

Netopil, M., Paunzen, E., Hümmerich, S., & Bernhard, K. 2017, *Mon. Not. R. Astron. Soc.*, **468**, 2745

Netopil, M., Paunzen, E., Maitzen, H. M., North, P., & Hubrig, S. 2008, *Astron. Astrophys.*, **491**, 545

North, P. 1998, *Astron. Astrophys.*, **334**, 181

Paunzen, E., Hensberge, H., Maitzen, H. M., et al. 2011a, *Astron. Astrophys.*, **525**, A16

Paunzen, E., Maitzen, H. M., Pintado, O. I., et al. 2006, *Astron. Astrophys.*, **459**, 871

Paunzen, E., Mikulášek, Z., Poleski, R., et al. 2013, *Astron. Astrophys.*, **556**, A12

Paunzen, E., Netopil, M., & Bord, D. J. 2011b, *Mon. Not. R. Astron. Soc.*, **411**, 260

Paunzen, E., Netopil, M., Maitzen, H. M., et al. 2014, *Astron. Astrophys.*, **564**, A42

Paunzen, E., Netopil, M., Pintado, O. I., & Rode-Paunzen, M. 2011c, *Astron. Nachr.*, **332**, 77

Preston, G. W. 1974, *Ann. Rev. Astron. Astrophys.*, **12**, 257

Reinhold, T. & Gizon, L. 2015, *Astron. Astrophys.*, **583**, A65

Renson, P. & Catalano, F. A. 2001, *Astron. Astrophys.*, **378**, 113

Stępień, K. & Landstreet, J. D. 2002, *Astron. Astrophys.*, **384**, 554

Stibbs, D. W. N. 1950, *Mon. Not. R. Astron. Soc.*, **110**, 395

Watson, C. L., Henden, A. A., & Price, A. 2006, *Society for Astronomical Sciences Annual Symposium*, **25**, 47

Wolff, S. C. 1967, *Astrophys. J., Suppl. Ser.*, **15**, 21

Wolff, S. C. 1975, *Astrophys. J.*, **202**, 127

Wraight, K. T., Fossati, L., Netopil, M., et al. 2012, *Mon. Not. R. Astron. Soc.*, **420**, 757

Zorec, J. & Royer, F. 2012, *Astron. Astrophys.*, **537**, A120

Melissa Munoz and Lilia Ferrario

Corinne Fletcher and Yaël Nazé

Contrib. Astron. Obs. Skalnaté Pleso **48**, 203 – 207, (2018)

Differential rotation in magnetic chemically peculiar stars

Z. Mikulášek[1], J. Krtička[1], E. Paunzen[1], M. Švanda[2], S. Hummerich[3], K. Bernhard[3], M. Jagelka[1], J. Janík[1], G. W. Henry[4] and M. E. Shultz[5]

[1] *Department of Theoretical Physics and Astrophysics, Masaryk University, Brno, Czech Republic, (E-mail: mikulas@physics.muni.cz)*

[2] *Astronomical Institute, Charles University, Prague, Czech Republic*

[3] *Bundesdeutsche Arbeitsgemeinschaft für Veränderliche Sterne e.V. (BAV), Berlin, Germany*

[4] *Center of Excellence in Information Systems, Tennessee State University, Nashville, Tennessee, USA*

[5] *Department of Physics and Astronomy, Uppsala University, Box 516, Uppsala 75120, Sweden*

Received: November 15, 2017; Accepted: December 28, 2017

Abstract. Magnetic chemically peculiar (mCP) stars constitute about 10% of upper-main-sequence stars and are characterized by strong magnetic fields and abnormal photospheric abundances of some chemical elements. Most of them exhibit strictly periodic light, magnetic, radio, and spectral variations that can be fully explained by a rigidly rotating main-sequence star with persistent surface structures and a stable global magnetic field. Long-term observations of the phase curves of these variations enable us to investigate possible surface differential rotation with unprecedented accuracy and reliability. The analysis of the phase curves in the best-observed mCP stars indicates that the location and the contrast of photometric and spectroscopic spots as well as the geometry of the magnetic field remain constant for at least many decades. The strict periodicity of mCP variables supports the concept that the outer layers of upper-main-sequence stars do not rotate differentially. However, there is a small, inhomogeneous group consisting of a few mCP stars whose rotation periods vary on timescales of decades. The period oscillations may reflect real changes in the angular velocity of outer layers of the stars which are anchored by their global magnetic fields. In CU Vir, V901 Ori, and perhaps BS Cir, the rotational period variation indicates the presence of vertical differential rotation; however, its exact nature has remained elusive until now. The incidence of mCP stars with variable rotational periods is currently investigated using a sample of fifty newly identified Kepler mCP stars.

Key words: stars: chemically peculiar – stars: rotation – stars: individual: σ Ori E, CU Vir, V901 Ori, and BS Cir – space vehicles: Kepler

1. Introduction

Main-sequence stars comprise an inhomogeneous group of stellar objects burning hydrogen in their cores. The most striking differences are encountered between stars of the upper and lower main sequence. Lower-main-sequence stars display solar-type activity powered by the dissipation of local magnetic fields that are generated by an interplay of convective motion in subphotospheric layers and differential latitudinal rotation (DLR). Characteristics of DLR can be traditionally derived by tracking solar-type spots and astero/helioseismology.

Unfortunately, we have only scarce information about the rotational periods of individual upper main sequence stars because of the lack of standard solar-type star rotation tracers such as spots, flares, and active regions. Nielsen et al. (2013) analysed more than 12 000 Kepler stars including a few representatives of early spectral types. They found that the early spectral-type stars rotate faster (one revolution in less than 5 days) than the late spectral types. No evidence was drawn about the possibility of a differential rotation. Based on a study of Kepler data, Balona & Abedigamba (2016); Balona et al. (2016) recently suggested the existence of stellar activity and differential rotation in A-type stars. However, their findings, although tempting, are controversial and not generally accepted.

Fortunately, the magnetic chemically peculiar stars (mCPs) of the upper main sequence boast stable photometric and spectroscopic spots and strong magnetic fields. These can be utilized for precise analyses of their rotation periods. Thus, we can determine whether or not hot main sequence stars rotate differentially (Mikulášek, 2016, and references therein).

2. On the variability and physics of magnetic CP stars

Most of the mCP stars exhibit strictly periodic light, magnetic, radio, and spectral variations that can be adequately explained by a rigidly rotating MS star with persistent surface structures and stable magnetic field frozen into the surface of the star. The phase curves of various rotation tracers (light curves, spectral line intensities, and the effective magnetic field $\langle B_z \rangle$) contain information about the rotation of regions of different latitude.

This enables us not only to determine the rotational period but also to search for the presence of latitudinal differential rotation. See e.g., the mutual phase shifts in V901 Ori depicted in Fig. 1, taken from Mikulášek (2016). The strict equality of the periods derived from the phase curves of different tracers supports the concept of solidly rotating mCP stars without any latitudinal differential rotation.

The hardening of the outer parts of the star is due to the global magnetic field intervening not only with the stellar body but also its close environment. Magnetic field plays its decisive role just in outer, rarified parts of the star - in the

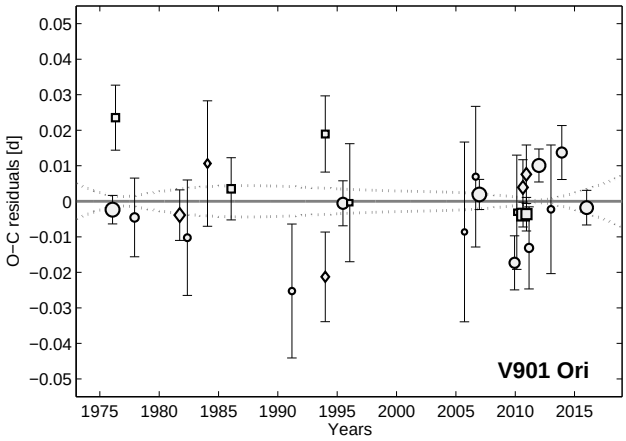

Figure 1. O-C residuals of individual sets of observations of V901 Ori that were obtained by different techniques and related to various structures on the surface (for details see Mikulášek, 2016). Circles mark results based on photometric measurements (silicon spots) while squares and diamond signs correspond to spectropolarimetric (magnetic field geometry) and spectroscopic (helium spots) observations. The areas of markers are proportional to the weights of individual phase shift determinations. Dotted lines denote the one σ uncertainty in the model fit.

magnetosphere and in the photospheric and subphotospheric layers, where the density of magnetic field energy exceeds the density of thermal kinetic energy.

Assuming magnetic induction of $B \sim 2$ kG at an optical depth $\tau = 1$ with a temperature of $T \sim 10^4$ K, density $\rho = 10^{-6}\,\mathrm{kg\,m^{-3}}$, and pressure $P_\mathrm{g} = 6{\times}10^{-4}$ atm $= 60$ Pa, we obtain a kinetic energy density of the thermal motion: $90\,\mathrm{J\,m^{-3}}$, while the magnetic field energy density amounts to $\eta_B = \frac{B^2}{2\,\mu_0} \sim 16\,000\,\mathrm{J\,m^{-3}}$.

Both energy densities are equal at an optical depth of $\tau \sim 100$. Outer layers of the star are dominated by a magnetic field, while in inner parts the role of stellar magnetism is essentially negligible. The mass of the shell dominated by the magnetic field is about $2{\times}10^{-9}\,\mathrm{M_\odot}$. Such a light shell will be able to glide on the inner part of the star and exhibit different rotation than the stellar interior. In this case, even a weak transport of the angular momentum through the stellar wind escaping the magnetosphere can brake the rotation of the visible part of a mCP star.

3. Magnetic CP stars with variable rotational periods

Using the method introduced and then developed by Mikulášek et al. (2008, 2011), and Mikulášek (2016), we analyzed archival, ground-based time series data of several dozens of mCP stars, with the hope of detecting possible varia-

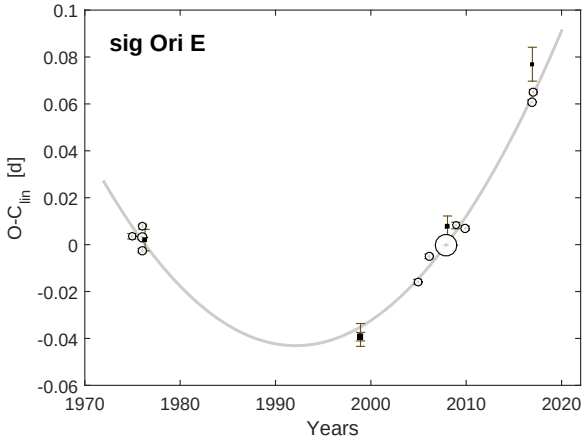

Figure 2. The O-C_{lin} diagram of σ Ori E with the parabolic fit and the mean values of individual sets of observations (see Mikulášek, 2016). Circles are based on the analysis of photometric data; black squares correspond to the analysis of helium lines' intensities. The areas of the symbols express the weights of observational sets.

tions in their rotational period. We found that the periods of almost all mCPs are constant to within the uncertainties of measurement.

However, some of mCPs (CU Vir, V901 Ori, σ Ori E, and BS Cir) were found to have slowly changing periods. These odd mCP stars form a very heterogeneous sample, and it is entirely possible that the mechanism(s) responsible for the observed period changes are different in each object. Unfortunately, the real incidence of mCP stars exhibiting period variations is unknown. A preliminary analysis of the sample of fifty new Kepler mCP stars has yielded no new candidates. However, research in this respect continues.

The nature of the lengthening period observed in BS Circini is still unknown. It may be the result of an internal differential rotation, or it could be the consequence of the precessional motion of the axis of the magnetically distorted star (Mikulášek et al., 2015, 2017). Magnetic braking through angular momentum loss caused by wind escaping from the extended magnetosphere apparently is only effective in particular cases of hot mCPs such as σ Ori E (Townsend et al., 2010; Mikulášek, 2016).

The period oscillations of at least CU Vir can be interpreted as a consequence of torsional waves that may disseminate in magnetic rotating stars (Krtička et al., 2017). Period changes in the hot mCP star V901 Ori may be caused by angular momentum loss through a stellar wind modulated by gradual reconfiguration of its extended magnetosphere, which is anchored in the stellar surface (Mikulášek et al., 2017).

4. Speculations on internal differential rotation

While the surface latitudinal differential rotation has been observed in the Sun and some sun-like stars, the properties of internal rotation in main-sequence stars remains unclear. Nevertheless, it is generally believed that the radiative regions rotate as a solid body while differential rotation develops in convective zones or cores.

Because the outer parts of mCP stars are dominated by the global magnetic field and envelopes overlying the convective cores are radiative, we do not expect any latitudinal differential rotation. However, some changes in the angular velocities of the envelopes and the 'solid' shell dominated by the magnetic field may exist in stars where the shell is braked by stellar wind escaping from the magnetosphere. It is important to note that the internal magnetic field provides an elastic connection between the outer envelopes and the surface 'solid' shell. Therefore we can expect either a firm interconnection between them (σ Ori E) or a more flexible one, allowing some cyclic oscillations (CU Vir). Possible changes in the intensity of the dynamical interaction with the environment may modulate the oscillations as well (V901 Ori).

Acknowledgements. This research was supported by the grant 16-01116S of the Grant Agency of Czech Republic.

References

Balona, L. A. & Abedigamba, O. P. 2016, *Mon. Not. R. Astron. Soc.*, **461**, 497

Balona, L. A., Švanda, M., & Karlický, M. 2016, *Mon. Not. R. Astron. Soc.*, **463**, 1740

Krtička, J., Mikulášek, Z., Henry, G. W., Kurfürst, P., & Karlický, M. 2017, *Mon. Not. R. Astron. Soc.*, **464**, 933

Mikulášek, Z. 2016, *Contributions of the Astronomical Observatory Skalnate Pleso*, **46**, 95

Mikulášek, Z., Janík, J., Krtička, J., Zejda, M., & Jagelka, M. 2015, in ASP Conf. Ser., Vol. **494**, *Physics and Evolution of Magnetic and Related Stars*, ed. Y. Y. Balega, I. I. Romanyuk, & D. O. Kudryavtsev, 189

Mikulášek, Z., Krtička, J., Henry, G. W., et al. 2011, *Astron. Astrophys.*, **534**, L5

Mikulášek, Z., Krtička, J., Henry, G. W., et al. 2008, *Astron. Astrophys.*, **485**, 585

Mikulášek, Z., Krtička, J., Janík, J., et al. 2017, in ASP Conf. Ser., Vol. **510**, *Stars: From Collapse to Collapse*, ed. Y. Y. Balega, D. O. Kudryavtsev, I. I. Romanyuk, & I. A. Yakunin, 220

Nielsen, M. B., Gizon, L., Schunker, H., & Karoff, C. 2013, *Astron. Astrophys.*, **557**, L10

Townsend, R. H. D., Oksala, M. E., Cohen, D. H., Owocki, S. P., & ud-Doula, A. 2010, *Astrophys. J., Lett.*, **714**, L318

Contrib. Astron. Obs. Skalnaté Pleso **48**, 208 – 212, (2018)

Magnetic field of massive chemically peculiar stars in the Orion OB1 association

I. I. Romanyuk, E. A. Semenko, D. O. Kudryavtsev and I. A. Yakunin

Special Astrophysical Observatory of Russian Academy of Sciences
Nizhny Arkhyz, 369167 Russia

Received: October 25, 2017; Accepted: November 6, 2017

Abstract. Spectropolarimetric observations of 55 chemically peculiar stars in the Orion OB1 association were obtained at the 6 m telescope of the Russian Academy of Sciences with the aim of searching for the presence of stellar magnetic fields. We found 8 new magnetic stars in addition to 20 previously known objects. The frequency of chemically peculiar A and B-type stars among normal A and B-type stars and the frequency of magnetic stars among all chemically peculiar stars decreases with age in the Orion OB1 association.

Key words: stars: magnetic field – stars: evolution – open clusters and associations: general

1. Introduction

The search for new magnetic stars is a complicated and time-consuming task, because magnetic field measurements require either special spectropolarimeric methods (Zeeman measurements), very high spectral resolution, or both. Chemically peculiar (CP) stars were the first objects other the Sun in which a magnetic field was found (Babcock, 1947), and currently magnetic fields were detected in about 450 CP stars. However, the latest catalogue of CP stars (Renson & Manfroid, 2009) contains a much larger number of 8200 objects, about half of them are non-magnetic Am stars, and the second half are potentially magnetic Ap and Bp stars.

The process of formation and evolution of magnetic CP stars is not clear yet, but the fossil field theory has a number of advantages compared to the alternative dynamo mechanism. Observations of magnetic CP stars in open clusters of different ages is the best way to study the formation and evolution of these objects. However, observations of stars in cluster areas also result in some selection effect towards more massive and brighter cluster members owing to the instrumental magnitude limit. Therefore, most of the observed Ap stars (70%) in cluster areas are actually field stars and their ages cannot be directly constrained, but most of the Bp stars (75%) are cluster members and provide a well-determined age (see discussion by Romanyuk et al., 2013).

2. CP stars in Orion OB1 association

For the observations with the 6-m telescope we selected 17 stellar populations of various ages that host at least three CP stars. Two groups, the Orion and the Scorpius-Centaurus associations, have been investigated in sufficient detail earlier, thus there are also a lot of additional data available in the literature.

In the Orion OB1 association we find 85 chemically peculiar stars based on the catalogue by Renson & Manfroid (2009), the by far largest number of CP stars in an association. Blaauw (1964) identified four regions inside the assocation: the subgoups (a), (b), (c), and (d) that slightly differ in the age and stellar content. The age ranges from about one million years to about 10 millions of years (see Romanyuk et al., 2013, for details). Additionally, Brown et al. (1994) provide a list of O, B, A and early F-star members of the Orion OB1 association. The average frequency of CP stars in the association is 10.4%, which is generally the same value as often quoted in the literature for the overall Galactic frequency of CP stars. Among the selected 85 CP stars we find 23 Am, 7 He-strong, 27 He-weak, 19 Si and Si+ stars, and nine stars of other types.

Table 1 shows the distribution of normal and peculiar stars for the individual Orion subgroups. The data indicate that the fraction of CP stars decreases with the age from 21.4% (subgroup d) to 7.7% (subgroup a).

Table 1. The age of the subgroups and the number of normal stars and CP objects in the Orion O B1 association.

Subgroup	Age, $\log t$	All stars	CP stars	Fraction
a	7.05	311	24	7.7%
b	6.23	139	21	15.1%
c	6.66	350	37	10.6%
d	<6.0	14	3	21.4%

However, parallaxes by the Hipparcos mission and proper motions indicate that the Am stars probably do not belong to the association and are most likely foreground objects. Thus, we exclude them from our investigation and continue our study with only 62 potentially magnetic Bp and Ap stars. For five of these objects we have no magnetic field measurements yet, therefore in our following analysis we consider 57 Bp and Ap stars: 15 in subgroup (a), 15 in subgroup (b), 24 in subgroup (c), and 3 in subgroup (d).

3. Magnetic field of CP stars in Orion OB1 association

Borra & Landstreet (1979) were among the first to measure the magnetic field of some CP stars in the Orion association. We continue these efforts using the 6 m telescope of the Russian Academy of Sciences (e.g. Romanyuk et al., 2016b). In

2011-2016 we obtained more than 500 polarized Zeeman spectra of 55 Ap and Bp stars in this association. The measurements have been published earlier: Yakunin (2013); Semenko et al. (2014); Romanyuk et al. (2016a, 2017).

The most interesting object among new detected magnetic stars in the association is certainly HD 34736. It belongs to the subgroup (c) and the spectrum shows strong silicon lines. The star has a very strong magnetic field with a longitudinal component that varies from -5 to $+5$ kG. We obtained more than 130 measurement of the longitudinal field B_e and constructed the B_e variability curve with a period of $P = 1.29$ days (Fig. 1). The curve is clearly anharmonic, suggesting that the magnetic field topology significantly deviates from that of a dipole configuration. Furthermore, the star is a SB2 system with effective temperatures for the primary and secondary component of 13700 K and 11500 K, respectively. The spectral lines of the primary component are broad and indicate a projected rotational velocity $v_e \sin i = 75$ km s^{-1}, while the spectral lines of the secondary component even show a $v_e \sin i$ of more than 100 km s^{-1}.

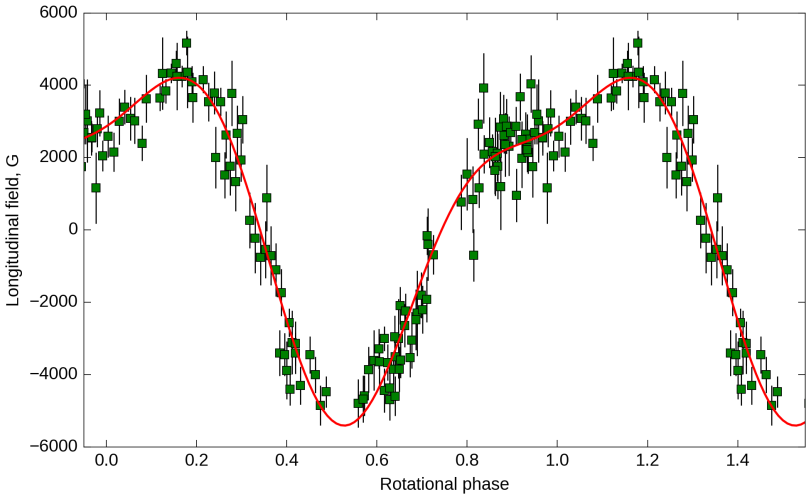

Figure 1. Longitudinal field B_e variations for HD 34736 with a period of $P = 1.29$ days.

We have collected all B_e measurements for stars in the Orion OB1 association, both our own and taken from the literature. Table 2 lists the magnetic stars with reliably measured magnetic fields, i.e. the stars for which $\langle B_e \rangle$ is larger than 3σ and/or for that Zeeman signatures are clearly seen in the spectra. The table provides the identifier in the HD catalog, the subgroup in the association, spectral and peculiarity types, the logarithm of the effective tem-

perature $\log T_{\rm eff}$, the root-mean-square magnetic field $\langle B_{\rm e}\rangle$, its error σ, and the number of measurements N.

Table 2. List of magnetic stars.

Star (subgroup)	Sp, pec	$\log T_{\rm eff}$	$\langle B_{\rm e}\rangle$, G	σ, G	N
HD 34736 (c)	B8 Si	4.11	4700	350	130
HD 34889 (c)	B9 Si	4.02	636	120	2
HD 35008 (a)	B9 Si	4.12	300	100	2
HD 35298 (a)	B6 He-wk	4.20	2145	139	30
HD 35456 (a)	B7 He-wk	4.16	441	96	8
HD 35502 (a)	B6 He-wk	4.20	1490	140	> 10
HD 36313 (b)	B8 He-wk	4.06	1020	450	15
HD 36429 (a)	B6 He-wk	4.23	425	170	5
HD 36485 (b)	B2 He-r	4.29	3220	318	15
HD 36526 (b)	B8 He-wk,Si	4.16	2820	380	15
HD 36540 (c)	B7 He-wk	4.20	470	220	10
HD 36668 (b)	B7 He-wk	4.10	1875	447	16
HD 36697 (c)	A0p	4.00	1137	64	2
HD 36916 (c)	B8 He-wk	4.15	464	180	8
HD 36955 (b)	A2 CrEu	3.99	920	230	6
HD 36982 (d)	B2 He-r	4.33	1150	330	1
HD 36997 (c)	B9 SiSr	4.04	1227	87	2
HD 37017 (c)	B2 He-r	4.32	1488	338	12
HD 37058 (c)	B3 He-wk,Sr	4.24	728	62	14
HD 37140 (b)	B8 SiSr	4.18	450	210	5
HD 37479 (b)	B2 He-r	4.39	1980	155	20
HD 37633 (b)	B9 EuSi	4.10	310	125	2
HD 37642 (c)	B9 He-wk,Si	4.15	2110	180	5
HD 37687 (c)	B7 He-wk	4.16	560	35	10
HD 37776 (b)	B2 He-r	4.36	1260	350	>10
HD 37808 (c)	B9 Si	4.12	480	130	2
HD 40759 (c)	B9 SrCrEu	3.98	1990	240	4
HD 290665 (b)	B9 SrCr Eu	3.99	1700	100	3

Reliable magnetic fields were detected for 28 stars in the Orion OB1 association. In subgroup (a) ($\log t = 7.05$) we find five magnetic stars out of 15 measured Ap/Bp stars (33.3%), in subgroup (b) ($\log t = 6.23$) there are 10 magnetic objects out of 15 Ap/Bp stars (66.7%), in subgroup (c) ($\log t = 6.66$) 12 magnetic stars out of 24 investigated Ap/Bp stars (50.0%), and finally a single magnetic star was found among three stars in subgroup (d).

If we exclude the three stars from subgroup (d) because of the very low statistics for this group, then we notice a clear correlation based on 27 stars with reliably measured magnetic fields: the fraction of magnetic stars decreases with age in the Orion OB1 ssociation. Most of the Bp stars in the youngest

subgroup (b) possess magnetic fields, and most of the Bp stars in the oldest subgroup (a) are non-magnetic.

4. Conclusion

We conclude that about 50% of all Ap/Bp stars in the Orion OB1 association possess strong magnetic fields and, in addition, about 20% of them are probably magnetic. No magnetic field has been found in approximately 30% of Ap/Bp stars. Furthermore, based on the analysis of subgroups of different ages, the fraction of CP stars among normal type stars and the fraction of magnetic stars among Ap/Bp stars decreases with age in the Orion OB1 association.

Acknowledgements. In the present work, we extensively used the information from the SIMBAD and VizieR astronomical databases. We thank the Russian Science Foundation for financial support (RSF grant 14-50-00043).

References

Babcock, H. W. 1947, *Astrophys. J.*, **105**, 105

Blaauw, A. 1964, *Ann. Rev. Astron. Astrophys.*, **2**, 213

Borra, E. F. & Landstreet, J. D. 1979, *Astrophys. J.*, **228**, 809

Brown, A. G. A., de Geus, E. J., & de Zeeuw, P. T. 1994, *Astron. Astrophys.*, **289**, 101

Renson, P. & Manfroid, J. 2009, *Astron. Astrophys.*, **498**, 961

Romanyuk, I. I., Kudryavtsev, D. O., Semenko, E. A., & Moiseeva, A. V. 2016a, *Astrophysical Bulletin*, **71**, 447

Romanyuk, I. I., Semenko, E. A., Yakunin, I. A., & Kudryavtsev, D. O. 2013, *Astrophysical Bulletin*, **68**, 300

Romanyuk, I. I., Semenko, E. A., Yakunin, I. A., Kudryavtsev, D. O., & Moiseeva, A. V. 2016b, *Astrophysical Bulletin*, **71**, 436

Romanyuk, I. I., Semenko, E. A., Yakunin, I. A., Kudryavtsev, D. O., & Moiseeva, A. V. 2017, *Astrophysical Bulletin*, **72**, 165

Semenko, E. A., Romanyuk, I. I., Kudryavtsev, D. O., & Yakunin, I. A. 2014, *Astrophysical Bulletin*, **69**, 191

Yakunin, I. A. 2013, *Astrophysical Bulletin*, **68**, 214

Contrib. Astron. Obs. Skalnaté Pleso **48**, 213 – 217, (2018)

Studying coherent scattering in the CP stars atmospheres

J. Fišák[1,2], J. Kubát[2] and J. Krtička[1]

[1] *Department of Theoretical Physics and Astrophysics, Masaryk University, Kotlárská 2, 611 37 Brno, Czech Republic, (E-mail: fisak@physics.muni.cz)*

[2] *Astronomical Institute of the Czech Academy of Sciences 251 65 Ondřejov, The Czech Republic*

Received: December 20, 2017; Accepted: December 28, 2017

Abstract. Chemically peculiar stars form a very interesting class of stars which frequently show variability. The variability is probably caused by the uneven surface distribution of chemical elements. Some elements are overabundant and some elements are underabundant compared to the solar chemical composition. In the case of chemically overabundant composition some of the rare photon-atom processes can be more important than in the atmospheres of stars with solar chemical composition. We study the importance of Rayleigh scattering by helium.

Key words: stars: chemically peculiar – stars: atmospheres – atomic processes – scattering

1. Introduction

Chemically peculiar (CP) stars have a complicated structure of their atmospheres. We call them "peculiar" because they differ from other stars whose chemical composition is very similar to the solar one. Several types of CP stars among A-type stars exist (see Preston, 1974). The B-type CP stars are less manifold and are typically divided to helium over- and under-abundant stars.

We study the effect of Rayleigh scattering on the atmospheres of CP stars. Rayleigh scattering is important in cool stellar atmospheres. It is much less important in hot stars, but may be more significant in CP stars.

2. Rayleigh scattering

Rayleigh scattering is a process of interaction of photon with a bound electron. The effect of Rayleigh scattering in the atmosphere of our planet is very well known, because it causes the blue colour of the sky.

The best and most accurate way to calculate the Rayleigh scattering cross section is to use quantum mechanics – using the Kramers-Heisenberg equation

in the form:

$$\frac{\mathrm{d}\sigma}{\mathrm{d}\Omega} = \frac{e^4\omega^4}{16c^4\pi^2\epsilon_0^2\hbar^2}\left|\sum_j\left(\frac{(\varepsilon_{\mathbf{k}_s}\cdot\mathbf{D}_{1j})\,(\varepsilon_{\mathbf{k}}\cdot\mathbf{D}_{j1})}{\omega_j-\omega}+\frac{(\varepsilon_{\mathbf{k}}\cdot\mathbf{D}_{1j})\,(\varepsilon_{\mathbf{k}_s}\cdot\mathbf{D}_{j1})}{\omega_j+\omega}\right)\right|^2, \tag{1}$$

where $\varepsilon_{\mathbf{k}}$ and $\varepsilon_{\mathbf{k}_s}$ denote polarization vectors of incoming and scattered photons, respectively, $\mathbf{D}_{ij} = \langle i\,|\mathbf{D}|\,j\rangle$, $\mathbf{D} = \sum_k \mathbf{r}_k$, where $\mathbf{r}_k$ is a position of the k-th electron, $\omega_j = (E_j - E_i)/(\hbar\nu)$, where E_i is the energy of the initial electron state and E_j is the energy of the virtual state. This equation describes coherent scattering of photons on an arbitrary atom. The equation accounts for polarization of radiation, which we will, however, neglect. Rewriting in terms of frequencies instead of ω we get

$$\sigma = \mathcal{K}(2\pi\nu)^4\frac{8}{3}\pi\left|\sum_j\left|\left\langle n_0,l_0\left|\hat{R}\right|n,l\right\rangle\right|^2\frac{2\nu_j}{\nu_j^2-\nu^2}\right|^2. \tag{2}$$

where $\mathcal{K}$ is a constant from Eq. 1 and $8/3\,\pi$ comes from the integration over angles. One can calculate the cross section numerically, but a simpler way is to rewrite Eq. 2 for frequencies much lower than the frequencies corresponding to the line transitions of the given ion. This is called the low frequency limit and it has a polynomial dependence:

$$\sigma = \nu^4(a_0 + a_1\nu^2 + a_2\nu^4 + \cdots + a_k\nu^{2k} + \dots),\ k\in\mathbb{N} \tag{3}$$

where a_i represent the corresponding coefficients in the series. Using this limit we get the well known dependence of the cross section on frequency (we will neglect higher powers than four). The plot of the cross section for hydrogen computed using Eq. 1 is shown in Hubeny & Mihalas (2014, Fig. 6.3). The analytical formula for hydrogen can be found in Lee & Kim (2004). It is significantly more complicated to calculate cross sections for heavier elements.

Rayleigh scattering cross sections can be found in several publications. For example, Colgan et al. (2016) contains cross sections for the neutral chemical elements. Here we list computed cross section for neutral hydrogen

$$\frac{\sigma_{\mathrm{H\ I}}(\nu)}{1\,\mathrm{cm}^2} = 7.18\times10^{-87}\cdot\nu^4 + 1.96\times10^{-117}\cdot\nu^6 + 4.27\times10^{-148}\cdot\nu^8,$$

and singly ionized helium

$$\frac{\sigma_{\mathrm{He\ II}}(\nu)}{1\,\mathrm{cm}^2} = 2.80\times10^{-89}\cdot\nu^4 + 4.79\times10^{-121}\cdot\nu^6 + 6.52\times10^{-153}\cdot\nu^8.$$

These cross-sections are plotted in comparison with the Thomson scattering cross section in Fig. 1.

3. Calculation of models

The procedure of model calculation was the following: it was necessary to choose a model atmosphere as input. For stars with solar chemical composition we used an existing model atmosphere grid on the TLUSTY web pages (Lanz & Hubeny, 2007). For non-solar chemical composition we computed stellar atmosphere models from scratch using the TLUSTY code (Hubeny, 1988; Hubeny & Lanz, 1995; Lanz & Hubeny, 2003, 2007).

In the sebsequent step it was possible to calculate the emergent spectrum from the stellar atmosphere model with Rayleigh scattering included. To this end we used the SYNSPEC code. This code does not calculate the model atmosphere but it calculates emergent synthetic spectra. We calculated synthetic spectra with and without Rayleigh scattering included. These spectra were convolved with the Gaussian function, since we were interested only in continuum radiation, not in lines. The convolution made the spectrum smoother. The Gaussian

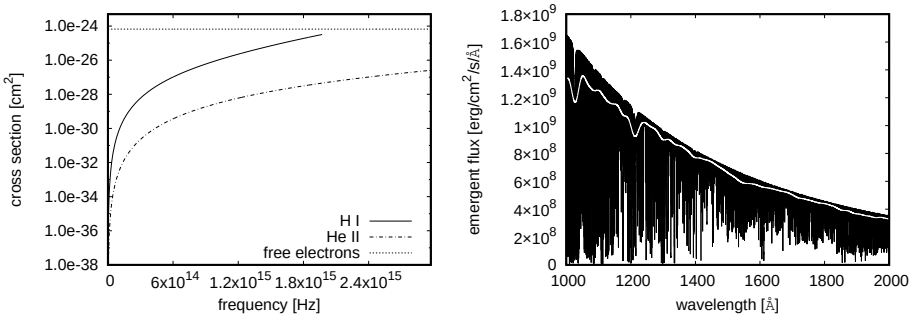

Figure 1. *Left*: Cross sections for neutral hydrogen and singly ionized helium. *Right*: Comparison of synthetic spectrum computed with the SYNSPEC code and the same synthetic spectrum after convolution with the Gaussian function.

function used to convolve the spectra was

$$(H * g)(\lambda) = \frac{1}{\sqrt{2\pi}\sigma} \int d\lambda' \, H(\lambda') \exp\left(-\frac{(\lambda - \lambda')^2}{2\sigma^2}\right), \tag{4}$$

where λ, λ' is the wavelength, $H(\lambda')$ is the flux and σ is a constant characterizing a half-width of the Gaussian curve. We choose to plot differences in magnitudes using the equation

$$\Delta m = -2.5 \log \frac{H_{\mathrm{RS}}}{H_{\mathrm{NO}}}, \tag{5}$$

where H_{RS} – flux with Rayleigh scattering included and H_{NO} – flux without Rayleigh scattering included.

4. Computed atmosphere models

We computed several series of atmosphere models. These models differ in helium abundance and in the effective temperature.

4.1. Stars with solar chemical composition

There were no significant differences between the measured and synthetic spectral energy distribution for stars with normal chemical composition. Consequently, we expected only very small changes caused by Rayleigh scattering by helium. Results confirmed our expectations and changes expressed in the form of Eq. 5 are about 10^{-4} mag large.

4.2. Helium overabundant stars

We were particularly interested in helium overabundant stars because for several stars of this type the light curves and the processes contributing to the measured spectra have not been fully explained yet.

We computed models in the temperature range 19–30 kK, with a surface gravity $\log(g) = 4$, and for helium ten times more abundant than hydrogen. The differences of the fluxes are of the order of 10^{-3} mag, see Fig. 2. These changes become one order of magnitude smaller with increasing effective temperature.

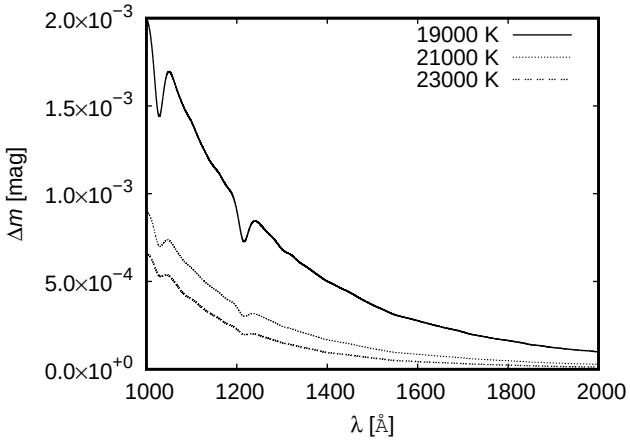

Figure 2. Calculated differences for helium rich B-type stars

4.3. Other objects

We computed several series of models for white dwarfs with $\log(g) = 8$ and subdwarfs with $\log(g) = 5.5$. The differences in the form of Eq. 5 are about 10^{-4} mag.

5. Conclusions

We computed several series of model atmospheres and we studied the importance of Rayleigh scattering in these cases. We obtained atmosphere models either from the existing grid or we computed models ourselves from scratch. We used these models as an input for the synthetic spectra calculation using the SYNSPEC code. The spectra were calculated with and without Rayleigh scattering included and were compared for the given temperature. We did not recalculate the temperature structure.

We can see that the largest differences in the flux are for helium stars for Rayleigh scattering by neutral helium. These changes are about 10^{-3} mag, which is not a very large value, however, it is possible to measure these changes with highly accurate instruments. A more detailed description of the results for hydrogen and singly ionized helium can be found in Fišák et al. (2016).

Acknowledgements. This research was supported by the grant GA ČR 16-01116S. Access to computing and storage facilities owned by parties and projects contributing to the National Grid Infrastructure MetaCentrum, provided under the programme "Projects of Large Infrastructure for Research, Development, and Innovations" (LM2010005), is greatly appreciated. We would like to thank prof. Dominik Munzar who consulted the theoretical part of this work.

References

Colgan, J., Kilcrease, D. P., Magee, N. H., et al. 2016, *Astrophys. J.*, **817**, 116

Fišák, J., Krtička, J., Munzar, D., & Kubát, J. 2016, *Astron. Astrophys.*, **590**, A95

Hubeny, I. 1988, *Comput. Phys. Commun.*, **52**, 103

Hubeny, I. & Lanz, T. 1995, *Astrophys. J.*, **439**, 875

Hubeny, I. & Mihalas, D. 2014, *Theory of stellar atmospheres* (Princeton, N.J.: Princeton University Press)

Lanz, T. & Hubeny, I. 2003, *Astrophys. J., Suppl.*, **146**, 417

Lanz, T. & Hubeny, I. 2007, *Astrophys. J., Suppl.*, **169**, 83

Lee, H.-W. & Kim, H. I. 2004, *Mon. Not. R. Astron. Soc.*, **347**, 802

Preston, G. W. 1974, *Ann. Rev. Astron. Astrophys.*, **12**, 257

Contrib. Astron. Obs. Skalnaté Pleso **48**, 218 – 222, (2018)

History of the Δa photometric system

H. M. Maitzen[1], E. Paunzen[2] and M. Netopil[1,2]

[1] *Institute for Astrophysics, University of Vienna, Türkenschanzstraße 17, 1180 Vienna, Austria, (E-mail: hans.michael.maitzen@univie.ac.at)*

[2] *Department of Theoretical Physics and Astrophysics, Masaryk University, Kotlárská 2, 611 37 Brno, Czech Republic*

Received: November 15, 2017; Accepted: November 20, 2017

Abstract. We review the invention of the Δa photometric system, which provides an efficient method to detect magnetic chemically peculiar stars, but also some other groups such as emission-line or metal-weak objects. Besides the investigation of numerous field stars, the photometric system was also applied to various stellar aggregates, from nearby Galactic open clusters over globular clusters up to field populations and clusters in the Large Magellanic Cloud. The study of star cluster members clearly provides the basis to improve knowledge connected with evolutionary topics. We discuss some results that were made during the four decades long history of Δa photometry.

Key words: stars: chemically peculiar – stars: emission-line, Be – stars: evolution – open clusters and associations: general – techniques: photometric

1. Introduction

Following a suggestion of K. D. Rakos in March 1969, a photoelectric mission at the 60 cm Bochum telescope at ESO-La Silla by HMM was devoted to a photometric variability search in Johnson UBV for objects in the catalogue of magnetic stars by Babcock (1958). During this two months run from the middle of May until July, 1969 the ApSi(Cr) star CS Vir (HD 125248) with already known 9 d photometric period was included to check the capability of the observing equipment. It had, however, not yet been observed in UBV and our results were astonishing: U and B confirmed the published period with roughly sinusoidal light curves, but in V a double wave variation appeared (Maitzen & Rakosch, 1970). This finding prompted us to refine the photometric filter coverage of the visual spectral range by including Strömgren *uvby* and Hβ wide and introducing two middle band filters g_1 and g_2 centered on 5030 and 5240Å, respectively. A subsequent run at the Bochum telescope revealed the presence of two flux depressions in v and g_2 (Maitzen & Moffat, 1972). While the former had already been known as metallicity enhancement from Strömgren photometry, the latter was so far present in a similar way only in the Ap-star HD 221568 observed by Kodaira (1969) who found flux depressions in its continuum at 4200, 5300 and 6300Å. The need for examining other magnetic stars in our new filter system became imminent.

2. Creating the Δa system

Further photoelectric missions on La Silla confirmed what had been found for CS Vir. Therefore it was advisable to compare the flux depression at 5240Å (g_2) with the arithmetic mean of the adjacent filters g_1 and y, expressed in magnitudes, by the definition:

$$a = g_2 - \frac{g_1 + y}{2} \tag{1}$$

Applying this to so-called normal stars (non-magnetic, non-peculiar) their photometry resulted in a slow, approximately linear increase with colour index (e.g. $b-y$) over the upper main sequence range. Standard deviations from this "normality line" are typically of the order of a few mmag. It turned out that nearly all of the well-known magnetic peculiar stars are lying above this line by more than 3σ (typically >10 mmag). This was the reason to create a new peculiarity index Δa defined as

$$\Delta a = a - a_{\mathrm{normal}} \tag{2}$$

where the second term refers to the a-value on the normality line corresponding to the colour of the peculiar star. Thus, the Δa-system was established after numerous observations in the first half of the 1970s (Maitzen, 1976). Its potential was evident: while the classical Ap-stars were detected by spectroscopy, limiting research to the immediate neighbourhood of the Sun, photometry would enable statistical research and much larger distances to be reached.

According to the definitions of chemically peculiar (CP) stars by Preston (1974) it is obvious that strong global magnetic fields are only present among CP2 (classical Ap-stars) and CP4 (He-weak stars, part of them). CP1 (Am-stars) and CP3 (HgMn-stars) lack those fields, and Δa has peculiar positive values only for the magnetic stars. The question arises: does a significant positive Δa mean that the star is a peculiar magnetic one? With high probability yes, but there is an impurity effect due to Be-stars which undergo their variation from their shell phase through normal and then to the emission line phase. This goes parallel from significant positive to significant negative Δa-values, e.g. for Pleione (Maitzen & Pavlovski, 1987). Negative Δa is also a characteristic for a large fraction of λ Bootis stars. The detection efficiency of Δa for different stellar groups has been discussed by Paunzen et al. (2005), confirming that almost all magnetic CP stars can be detected by Δa. It is therefore also a valuable pre-selection tool for spectroscopic or polarimetric follow-up observations.

3. Open cluster survey in Δa

After establishing the Δa-system by field stars relatively near to the Sun, the 1980s were devoted to the search of peculiar/magnetic stars in open clusters using the photoelectric technique (see for details and references Paunzen et al.,

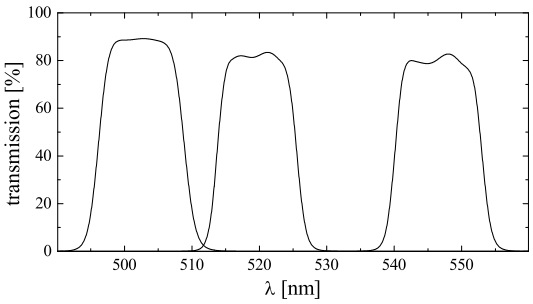

Figure 1. The Δa filters were adjusted over the years to improve the efficiency of the system, the currently last one is shown here.

2014b). Due to the lower magnitude limit (one star at one time) this way the closer galactic clusters were observed, altogether 48 of them. This situation changed dramatically with the transition of Δa to CCD observations as of 1995. 47 open clusters were published so far with this technique, increasing the galactic surrounding for this investigation enormously. These are presented in a series of papers (the currently last one by Netopil et al., 2007) and in studies of two individual open clusters (Netopil et al., 2005; Cariddi et al., 2018). As a result, about 100 Ap cluster stars were detected, their mass distribution resembling in general that of the field stars. The formation of Ap stars turns out to be more efficient in the range of objects with masses of 3–4 $M_\odot$, reaching a maximum value near five percent of all stars (Netopil et al., 2014).

4. Δa photometry of globular clusters

After the discovery of chemical abundance variations especially on the Blue Horizontal Branch of globular clusters observations were undertaken in order to verify whether similar effects as on the main sequence where quiet atmospheres are present would produce measurable consequences to be registered also by Δa. Paunzen et al. (2014a) presented an analysis of three globular clusters in this photometric system and find that about 3 per cent of the stars lie in abnormal regions in the diagnostic diagrams. A comparison with published abundances for few horizontal-branch stars yields an excellent agreement. Therefore, the observations provide very promising results, which will serve as a solid basis for follow-up observations.

5. CP stars in the Large Magellanic Cloud

Some fields in the Large Magellanic Cloud (LMC) were subject to Δa photometry and clearly deviating Δa-objects were found, both above and below the

normality line of field and cluster stars. Hence the first extragalactic chemically peculiar stars of the upper main sequence were discovered this way, but also Be-stars, detected by Δa-photometry (Paunzen et al., 2006). Spectroscopic confirmation took place for a classical magnetic CP2 star (NGC 1866-1005) and the Be-star NGC 1866-257 using the Si-doublet λ4128/31Å and the Hβ line, respectively, using the 6.5 m Magellan II telescope at Las Campanas (Paunzen et al., 2011). However, the derived occurrence of classical chemically peculiar stars in the LMC is only about half the value found in the Milky Way, while the age and mass distributions apparently do not differ from those of CP stars in galactic open clusters. For some of the detected CP stars in the LMC photometric timeseries data are available from the Optical Gravitational Lensing Experiment (OGLE)-III survey. Paunzen et al. (2013) only found two objects that may show some weak rotationally modulated light variations. This can be explained by the absence of photometric spots of overabundant optically active chemical elements, a behaviour which is probably caused by different conditions during the star formation in the LMC and the Galaxy.

6. Detection by serendipity

An unexpected success was reached by the application of Δa-photometry to the list of Ap stars by Renson et al. (1991). One object (Renson 31250), later denominated HIP 60350 in the Hipparcos/Tycho catalogue, had an entry as "A5m:" and with a visual magnitude of about 11 mag one of the faintest object therein. A positive Δa mean obtained from an (insufficient) number of individual measurements suggested possible peculiarity. It was therefore observed spectroscopically for spectral classification at the Figl Observatory for Astrophysics of the Vienna University. It turned out that its late A-type was wrong and that this star, exhibiting He-4026Å, was an early B-type object with unusual red shifted radial velocity of $+210\,\mathrm{km\,s^{-1}}$. Together with the proper motion results of Hipparcos a galactocentric velocity of about $600\,\mathrm{km\,s^{-1}}$ resulted, hence identifying HIP 60350 as fastest star of the Galactic disc moving in the direction to the Andromeda Galaxy (Maitzen et al., 1998), detected thanks to a chance value of Δa!

7. Conclusions

We reviewed the invention of the Δa photometric system and achievements that were made in CP star research based on this efficient detection tool. It was applied to several environments, from Galactic field stars and open clusters to globular clusters or stellar populations in the LMC. Cluster stars certainly provide a unique opportunity to study evolutionary topics thanks to the tight constraints on the age. However, we still lack of homogeneous cluster parameters for numerous objects (see discussion by Netopil et al., 2015). For many open

clusters of the Δa survey these were already derived (Netopil & Paunzen, 2013) and upcoming data releases of the Gaia satellite mission will allow thorough membership analyses for a proper identification of cluster member stars. This will significantly improve our knowledge of the evolutionary status of CP stars. Nevertheless, more CP star detections in clusters are desirable and we continue our efforts using the Δa system.

Acknowledgements. We acknowledge the support by the Austrian Agency for International Cooperation in Education and Research (WTZ CZ-15/2017).

References

Babcock, H. W. 1958, *Astrophys. J., Suppl. Ser.*, **3**, 141

Cariddi, S., Azatyan, N. M., Kurfürst, P., et al. 2018, *New Astronomy*, **58**, 1

Kodaira, K. 1969, *Astrophys. J., Lett.*, **157**, L59

Maitzen, H. M. 1976, *Astron. Astrophys.*, **51**, 223

Maitzen, H. M. & Moffat, A. F. J. 1972, *Astron. Astrophys.*, **16**, 385

Maitzen, H. M., Paunzen, E., Pressberger, R., Slettebak, A., & Wagner, R. M. 1998, *Astron. Astrophys.*, **339**, 782

Maitzen, H. M. & Pavlovski, K. 1987, *Astron. Astrophys.*, **178**, 313

Maitzen, H. M. & Rakosch, K. D. 1970, *Astron. Astrophys.*, **7**, 10

Netopil, M. & Paunzen, E. 2013, *Astron. Astrophys.*, **557**, A10

Netopil, M., Paunzen, E., & Carraro, G. 2015, *Astron. Astrophys.*, **582**, A19

Netopil, M., Paunzen, E., Maitzen, H. M., et al. 2005, *Astron. Nachr.*, **326**, 734

Netopil, M., Paunzen, E., Maitzen, H. M., et al. 2007, *Astron. Astrophys.*, **462**, 591

Netopil, M., Paunzen, E., Maitzen, H. M., Pintado, O. I., & Iliev, I. K. 2014, in *Putting A Stars into Context: Evolution, Environment, and Related Stars*, ed. G. Mathys, E. R. Griffin, O. Kochukhov, R. Monier, & G. M. Wahlgren, 10–18

Paunzen, E., Iliev, I. K., Pintado, O. I., et al. 2014a, *Mon. Not. R. Astron. Soc.*, **443**, 2492

Paunzen, E., Maitzen, H. M., Pintado, O. I., et al. 2006, *Astron. Astrophys.*, **459**, 871

Paunzen, E., Mikulášek, Z., Poleski, R., et al. 2013, *Astron. Astrophys.*, **556**, A12

Paunzen, E., Netopil, M., & Bord, D. J. 2011, *Mon. Not. R. Astron. Soc.*, **411**, 260

Paunzen, E., Netopil, M., Maitzen, H. M., et al. 2014b, *Astron. Astrophys.*, **564**, A42

Paunzen, E., Stütz, C., & Maitzen, H. M. 2005, *Astron. Astrophys.*, **441**, 631

Preston, G. W. 1974, *Ann. Rev. Astron. Astrophys.*, **12**, 257

Renson, P., Gerbaldi, M., & Catalano, F. A. 1991, *Astron. Astrophys., Suppl. Ser.*, **89**, 429

Contrib. Astron. Obs. Skalnaté Pleso **48**, 223 – 227, (2018)

Evolution of magnetic field of massive stars

A. S. Medvedev[1], A. F. Kholtygin[2], S. Hubrig[3], S. N. Fabrika[1], G. G. Valyavin[1], M. Schöller[4] and O. A. Tsiopa[5]

[1] *Special Astrophysical Observatory, Russia*
(E-mail: a.s.medvedev@gmail.com)

[2] *Saint-Petersburg State University, Russia, (E-mail: afkholtygin@gmail.com)*

[3] *Leibniz-Institut für Astrophysik Potsdam (AIP), Potsdam, Germany*

[4] *European Southern Observatory, Garching, Germany*

[5] *Main (Pulkovo) Astronomical Observatory, Russia*

Received: November 19, 2017; Accepted: November 28, 2017

Abstract. We model the evolution of massive magnetic stars in the Galaxy using our own population synthesis code. A comparison of our model magnetic field distribution with that obtained from an analysis of measurements of magnetic fields shows that both model and real distributions can be approximated by a log-normal law with a mean $\log(B) = 2.5$. Based on this comparison we conclude that the magnetic flux variations of OBA stars on the main sequence (MS) are very slow. The shape of the magnetic field distribution for O, B and A stars appeared to be similar. This means that the mechanisms of the generation of their magnetic field are probably identical.

Key words: stars: magnetic field – stars: evolution – stars: early type

1. Introduction

Studies of the age, environment, and kinematic characteristics of magnetic stars are promising to give us new insight into the origin of the magnetic fields (e.g. Hubrig et al., 2011, 2013; González et al., 2017). The first magnetic field detection in an O-type star was made in 2002 by Donati et al. (2002) only.

The recent systematic surveys BOB (The B fields in OB stars; Morel et al., 2014) and MiMeS (The Magnetism in Massive Stars; Wade et al., 2016) significantly enhanced the number of known magnetic OBA stars in comparison with ∼500 OBA stars with confirmed magnetic field in the catalog by Bychkov et al. (2009). The fraction of massive magnetic stars was found about of 6 – 7% only (Wade et al., 2014; Schöller et al., 2017).

Measuring of magnetic fields in hundreds of OBA stars open the possibility to study the magnetic field distribution (MFD) for different types of stars (e.g. Kholtygin et al., 2010a) which is important to understand the nature of the magnetic field of massive stars. An employment of the real MFD showed that some previous ideas about the magnetic field evolution can be incorrect. In this paper we consider the evolution of the magnetic fields and fluxes of OBA stars at the main sequence stage.

2. Model

The first step of our modelling is a creation of the initial ensemble of stars supposing that a total number of stars in the ensemble is $N_{\rm tot}$ and the stellar masses $M \in [M_{\rm min}, M_{\rm max}]$. The stellar mass distribution at the Zero-Age-MS (ZAMS) is described by a power law with an exponent of -2.3 (Kroupa, 2002). The appearance time t_* of each star at ZAMS is generated using the uniform distribution in the range $[0, T]$, where T is the total simulation time. The simulation time T has to be at least three times longer than the main sequence lifetime $\tau_{\rm MS}$ of a least massive star in the ensemble. The stellar birthrate λ is supposed to be constant.

Evolution of the stars in our ensemble is simulated using the single-star evolution code SSE by Hurley et al. (2000). This code is based on analytical approximations of evolutionary tracks by Pols et al. (1998). Our population synthesis code is created on the base of the Astrophysical Multipurpose Software Environment[1] (AMUSE) developed by Pelupessy et al. (2013).

The magnetic field of a star in our model is defined via the net magnetic flux Φ at the stellar surface: $\Phi = \int_S |B_r| dS$. Here B_r is the radial projection of the B-field and dS is a surface element. We use the root-mean-square (*rms*) field $\mathcal{B}$ instead of $B_{\rm d}$ as the main characteristic of stellar magnetic fields. If N is the total number of the field measurements B_l^k $(k = 1 \dots N)$, then the *rms*-field is given by the formula (e.g. Bohlender et al., 1993):

$$\mathcal{B} = \sqrt{\frac{1}{N} \sum_{k=1}^{N} \left(B_l^k\right)^2}. \tag{1}$$

The phase-averaged ratio $\mathcal{B}/B_{\rm d}$ and its asymptotical behaviour at $N \to \infty$ were investigated by Kholtygin et al. (2010a). They demonstrated that in the case of a dipole configuration the *rms*-field $\mathcal{B}$ weakly depends on random values of the rotational phase ϕ, inclination i and the angle β between magnetic and rotational axes. Following this paper we adopt $\Phi = 4\pi R^2 \mathcal{B}$, $\mathcal{B} \approx 0.2 B_{\rm d}$. We assume the lognormal distribution of the net magnetic fluxes:

$$f(\Phi \mid t = 0) = \frac{1}{\sqrt{2\pi} \ln 10 \Phi \sigma} \exp\left\{ -\frac{1}{2} \left(\frac{\log \Phi - \langle \log \Phi \rangle}{\sigma} \right)^2 \right\}, \tag{2}$$

where Φ is the net magnetic flux, $\langle \log \Phi \rangle$ is the mean value of the $\log \Phi$, σ is the width (in dex) of the distribution.

We chose the lognormal distribution of the magnetic fluxes mainly due to similarity between the lognormal and empirical distributions derived from real samples of magnetic stars (e.g. Medvedev et al., 2017). A lognormal magnetic flux distribution (magnetic flux function) can be generated due to of multiple

[1] see http://www.amusecode.org for details

merging of the protostars at the stage of the evolution before MS (see for details Medvedev & Kholtygin, 2017). Observational evidences imply that the magnetic fields of Ap stars can be decayed (e.g. Landstreet et al., 2008). According to Kholtygin et al. (2010b) the dissipation of magnetic fields can be described by the exponential function: $\Phi(t) = \Phi(0)e^{-\tau/t_{\rm d}}$.

3. Statistical criteria

Suppose that we want to analyse some empirical magnetic field distribution derived from a sample of N_* stars, using our model. Let n_i be the number of stars in each of N bins of the empirical distribution and let e_i be the expected number of stars, given by our model. Unfortunately, the number of known magnetic massive stars is not large. Therefore, the standard χ^2 statistics is not suitable for the analysis of empirical distributions. Instead we use the C-statistics, introduced by Cash (1979). In our model we use the following modification of the C-statistics:

$$C = 2\sum_{i=1}^{N_{\rm bins}} \left[e_i - n_i + n_i(\ln n_i - \ln e_i)\right]. \tag{3}$$

This form of C-statistics is often used in X-ray astronomy especially in cases when the number of photons is low (e.g. Arnaud, 1996).

Humphrey et al. (2009) found that the C-statistics allows to find unbiased estimates of fitting parameters even if a number of counts in data is low. However they also noted the main problem associated with the C-statistics that there is no simple way to implement a goodness-of-fit test. For example, in our model we first find the minimum of C-statistics using the Nelder-Mead algorithm and then find confidence intervals for fitting parameters using Monte-Carlo simulations. Hence in a recent paper, Kaastra (2017) presented the analytical and numerical approximations of expected values and variances for the C-statistics that can be used to evaluate the goodness-of-fit.

Additionally, the C-statistics can be expanded for simultaneous fitting of different samples of empirical distributions. If N is the number of samples and N_k is the number of bins in k-th sample, then we get

$$C_{\rm sim} = 2\sum_{k=1}^{N}\sum_{i=1}^{N_k}\left[e_i^k - n_i^k + n_i^k\Big(\ln n_i^k - \ln e_i^k\Big)\right]. \tag{4}$$

4. Results and Conclusions

Results of simultaneous fitting are presented in Fig. 1. For the model without dissipation of magnetic field we find: $\langle\log\Phi\rangle = 26.45^{+0.05}_{-0.05}$, $\sigma = 0.50^{+0.04}_{-0.05}$, $C/{\rm dof} = 39.1/53$ (here "dof" denotes "degrees of freedom"). For the model with $\tau_{\rm d} = 0.5$ the corresponding values are: $\langle\log\Phi\rangle = 26.87^{+0.05}_{-0.07}$, $\sigma = 0.35^{+0.04}_{-0.09}$,

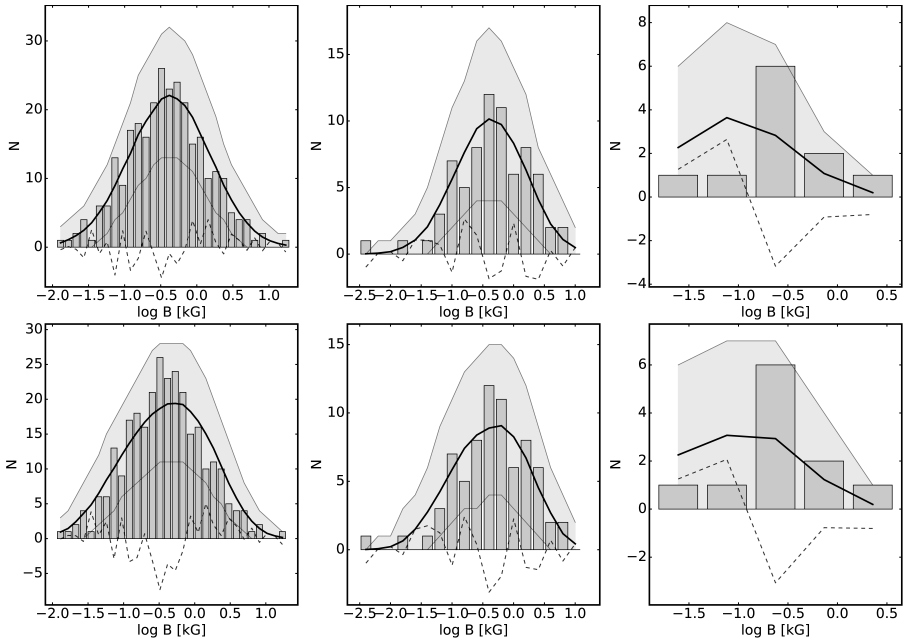

Figure 1. Simultaneous fitting of the magnetic field distributions for BA, OB and O-type stars (from left to right) for the model without dissipation of magnetic fields (*upper panel*) and for the model with dissipation parameter $\tau_{\rm d} = 0.5$ (*lower panel*). The gray histograms represent the empirical data, while the black lines and dashed lines show the mean model distribution and residuals. The gray filled area corresponds to the 95% confidence limits for possible variations.

$C/\mathrm{dof} = 48.3/53$. Our results show that all three empirical distribution of magnetic fields can be fitted with a common magnetic field function.

Acknowledgements. ASM, AFK, SF and GGV thank the RFBR grant 16-02-00604 A for the support.

References

Arnaud, K. A. 1996, in ASP Conf. Ser., Vol. **101**, *Astronomical Data Analysis Software and Systems V*, ed. G. H. Jacoby & J. Barnes, 17

Bohlender, D. A., Landstreet, J. D., & Thompson, I. B. 1993, *Astron. Astrophys.*, **269**, 355

Bychkov, V. D., Bychkova, L. V., & Madej, J. 2009, *Mon. Not. R. Astron. Soc.*, **394**, 1338

Cash, W. 1979, *Astrophys. J.*, **228**, 939

Donati, J.-F., Babel, J., Harries, T. J., et al. 2002, *Mon. Not. R. Astron. Soc.*, **333**, 55

González, J. F., Hubrig, S., Przybilla, N., et al. 2017, *Mon. Not. R. Astron. Soc.*, **467**, 437

Hubrig, S., Schöller, M., Ilyin, I., et al. 2013, *Astron. Astrophys.*, **551**, A33

Hubrig, S., Schöller, M., Kharchenko, N. V., et al. 2011, *Astron. Astrophys.*, **528**, A151

Humphrey, P. J., Liu, W., & Buote, D. A. 2009, *Astrophys. J.*, **693**, 822

Hurley, J. R., Pols, O. R., & Tout, C. A. 2000, *Mon. Not. R. Astron. Soc.*, **315**, 543

Kaastra, J. S. 2017, *Astron. Astrophys.*, **605**, A51

Kholtygin, A. F., Fabrika, S. N., Drake, N. A., et al. 2010a, *Astronomy Letters*, **36**, 370

Kholtygin, A. F., Fabrika, S. N., Drake, N. A., et al. 2010b, *Kinematics and Physics of Celestial Bodies*, **26**, 181

Kroupa, P. 2002, *Science*, **295**, 82

Landstreet, J. D., Silaj, J., Andretta, V., et al. 2008, *Astron. Astrophys.*, **481**, 465

Medvedev, A. & Kholtygin, A. 2017, in ASP Conf. Ser., Vol. **510**, *Stars: From Collapse to Collapse*, ed. Y. Y. Balega, D. O. Kudryavtsev, I. I. Romanyuk, & I. A. Yakunin, 265

Medvedev, A. S., Kholtygin, A. F., Hubrig, S., et al. 2017, *Astron. Nachr.*, **338**, 910

Morel, T., Castro, N., Fossati, L., et al. 2014, *The Messenger*, **157**, 27

Pelupessy, F. I., van Elteren, A., de Vries, N., et al. 2013, *Astron. Astrophys.*, **557**, A84

Pols, O. R., Schröder, K.-P., Hurley, J. R., Tout, C. A., & Eggleton, P. P. 1998, *Mon. Not. R. Astron. Soc.*, **298**, 525

Schöller, M., Hubrig, S., Fossati, L., et al. 2017, *Astron. Astrophys.*, **599**, A66

Wade, G. A., Grunhut, J., Alecian, E., et al. 2014, in IAU Symp., Vol. **302**, *Magnetic Fields throughout Stellar Evolution*, ed. P. Petit, M. Jardine, & H. C. Spruit, 265–269

Wade, G. A., Neiner, C., Alecian, E., et al. 2016, *Mon. Not. R. Astron. Soc.*, **456**, 2

Contrib. Astron. Obs. Skalnaté Pleso **48**, 228 – 235, (2018)

The properties and origin of magnetic fields in white dwarfs

A. Kawka

Astronomical Institute of the Czech Academy of Sciences
251 65 Ondřejov, The Czech Republic, (E-mail: kawka@asu.cas.cz)

Received: November 22, 2017; Accepted: November 28, 2017

Abstract. A significant fraction of white dwarfs harbour a magnetic field with strengths ranging from a few kG up to about 1000 MG. The fraction appears to depend on the specific class of white dwarfs being investigated and may hold some clues to the origin of their magnetic field. The number of white dwarfs with variable fields as a function of their rotation phase have revealed a large field structure diversity, from a simple offset dipole to structures with spots or multipoles. A review of the current challenges in modelling white dwarf atmospheres in the presence of a magnetic field is presented, and the proposed scenarios for the formation of magnetic fields in white dwarfs are examined.
Key words: white dwarfs – stars: magnetic fields – stars: evolution

1. Introduction

White dwarfs represent the final stage of stellar evolution for the majority of stars and a significant fraction of them harbour a magnetic field ranging from a few kG up to several hundred MG. The presence of a magnetic field affects the external appearance of the white dwarf (emerging flux), its temperature structure as well as its evolutionary prospects (cooling age).

In this review I examine the incidence of magnetism in the white dwarf population, and how it differs between different subclasses. The challenges in modelling white dwarf atmospheres in the presence of a magnetic field are discussed in Sect. 3. Finally, eligible scenarios for the origin of magnetic fields in white dwarfs are explored in Sect. 4.

2. Magnetic field incidence

The measured fraction of magnetism in white dwarfs varies between various surveys. Magnetic white dwarfs are identified via polarization measurements (P) or characteristic Zeeman patterns (H). Colourimetric and photometric limited surveys (e.g., Schmidt & Smith, 1995; Kepler et al., 2013) delivered fractions as low as 5% but volume limited surveys (Kawka et al., 2007) resulted in fraction estimates as high as 20%. The number of known magnetic white dwarfs has grown considerably in recent years which helped uncover specific classes of white dwarfs showing a significantly higher incidence of magnetism.

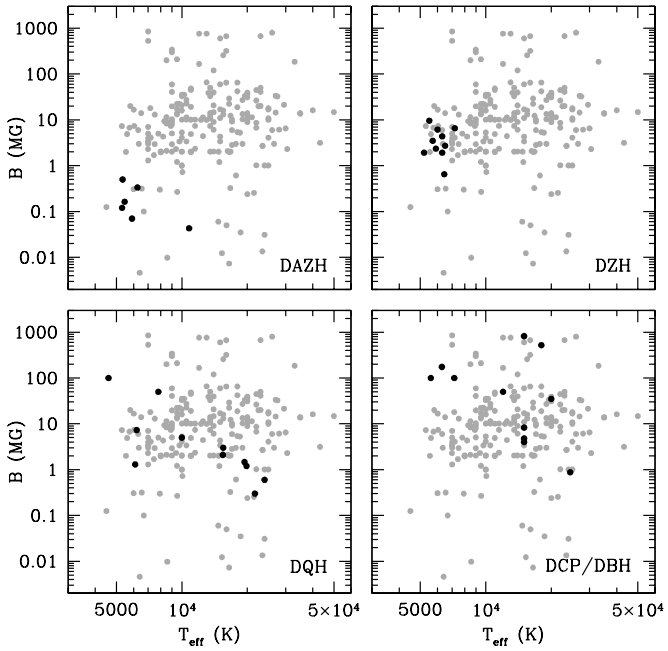

Figure 1. The distribution of known white dwarfs as a function of the magnetic field and effective temperature. The grey points in all panels are magnetic DA white dwarfs. Each panel highlights (in black) the properties of the various spectral type of magnetic white dwarfs (DAZ, DZ, DQ and DC/DB).

Most white dwarfs have a hydrogen-rich atmosphere (DA), with the remainder having an atmosphere dominated by helium, with a visual helium spectrum (DB) or without (DC). A few, rare carbon-dominated objects are known as hot DQ white dwarfs (Dufour et al., 2008) that appear to be high temperature counterparts to the cool helium-dominated but carbon-polluted DQ white dwarfs (Dufour et al., 2005). Approximately 25 to 30% of white dwarfs show traces of heavy elements (Zuckerman et al., 2003, 2010) and for such objects the suffix Z is added to the respective spectral classes, e.g., DAZ, DBZ, DZ (i.e., DC with metal lines).

Figure 1 shows all currently known magnetic white dwarfs segregated into various spectral types as a function of their field strength and effective temperature. Table 1 lists the number of known magnetic white dwarfs and the incidence of magnetism per spectral class. For hot DQs, 12 are known, but only 6 of these have a published magnetic field measurement. There is no apparent correlation between effective temperature and magnetic field strength for DAH and DCP/DBH white dwarfs. Although only a few are known, polluted mag-

Table 1. Incidence of magnetism among different classes of white dwarfs

Spectral type	Prototype	Number	Fraction (%)	Reference
DAH	Grw+70°8247	208	4 ± 1.5	Schmidt & Smith (1995)
DAZH	G77-50	6	~ 50	Table 2
DBH	GD229	8	~ 1.5	estimated
DCP	G195-19	3	~ 5	Putney (1997)
DZH	LHS2534	10	13 ± 4	Hollands et al. (2015)
DQH (hot)	SDSS J1337+0026	12 (6)	~ 70	Dufour et al. (2013)
DQH (cool)	G99-37	4	~ 4	Vornanen et al. (2013)

netic white dwarfs (DAZH, DZH) are clustered at cooler temperatures, with the DAZH at systematically lower field strengths. Featureless DC white dwarfs are difficult to diagnose and only a handful of high-field DCP are known.

2.1. Cool polluted white dwarfs

Studies of cool, polluted white dwarfs have revealed a higher incidence of magnetism than in the general population of white dwarfs. Kawka & Vennes (2014) showed an incidence of 40% in cool, polluted hydrogen-rich (DAZ) white dwarfs. These objects have relatively low fields ($B_S < 1$ MG). Here we revisit this sample and confirm this high incidence. Table 2 lists the known magnetic DAZs. Comparing this sample to all the other known DAZ white dwarfs that have been observed at sufficiently high resolution we find that close to 50% of DAZ white dwarfs with $T_{\rm eff} < 6000$ K are magnetic. The abundance patterns of magnetic DAZs does not appear to differ from those of non-magnetic DAZs and we cannot establish a correlation between magnetic field strengths and abundances. Above a temperature of 6000 K, only 2 magnetic DAZs are known, NLTT 53908 is only slightly warmer at 6250 K and WD2105-820 is hotter with $T_{\rm eff} = 10\,800$ K.

A high incidence of magnetism is also observed in the cool, polluted, helium-rich class (DZ) of white dwarfs. Hollands et al. (2015) reported an incidence of 13% in DZ white dwarfs with $T_{\rm eff} < 8000$ K. The magnetic fields in this case are higher than those in cool DAZs with $1.9 < B_S < 9.6$ MG. Hollands et al. (2015) noted that the incidence of magnetism in DZs hotter than 8000 K is significantly lower in their sample.

2.2. Hot DQ white dwarfs

Hot DQ white dwarfs have temperatures ranging from about 18 000 K up to 24 000 K and an atmosphere dominated by carbon. Half of these stars were found to be photometrically variable with periods ranging from ≈ 5 min up to 2.1 days. Initially, these variations were attributed to pulsations, however, following the discovery of a 2.1 day period in SDSS J0005-1002 (Lawrie et al.,

Table 2. Properties of known magnetic DAZ white dwarfs

Name	$T_{\rm eff}$ (K)	$\log g$	B_S (kG)	V (mag)	Reference
NLTT07547	5460	8.04	163	18.3	1
NLTT10480	5410	8.0	519	17.5	2
NLTT43806	5900	8.0	70	15.9	3,4
NLTT53908	6250	7.87	334	18.0	5
G77-50	5310	8.05	120	16.2	6
WD2105-820	10800	8.19	43	13.6	7,8

References: (1) Kawka et al., in prep; (2) Kawka & Vennes (2011); (3) Kawka & Vennes (2006); (4) Zuckerman et al. (2011); (5) Kawka & Vennes (2014); (6) Farihi et al. (2011); (7) Koester et al. (2009); (8) Landstreet et al. (2012)

2013), the preferred explanation is that they are caused by a rotating field. Recently, Dufour et al. (2013) reported an incidence of 70% in this class of objects, suggesting that all hot DQs may be magnetic at some level. The magnetic fields range from $\sim$ 0.3 up to 2.1 MG. Dufour et al. (2013) also propose that these stars may be more massive than the general white dwarf population. Dunlap & Clemens (2015) also suggests that hot DQs are likely massive, and, since most of them show rapid variability which may be attributed to rotation, they are possibly the product of white dwarf mergers.

3. Modelling magnetic atmospheres

Magnetic fields, particular strong ones, are detected in intensity spectra while weak fields are readily detectable in Stokes V spectra. A combination of intensity and circular polarization spectra are useful for detailed studies of field geometry. Different Zeeman regimes need to be used depending on the field strength. The linear Zeeman regime can be assumed for weak fields, and as the field strength increases, the quadratic effect becomes important. For the strongest magnetic fields the strong field mixing regime needs to be adopted. For more details about these regimes see Wickramasinghe & Ferrario (2000).

In general the magnetic field in white dwarfs is assumed to be a centred or offset dipole. However, rotating magnetic white dwarfs have revealed a diversity in the field topology. Landstreet et al. (2017) showed that the rotating magnetic white dwarf WD 2047+372 which has a weak field of $B_P = 91.8 \pm 0.8$ kG can be modelled by a simple dipole. Their analysis of a second low-field white dwarf WD 2359-434 required the combination of a dipolar and a non-aligned quadrupole to model the spectropolarimetric observations. Some white dwarfs were found to have even more complex structures. For example, the high-field, massive and hot white dwarf EUVE J0317-855 shows a field of 185 MG with a likely 425 MG magnetic spot (Burleigh et al., 1999; Vennes et al., 2003). WD 1953-011 also shows a complex field structure (Maxted et al., 2000; Valyavin et al., 2008) as it rotates with a period of 1.4418 days (Brinkworth et al., 2005).

White dwarfs with hydrogen-rich atmospheres become convective below $T_{\rm eff}$ $\sim$ 15 000 K. Helium-rich atmospheres develop convection zones at much higher temperatures $T_{\rm eff} \lesssim 30\,000$ K. Valyavin et al. (2014) proposed that convection is suppressed in magnetic white dwarfs and slows down the white dwarf cooling rate. Using radiative magnetohydrodynamic simulations Tremblay et al. (2015) confirmed that convection is indeed suppressed, but that the cooling rate is not affected until the convective zone couples with the degenerate core which occurs around 5500 K. Observationally, Gentile Fusillo et al. (2018) fitted far ultraviolet (UV) spectra as well as optical Balmer line spectra of magnetic and non-magnetic white dwarfs with temperatures ranging from 9000 to 10 000 K. They used models with convection and without convection and found that for the magnetic white dwarf WD 2105-820 they could only produce consistent results between the best fitting UV and optical data using radiative models.

4. Origin of magnetic fields in white dwarfs

Magnetic fields in white dwarfs have often been assumed to be fossil fields, and that the progenitors of magnetic white dwarfs are predominantly magnetic Ap and Bp stars. Assuming magnetic flux conservation, the field strengths observed in Ap/Bp stars would correspond to white dwarf fields in excess of 10 MG (Kawka & Vennes, 2004; Wickramasinghe & Ferrario, 2005). Therefore, the progenitors of white dwarfs with weak magnetic fields may be other main-sequence stars that have magnetic fields well below current detection limits.

The fossil field theory implies that magnetic white dwarfs should be found in equal proportion in binary systems with main-sequence stars. However, this does not appear to be the case. Extensive surveys, like those of the Sloan Digital Sky Survey (SDSS), have been unable to find any non-interacting magnetic white dwarf plus main-sequence pairs (Liebert et al., 2015), thus leaving magnetic cataclysmic variables without direct progenitors. Therefore, other mechanisms for producing magnetic fields in white dwarfs have been recently proposed.

Tout et al. (2008) proposed a binary origin where the magnetic field is formed via a dynamo created during a common envelope (CE) phase. In systems that merge during the CE phase, single magnetic white dwarfs are created, but failed mergers would result in binary systems with a secondary nearly filling its Roche lobe. Following up on this theory, Potter & Tout (2010) and Wickramasinghe et al. (2014) showed that a magnetic field can be generated by a dynamo created by differential rotation within the CE, with the strongest fields being created if the merged objects are differentially rotating near break-up. A variation on the merger scenario was proposed by Nordhaus et al. (2011) who proposed that during a CE phase a low-mass star will be tidally disrupted by its proto-white dwarf companion forming an accretion disk. This would generate a dynamo in the disk which is then transferred to the degenerate core via accretion. Magnetic fields can also be produced by the merger of two white dwarfs. García-Berro

et al. (2012) have shown that the merger of two white dwarfs can generate a hot, convective and differentially rotating corona producing a dynamo and the resulting magnetic field.

Isern et al. (2017) proposed that magnetic fields with $B \lesssim 0.1$ MG may be produced by phase separation during the onset of crystallization in the white dwarf core. They show that as white dwarfs begin to crystallize at sufficiently low temperatures (~ 8000 K), phase separation of the main elements (in most cases O and C) occurs leading to an unstable, convective liquid mantle on top of a solid core. This produces a dynamo allowing the creation of a magnetic field.

Briggs et al. (2015) conducted a population synthesis of binary systems to investigate which type of system could result in a magnetic white dwarf. They found that the contribution from the double degenerate merger scenario is much smaller than the contribution from the CE merger. Both merger scenarios are able to explain the higher than average mass of magnetic white dwarfs. Once the field is established, the predicted magnetic field strengths should remain throughout the white dwarf life-time since the magnetic flux is not expected to decay significantly once the magnetic field is frozen into the white dwarf.

Evidence for the binary origin of magnetic fields in white dwarfs can be found in a few double degenerate systems. The fast rotating magnetic white dwarf EUVE J0317-855 is in a common proper motion (CPM) binary with LP9802 (Külebi et al., 2010) and has $B \approx 450$ MG magnetic spot with an underlying lower field of $B \approx 185$ MG (Ferrario et al., 1997; Vennes et al., 2003). The cooling age of EUVE J0317-855 which is also the more massive white dwarf in the system is much shorter than that of its CPM companion LP9802 and therefore EUVE J0317-855 is the result of a merger. The CPM binary PG1258+593 plus SDSS J1300+5904 have similar masses, however SDSS J1300+5904 is much cooler (Girven et al., 2010) resulting in an age discrepancy and therefore implying that PG1258+593 is the product of a merger.

Only a few magnetic plus non-magnetic double degenerate systems are known (for a list see Kawka et al., 2017). In some cases, the magnetic white dwarf is hotter and hence younger than its non-magnetic companion, despite being the more massive component. Failed merger may also deliver double degenerate systems with a magnetic component. A magnetic field can be created during the CE without the stars merging. This is the case of the close double degenerate system NLTT 12758 which contains a magnetic white dwarf. The field in the magnetic white dwarf was probably not formed during the merger of two stars, but would have formed in the second CE phase where the differential rotation was greater (Kawka et al., 2017).

5. Summary

The growing sample of known magnetic white dwarfs is revealing a diversity in the properties of magnetic fields. The incidence of magnetism appears to vary

between various classes of white dwarfs. This suggests that magnetic fields in white dwarfs are created by several discernible processes.

Acknowledgements. A.K. thanks S. Vennes and L. Ferrario for stimulating discussions. This work was supported by the Czech Science Foundation (15-15943S).

References

Briggs, G. P., Ferrario, L., Tout, C. A., Wickramasinghe, D. T., & Hurley, J. R. 2015, *Mon. Not. R. Astron. Soc.*, **447**, 1713

Brinkworth, C. S., Marsh, T. R., Morales-Rueda, L., et al. 2005, *Mon. Not. R. Astron. Soc.*, **357**, 333

Burleigh, M. R., Jordan, S., & Schweizer, W. 1999, *Astrophys. J., Lett.*, **510**, L37

Dufour, P., Bergeron, P., & Fontaine, G. 2005, *Astrophys. J.*, **627**, 404

Dufour, P., Fontaine, G., Liebert, J., Schmidt, G. D., & Behara, N. 2008, *Astrophys. J.*, **683**, 978

Dufour, P., Vornanen, T., Bergeron, P., & Fontaine, A., B. 2013, in ASP Conf. Ser., Vol. **469**, *18th European White Dwarf Workshop.*, 167

Dunlap, B. H. & Clemens, J. C. 2015, in ASP Conf. Ser., Vol. **493**, *19th European Workshop on White Dwarfs*, ed. P. Dufour, P. Bergeron, & G. Fontaine, 547

Farihi, J., Dufour, P., Napiwotzki, R., & Koester, D. 2011, *Mon. Not. R. Astron. Soc.*, **413**, 2559

Ferrario, L., Vennes, S., Wickramasinghe, D. T., Bailey, J. A., & Christian, D. J. 1997, *Mon. Not. R. Astron. Soc.*, **292**, 205

García-Berro, E., Lorén-Aguilar, P., Aznar-Siguán, G., et al. 2012, *Astrophys. J.*, **749**, 25

Gentile Fusillo, N. P., Tremblay, P.-E., Jordan, S., et al. 2018, *Mon. Not. R. Astron. Soc.*, **473**, 3693

Girven, J., Gänsicke, B. T., Külebi, B., et al. 2010, *Mon. Not. R. Astron. Soc.*, **404**, 159

Hollands, M. A., Gänsicke, B. T., & Koester, D. 2015, *Mon. Not. R. Astron. Soc.*, **450**, 681

Isern, J., García-Berro, E., Külebi, B., & Lorén-Aguilar, P. 2017, *Astrophys. J., Lett.*, **836**, L28

Kawka, A., Briggs, G. P., Vennes, S., et al. 2017, *Mon. Not. R. Astron. Soc.*, **466**, 1127

Kawka, A. & Vennes, S. 2004, in IAU Symposium, Vol. **224**, *The A-Star Puzzle*, ed. J. Zverko, J. Ziznovsky, S. J. Adelman, & W. W. Weiss, 879–885

Kawka, A. & Vennes, S. 2006, *Astrophys. J.*, **643**, 402

Kawka, A. & Vennes, S. 2011, *Astron. Astrophys.*, **532**, A7

Kawka, A. & Vennes, S. 2014, *Mon. Not. R. Astron. Soc.*, **439**, L90

Kawka, A., Vennes, S., Schmidt, G. D., Wickramasinghe, D. T., & Koch, R. 2007, *Astrophys. J.*, **654**, 499

Kepler, S. O., Pelisoli, I., Jordan, S., et al. 2013, *Mon. Not. R. Astron. Soc.*, **429**, 2934

Koester, D., Voss, B., Napiwotzki, R., et al. 2009, *Astron. Astrophys.*, **505**, 441

Külebi, B., Jordan, S., Nelan, E., Bastian, U., & Altmann, M. 2010, *Astron. Astrophys.*, **524**, A36

Landstreet, J. D., Bagnulo, S., Valyavin, G., & Valeev, A. F. 2017, *Astron. Astrophys.*, **607**, A92

Landstreet, J. D., Bagnulo, S., Valyavin, G. G., et al. 2012, *Astron. Astrophys.*, **545**, A30

Lawrie, K. A., Burleigh, M. R., Dufour, P., & Hodgkin, S. T. 2013, *Mon. Not. R. Astron. Soc.*, **433**, 1599

Liebert, J., Ferrario, L., Wickramasinghe, D. T., & Smith, P. S. 2015, *Astrophys. J.*, **804**, 93

Maxted, P. F. L., Ferrario, L., Marsh, T. R., & Wickramasinghe, D. T. 2000, *Mon. Not. R. Astron. Soc.*, **315**, L41

Nordhaus, J., Wellons, S., Spiegel, D. S., Metzger, B. D., & Blackman, E. G. 2011, *Proc. Natl. Acad. Sci.*, **108**, 3135

Potter, A. T. & Tout, C. A. 2010, *Mon. Not. R. Astron. Soc.*, **402**, 1072

Putney, A. 1997, *Astrophys. J., Suppl. Ser.*, **112**, 527

Schmidt, G. D. & Smith, P. S. 1995, *Astrophys. J.*, **448**, 305

Tout, C. A., Wickramasinghe, D. T., Liebert, J., Ferrario, L., & Pringle, J. E. 2008, *Mon. Not. R. Astron. Soc.*, **387**, 897

Tremblay, P.-E., Fontaine, G., Freytag, B., et al. 2015, *Astrophys. J.*, **812**, 19

Valyavin, G., Shulyak, D., Wade, G. A., et al. 2014, *Nature*, **515**, 88

Valyavin, G., Wade, G. A., Bagnulo, S., et al. 2008, *Astrophys. J.*, **683**, 466

Vennes, S., Schmidt, G. D., Ferrario, L., et al. 2003, *Astrophys. J.*, **593**, 1040

Vornanen, T., Berdyugina, S. V., & Berdyugin, A. 2013, *Astron. Astrophys.*, **557**, A38

Wickramasinghe, D. T. & Ferrario, L. 2000, *Publ. Astron. Soc. Pac.*, **112**, 873

Wickramasinghe, D. T. & Ferrario, L. 2005, *Mon. Not. R. Astron. Soc.*, **356**, 1576

Wickramasinghe, D. T., Tout, C. A., & Ferrario, L. 2014, *Mon. Not. R. Astron. Soc.*, **437**, 675

Zuckerman, B., Koester, D., Dufour, P., et al. 2011, *Astrophys. J.*, **739**, 101

Zuckerman, B., Koester, D., Reid, I. N., & Hünsch, M. 2003, *Astrophys. J.*, **596**, 477

Zuckerman, B., Melis, C., Klein, B., Koester, D., & Jura, M. 2010, *Astrophys. J.*, **722**, 725

Contrib. Astron. Obs. Skalnaté Pleso **48**, 236 – 244, (2018)

A high-precision survey of magnetic white dwarfs

S. Bagnulo[1], J. D. Landstreet[1,2], A. J. Martin[3] and G. Valyavin[4]

[1] *Armagh Observatory & Planetarium, College Hill, Armagh BT61 9DG, UK*

[2] *Dept. of Physics & Astronomy, University of Western Ontario, London, Ontario N6A 3K7, Canada*

[3] *LESIA, 5 place Jules Janssen, F-92195 Meudon, France*

[4] *Special Astrophysical Observatory, RAS, Nizhnij Arkhiz, Zelenchukskij Region, 369167 Karachai-Cherkessian Republic, Russia*

Received: Dezember 22, 2017; Accepted: Dezember 27, 2017

Abstract. We have carried out a survey of magnetic fields in 60 bright white dwarfs. Our observations have a mean uncertainty of about 0.5 kG. The large sample and high accuracy of our measurements allows us to obtain a clearer picture of the frequency of magnetic fields in degenerate stars, and shows that even relatively weak fields are in fact quite rare in white dwarfs.

Key words: polarization – stars: white dwarfs – stars: magnetic field

1. Introduction

There are many important questions to be explored concerning magnetic fields in white dwarfs (WDs). Primarily: is there a lower limit for field strength in WDs below which all, or none, have magnetic fields? We know that the strength of the fossil field of Ap stars is always above a threshold of about 300 G (Aurière et al., 2007). Does the field of WDs exhibit a similar behaviour? Finding this limit, if it exists, will help to define similarities between the fields of Ap stars and those of WDs, which will in turn guide the development of new theories and models for how WD magnetic fields form and evolve. Motivated by this and other important questions about stellar magnetism we have started a high-precision magnetic survey of WDs. Here we present our preliminary results. This workshop, which is dedicated to the general theme of stellar magnetic fields, is in fact a direct descendant of a series of conferences that were dedicated to Ap/Bp stars. Accordingly we have decided to present our work making references to our experience in detection and modelling of magnetic fields of Ap/Bp stars.

2. Detection techniques for the magnetic field of WDs

Together with Ap/Bp stars, WDs are the kinds of star to which we most commonly associate the idea that a magnetic field may be present and possibly be a predominant feature of the stellar atmosphere. Like Ap/Bp stars, there exist

different varieties of WDs. The classification (developed by Sion et al., 1983) includes a first letter D which means "Degenerate", followed by a capital letter that reflects the spectral features. For instance, we have DA WDs, with spectra that show only H lines, DB WDs, that show only He lines, DC WDs, with featureless spectra, etc. To these two letters, a number from 0 to 9 is usually added to report about the stellar temperature, 9 being the coolest end, and 0 the hottest end. Most WDs show only a single atom in their spectra because gravitational diffusion leads to the lightest surviving element floating on everything else.

Prior to the presentation of our survey we need to discuss the observing techniques for WDs, which may be quite different from those commonly used for other kinds of stars.

The top left panel of Fig. 1 shows the intensity spectrum of an Ap star observed at medium-low resolution ($R \sim 8\,000$). This spectrum exhibits Balmer lines from Hβ down to the Balmer jump. What we see between Balmer lines is not noise, but the superposition of hundreds of metal lines. Balmer lines are sensitive to the magnetic field, but for various reasons, the magnetic field of Ap/Bp stars is usually measured from metal lines observed with high-resolution spectropolarimetry.

The top right panel of Fig. 1 shows the spectrum of the DA star WD 1647+591 observed with the same instrument setting as the Ap star. The two spectra are not very dissimilar, except that the continuum of the spectrum of the WD is actually featureless (any wrinkle is actually due to noise). Compared to Ap/Bp stars, WDs are generally much fainter objects (there exist only about 60 WDs known to be brighter than $V = 13$). We note that the intensity spectrum of this DA WD represents a best-case situation. Some spectra appear like the one of WD 0426+588 (mid left panel of Fig. 1), or like WD 1900+705 (mid right panel).

Regarding polarisation, in Ap/Bp stars we are used to Stokes V/I profiles spectra like the one in the left bottom panel of Fig. 1, i.e., with the continuum oscillating around zero, and with large amplitude in proximity of spectral lines. This polarisation spectrum was obtained at low resolution and only Balmer lines show a prominent signal of polarisation. However, this example is qualitatively also representative of the polarised spectrum of metal lines when observed in high-resolution. The polarisation spectrum of WDs may be totally different, like the one of WD 1900+705 shown in the bottom right panel of Fig. 1, where also the continuum is polarised.

Compared to field measurements in Ap stars, two new characteristics appear for WDs: 1) Some WDs have featureless spectra, which simply makes it impossible to detect the magnetic field from the analysis of Zeeman effect on the Stokes profiles of spectral lines. 2) Magnetic fields of WDs may be very strong, so strong that Hydrogen Balmer lines wander around in wavelength, and that even the continuum becomes polarised. For instance, the spectral feature around 4100 Å observed in the intensity spectrum of WD 1900+705 is one

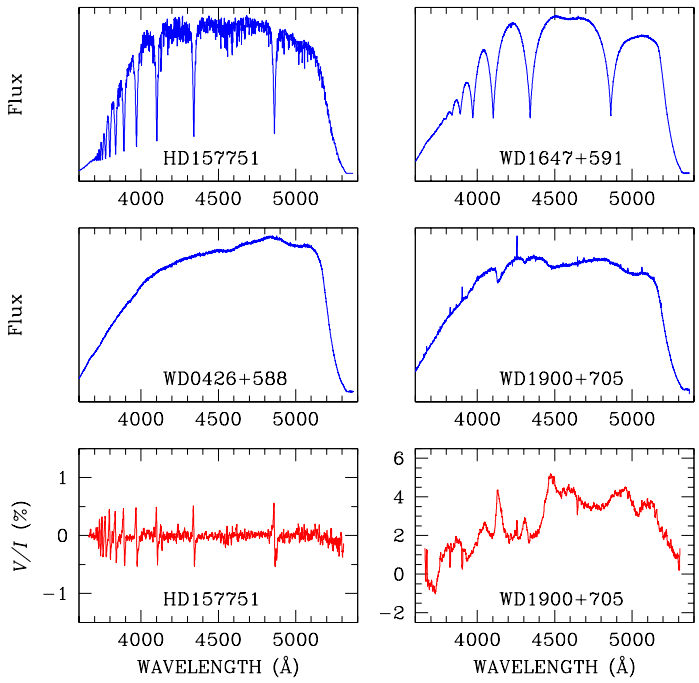

Figure 1. Low-resolution intensity and circularly polarised spectra of the Ap star HD 157751 and of three WDs observed with the blue arm of the ISIS instrument of the WTH.

of the component of Hβ shifted by 700 Å by the presence of a magnetic field. Both stars (WD 1900+705 and WD 1647+591) have a H-rich atmosphere with a similar temperature!

A simple introduction to the effects of strong magnetic fields in stellar atmospheres was presented by Putney (1997) as follows.
1) For field strength $|B| > 50$ MG the magnetic force acting on the electrons is comparable to the Coulomb force due to the atom nucleus; the continuum is polarised and spectral lines may be shifted; e.g., in presence of a 10^9 G magnetic field, some of the Balmer and Paschen transitions of H are in the ultraviolet. Many of line transitions have extrema, or stationary points where a transition occurs at a particular wavelength, or over a very small wavelength range (e.g., 50 Å), for a large range of magnetic fields (e.g., 100 MG). A spectral feature may develop at the wavelength of a stationary point if a large enough fraction of the star is characterised by a magnetic field in the corresponding range of magnetic field strength. Calculations have been made by Wunner et al. (1985).

2) For 1 MG< $|B|$ < 50 MG we are in the Zeeman quadratic regime. We still need numerical computation to interpret line polarisation and splitting in terms of field strength (e.g. Kemic, 1974).
3) In the linear Zeeman regime we can adopt formulas that are similar to those used for Ap/Bp stars, e.g. the relationship between Zeeman splitting and field modulus is linear.
4) Zeeman splitting is not detectable for field strength less than 50 kG, a regime that may be probed only by means of spectropolarimetric techniques.

It is important to note that there is no instrument that suits perfectly well all these regimes, which as we will discuss later may introduce a bias in the survey.

3. S, M, L, XL, XXL WD surveys

Kemp et al. (1970) obtained the first field detection in a WD using broadband circular polarisation (BBCP) measurements. This work was followed by various BBCP surveys, e.g., by Angel et al. (1981). Over the last few five decades, several surveys of WDs have been performed to search for magnetic fields. In the following we shall mention some of those, highlighting the technique used, their sample size, mean uncertainty of the field measurements and the field detection rate.
– Schmidt & Smith (1995) carried out a large spectropolarimetric survey of 170 DA WDs characterised by a mean uncertainty of 8.6 kG, with a 4 % detection rate.
– Putney (1997) carried out a medium-size spectropolarimetric survey of 46 WDs, with typical uncertainty > 10 kG and a claimed (but overestimated) detection rate of $15 - 20$ %.
– Koester et al. (1998) carried out a medium-size high-resolution spectroscopic survey of 30 stars with a 16 % detection rate.
– Aznar Cuadrado et al. (2004) and Jordan et al. (2007) obtained FORS circular spectropolarimetry of 12 and 10 stars, respectively, with an uncertainty < 1 kG and a detection rate of 25 % and 10 % respectively. These two small surveys introduced the concept that it could be very interesting to investigate WDs with high-precision spectropolarimetry.
– Valyavin et al. (2006) used the 6 m Russian telescope (BTA) for a small spectropolarimetric survey of six WDs, with typical uncertainties of 1 to 3 kG, and a formal detection rate of 17 %.
– Koester et al. (2009) used the extremely large SPY UVES high-resolution spectroscopic survey of 1 000 isolated WDs and WD+dM systems for a detection rate of 1.6 % for fields small enough (less than about 1 MG) or sufficiently non-obvious to have been missed in low-resolution spectroscopic surveys.
– Landstreet et al. (2012) presented a small FORS specpolarimetric survey of 8 WDs field measurements with an uncertainty of 1 kG, for a 12 % detection rate.

Landstreet et al. (2012) also presented a reassessment of the results obtained in previous surveys.
– Kawka & Vennes (2012) presented a medium-size FORS spectropolarimetric survey of 58 cool WDs with uncertainty $> 2 - 5$ kG, and resulting in a 3.5 % detection rate.
– Külebi et al. (2009), Kleinman et al. (2013) and Kepler et al. (2013) analysed 20 000 spectra of WD from the SDSS spectroscopic survey, and scored a 5 % detection rate.

Without going into details, one can see that different surveys had a different success in detecting new magnetic stars. It is not easy to get a comprehensive view of the incidence of magnetic fields in WDs from individual surveys, because different surveys have a target list with different size and compiled with different criteria, and because observations were carried out with different techniques and with different typical S/N (resulting in different sensitivity). Note also that magnetic fields in WDs with featureless spectra (DC) can be detected only if the magnetic field is strong enough to polarise the continuum ($|B| > 50$ MG). Most of surveys include stars that were already known as magnetic or suspected magnetic stars. Finally we note that some surveys report results with an ambiguous to misleading language. For instance, sentences like "The WD has a field strength less than N kG" (where N kG is the detection threshold) or "Field was detected at $2\,\sigma$ level" mean both that no field was detected, but may give the impression that the stars are indeed magnetic.

4. This survey

We have surveyed about 60 WDs in low and/or medium and/or high-resolution spectropolarimetric mode using three different instruments: the FORS instrument of the ESO VLT, the ISIS instrument of the WHT, and the ESPaDOnS instrument of the CHFT. Most of the targets of our survey were never observed before with high precision polarimetric techniques (or never observed at all in polarimetric mode). With FORS and ISIS we adopted the slope technique described by Bagnulo et al. (2002) and with ESPaDOnS we used the technique introduced by Landstreet et al. (2015).

FORS and ISIS are somehow very similar instruments, but they have some important differences that are interesting to emphasise. First of all, ISIS reaches a higher spectral resolution than FORS, up to 8 000 (compared to 2-3 000 with FORS). ISIS has two arms and covers double the spectral range of FORS. At the highest spectral resolution ISIS may cover the ranges 3700–5200 and 6100–6800 Å, while FORS covers only one of these spectral regions at a time. For our survey we decided to observe with FORS in the blue spectral region.

With ISIS, grisms cannot be exchanged quickly during the night, and grism insertion must be generally followed by some fine tuning and calibration procedures, whereas with FORS, changing a grism is as fast and simple as exchang-

ing a filter. Practically speaking, the instrument mode with ISIS is fixed for the entire observing night, while FORS gives much more flexibility. Once the instrument mode is set, ISIS has much shorter overheads than FORS, e.g., CCD readout and rotation of the wave plate require 15 secs at most, against at least 1 minute with FORS. Since polarimetry requires multiple exposure, this difference in overheads is really felt by the observer. On the other hand, ISIS operations are less automatised than with FORS, therefore it is easier to make errors and waste telescope time at the console.

Both ISIS and FORS are Cassegrain-mounted instruments, which means they are prone to flexures when the telescope is pointed. Also, because of the alt-az mounting of the telescope, the instrument is continuously rotating to keep the field of view fixed in the camera. If flexures happen during an exposure or an exposure series, it means that that the image or the spectrum on the CCD may be slightly blurred or move from one exposure to the next. The implication for spectropolarimetric measurements has been thoroughly discussed by Bagnulo et al. (2013), and we will not come back to this point here, but we shall just remember that *flexures are much more likely to produce spurious detections than to hide a magnetic field*.

The third instrument that we have used, ESPaDOnS, does not have problems with flexures as it sits on a bench and it is fibre fed from a polarimetric module attached at the Cassegrain focus. Since the telescope has an equatorial mounting, the instrument does not have to rotate. The caveat is that a high-resolution spectropolarimeter may not be the ideal instrument for the measurement of the magnetic field in stars with very broad spectral lines, for the following reason. As the retarders rotate, or simply as time passes and fibres are moved, the way in which fibres are fed and transmit the signal may change, in particular the ratio between the signal in the two beams of the Wollaston prism or any other beam splitter device may change. This produces a nearly unavoidable and spurious polarisation signal in the continuum which is usually removed by a normalisation procedure that assumes that the continuum is not polarised. The Balmer lines are very broad and may even extend beyond an individual order of the echelle spectrograph, making it very difficult to disentangle in the line wings the polarisation due to a magnetic field from that due to instrument polarisation. However, Landstreet et al. (2015) showed that the core of Hα behaves somehow like a metal line, so that Stokes profile may be analysed with the usual technique that measures the first order moment of Stokes V about the line centre and converts this quantity into an estimate of the mean longitudinal magnetic field $\langle B_z \rangle$. Landstreet et al. (2015) introduced and validated the use of this technique and at the same time failed to confirm the magnetic nature of the WD 40 Eri B (this conclusion was based also on ISIS data).

An obvious advantage of ESPaDOnS is that it allows us also to measure the mean magnetic field modulus $\langle |B| \rangle$ even in relatively weak-field stars: we estimate that ESPaDOnS can measure $\langle |B| \rangle \geq 20\,\mathrm{kG}$, and detect clear Zeeman splitting in stars with $\langle |B| \rangle$ as weak as 40 kG, while the detection limit with

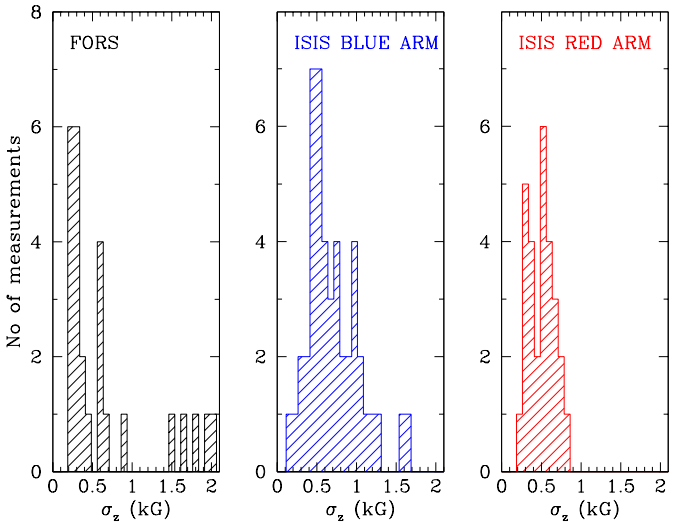

Figure 2. Histograms showing the distribution of the error bars obtained with FORS and with the two ISIS arms.

ISIS would be twice as much, and FORS can detect Zeeman splitting in the intensity spectrum only in stars that have at least a 2-300 kG field.

At the moment of writing we are in the process of revising the technique used to measure the mean longitudinal magnetic field with ESPaDOnS, therefore in these proceedings we will discuss only FORS and ISIS measurements.

The precision of the $\langle B_z \rangle$ field measurements of our survey is shown in Fig. 2 with the histograms of the error bars. We have considered separately the observations obtained with the blue arm and with the red arm of ISIS. This allows us to see that observing Hα alone leads to measurements that have the same precision as those obtained observing several Balmer lines from Hβ down. The explanation is that Zeeman effect is proportional to λ^2, therefore the higher number of spectral lines in the blue region is balanced by the higher sensitivity of Hα. In fact, about 2/3 of the ISIS observations used the blue and red arm to observe (simultaneously) the same star. These observations may be combined, leading to even higher precisions for individual stars. Our survey led to very few field detections, mostly in stars that were already known to be magnetic from previous investigations. The full results of our surveys will be presented in two forthcoming papers by Bagnulo et al. (in prep.) and Landstreet et al. (in prep.).

We finally would like to mention that we also used telescope time to monitor individual WDs that show variability to measure their rotation period and eventually to model their magnetic field. The special case of stars WD 2047+372 and WD 2359-434 is presented by Landstreet et al. (2017, and these proceedings).

References

Angel, J. R. P., Borra, E. F., & Landstreet, J. D. 1981, *Astrophys. J., Suppl.*, **45**, 457

Aurière, M., Wade, G. A., Silvester, J., et al. 2007, *Astron. Astrophys.*, **475**, 1053

Aznar Cuadrado, R., Jordan, S., Napiwotzki, R., et al. 2004, *Astron. Astrophys.*, **423**, 1081

Bagnulo, S., Fossati, L., Kochukhov, O., & Landstreet, J. D. 2013, *Astron. Astrophys.*, **559**, A103

Bagnulo, S., Szeifert, T., Wade, G. A., Landstreet, J. D., & Mathys, G. 2002, *Astron. Astrophys.*, **389**, 191

Jordan, S., Aznar Cuadrado, R., Napiwotzki, R., Schmid, H. M., & Solanki, S. K. 2007, *Astron. Astrophys.*, **462**, 1097

Kawka, A. & Vennes, S. 2012, *Mon. Not. R. Astron. Soc.*, **425**, 1394

Kemic, S. B. 1974, *Astrophys. J.*, **193**, 213

Kemp, J. C., Swedlund, J. B., Landstreet, J. D., & Angel, J. R. P. 1970, *Astrophys. J., Lett.*, **161**, L77

Kepler, S. O., Pelisoli, I., Jordan, S., et al. 2013, *Mon. Not. R. Astron. Soc.*, **429**, 2934

Kleinman, S. J., Kepler, S. O., Koester, D., et al. 2013, *Astrophys. J., Suppl.*, **204**, 5

Koester, D., Dreizler, S., Weidemann, V., & Allard, N. F. 1998, *Astron. Astrophys.*, **338**, 612

Koester, D., Voss, B., Napiwotzki, R., et al. 2009, *Astron. Astrophys.*, **505**, 441

Külebi, B., Jordan, S., Euchner, F., Gänsicke, B. T., & Hirsch, H. 2009, *Astron. Astrophys.*, **506**, 1341

Landstreet, J. D., Bagnulo, S., Fossati, L., Jordan, S., & O'Toole, S. J. 2012, *Astron. Astrophys.*, **541**, A100

Landstreet, J. D., Bagnulo, S., Valyavin, G., & Valeev, A. F. 2017, *Astron. Astrophys.* **607**, A92

Landstreet, J. D., Bagnulo, S., Valyavin, G. G., et al. 2015, *Astron. Astrophys.*, **580**, A120

Putney, A. 1997, *Astrophys. J., Suppl.*, **112**, 527

Schmidt, G. D. & Smith, P. S. 1995, *Astrophys. J.*, **448**, 305

Sion, E. M., Greenstein, J. L., Landstreet, J. D., et al. 1983, *Astrophys. J.*, **269**, 253

Valyavin, G., Bagnulo, S., Fabrika, S., et al. 2006, *Astrophys. J.*, **648**, 559

Wunner, G., Roesner, W., Herold, H., & Ruder, H. 1985, *Astron. Astrophys.*, **149**, 102

Stefano Bagnulo, Lilia Ferrario, Adela Kawka and Stéphane Vennes

Gregg Wade

Contrib. Astron. Obs. Skalnaté Pleso **48**, 245 – 249, (2018)

Optical polarimetry studies of white dwarfs

A. Słowikowska[1], **K. Krzeszowski**[2], **M. Żejmo**[2], **D. Blinov**[3,4,5] **and P. Reig**[3,4]

[1] *Toruń Centre for Astronomy, Nicolaus Copernicus University in Toruń, ul. Gagarina 11, 87-100 Toruń, Poland, (E-mail: aga@umk.pl)*

[2] *Janusz Gil Institute of Astronomy, University of Zielona Góra, Szafrana 2, 65-417 Zielona Góra, Poland*

[3] *Foundation for Research and Technology, 711 10 Heraklion, Crete, Greece*

[4] *University of Crete, Physics Department, 710 03 Heraklion, Crete, Greece*

[5] *Astronomical Institute, St. Petersburg State University, Universitetsky pr. 28, Petrodvoretz, 198504 St. Petersburg, Russia*

Received: December 13, 2017; Accepted: December 20, 2017

Abstract. We present results of the optical linear polarimetric survey of 101 white dwarfs (WDs) performed in R band with the RoboPol polarimeter. Our study shows that highly linear polarized white dwarfs are very rare. Moreover, we found that the median polarization degree of isolated DA WDs and DB WDs are similar, but lower than the median polarization of isolated DC WDs. The DB WDs in binaries seem to be more polarized than binaries containing DA+dM or double degenerated systems (DDSs) with DA component. We also present the measurements of the optical linear polarization of both components in two common proper motion binary systems (CPMBs): WD1336+123 and the Sirius-like system (SLS) WD2129+000. Because the vast majority of WDs have very low polarization degree on the level of less than 0.5%, they can be used as faint linear polarization standards.

Key words: white dwarfs – techniques: polarimetric

1. Introduction

Recently, optical polarimetry studies of astrophysical sources are booming. More and more dedicated polarimeters are built, thus more polarimetric observations are performed. The RoboPol polarimeter dedicated to monitoring the polarization of blazars (Blinov et al., 2016) is a good example. At the same time, polarization observations performed with different telescope classes, from the small to the big, urgently require fainter polarization standards of both types – polarized and zero-polarized. The polarized standards are required to establish the intrinsic depolarization caused by the instrument and zero-point of its position angle (PA), while the zero-polarized standards are necessary to determine the instrumental polarization (e.g. the RINGO3 polarimeter at the Liverpool Telescope, see Słowikowska et al., 2016).

There are more than 23,000 WDs known up to date. For many of them, the spectral type is known. Most WD atmospheres are hydrogen-rich (DA), and almost all others are helium-rich (DB). However, a significant fraction of WDs also contain traces of heavier elements in their atmospheres, and these are labelled with Z for metals or Q for carbon, for example, DZ or DQ. There are also WDs for which the spectrum does not show any strong lines, but their atmospheres are still helium-rich. Such WDs are classified as DC-type WDs.

In 2014 we started a long-term project to measure the linear optical polarization of selected WDs (for the description of the selected sample see Sec. 2 of Żejmo et al., 2017). We aim to perform a statistical analysis of the linear polarization properties of a WD sample and provide observers with a new list of faint linear polarimetric standard sources. In Żejmo et al. (2017) we presented the results of analysis of the optical linear polarization degree of 74 WDs of DA and DC spectral types, both isolated and in binary systems. Their SDSS r magnitudes range from 13 to 17. Almost all measured WDs show low polarization degree (PD $< 1\%$). Only two of them, WD1440−025 and WD2213+317, have PD higher than 1%. Żejmo et al. (2017) claim that the DC-type white dwarfs on average have higher PD (with the median PD of 0.78%) than DA type WDs (with the median PD of 0.36%), but there is no difference between PD of isolated DA type WDs (0.36%) and PD of DA+dM binary systems (0.33%).

Because most of WDs from our sample have low PD and they are well distributed over the sky in the right ascension range from $13^{\rm h}$ to $24^{\rm h}$ and declination from -11° up to 78° , they can be treated as a good set of faint linear polarimetric standard stars. With our sample[1] we increased the low linear polarization standard list (e.g. Fossati et al., 2007) substantially. WDs were, and still are, commonly used as zero-polarization standard stars. Apart from our list, there are eleven well known zero-polarized WDs in the literature. Two of them, namely G 191-B2B (PD=0.09%) and GD 319 (PD=0.045%), were proposed by Turnshek et al. (1990) as the Hubble Space Telescope polarimetric standards. Long-term monitoring of G 191-B2B is presented by Słowikowska et al. (2016). Another nine were proposed by Fossati et al. (2007) as main zero-polarization standards for the FORS1 instrument on the Very Large Telescope. Their goal was to find a group of faint polarized and zero-polarized standards appropriate for telescopes with big mirrors. Their sample consists of 30 stars of different spectral types in the magnitude range from 6 to 14. However, WDs given by Fossati et al. (2007) are in the magnitude range from 11 to 13, with only one exception of 14 mag. Therefore, our list is complementary to Fossati et al. (2007) in respect of the brightness. Seventy WDs extended the existing polarimetric standard lists by a factor of 7. A larger group of zero-polarization standards facilitates the selection of standards at a convenient time of the night and position on the sky.

[1] `http://astro.ia.uz.zgora.pl/~chriss/grant/tables_en.html`

Additionally, we found that for low extinction values (E(B–V) < 0.04), the best model that describes the dependence of PD on E(B–V) is given by the equation $\mathrm{PD_{max,ISM}}[\%] = 0.65\ \mathrm{E(B-V)}^{0.12}$. This differs from the Fosalba et al. (2002) equation $\mathrm{PD_{max,ISM}}[\%] = 3.5\ \mathrm{E(B-V)}^{0.8}$ that was derived from the fit in the E(B–V) range from 0.1 to 1.

2. Observations and data analysis

Our observations were performed at the Skinakas Observatory located in Crete (Greece) in 2014 and 2016. We used the RoboPol[2] linear polarimeter, equipped with two Wollaston prisms and two half-wave plates. It allows to measure the Stokes I, Q, U parameters simultaneously for all stellar objects within $13' \times 13'$ field of view and the scale of $0.435''\ \mathrm{px}^{-1}$ (King et al., 2014). The measurements were performed with an aperture defined as $2.5 \times$ FWHM, where FWHM is an average full width at half maximum of stellar images, which has a median value of $2.1''$(4.0 pixels). All observations with the RoboPol were performed with the R Johnson-Cousins filter. The exposure time was adjusted according to the brightness of each target, as estimated during short pointing exposures.

The data were analysed with the standard RoboPol pipeline (King et al., 2014), whose output gives the normalised Stokes parameters $q = Q/I$ and $u = U/I$ [3]. To account for the instrumental polarization, we measured the polarization degree of 14 zero-polarized standards. The data corrected for instrumental polarization were later used to obtain the PD according to Eq. 1, while the corresponding error (σ_{PD}) is calculated from Eq. 5 in King et al. (2014). For low polarization signal-to-noise ratio (PD / $\sigma_{\mathrm{PD}} < 3$) distribution of the PD is not normal (Gaussian) and the PD values must always be positive so their uncertainties are not symmetric. This introduces a bias into any estimate. To deal with this problem we applied the debias method described by Vaillancourt (2006). Details are given in Sec. 4 of Żejmo et al. (2017).

3. Results

The most intriguing object from our sample is WD1415+234. It shows the highest measured linear polarization in our total sample of 101 WDs measured in 2014 and 2016 and is an isolated DB WD with PD of 2.66% ($\mathrm{PD_c} = 2.56\%$). This value of the PD does not depend on the chosen aperture. A close examination of its neighbourhood stars indicates that the WD polarization is intrinsic. The other two WDs with reasonably high PD are WD1336+123 and WD1619+123 with PD values of 1.14% and 1.25%, respectively, and both are in binary systems. WD1336+123 is a DB WD with a dwarf M4 companion (Silvestri et al.,

[2] `http://robopol.org/`

[3] Hereafter we follow the IAU convention, where the position angle is measured from the North direction increasing counter-clockwise.

2005) and WD1619+123 is of DA type with a dG0 companion (Farihi et al., 2005). Below we discuss binary and multiple systems observed within our 2016 sample.

WD0119-004 (GR 516, LP 587-44): its companion is a subdwarf M5 (Silvestri et al., 2005) and is not a common proper motion binary.

WD1336+123 (PG 1336+124, LP 498-26): we were able to measure its companion (dwarf M4) separated by 87″(Oswalt et al., 1988). It has PD = 0.34% ± 0.33%, while PA = 82.°4 ± 25.°4. This compares with WD PD = 1.14% ± 0.15% and PA = 2.°3 ± 3.°9. The maximum PD caused by the ISM is ∼ 0.42%.

WD1419+576: it is a multiple system resolved only in the HST images and consists of a DB WD and two dwarfs of M2 types (Farihi et al., 2010). It cannot be resolved with RoboPol because the separation between components is less than 0.″7. Therefore, the measured PD is the net PD (0.44% ± 0.28%) of all three. The same is for PA, −37.°5 ± 16.°1. The position angle of secondary stars is 304.°04 ± 0.°12.

WD1619+123: this is a SLS with a dwarf G0 companion separated by 63″(Farihi et al., 2005). It can be resolved by RoboPol, but was unfortunately covered by the mask even in the pointing exposures. Holberg et al. (2013) give the position angle of the companion, where the orientation is measured from the WD to the companion, being 311.°39 (that corresponds to 131.°39) and it is aligned with the proper motion PA of 135.°8 found by Farihi et al. (2005).

WD2129+000: it is the second SLS in our sample. We were able to measure the polarization of its K2 star (Holberg et al., 2013) separated by 133.″1 (Oswalt et al., 1988) and obtained PD = 0.29% ± 0.05% and PA = -85.°9 ± 4.°9. The WD in this system has PD = 0.42% ± 0.28% and PA = −24.°6 ± 17.°4. The contribution from the ISM is estimated to be less than 0.44%. Holberg et al. (2013) give PA = 29.°04 of the companion measured from the WD.

For two CPMBs, WD1336+123 and WD2129+000, we were able to measure the PD of their companions. In both cases the measured PD of the companions (dwarf M4 in case of WD1336+123 and K2 in case of WD2129+000) is smaller than the expected maximum PD_{ISM}. Such measurements give an independent check on the contribution of the PD from the ISM, assuming that no intrinsic PD is expected from the companions – M4 and K2 type dwarfs.

We used the combined dataset from 2014 and 2016 to check the correlation between the interstellar polarization and the extinction. We found that for the E(B–V) range from 0.0 to 0.045 the maximum PD caused by the ISM is given by the relation $PD_{max,ISM}(\%) = 0.65\ E(B-V)^{0.12}$. We concluded that for three WDs with the highest PD their measured linear polarization is intrinsic.

The spatial distribution of our joined sample is in good agreement with the Berdyugin et al. (2014) measurements. There are regions in the Galaxy that show a higher PD, however, most of WDs from our sample are not located in these regions. Our statistical analysis shows that the isolated DB type WDs, similarly to isolated DA type WDs, have lower median PD values in comparison to isolated DC type WDs (0.3%, 0.36% and 0.66%, respectively). On the other

hand, the DB WDs in binary systems have much higher PD than the PD of all other binary systems in our sample (i.e. binary DA+dM and DDSs). However, the DB binaries sample size is small, therefore our result is not conclusive.

Acknowledgements. This work has been supported by Polish National Science Centre grants DEC-2011/03/D/ST9/00656 (AS, KK, MŻ) and UMO-2014/13/B/ST9/00570 (AS). DB acknowledges support from the St. Petersburg Univ. research grant 6.38.335.2015. RoboPol is a collaboration involving the University of Crete, the Foundation for Research and Technology - Hellas, the California Institute of Technology, the Max-Planck Institute for Radioastronomy, the Nicolaus Copernicus University, and the Inter-University Centre for Astronomy and Astrophysics. This work was partially supported by the "RoboPol" project, which is co-funded by the European Social Fund (ESF) and Greek National Resources, and by the European Comission Seventh Framework Programme (FP7) through grants PCIG10-GA-2011-304001 "JetPop" and PIRSES-GA-2012-31578 "EuroCal". Data analysis and figures were partly prepared using R (R Core Team, 2013).

References

Berdyugin, A., Piirola, V., & Teerikorpi, P. 2014, *Astron. Astrophys.*, **561**, A24

Blinov, D., Pavlidou, V., Papadakis, I., et al. 2016, *Mon. Not. R. Astron. Soc.*, **462**, 1775

Farihi, J., Becklin, E. E., & Zuckerman, B. 2005, *Astrophys. J., Suppl.*, **161**, 394

Farihi, J., Hoard, D. W., & Wachter, S. 2010, *Astrophys. J., Suppl.*, **190**, 275

Fosalba, P., Lazarian, A., Prunet, S., & Tauber, J. A. 2002, *Astrophys. J.*, **564**, 762

Fossati, L., Bagnulo, S., Mason, E., & Landi Degl'Innocenti, E. 2007, in ASP Conf. Ser., Vol. **364**, *The Future of Photometric, Spectrophotometric and Polarimetric Standardization*, ed. C. Sterken, 503

Holberg, J. B., Oswalt, T. D., Sion, E. M., Barstow, M. A., & Burleigh, M. R. 2013, *Mon. Not. R. Astron. Soc.*, **435**, 2077

King, O. G., Blinov, D., Ramaprakash, A. N., Myserlis, I., & et al., A. 2014, *Mon. Not. R. Astron. Soc.*, **442**, 1706

Oswalt, T. D., Hintzen, P. M., & Luyten, W. J. 1988, *Astrophys. J., Suppl.*, **66**, 391

R Core Team. 2013, R: A Language and Environment for Statistical Computing, R Foundation for Statistical Computing, Vienna, Austria

Silvestri, N. M., Hawley, S. L., & Oswalt, T. D. 2005, *Astron. J.*, **129**, 2428

Słowikowska, A., Krzeszowski, K., Żejmo, M., Reig, P., & Steele, I. 2016, *Mon. Not. R. Astron. Soc.*, **458**, 759

Turnshek, D. A., Bohlin, R. C., Williamson, II, R. L., et al. 1990, *Astron. J.*, **99**, 1243

Vaillancourt, J. E. 2006, *Publ. Astron. Soc. Pac.*, **118**, 1340

Żejmo, M., Słowikowska, A., Krzeszowski, K., Reig, P., & Blinov, D. 2017, *Mon. Not. R. Astron. Soc.*, **464**, 1294

Contrib. Astron. Obs. Skalnaté Pleso **48**, 250 – 258, (2018)

Highly magnetized super-Chandrasekhar white dwarfs and their consequences

B. Mukhopadhyay[1], U. Das[2] and A. R. Rao[3]

[1] *Indian Institute of Science, Bangalore, India, (E-mail: bm@iisc.ac.in)*
[2] *University of Colorado, Boulder, USA*
[3] *Tata Institute of Fundamental Research, Mumbai, India*

Received: November 17, 2017; Accepted: November 22, 2017

Abstract. Since 2012, we have been exploring possible existence of highly magnetized significantly super-Chandrasekhar white dwarfs with a new mass-limit. This explains several observations, e.g. peculiar over-luminous type Ia supernovae, some white dwarf pulsars, soft gamma-ray repeaters and anomalous X-ray pulsars, which otherwise puzzled us enormously. We have proceeded to uncover the underlying issues by exploiting the enormous potential in quantum, classical and relativistic effects lying with magnetic fields present in white dwarfs. We have also explored the issues related to the stability and gravitational radiation of these white dwarfs.

Key words: white dwarfs – supernovae: general – stars: magnetic fields – pulsars: general – gravitation – x-rays: general

1. Introduction

In the last five years or so, we have initiated modeling highly magnetized super-Chandrasekhar white dwarfs (B-WDs). We initiated our exploration by considering a simplistic spherically symmetric Newtonian model to study the quantum mechanical effects of a strong magnetic field on the composition of the white dwarf (Das & Mukhopadhyay, 2012). This in turn led to the discovery of a new mass-limit significantly larger than the Chandrasekhar limit (Das & Mukhopadhyay, 2013), thus heralding the onset of a paradigm shift. Note that although the possibility of super-Chandrasekhar white dwarfs has been mentioned in the literature (e.g. Ostriker & Hartwick, 1968), there was no prediction of a new (super-Chandrasekhar) mass-limit. Rather the existing idea was mostly to establish magnetized white dwarfs of larger size, which need not be the case. After our preliminary success with impressive results, we have progressed to a general relativistic framework, however, still within the assumption of spherical symmetry (Das & Mukhopadhyay, 2014a) and again showed the existence of magnetized super-Chandrasekhar white dwarfs. Finally, we have constructed a sophisticated general relativistic magnetohydrodynamic (GRMHD) model with self-consistent departure from spherical symmetry, due to the presence of strong magnetic field as well as rotation, which confirmed our previous results by yield-

ing highly super-Chandrasekhar B-WDs (Das & Mukhopadhyay, 2015; Subramanian & Mukhopadhyay, 2015). It has also been shown that B-WDs, depending on their field geometry, could be much smaller or bigger in size compared to the standard white dwarfs following Chandrasekhar's theory (C-WDs). More so, we have argued for a possible evolutionary scenario from C-WDs with weaker magnetic fields to B-WDs, by accretion (Das et al., 2013).

In this proceedings, we highlight the basic tenets of B-WDs – the observational motivations, main theoretical results and its multiple astrophysical implications. The various notations used here, if not defined, have their usual meaning and follow from our past work mentioned here.

2. Observational motivations

At least 10% of white dwarfs are known to be highly magnetized with surface fields $> 10^6$ G (Ferrario & Wickramasinghe, 2005) and, hence, they are likely to harbor much stronger interior fields. More interestingly, magnetized white dwarfs tend to be more massive (mean mass $0.784 \pm 0.4 M_\odot$) than their non-magnetized counterparts (mean mass $0.663 \pm 0.136 M_\odot$) (Ferrario et al., 2015). Thus, it is an important question in itself to study the effect of a stronger interior magnetic field on the structure and properties of white dwarfs. The theory of weakly magnetized white dwarfs was explored by a few authors (e.g. Ostriker & Hartwick, 1968; Suh & Mathews, 2000), however, we have initiated the investigation into strong magnetic fields in white dwarfs. The most compelling motivation behind the initiation of super-Chandrasekhar B-WDs, however, was the recent discovery of several peculiar, highly over-luminous type Ia supernovae (SNeIa), which invoke highly super-Chandrasekhar white dwarfs in the mass range $2.1 - 2.8 M_\odot$ as their most plausible progenitors (Scalzo et al., 2010).

3. Newtonian model of B-WDs and new mass-limit

An interior field $> B_c = 4.414 \times 10^{13}$ G introduces the quantum mechanical effect of Landau orbital, which stiffens the equation of state (EoS) of the underlying electron degenerate matter in the high density regime. In order to focus solely on this effect, we have assumed a simple Newtonian framework, a fluctuating (or constant) magnetic field and spherical symmetry. This led to significantly super-Chandrasekhar white dwarfs having mass $> 2 M_\odot$. The length scale over which the field is fluctuating is assumed to be large compared to the underlying electron Compton wavelength for quantum mechanical effects to work. However, this length scale is small enough to reveal an averaged magnetic field that does not produce any significant Lorentz force on the stellar matter. The magnetic field in this scenario affects only EoS, hence the emergence of super-Chandrasekhar B-WDs in this framework is due to the modified EoS alone.

Following Das & Mukhopadhyay (2013) the EoS of degenerate electron gas at high density (e.g. central region of the star) is approximately given by $P = K_m(B)\rho^{\Gamma} = K_m(B)\rho^{1+1/n}$, when $\Gamma = 2$. The spherical B-WD obeys the conditions for magnetostatic equilibrium and the estimate of mass, given by

$$\frac{1}{\rho+\rho_B}\frac{d}{dr}\left(P+\frac{B^2}{8\pi}\right) = F_g + \left.\frac{\boldsymbol{B}\cdot\nabla\boldsymbol{B}}{4\pi(\rho+\rho_B)}\right|_r, \quad \frac{dM}{dr} = 4\pi r^2(\rho+\rho_B). \tag{1}$$

As argued above, the magnetic terms could be neglected in the present framework and following Lane-Emden formalism (Das & Mukhopadhyay, 2013), the scalings of mass and radius with central density ρ_c are obtained as

$$M \propto K_m^{3/2}\rho_c^{(3-n)/2n}, \quad R \propto K_m^{1/2}\rho_c^{(1-n)/2n}, \quad K_m = K\rho_c^{-2/3}. \tag{2}$$

Clearly $n = 1$ ($\Gamma = 2$) corresponds to ρ_c-independent M (unlike Chandrasekhar's case when K_m is independent of B and the limiting mass corresponds to $n = 3$).

Substituting for the proportionality constants appropriately, we obtain the limiting mass

$$M_l = \left(\frac{hc}{2G}\right)^{3/2}\frac{1}{(\mu_e m_H)^2} \approx \frac{10.312}{\mu_e^2}\mathrm{M}_\odot, \tag{3}$$

when the limiting radius $R_l \to 0$. For $\mu_e = 2$, $M_l = 2.58\mathrm{M}_\odot$. This may establish the aforementioned peculiar, over-luminous SNeIa as new standard candles for cosmic distance measurement. Note that this result is in the spirit of original Chandrasekhar-limit, which also corresponds to zero radius at infinite density. Realistically, at a finite but high density and a finite magnetic field – e.g., $\rho_c = 2\times10^{10}$gm/cc and $B = 8.8\times10^{15}$G when $E_{Fmax} = 20m_ec^2$ – one obtains $M = 2.44\mathrm{M}_\odot$ and $R = 650$km, as opposed to $M = 1.39\mathrm{M}_\odot$ for the $B = 0$ case. Note that these ρ_c and B are below their respective upper limits set by the instabilities of pycnonuclear fusion, inverse-β decay and general relativistic effects (Das & Mukhopadhyay, 2014b).

4. General relativistic model of B-WDs with rotation

To self-consistently account for generalized cases when the magnetic fields need not be fluctuating, we have constructed equilibrium models of B-WDs in a general relativistic framework, both with and without rotation, using the well-tested codes *XNS* and *Lorene*. Even if we restrict the ratios of magnetic-to-gravitational and rotational-to-gravitational energies following Ostriker & Hartwick (1968); Braithwaite (2009) (in order to assure stable-equilibria), the mass range turns out to be $\sim 2-2.5\mathrm{M}_\odot$ depending upon the field geometry. The equilibrium sequences shown in Fig. 1 reveal the shape of B-WDs obtained by *XNS*. Larger the fields and/or rotation, larger is the mass. Note that we did a thorough investigation by invoking all possible rotation profiles in B-WDs, including uniform and differential. Here, we report only the differentially rotating cases. However,

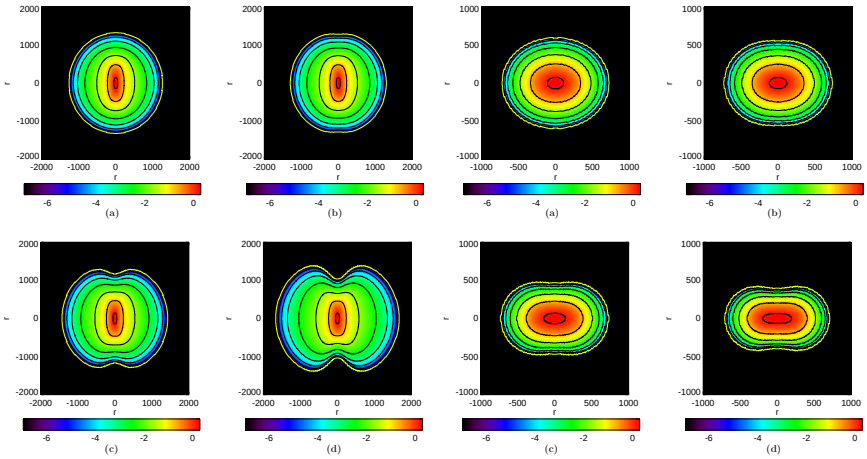

Figure 1. *Left panels*: Sequence of differentially rotating configurations with a purely toroidal magnetic field with maximum field $\approx 3.1 \times 10^{14}$ G fixed. The panels are density (ρ) contour plots of $\log\left(\frac{\rho}{\rho_0}\right)$, with $\rho_0 = 10^{10}$ gm/cc, corresponding to the values of central angular velocity in s^{-1} (a) 0.003, (b) 8.112, (c) 18.252, (d) 28.392. *Right panels*: The same, but for a purely poloidal magnetic field and values of central angular velocity in s^{-1} (a) 2.028, (b) 12.168, (c) 24.336, (d) 32.448. See, Subramanian & Mukhopadhyay (2015) for other details.

the magnetic braking effect might eventually cause the B-WDs to rotate uniformly. It is important to check the timescale over which differential rotation could be maintained in B-WDs, which needs further detailed exploration.

5. Astrophysical implications of B-WDs

B-WDs have many important astrophysical implications.

5.1. B-WDs as sources of SGRs/AXPs

B-WDs appear to be ideal candidates to explain SGRs/AXPs, as they resolve several discrepancies in the magnetar model (Duncan & Thompson, 1992) and also the weakly magnetized C-WD model (Paczynski, 1990). Some problems (Mereghetti, 2013) with the magnetar model are (1) no observational evidence has been found so far for strongly magnetized neutron stars, as required by the magnetar model to work, (2) Fermi observations are inconsistent with high energy gamma-ray emissions in magnetars, (3) inferred upper limit of surface field, e.g. for SGR 0418+5729, is quite smaller than the field required to explain the observed X-ray luminosity. Weakly magnetized C-WDs are challenged by the observed short spin periods and low UV-luminosities (L_{UV}). The advantage of

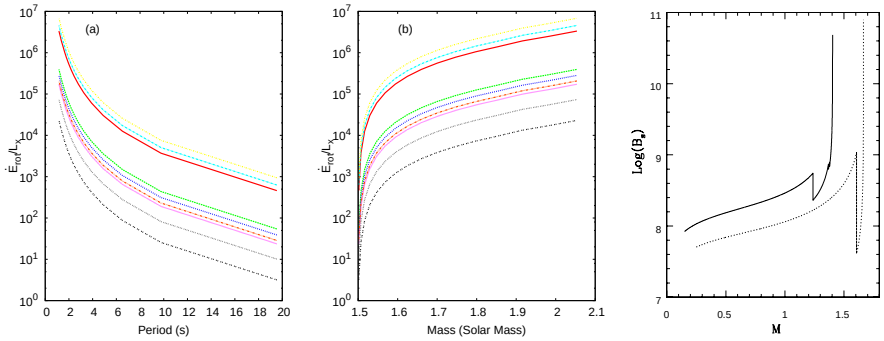

Figure 2. *Left*: The ratio of rate of rotational energy release to observed X-ray luminosity as a function of (a) spin period, (b) mass, for B-WDs when from the top to bottom various curves correspond to 1E 1547-54, 1E 1048-59, SGR 1806-20, SGR 1900+14, SGR 0526-66, SGR 1822-1606, 1E 1841-045, SGR 0418+5729 and 1E 2259+586. For details, see Mukhopadhyay & Rao (2016). *Right*: Time evolution of surface magnetic field in G as a function of mass in units of solar mass. Other parameters are accretion rate $\dot{M} = 10^{-8} \mathrm{M}_\odot\,\mathrm{yr}^{-1}$, the angle between rotational and magnetic axes $\alpha = 10^\circ$ and stellar radius $R = 10^4$ km at $t = 0$. See Mukhopadhyay et al. (2017) for details.

B-WDs chiefly lies in their intermediate size between neutron stars and weakly magnetized C-WDs, as well as a strong enough magnetic field. This magnetic field is, however, much weaker than that of neutron stars. Hence, B-WDs assure low L_{UV}.

We explore the possibility to explain the high energy phenomena in SGRs and AXPs by rotationally powered magnetic energy ($\dot{E}_{rot}$) of B-WDs – there is no need to invoke extraordinary, yet observationally unconfirmed, sources of energy. Figure 2 (left panels) shows that $\dot{E}_{\rm rot}$ computed based on B-WD model, with a fixed inclination angle between rotation and magnetic axes, is several orders of magnitude larger than the observed X-ray luminosity L_x for nine sources.

More sources are to be observed by the Indian satellite AstroSat's wide band spectroscopic capabilities, with cyclotron resonance energy $E = 11.6\ (B/10^{12}\,G)$ keV in the spectrum. This would confirm B-WDs' surface field strength. Also other features such as, a wide band spectral shape (like a tail or second peak), can be examined in the context of beamed emission from the pole of a B-WD having X-ray luminosity similar to SGRs/AXPs ($\sim 10^{36}$ erg s^{-1}).

5.2. B-WDs as descendents of white dwarf pulsar AR Scorpii

Recent observation of the first white dwarf radio pulsar AR Scorpii (AR Sco) justifies the existence of strongly magnetized white dwarfs in nature. Although

based on the current observational evidence AR Sco does not appear to have fields as strong as a B-WD could have, we have proposed in our latest work (Mukhopadhyay et al., 2017) a possible mechanism by which AR Sco can evolve to a B-WD eventually, due to binary interaction. This essentially involves repeated, alternating cycles of accretion-induced spin-up and increase in magnetic field due to flux freezing, followed by spin-down during radio emission when accretion is inhibited due to a strong magnetic field.

Figure 2 (right panel) reveals by a couple of possible evolutions of magnetic field with mass (which is varying with time) that initial smaller surface field B_s is seen to increase with accretion, but drops during the spin-powered phase (when accretion stops and hence there is no change in mass), followed by a phase with increasing trend again. Also, there is a sharp rise ($B_s \sim 10^{11}$ G) at the last cycle. This corresponds to the increase of central field B_c as well, leading to a B-WD. Of course, these are just representative samples and they may depend on many other factors. Hence, they may not match exactly with what is expected to happen in AR Sco itself.

5.3. B-WDs as sources of gravitational waves

Figure 1 shows that B-WDs are deformed due to the strong magnetic field as well as rotation, and they assume a triaxial shape. If their rotation axis is misaligned with the magnetic axis, then there is a time-varying quadrupole moment that leads to gravitational radiation with amplitude (Palomba et al., 2012)

$$h_+(t) = h_0 \left(\frac{1 + \cos^2 \alpha_0}{2} \right) \cos \Phi(t), \;\; h_\times(t) = h_0 \cos \alpha_0 \sin \Phi(t), \tag{4}$$

where α_0 is the inclination of the star's rotation axis with respect to the line of sight and

$$h_0 = \frac{4\pi^2 G}{c^4} \frac{I_{zz} \epsilon}{P_s^2 d}, \tag{5}$$

$\Phi(t)$ is the signal phase function, I_{zz} is the moment of inertial about z-axis, ϵ is the measure of ellipticity of the star and d is the distance of the star from the detector. In our latest work (Mukhopadhyay et al., 2017), we have justified B-WDs as potential sources for gravitational wave to be detected. A B-WD with mass $\sim 2\mathrm{M}_\odot$, polar radius ~ 700 km, rotational period $P_s \sim 1$ s (Subramanian & Mukhopadhyay, 2015), $\epsilon \sim 5 \times 10^{-4}$ and at ~ 100 pc away from us would produce $h_0 \sim 10^{-22}$, which is within the sensitivity of the Einstein@Home search for early LIGO S5 data (Palomba et al., 2012). If the B-WD's polar radius is ~ 2000 km, $P_s \sim 10$ s and other parameters intact as above, a firm confirmation of gravitational wave emission can be provided by DECIGO/BBO (Yagi & Seto, 2011) with $h_0 \sim 10^{-23}$. Nevertheless, high magnetic field rotating white dwarfs approaching a B-WD would be common and it is possible that such white dwarfs of radius ~ 7000 km, $P_s \sim 20$ s and $d \sim 10$ pc will have a $h_0 \geq 10^{-22}$, which is detectable by LISA.

6. Discussion and conclusion

A lot of groups have adopted and pursued our model of B-WDs: exploring polytropes for anisotropic matter (Herrera et al., 2014), explaining SGRs/AXPs (Belyaev et al., 2015), constructing magnetic compressible fluid stars (Federbush et al., 2015), to construct ungravity-inspired model (Bertolami & Mariji, 2016), possible exploration of third family of compact stars (Sotani & Tatsumi, 2017), for emission of gravitational wave (Franzon & Schramm, 2017), establishing central magnetic field of a magnetic white dwarf (Shah & Sebastian, 2017), to mention a few.

However, there have also been concerns regarding instability to neutronization and pycnonuclear reactions, general relativistic instability and MHD instabilities (Chatterjee et al., 2017; Bera & Bhattacharya, 2017). We have, however, argued/established that these are non-issues. First, our simplistic models (Das & Mukhopadhyay, 2012, 2013) were constructed in the spirit of Chandrasekhar's calculations, whose actual mass-limit also corresponds to infinite density and zero radius – an ideal case. Moreover, these models assumed a fluctuating (or constant) magnetic field, as mentioned above, such that the net averaged field does not contribute significantly to the Lorentz force, but affects the white dwarf properties on a quantum mechanical scale. In this scenario the above concerns do not hold. Next, all these concerns are automatically resolved in our fully self-consistent GRMHD model (with and without rotation), which invokes magnetic field strengths that satisfy all constraints from general relativity and neutronization. It is additionally important to note that the rates for pycnonuclear reactions are extremely uncertain, and if the chosen rates (Chatterjee et al., 2017) were to be accurate, then that poses a concern for even the weakly magnetized white dwarfs. As far as the underlying magnetic field configurations and related stability are concerned, purely toroidal and purely poloidal field configurations have been long known to be subjected to MHD instabilities (Tayler, 1973), as we pointed in our work (Das & Mukhopadhyay, 2015; Mukhopadhyay et al., 2017). So arguments based on solely these configurations (Bera & Bhattacharya, 2017) are too premature and may be misleading. One needs to construct mixed field configurations which are more likely to occur in nature (Ciolfi & Rezzolla, 2013), for further stability analysis.

B-WDs have enormous astrophysical significance – they can be ideal progenitors for the recently discovered peculiar, highly over-luminous, SNeIa; they can explain the origin of SGRs and AXPs; they are potential sources of gravitational waves for future detectors; their new mass-limit altogether offers a new standard candle – to list a few. Hence, more explorations are needed, both theoretical and observational, for thoroughly understanding the physics behind B-WDs, in order to fully utilize them for explaining a wide range of astrophysical phenomena.

References

Belyaev, V. B., Ricci, P., Šimkovic, F., et al. 2015, *Nucl. Phys. A*, **937**, 17

Bera, P. & Bhattacharya, D. 2017, *Mon. Not. R. Astron. Soc.*, **465**, 4026

Bertolami, O. & Mariji, H. 2016, *Phys. Rev. D*, **93**, 104046

Braithwaite, J. 2009, *Mon. Not. R. Astron. Soc.*, **397**, 763

Chatterjee, D., Fantina, A. F., Chamel, N., Novak, J., & Oertel, M. 2017, *Mon. Not. R. Astron. Soc.*, **469**, 95

Ciolfi, R. & Rezzolla, L. 2013, *Mon. Not. R. Astron. Soc.*, **435**, L43

Das, U. & Mukhopadhyay, B. 2012, *Phys. Rev. D*, **86**, 042001

Das, U. & Mukhopadhyay, B. 2013, *Phys. Rev. Lett.*, **110**, 071102

Das, U. & Mukhopadhyay, B. 2014a, *J. Cosmol. Astropart. Phys.*, **6**, 050

Das, U. & Mukhopadhyay, B. 2014b, *Mod. Phys. Lett. A*, **29**, 1450035

Das, U. & Mukhopadhyay, B. 2015, *J. Cosmol. Astropart. Phys.*, **5**, 016

Das, U., Mukhopadhyay, B., & Rao, A. R. 2013, *Astrophys. J., Lett.*, **767**, L14

Duncan, R. C. & Thompson, C. 1992, *Astrophys. J., Lett.*, **392**, L9

Federbush, P., Luo, T., & Smoller, J. 2015, *Arch. Ration. Mech. Anal.*, **215**, 611

Ferrario, L., de Martino, D., & Gänsicke, B. T. 2015, *Space Sci. Rev.*, **191**, 111

Ferrario, L. & Wickramasinghe, D. T. 2005, *Mon. Not. R. Astron. Soc.*, **356**, 615

Franzon, B. & Schramm, S. 2017, *Mon. Not. R. Astron. Soc.*, **467**, 4484

Herrera, L., Di Prisco, A., Barreto, W., & Ospino, J. 2014, *Gen. Rel. Gravit.*, **46**, 1827

Mereghetti, S. 2013, *Braz. J. Phys.*, **43**, 356

Mukhopadhyay, B. & Rao, A. R. 2016, *J. Cosmol. Astropart. Phys.*, **5**, 007

Mukhopadhyay, B., Rao, A. R., & Bhatia, T. S. 2017, *Mon. Not. R. Astron. Soc.*, **472**, 3564

Ostriker, J. P. & Hartwick, F. D. A. 1968, *Astrophys. J.*, **153**, 797

Paczynski, B. 1990, *Astrophys. J., Lett.*, **365**, L9

Palomba, C., for the LIGO Scientific Collaboration, & for the Virgo Collaboration. 2012, *ArXiv e-prints* [arXiv:1201.3176]

Scalzo, R. A., Aldering, G., Antilogus, P., et al. 2010, *Astrophys. J.*, **713**, 1073

Shah, H. & Sebastian, K. 2017, *Astrophys. J.*, **843**, 131

Sotani, H. & Tatsumi, T. 2017, *Mon. Not. R. Astron. Soc.*, **467**, 1249

Subramanian, S. & Mukhopadhyay, B. 2015, *Mon. Not. R. Astron. Soc.*, **454**, 752

Suh, I.-S. & Mathews, G. J. 2000, *Astrophys. J.*, **530**, 949

Tayler, R. J. 1973, *Mon. Not. R. Astron. Soc.*, **161**, 365

Yagi, K. & Seto, N. 2011, *Phys. Rev. D*, **83**, 044011

Alfio Bonanno and Banibrata Mukhopadhyay

Jan Janík and Eugene Semenko

Contrib. Astron. Obs. Skalnaté Pleso **48**, 259 – 261, (2018)

Have we seen all glitches?

M. Yu

National Astronomical Observatories of China, Beijing 100012, China
(E-mail: vela.yumeng@gmail.com)

Received: October 31, 2017; Accepted: November 7, 2017

Abstract. Neutron star glitches are observed via artificially scheduled pulsar pulse arrival-time observations. The detection probability density of glitch events for a given data set is an essentially required knowledge for realizing glitch detectability with a specified observing system and schedule. In Yu & Liu (2017), the detection probability density was derived for the Yu et al. (2013) data set. In this proceeding, further discussions are presented.

Key words: pulsars: general – stars: neutron

Hundreds of pulsars have been observed at the Parkes Observatory over decades by a number of timing programmes. A search for pulse frequency glitches in a data set that contains 1911 yr of observations in total for 165 pulsars was done by Yu et al. (2013). The result is that 107 glitches were identified in 36 pulsars. For the Yu et al. (2013) data set, glitch identification depends on the observing cadences and the observed timing noise. Yu & Liu (2017) thus defined the complete probability formula of identifying glitch events (see Eq. 1 therein). They found that the derived detection probability densities for both the group and individual cases are not uniform; as the glitch becomes larger the density increases (see Figs. 5, 7 and 8 therein). The high-cadence observations of the Crab pulsar showed that the $\Delta\nu$ values of glitches are significantly larger than those of the timing noise (Espinoza et al., 2014). This implies that the cadences with which the Yu et al. (2013) pulsars were observed were not adequate to observe all occurred glitches.

In Fig. 1, the average pulse time-of-arrival (ToA) interval for each of the 165 pulsars is plotted on the $P-\dot{P}$ diagram. For the non-glitching pulsars, the averages range between 10.4 d for PSR J1359−6038 and 798.7 d for PSR J1047−6709; most averages are a few tens of days. For the glitching pulsars, the averages range between 8.3 d for the Vela pulsar and 240.6 d for PSR J1740−3015. For PSR J1740−3015, the low observing cadences result in the unidentification of thirteen glitches in the Yu et al. (2013) data. PSR J1341−6220 which shows seventeen glitches was on average observed every 23.5 d. Figure 2 shows the ToA interval modulation index of the average over the intervals' standard deviation for each pulsar. For the non-glitching pulsars, the indices range between 0.08 for PSR J1456−6843 and 1.20 for PSR J1721−3532. For the glitching pulsars, the indices range between 0.06 for PSR J1105−6107 and 1.12 for PSR J1531−5610, while PSR J1341−6220 has 0.73. In Fig. 3, the amplitude of the power spectral

density of the observed timing noise is shown. PSR J1341−6220 has the maximum amplitude in the sample. In general, young pulsars show large timing noise while timing noise does not seem to correlate with the magnetic field.

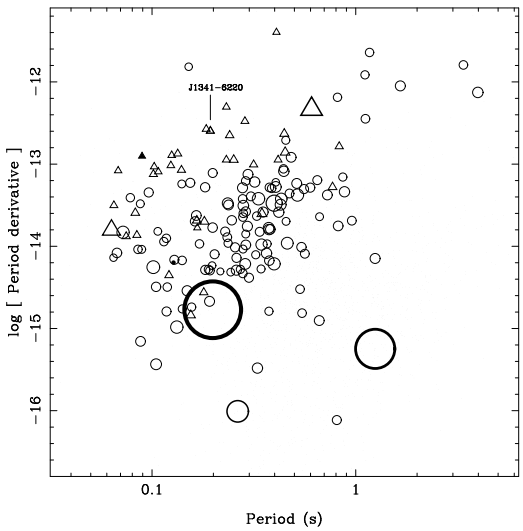

Figure 1. Average ToA intervals on the $P-\dot{P}$ diagram. Circles indicate the non-glitching pulsars, triangles indicate the glitching pulsars. Minima are shown by solid symbols. The symbol size is a linear function of the value with positive slope.

Acknowledgements. The work Yu & Liu (2017) is supported by the National Natural Science Foundation of China (No. 11403060), the Joint Research Fund in Astronomy (U1531246) under cooperative agreement between the National Natural Science Foundation and Chinese Academy of Sciences, the Strategic Priority Research Program 'The Emergence of Cosmological Structures' of the Chinese Academy of Sciences (No. XDB09000000), the International Partnership Program of the Chinese Academy of Sciences (No. 114A11KYSB20160008) and the Strategic Priority Research Program of the Chinese Academy of Sciences (No. XDB23000000).

References

Espinoza, C. M., Antonopoulou, D., Stappers, B. W., Watts, A., & Lyne, A. G. 2014, *Mon. Not. R. Astron. Soc.*, **440**, 2755

Yu, M. & Liu, Q.-J. 2017, *Mon. Not. R. Astron. Soc.*, **468**, 3031

Yu, M., Manchester, R. N., Hobbs, G., et al. 2013, *Mon. Not. R. Astron. Soc.*, **429**, 688

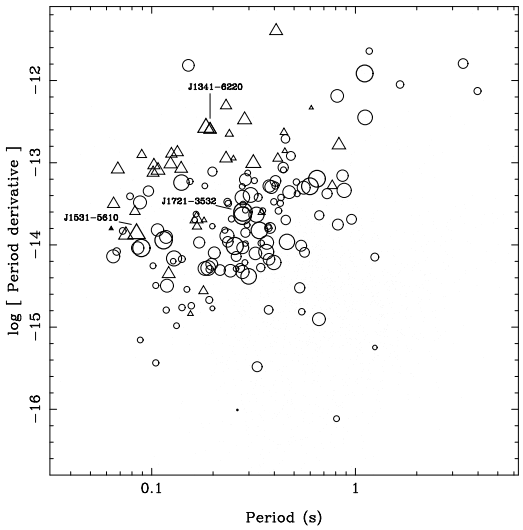

Figure 2. ToA interval modulation index on the $P - \dot{P}$ diagram. Circles indicate the non-glitching pulsars, triangles indicate the glitching pulsars. Minima are shown by solid symbols. The symbol size is a linear function of the value with positive slope.

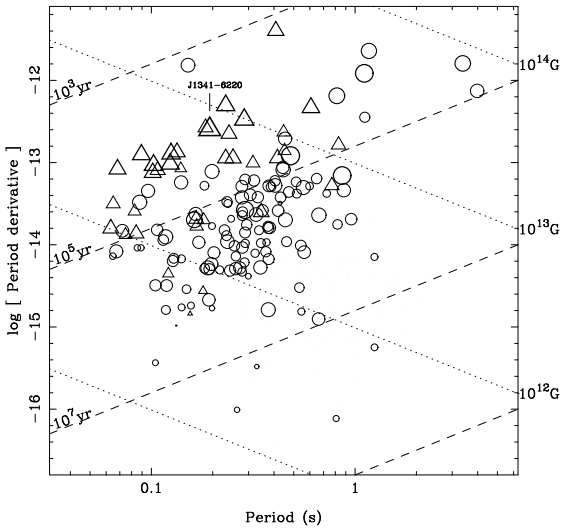

Figure 3. Amplitude of power spectral density of the observed timing noise on the $P - \dot{P}$ diagram. Circles indicate the non-glitching pulsars, triangles indicate the glitching pulsars. The symbol size is a linear function of the value with positive slope.

Contrib. Astron. Obs. Skalnaté Pleso **48**, 262 – 270, (2018)

Impact of space-based instruments on magnetic star research: past and future

W W. Weiss[1], C. Neiner[2] and G. A. Wade[3]

[1] *Institute for Astrophysics, University of Vienna, Tuerkenschanzstrasse 17, 1180 Vienna, Austria (E-mail: Werner.Weiss@univie.ac.at)*

[2] *LESIA, bat. 14, Observatoire de Paris, 5, place Jules Janssen, 92195 Meudon Cedex, France (E-mail: Coralie.Neiner@obspm.fr)*

[3] *Dept. of Physics and Space Science, RMC, Kingston, ON, K7K 7B4, Canada (E-mail: Gregg.Wade@rmc.ca)*

Received: December 8, 2017; Accepted: December 12, 2017

Abstract. Magnetic stars are observed at a large variety of spectral ranges, frequently with photometric and spectroscopic techniques and on time scales ranging from a 'snap shot' to years, sometimes using data sets which are continuous over many months. The outcome of such observations has been discussed during this conference and many examples have been presented, demonstrating the high scientific significance and gains in our knowledge that result from these observations. A key question that should be addressed is, what are the advantages and requirements of space based research of magnetic stars, particularly in relation to ground based observations? And what are the drawbacks? What are the hopes for the future? In the following, we intend to present an overview that addresses these questions.

Key words: stars: magnetic field – space vehicles: instruments

1. Observations from space

The principal advantages of space-based observations are (i) quasi-continuous monitoring, avoiding the strict diurnal cycle imposed by the sun, and (ii) access to wavelength ranges invisible from Earth's surface.

Space-based observations in the visual spectral domain have delivered information about stellar surface properties and internal stellar structure by observing flux and spectral line variations in a wide range of frequencies. Non-periodic phenomena, like flares, have been particularly helpful to understand the interaction of stars and their environment with a magnetic field. In the UV range, effects of a stellar wind confined by (oblique) magnetic fields have been prominently investigated. Extending the energy range of observations to the X-ray regime has provided access to understanding large-scale shocks in magnetospheres. Figure 1 illustrates the utility of such multispectral observations for investigating the magnetospheric physics of hot stars.

Of course, there are also drawbacks associated with space-based observations. Instruments for observations in space are typically more expensive and

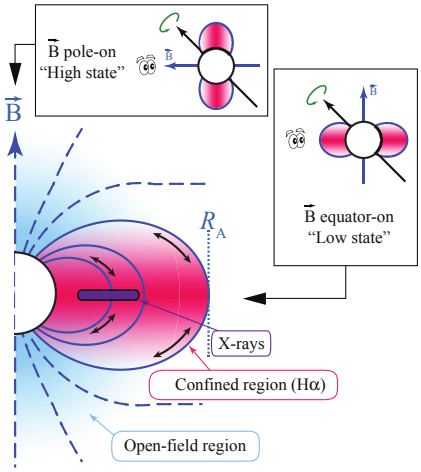

Figure 1. Schematic of the dynamical magnetosphere of a magnetic O-type star. Solid blue lines indicate regions below the last closed magnetic loop that confine the wind, located near the Alfvén radius R_A. The bulk of the X-rays are produced in the region indicated in purple. The insets illustrate the view of an observer as the star's rotation changes the orientation of the magnetosphere, which allows disentangling of the effects due to the star and its environment. Source: (Petit et al., 2015)

less advanced than that available for ground based observations. Space missions are also inherent more risky, and usually limited in lifetime. However, the most long-lived space telescope is probably the Hubble Space Telescope (**HST**), which still produces amazing science after the first successful servicing mission in December 1993 - 25 years ago!

2. Current and past satellite projects

Quite a number of space instruments have contributed significantly to the topic of this conference. We present here only a subset of the most productive projects, which is necessarily incomplete and biased.

2.1. X-ray

ESA's **XMM-Newton** (launched in 1999) is working with a 0.7 m telescope and operates in the 0.15 to 15 keV range. In the same year, NASA launched the **Chandra** telescope, with a 1.2 m telescope and operating in the 0.1 to 10 keV range. Each of these facilities boasts imaging and spectroscopic capabilities. In particular, the Chandra high resolution grating spectrometer provides the capability to resolve X-ray emission line shapes, and to infer detailed velocity fields and regions of spectrum formation. We address in the following four, of many more highlights:

– Magnetically confined winds are X-ray sources and a large series of Chandra and XMM-Newton observations of massive magnetic stars have been analysed, with the evidence that X-ray luminosity is strongly correlated with the stellar wind mass-loss-rate (Nazé et al., 2014), what is confirmed by additional XMM observations (see Fletcher et al., 2017, and these proceedings, and Fig. 2).

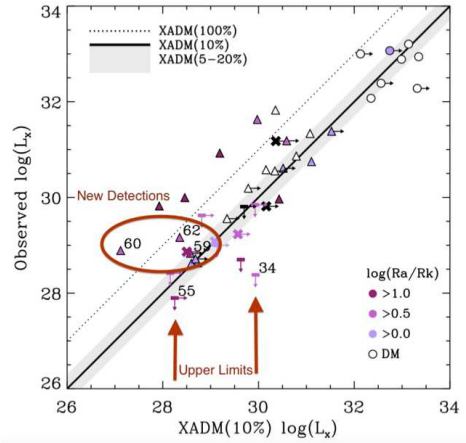

Figure 2. The predicted versus observed X-ray luminosity (Nazé et al., 2014), updated with new X-ray observations. The B-type stars in triangles, the O-type stars in circles and the undetected sources in rectangles (indicating upper limits). The color scheme corresponds to the size of the centrifugal magnetosphere (CM) with the darker the color having a larger CM and the white only having a dynamical magnetosphere (DM). Source: Fletcher et al. (2017)

– X-ray studies of cataclysmic variable and symbiotic stars teach a lot about the physics of accretion, disks and the interaction between accretion flow and magnetic field. They are important for the study of the Galaxy we live in, including its collective X-ray emission, and they provide valuable insight into the evolution of close binaries (Mukai, 2017).

– An impressive systematic study of all magnetar-like outbursts for which extensive X-ray monitoring campaigns are available is published by Coti Zelati et al. (2018). Magnetars are strongly magnetised (up to $B \approx 10^{15}$ G) isolated X-ray pulsars with luminosities $L_X \approx 10^{31} - 10^{36}\,\mathrm{erg\,s^{-1}}$. The authors investigate the correlation between different parameters (e.g., the luminosity at the peak of the outburst and in quiescence, the maximum luminosity increase, the decay timescale and energy of the outburst, the neutron star surface dipolar magnetic field and characteristic age).

– Isolated neutron stars (INS) come in an unexpected variety. The observed spectral and timing properties indicate that different energy sources, besides the obvious cooling of the primeval internal heat, are at play in powering such thermal-like components. The effects of a strong and dynamic magnetic field are especially evident in the paroxysmic behaviour of soft gamma-ray repeaters (SGRs) and anomalous X-ray pulsars (AXPs). There is evidence for a closer connection between radio pulsars and magnetars than previously thought (see the review by Mereghetti, 2011).

2.2. UV

The most prominent UV satellite was probably the International Ultraviolet Explorer (**IUE**), which was observing between 1978 and 1996 with a 0.45 m telescope in the 115 to 325 nm spectral range. The **HST** produced science also in the optical and IR regions, but was ground braking in UV, when launched in 1990 with a 2.5 m telescope and *STIS* working in the 114 to 318 nm range and

COS in the 90 to 320 nm range. Contrary to IUE, which delivered high cadence, long timebase data, HST primarily produces snapshots. Also for UV we present some highlights:

– The appearance and evolution of discrete absorption components (DACs) is interpreted by Kaper et al. (1999) for O-type stars in terms of a model invoking fast and slow streams which interact due to the rotation of the underlying star. The interacting regions (CIRs) corotate with the star while the wind material is flowing through them. The observations suggest that the stellar wind includes more than one CIR, most likely two (cf. Kaper et al., 1997). The wind variability periods they derive are a direct measure of the DAC recurrence timescales and, in their interpretation, is equal to an integer fraction (most likely 1/2) of the stellar rotation period. The authors discuss the origin of the CIRs: are non-radial pulsations, surface magnetic fields, or other physical mechanisms responsible for the surface structure creating fast and slow wind streams?

– β Cep is the first upper main-sequence pulsating star with confirmed detection of a weak dipolar magnetic field (less than about $B_{long} = 100$ G). The data seem to be consistent with an oblique dipolar magnetic rotator model and the maximum wind absorption, derived from IUE spectra, originates in the magnetic equatorial plane (Henrichs et al., 2013).

– V 2052 Oph (B2IV-V) is the second discovered magnetic pulsating B star. UV delivered a very precise value of the rotation period. The star has no extra internal mixing due to the presence of the magnetic field which inhibits mixing (Briquet et al., 2012). A magnetic analysis of this star is presented by Neiner et al. (2012).

– ω Ori (B3Ve) is the first classical Be star showing indirect magnetic indicators (Neiner et al., 2003).

2.3. Optical

The majority of space instruments contributing to understanding magnetic fields associated to stars are working in the visual spectral range and we address some of the highlights in the following:

MOST

This is a Canadian Space Agency funded mission, launched in 2003 and still working. It was jointly operated by Dynacon Inc., the University of Toronto Institute for Aerospace Studies and the University of British Columbia, with the assistance of the University of Vienna, and now by Microsat Systems Canada Inc (MSCI). Please consult https://science.ubc.ca/feature/MOST for more details. Some MOST research highlights in the field are:

– ξ Per (B1Ib): This is the first convincing case '...with possible bright-spot generation via a breakout at the surface of a global magnetic field generated by a subsurface convection zone...' (Ramiaramanantsoa et al., 2014).

– HR 5907 (B2V): detection of a large-scale polar surface magnetic field of 10 to 16 kG. Longitudinal magnetic field and Hα variations are consistent with an oblique rotator, indicating a non-degenerate and magnetic massive star (5.5 $M_\odot$) with the shortest period (0.51 d) yet known (Grunhut et al., 2012).

– WR 110 has revealed during a month of observations properties of a co-rotating interaction region (CIR), which allows probing the mysterious origin of the CIR phenomenon rooted at the stellar surface, e.g. as a phenomenon related to magnetism or pulsations (Chené et al., 2011).

– 10 Aql (A7VpSrEu) provided first evidence for finite mode lifetimes in roAp stars (Huber et al., 2008).

– κ^1 Cet (G5V): all of the photometric periods found to date can be explained by spots at different latitudes. The apparent persistence of this period for some 35 years, corresponding to spot latitude-ranges of 50° to 60°, might be due to large-scale magnetic structures with solar-like differential rotation (see Fig. 3).

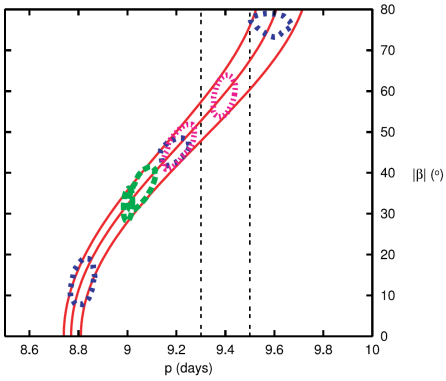

Figure 3. κ^1 Ceti: Likelihood contours for the latitude and spot period are shown by dots for each spot – 2003 (green), 2004 (blue) and 2005 (pink). The central red curve is the solar-period, latitude relation, indicating a differential rotation being closely solar. Source: (Walker et al., 2007)

CoRoT

It is based on a concept which was proposed already in 1993 by C. Catala, M. Auvergne and A. Baglin in answer to a call for ideas for "small missions". CoRoT was developed under the lead of CNES with a wide European cooperation, was launched in 2006 and operated till 2012. For more details please consult https://corot.cnes.fr/en/COROT/index.htm. Some highlights are:

– HD 43317 (B3IV): photometric data of unprecedented precision, complemented by ground-based spectroscopy and polarimetry, allow to study the effect of magnetism in the mixing processes inside a star (Briquet et al., 2013).

– Close-in massive planets interact with their host stars through tidal and magnetic mechanisms, possibly related with hot Jupiters. The unique advantages of CoRoT and Kepler observations to test these models are pointed out by Lanza (2011).

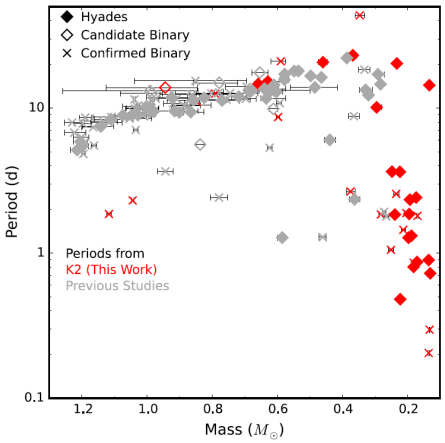

Figure 4. Mass-period distribution for all Hyades with measured periods. Source: Douglas et al. (2016)

– HD 49933 (F3V): observed variations in mode frequencies are related to its magnetic activity. HD 49933 is thus the second star after the Sun for which the frequency dependence of the p-mode frequency shifts with magnetic activity has been measured (Salabert et al., 2011).

Kepler

Kepler was launched in 2009, fully operational till 2013, then in a modified operation active in K2-mode. Few highlights:

– Beyond stellar middle-age the efficiency of magnetic braking is dramatically reduced, implying a fundamental change in angular momentum loss beyond a critical Rossby number (Metcalfe et al., 2016).

– K2 is the first opportunity to measure rotation periods for many Hyades simultaneously (Fig. 4), being also sensitive to fully convective M dwarf members. The deficit of single rapid rotators more massive than $\approx 0.3\,M_\odot$ indicates that magnetic braking is more efficient than previously thought, and that age-rotation studies must account for multiplicity (Douglas et al., 2016).

– The asteroseismology of Red Giant stars has continued to yield surprises. The observed suppression of dipole oscillation modes in Red Giants can be used to detect indirect evidence of the presence of strong magnetic fields in the stellar cores (Stello et al., 2016).

– HD 188774 (A7.5 IV-III) is the first known magnetic main-sequence δ Sct star. This challenges analysis and interpretation of the Kepler results for the class of A-type stars (Neiner & Lampens, 2015).

BRITE-Constellation

BRITE-Constellation was built, launched and is operated thanks to support from the Austrian Research Promotion Agency (FFG) and the University of

Vienna, the Canadian Space Agency (CSA), the Foundation for Polish Science & Technology (FNiTP MNiSW), and the National Science Centre (NCN). Please consult http://www.brite-constellation.at for more details. The BRITE observations are completed by a ground-based spectropolarimetric survey (see Neiner et al., 2016). Recent science highlights are:

– ρ Pup (F5IIkF2IImF5II) is the second confirmed magnetic δ Scuti star (Neiner et al., 2017)

– γ Gem (A1.5 IV): the BRITE spectropolarimetric survey provided first detection of a standard Zeeman pattern in an Am star, with $B_{pol} \approx 30$ G, while all other magnetic Am stars show peculiar Zeeman profiles with a single lobe and ultra-weak field strengths (Blazère et al., 2016).

– i Car (B3V) & 27 Tau (B8 III): combining magnetic and seismic information is the only way to probe the impact of magnetism on the physics of non-standard mixing processes inside hot stars (Neiner et al., 2015).

3. Projects in the future

Several space missions are in preparation for the coming decades that will contribute to drastically extend our knowledge of stellar magnetism. In particular high-resolution UV spectropolarimetry is being developed for the **Arago** project and the **Pollux** instrument on LUVOIR. These missions would open a brand new window on magnetic stars and their environment. On the X-ray side, the **Athena** mission will have capacities well beyond XMM-Newton and Chandra and allow us in particular to study magnetospheres.

Arago

Arago is a space project candidate for a M-size mission at ESA led by France (PI: C. Neiner). Arago is a 1.3-m telescope that would perform high-resolution full-Stokes (IQUV) spectropolarimetry simultaneously in the UV and Visible wavelength ranges from 119 to 888 nm. The targets would be observed during a full stellar rotation period to obtain comprehensive 3D maps all the way from their sub-photosphere to the frontiers of their immediate circumstellar environment (Fig. 5). In addition, high-fidelity multi-parameter information on statistical stellar and planetary samples would be obtained thanks to snapshot observations of a large number of targets.

The final goal of Arago is to follow the life cycle of matter, and, therefore, the entire life cycle of stars and planets from their formation from interstellar gas and grains to their death and feedback into the interstellar medium (ISM). Arago's high-resolution spectropolarimeter would be the only facility able to simultaneously deliver all pertinent diagnostics throughout the UV and Visible domains.

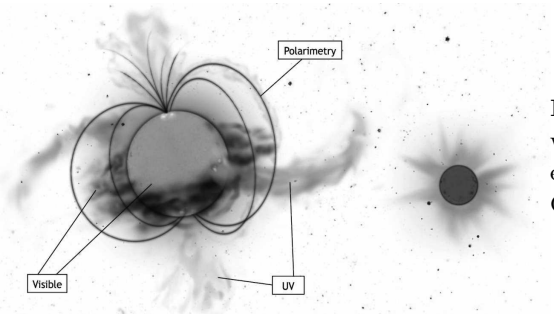

Figure 5. Core issues for Arago will be the links of circumstellar events to stellar surface structures. Copyright: S. Cnudde

Pollux on the LUVOIR

LUVOIR is one of four Decadal Survey Mission Concept Studies initiated by NASA in January 2016. It is a concept for a highly capable, multi-wavelength 15-m observatory with ambitious science goals, led by NASA. This mission would enable a great leap forward in a broad range of astrophysics, from the epoch of re-ionization, through galaxy formation and evolution, to star and planet formation. LUVOIR also has the major goal of characterizing a wide range of exoplanets, including those that might be habitable - or even inhabited.

LUVOIR will be equipped with 4 instruments: a coronagraph, a multi-resolution visible and IR spectrograph, a multi-object low and medium resolution UV spectrograph and imager, and a high-resolution UV spectropolarimeter called Pollux.

Pollux is a European instrument led by France (co-PIs: C. Neiner and J.-C. Bouret). It is a full-Stokes (IQUV) spectropolarimeter working at very high-resolution (120000) in 3 bands from the FUV (92 nm) to the near-UV (390 nm).

Athena

Athena is an ESA L-size mission planned to be launched in 2028 (PI: P. Nandra). The main goals of Athena are to map the hot gas structures in the Universe, determine their physical properties, track their evolution, find and study massive black holes. However, Athena will also be an ideal tool to study magnetospheres around stars.

Athena includes two instruments: X-IFU which provides high spectral resolution imaging in the 0.2–12 keV domain, and WFI which permits high count rate, mid-resolution spectroscopy over a large field-of-view in the 0.2–15 keV domain.

References

Blazère, A., Neiner, C., & Petit, P. 2016, *Mon. Not. R. Astron. Soc.*, **459**, L81

Briquet, M., Neiner, C., Aerts, C., et al. 2012, *Mon. Not. R. Astron. Soc.*, **427**, 483

Briquet, M., Neiner, C., Leroy, B., Pápics, P. I., & MiMeS Collaboration. 2013, *Astron. Astrophys.*, **557**, L16

Chené, A.-N., Moffat, A. F. J., Cameron, C., et al. 2011, *Astrophys. J.*, **735**, 34

Coti Zelati, F., Rea, N., Pons, J. A., Campana, S., & Esposito, P. 2018, *Mon. Not. R. Astron. Soc.*, **474**, 961

Douglas, S. T., Agüeros, M. A., Covey, K. R., et al. 2016, *Astrophys. J.*, **822**, 47

Fletcher, C. L., Petit, V., Nazé, Y., et al. 2017, in IAU Symposium, Vol. **329**, *The Lives and Death-Throes of Massive Stars*, ed. J. J. Eldridge, J. C. Bray, L. A. S. McClelland, & L. Xiao, 369–372

Grunhut, J. H., Rivinius, T., Wade, G. A., et al. 2012, *Mon. Not. R. Astron. Soc.*, **419**, 1610

Henrichs, H. F., de Jong, J. A., Verdugo, E., et al. 2013, *Astron. Astrophys.*, **555**, A46

Huber, D., Saio, H., Gruberbauer, M., et al. 2008, *Astron. Astrophys.*, **483**, 239

Kaper, L., Henrichs, H. F., Fullerton, A. W., et al. 1997, *Astron. Astrophys.*, **327**, 281

Kaper, L., Henrichs, H. F., Nichols, J. S., & Telting, J. H. 1999, *Astron. Astrophys.*, **344**, 231

Lanza, A. F. 2011, *Astrophys. Space Sci.*, **336**, 303

Mereghetti, S. 2011, *Astrophys. Space Sci. Proc.*, **21**, 345

Metcalfe, T. S., Egeland, R., & van Saders, J. 2016, *Astrophys. J., Lett.*, **826**, L2

Mukai, K. 2017, *Publ. Astron. Soc. Pac.*, **129**, 062001

Nazé, Y., Petit, V., Rinbrand, M., et al. 2014, *Astrophys. J., Suppl.*, **215**, 10

Neiner, C., Alecian, E., Briquet, M., et al. 2012, *Astron. Astrophys.*, **537**, A148

Neiner, C., Buysschaert, B., Oksala, M. E., & Blazère, A. 2015, *Mon. Not. R. Astron. Soc.*, **454**, L56

Neiner, C., Hubert, A.-M., Frémat, Y., et al. 2003, *Astron. Astrophys.*, **409**, 275

Neiner, C. & Lampens, P. 2015, *Mon. Not. R. Astron. Soc.*, **454**, L86

Neiner, C., Wade, G., Marsden, S., & Blazère, A., 2016, *ArXiv e-prints* [arXiv:1611.03285]

Neiner, C., Wade, G. A., & Sikora, J. 2017, *Mon. Not. R. Astron. Soc.*, **468**, L46

Petit, V., Cohen, D. H., Wade, G. A., et al. 2015, *Mon. Not. R. Astron. Soc.*, **453**, 3288

Ramiaramanantsoa, T., Moffat, A. F. J., Chené, A.-N., et al. 2014, *Mon. Not. R. Astron. Soc.*, **441**, 910

Salabert, D., Régulo, C., Ballot, J., García, R. A., & Mathur, S. 2011, *Astron. Astrophys.*, **530**, A127

Stello, D., Cantiello, M., Fuller, J., Garcia, R. A., & Huber, D. 2016, *Publ. Astron. Soc. Aust.*, **33**, 11

Walker, G. A. H., Croll, B., Kuschnig, R., et al. 2007, *Astrophys. J.*, **659**, 1611

Contrib. Astron. Obs. Skalnaté Pleso **48**, 271 – 272, (2018)

Magnetic Fields in Interacting Binaries

G. Briggs[1], L. Ferrario[1], C. A. Tout[2] and D. T. Wickramasinghe[1]

[1] *Mathematical Sciences Institute, The Australian National University, Australia, (E-mail: Gordon.Briggs@anu.edu.au)*

[2] *Institute of Astronomy, University of Cambridge, U.K.*

Received: November 12, 2017; Accepted: November 16, 2017

Abstract. Wickramasinghe et al. (2014) and Briggs et al. (2015) have proposed that the strong magnetic fields observed in some single white dwarfs (MWDs) are formed by an α–Ω dynamo driven by differential rotation when two stars, the more massive one with a degenerate core, merge during common envelope (CE) evolution (Ferrario et al., 2015b). We synthesise a population of binaries to investigate if fields in the magnetic cataclysmic variables (MCVs) may also originate during stellar interaction in the CE phase.

Key words: magnetic field – white dwarfs – binaries: general – novae, cataclysmic variables

1. Methods and Discussion

In the MCVs, a red dwarf transfers matter to a MWD via magnetically confined accretion flows. Cyclotron and Zeeman spectroscopy have revealed fields of a few 10^7–10^8 G (Ferrario et al., 1992, 1993a, 1996) in the high field MCVs (the polars; Ferrario & Wehrse, 1999). Fields of a few 10^6–10^7 G are inferred in the intermediate polars (Ferrario & Wickramasinghe, 1993; Ferrario et al., 1993b).

We have synthesised a population of binaries with the BSE code of Hurley et al. (2002) for a CE efficiency parameter α in the range 0.1–0.9. We have assumed that the field B, achieved by the WD during CE evolution, is proportional to the orbital angular velocity Ω of the binary when the envelope gets ejected. If 10^{13} G is the highest field that can be stably generated in a WD then

$$B = \gamma 10^{13} \left(\frac{\Omega}{\Omega_{\rm crit}}\right) \text{ G}. \quad (1)$$

where $\Omega_{\rm crit}$ is the break-up angular velocity of the WD and γ is a parameter that determines the efficiency with which the poloidal field is regenerated by the decaying toroidal field. The best fit to observations requires $\gamma \sim 10^{-3}$.

We find that if $\alpha < 0.4$ we can produce binaries emerging from the CE that are close to contact, in agreement with Schwope et al. (2009) who proposed that those detached magnetic binaries where the MWD accretes matter from the wind of its companion are the progenitors of the MCVs. The theoretical and observed field and mass distributions are overlapped and shown in Fig. 1.

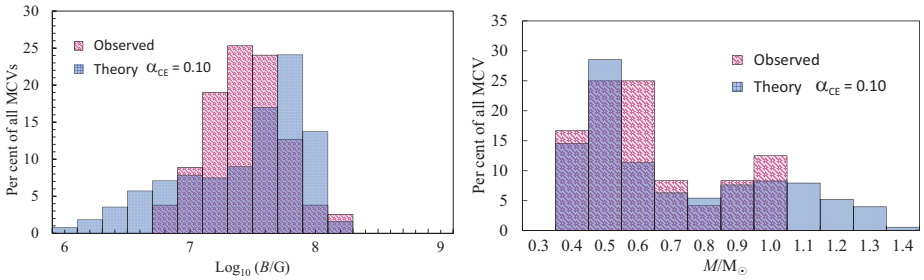

Figure 1. *Left*: Comparison of the theoretical field strength for $\alpha = 0.1$ and observations from Ferrario et al. (2015a). *Right*: Comparison of the theoretical mass distributions to observations from Zorotovic et al. (2011).

Acknowledgements. L.F. acknowledges support from the Grant Agency of the Czech Republic (15-15943S) and the organisers of the conference.

References

Briggs, G. P., Ferrario, L., Tout, C. A., Wickramasinghe, D. T., & Hurley, J. R. 2015, *Mon. Not. R. Astron. Soc.*, **447**, 1713

Ferrario, L., Bailey, J., & Wickramasinghe, D. 1996, *Mon. Not. R. Astron. Soc.*, **282**, 218

Ferrario, L., Bailey, J., & Wickramasinghe, D. T. 1993a, *Mon. Not. R. Astron. Soc.*, **262**, 285

Ferrario, L., de Martino, D., & Gänsicke, B. T. 2015a, *Space Sci. Rev.*, **191**, 111

Ferrario, L., Melatos, A., & Zrake, J. 2015b, *Space Sci. Rev.*, **191**, 77

Ferrario, L. & Wehrse, R. 1999, *Mon. Not. R. Astron. Soc.*, **310**, 189

Ferrario, L. & Wickramasinghe, D. T. 1993, *Mon. Not. R. Astron. Soc.*, **265**, 605

Ferrario, L., Wickramasinghe, D. T., Bailey, J., Hough, J. H., & Tuohy, I. R. 1992, *Mon. Not. R. Astron. Soc.*, **256**, 252

Ferrario, L., Wickramasinghe, D. T., & King, A. R. 1993b, *Mon. Not. R. Astron. Soc.*, **260**, 149

Hurley, J. R., Tout, C. A., & Pols, O. R. 2002, *Mon. Not. R. Astron. Soc.*, **329**, 897

Schwope, A. D., Nebot Gomez-Moran, A., Schreiber, M. R., & Gänsicke, B. T. 2009, *Astron. Astrophys.*, **500**, 867

Wickramasinghe, D. T., Tout, C. A., & Ferrario, L. 2014, *Mon. Not. R. Astron. Soc.*, **437**, 675

Zorotovic, M., Schreiber, M. R., & Gänsicke, B. T. 2011, *Astron. Astrophys.*, **536**, A42

Contrib. Astron. Obs. Skalnaté Pleso **48**, 273 – 274, (2018)

First results of the magnetic field measurements on the G0 IV η Boo

V. V. Butkovskaya, S. I. Plachinda, D. Baklanova and N. F. Pankov

Crimean Astrophysical Observatory of RAS, Nauchny, Russia, 298409
(E-mail: vb@craocrimea.ru)

Received: October 28, 2017; Accepted: November 7, 2017

Abstract. Search for a magnetic field on η Boo has been performed over 50 nights in 1999 – 2014. Statistically significant magnetic field has been detected over 5 out of 50 nights. The total range of the longitudinal magnetic field variations is from -15.1 ± 6.4 G to 23.1 ± 9.6 G.

Key words: stars: activity – stars: late-type – stars: magnetic fields – stars: individual: η Boo

1. Introduction

η Boo (HD 121370, HR 5235, Sp G0 IV) is a yellow subgiant with a thin convective envelope containing less than 1% of the total mass of the star (van Belle *et al.*, 2007). Carrier et al. (2005) have obtained $T_{\rm eff} = 6030 \pm 90$ K, $M/{\rm M}_{\odot} = 1.57 \pm 0.07$, and the age $t = 2.67 \pm 0.10$ Gyr for this star. $\log g = 3.817 \pm 0.016$ and $R/{\rm R}_{\odot} = 2.672 \pm 0.028$ have been reported by van Belle *et al.* (2007). The S-index 0.144 ± 0.005 has been estimated by Hempelmann et al. (2016). We present the preliminary result of our study of the magnetic field on η Boo.

2. Results

Spectropolarimetric observations of η Boo have been performed over 50 nights from 1999 to 2014 with the 2.6-m Shajn telescope at the Crimean Astrophysical Observatory using the long-slit spectrograph (45 nights in 1999 – 2013, spectral resolution $R \sim 30000$, spectral range 6200 – 6270 Å) and echelle spectrograph (5 nights in 2014, spectral resolution $R \sim 57000$, spectral range 5200 – 6420 Å). The calculation of the longitudinal magnetic field (LMF) has been performed with the procedure discussed by Butkovskaya & Plachinda (2007).

Figure 1 shows the LMF, $B_{\rm e}$, of η Boo measured from 1999 to 2014. The total range of LMF variations is from -15.1 ± 6.4 G to 23.1 ± 9.6 G. We have detected a statistically significant magnetic field over 5 out of 50 dates (see Table 1). Most of the $B_{\rm e}$ values are in the range from about -5 to 10 G, whereas the average error is $\sim$5 G. Thus, if the magnetic field of η Boo has large-scale and small-scale components as, for example, the magnetic field of β Aql (Butkovskaya

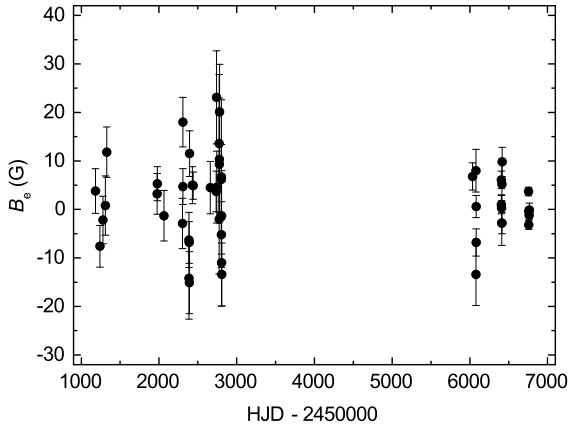

Figure 1. Longitudinal magnetic field of η Boo in 1999 – 2014.

Table 1. Statistically significant magnetic field B_e of η Boo.

HJD	B_e	σ	B_e/σ
2452307.540	18.0	5.1	3.5
2456405.478	6.1	1.8	3.4
2456415.318	9.8	3.0	3.3
2456756.440	3.7	0.9	4.1
2456757.486	−3.2	0.9	3.6

et al., 2017), long-term and more precise measurements are needed to identify both of these components.

Acknowledgements. The study was funded by RFBR and Ministry of Education of the Crimean Republic according to the research projects No. 16-02-00689, 16-42-910813 r_a.

References

Butkovskaya, V. V. & Plachinda, S. I. 2007, *Astron. Astrophys.*, **469**, 1069

Butkovskaya, V. V., Plachinda, S. I., Bondar', N. I., & Baklanova, D. N. 2017, *Astron. Nachr.*, accepted

Carrier, F., Eggenberger, P., & Bouchy, F. 2005, *Astron. Astrophys.*, **434**, 1085

Hempelmann, A., Mittag, M., Gonzalez-Perez, J. N., et al. 2016, *Astron. Astrophys.*, **586**, A14

Contrib. Astron. Obs. Skalnaté Pleso **48**, 275 – 276, (2018)

Result of the magnetic field measurements on β Aql using different sets of spectral lines

V. V. Butkovskaya and S. I. Plachinda

Crimean Astrophysical Observatory, Nauchny, Crimea, 298409
(E-mail: vb@craocrimea.ru)

Received: October 28, 2017; Accepted: November 7, 2017

Abstract. The magnetic field of β Aql has been studied using different sets of lines in spectra obtained on October 6, 2014. We identify two sets of lines that give different values of the magnetic field of 40.8 ± 1.9 G and 8.7 ± 2.0 G, respectively. We conclude that for the calculation of the magnetic field and its geometry on a convective star it is necessary to take into account the distribution of physical conditions over the stellar surface and to select homogeneous sets of spectral lines.

Key words: stars: late-type – stars: magnetic fields – stars: individual: β Aql

1. Introduction

The effect of physical condition irregularities on the surface of the Sun is well known in the solar physics: magnetic field measured using different spectral lines significantly differs (e.g. Rezaei et al., 2007; Stenflo et al., 2013; Lozitsky, 2015). We present the result of our study of the magnetic field on the convective subgiant β Aql (G8 IV–V) using two different sets of lines in circularly polarized spectra obtained on October 6, 2014.

2. Results

To test our method of magnetic field calculation a synthetic spectrum has been computed for a longitudinal field of about 60 G. Each contour was normalized to the selected wavelength λ, the Landé factor g and the central residual intensity R_0 independently. The circularly polarized σ-components were calculated using the dependence $r_{\rm n,k} = f(R_{\rm k}^{\rm center})$ (1), where $r_{\rm n,k}$ is the residual intensity in each n-th point of each k-th contour; $R_{\rm k}^{\rm center}$ is the residual intensity in the center of gravity or in the minimum intensity of the contour (n = 1, 2,..., N and k = 1, 2,..., K). An example of Stokes V computed by our code is shown on the left bottom panel of Fig. 1.

Butkovskaya et al. (2017) have supposed that two components of the magnetic field are present on β Aql. The low amplitude one is due to the global

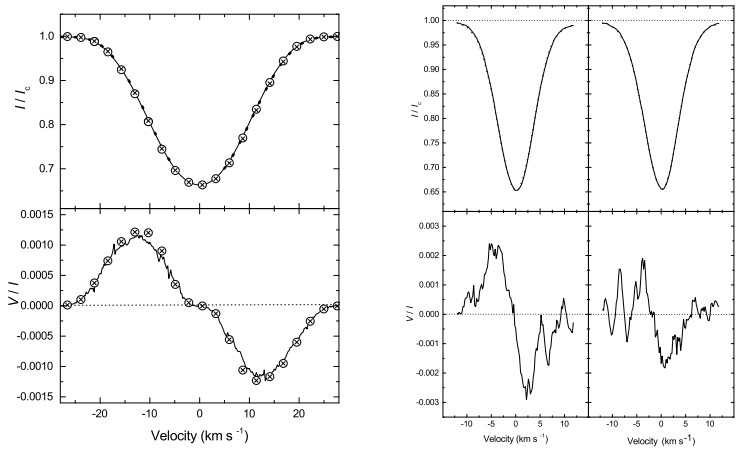

Figure 1. *Left*: Top panel: origin synthetic σ-components calculated for the longitudinal field of 60 G (open circles and crosses); σ-components calculated by Eq. (1) (solid and dotted lines). Bottom panel: Stokes V calculated using polarized synthetic contours of a single line with selected λ, g, R_0 (open circles and crosses); Stokes V calculated by Eq. (1) (solid line). *Right*: σ-components (top panels) and Stokes V (bottom panels) calculated by Eq. (1). All lines from the first set demonstrate a stronger field (left). Longitudinal magnetic field calculated using these lines is 40.8 ± 1.9 G. All lines from the second set give a weaker field (right) of 8.7 ± 2.0 G. Longitudinal magnetic field calculated using centers of gravity of all unblended lines is 23.6 ± 1.0 G.

large-scale magnetic field and the large-amplitude one originates from the small-scale magnetic activity. The right panels of Fig. 1 show that the magnetic field of β Aql significantly differs if measured using two different sets of spectral lines. This agrees with the solar magnetic field measurements. We conclude that for the calculation of the magnetic field and its geometry on a convective star it is necessary to take into account the distribution of physical conditions over the stellar surface and to select homogeneous sets of spectral lines.

References

Butkovskaya, V. V., Plachinda, S. I., Bondar', N. I., & Baklanova, D. N. 2017, *Astron. Nachr.*, **338**, 896

Lozitsky, V. G. 2015, *Adv. Space Res.*, **55**, 958

Rezaei, R., Schlichenmaier, R., Schmidt, W., & Steiner, O. 2007, *Astron. Astrophys.*, **469**, L9

Stenflo, J. O., Demidov, M. L., Bianda, M., & Ramelli, R. 2013, *Astron. Astrophys.*, **556**, A113

Contrib. Astron. Obs. Skalnaté Pleso **48**, 277 – 279, (2018)

A Search for Photometrically Variable Magnetic CP Stars in Sky Survey Data

S. Hümmerich[1,2], K. Bernhard[1,2] and E. Paunzen[3]

[1] *American Association of Variable Star Observers (AAVSO), Cambridge, MA, 02138, USA (E-mail: ernham@rz-online.de)*

[2] *Bundesdeutsche Arbeitsgemeinschaft für Veränderliche Sterne e.V. (BAV), D-12169 Berlin, Germany*

[3] *Department of Theoretical Physics and Astrophysics, Masaryk University, CZ-611 37 Brno, Czech Republic*

Received: November 10, 2017; Accepted: November 12, 2017

Abstract. The magnetic chemically peculiar (mCP) stars of the upper main sequence are natural laboratories well-suited for the investigation of such diverse phenomena as e.g. atmospheric structure, magnetic fields and stellar rotation. We here present our efforts towards increasing the sample of known mCP stars by using publicly available photometric time series data, which has already led to the discovery of more than 850 photometrically variable mCP stars and candidates.

Key words: stars: chemically peculiar – variables: general – surveys

1. Introduction

Chemically peculiar (CP) stars make up about 10 % of upper main-sequence stars (spectral types early B to early F). They are characterized by peculiar atmospheric abundances that differ significantly from the solar pattern. The CP2 (Bp/Ap) stars and the CP4 (helium-weak) stars (also referred to collectively as the magnetic CP or mCP stars) are set apart by the presence of strong, stable and globally-organized magnetic fields (Babcock, 1947; Aurière et al., 2007). They exhibit a non-uniform distribution of chemical elements on their surfaces, which leads to spectral and photometric variability with the rotation period. mCP stars exhibiting photometric variability are traditionally referred to as α^2 Canum Venaticorum (ACV) variables.

During recent decades, automated sky surveys have advanced to become the dominant data source in astronomy. An increasing number of surveys routinely produce high-quality photometric time-series data well suited to the investigation of stellar variability. We have taken advantage of these data in the identification and investigation of new ACV variables. Two different approaches were taken: (i) mCP stars from the Catalogue of Ap, HgMn, and Am stars (Renson & Manfroid, 2009) were selected and cross-matched with archival sky survey data, and (ii) a search for the typical variability pattern of ACV variables was carried

out among the light curves of early-type (spectral types B/A or colour-selected) variable stars of undetermined type in the AAVSO International Variable Star Index (VSX Watson et al., 2006).

2. Results

We here present an overview over the present state of our project. Following the methodology outlined above, we have established light variability in a large number of mCP stars not hitherto known as photometric variables (Table 1).

Table 1. New photometrically variable ACV stars and candidates.

Data Source	#ACVs	Ref.
All Sky Automated Survey (ASAS)	316	Bernhard et al. (2015a)
	357	Hümmerich et al. (2016)
SuperWASP (SWASP)	80	Bernhard et al. (2015b)
KELT Transit Survey	49	[unpublished]
Kepler (also K2 mission)	>50	[unpublished]
total of new variables	852+	

Among our sample, there are 14 eclipsing binary systems hosting an mCP star component. A lack of close binaries is generally observed among mCP stars; therefore, this finding is of great interest. Furthermore, we have identified several stars exhibiting variability on time-scales typical of δ Scuti variables (periods between about 15 minutes and 5 hours). While most of these stars are actually non-magnetic CP1 (Am) stars, several mCP star candidates are present. Spectroscopic verification, however, is needed and under way. In additon, some objects of special interest have been found, such as HD 66051, which has been identified as an eclipsing binary system hosting a highly-peculiar CP3(HgMn)-related star. Obvious out-of-eclipse variability is present in the light curve and interpreted as a signature of surface inhomogeneities (Niemczura et al., 2017).

Some future research fields deriving from our main project are outlined in the following: (i) extension of the search for new ACV variables to other photometric survey databases, (ii) spectroscopic confirmation of the 'photometric' ACV candidates (first results have shown that this might be a viable and efficient means of discovering new mCP stars), (iii) datamining of spectroscopic survey archives (LAMOST and SDSS) for new mCP stars, (iv) search for very long-period ($P > 1\,yr$) ACV variables in survey data, and (v) investigation into the properties of the mCP stars that do not show photometric variability in the accuracy limit of the employed sky survey data.

References

Aurière, M., Wade, G. A., Silvester, J., et al. 2007, *Astron. Astrophys.*, **475**, 1053

Babcock, H. W. 1947, *Astrophys. J.*, **105**, 105

Bernhard, K., Hümmerich, S., Otero, S., & Paunzen, E. 2015a, *Astron. Astrophys.*, **581**, A138

Bernhard, K., Hümmerich, S., & Paunzen, E. 2015b, *Astron. Nachr.*, **336**, 981

Hümmerich, S., Paunzen, E., & Bernhard, K. 2016, *Astron. J.*, **152**, 104

Niemczura, E., Hümmerich, S., Castelli, F., et al. 2017, *Sci. Rep.*, **7**, 5906

Renson, P. & Manfroid, J. 2009, *Astron. Astrophys.*, **498**, 961

Watson, C. L., Henden, A. A., & Price, A. 2006, *Society for Astronomical Sciences Annual Symp.*, **25**, 47

Shinsuke Takasao, Christian Fendt and Wouter Vlemmings

Contrib. Astron. Obs. Skalnaté Pleso **48**, 280 – 281, (2018)

Impact of magnetic fields on the structure of convective atmospheres of red giant stars

J. Klevas[1], A. Kučinskas[1], S. Wedemeyer[2,3] and H.-G. Ludwig[4]

[1] *Astronomical Observatory, Vilnius University, Vilnius LT-10222, Lithuania, (E-mail: jonas.klevas@tfai.vu.lt)*

[2] *Rosseland Centre for Solar Physics, University of Oslo, P.O. Box 1029 Blindern, N-0315 Oslo, Norway*

[3] *Institute of Theoretical Astrophysics, University of Oslo, P.O. Box 1029 Blindern, N-0315 Oslo, Norway*

[4] *ZAH Landessternwarte Königstuhl, D-69117 Heidelberg, Germany*

Received: November 23, 2017; Accepted: November 25, 2017

Abstract. We use 3D magnetohydrodynamic CO^{5}BOLD model atmospheres to study the interplay between magnetic fields and convection in the atmospheres of red giant stars. We find that vortex-like structures occur prominently in stars with stronger magnetic fields and lead to alterations of their thermal structures.

Key words: stars: atmospheres – convection – hydrodynamics – magnetohydrodynamics (MHD) – stars: late-type

1. Introduction

It is well-known that magnetic fields are present in stellar atmospheres even in the regions which can be regarded as magnetically quiet. In the Sun, such regions can experience a noticeable influence from the magnetic fields resulting, for example, in the formation of vortex-like structures and thereby affecting the overall structure of the solar atmosphere. As such effects are still largely unexplored in other types of stars, we investigate the interaction of convection and magnetic field and their combined impact on the atmospheric structure of red giant stars.

In this study we used 3D hydrodynamical CO^{5}BOLD model atmospheres (Freytag et al., 2012). 3D hydrodynamical CO^{5}BOLD model atmospheres from the CIFIST grid (Ludwig et al., 2009) were used as starting models for the MHD simulations. The CIFIST models were extended both vertically and horizontally to avoid expanding shockwaves colliding with themselves in the outer chromosphere due to periodic horizontal boundary conditions. To construct the model atmospheres of appropriate size, we have extended CIFIST model atmospheres by 1.5 – 2 times horizontally and 1.5 times vertically. In the vertical direction, the goal was to include layers up to the Rosseland optical depth $\log \tau_{\mathrm{Ross}} \approx -10$.

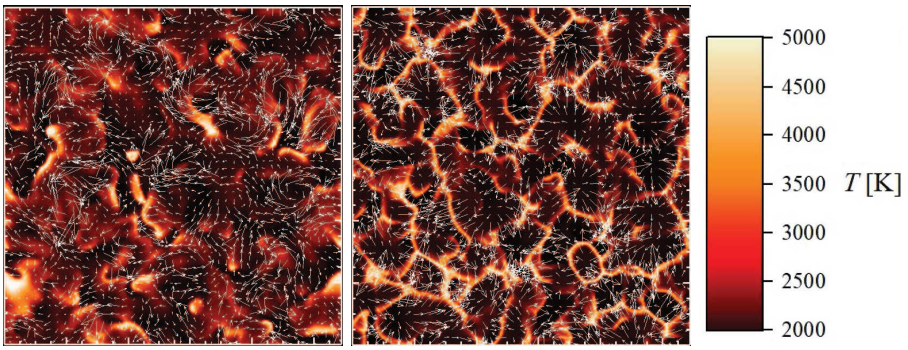

Figure 1. Horizontal cuts through the model atmosphere of a red giant ($T_{\rm eff}$ = 4500 K, $\log g$ = 2.5, [M/H] = –2.0). The color maps show the thermal structure in the outer atmosphere ($\langle \log \tau_{\rm Ross} \rangle \approx -8$), white vectors delineate the horizontal velocity field. *Left*: MHD model atmosphere with the inital mean magnetic field strength $\langle |B| \rangle \approx 50$ G. *Right*: purely hydrodynamic model atmosphere ($\langle |B| \rangle = 0$).

2. Influence of magnetic fields on the atmospheric structure

At solar metallicity, the presence of a magnetic field typically results in the increase of atmospheric velocities and higher temperatures in the chromosphere, whereas in the red giant model at [M/H] = –2.0 the velocity field is noticeably dampened. In both cases the mean temperature profiles are only weakly affected by the magnetic field, whereas stronger initial magnetic field of 50 G results in the decrease of RMS temperature.

Horizontal cuts through the model atmosphere at the Rosseland optical depth $\langle \log \tau_{\rm Ross} \rangle = -8$ show that whereas the non-magnetic model atmosphere exhibits usual filamentary structure in the outer layers, this pattern is replaced with an apparently more uniform temperature distribution in the magnetic model atmosphere where vortex structures are clearly prominent (Fig. 1).

Acknowledgements. This work was supported by a grant from the Research Council of Lithuania (MIP-089/2015). HGL acknowledges financial support by Sonderforschungsbereich SFB 881 "The Milky Way System" (subproject A4) of the German Research Foundation (DFG).

References

Freytag, B., Steffen, M., Ludwig, H.-G., et al. 2012, *J. Comput. Phys.*, **231**, 919

Ludwig, H.-G., Caffau, E., Steffen, M., et al. 2009, *Mem. Soc. Astron. Ital.*, **80**, 711

Contrib. Astron. Obs. Skalnaté Pleso **48**, 282 – 283, (2018)

Some astrophysical processes around magnetized black hole

M. Kološ, A. Tursunov and Z. Stuchlík

Silesian University in Opava, Czech Republic
(E-mail: martin.kolos@fpf.slu.cz)

Received: October 10, 2017; Accepted: October 25, 2017

Abstract. We study the dynamics of charged test particles in the vicinity of a black hole immersed into an asymptotically uniform external magnetic field. A real magnetic field around a black hole will be far away from to be completely regular and uniform, a uniform magnetic field is used as linear approximation. Ionized particle acceleration, charged particle oscillations and synchrotron radiation of moving charged particle have been studied.

Key words: magnetic fields – black holes – charged particle

The motion of a charged particle with the charge q and mass m in Kerr black hole spacetime with mass M and spin a in the presence of a uniform magnetic field b is governed by the Lorentz equation

$$\frac{\mathrm{d}u^\mu}{\mathrm{d}\tau} + \Gamma^\mu_{\alpha\beta} u^\alpha u^\beta = \frac{q}{m} g^{\mu\rho} F_{\rho\sigma} u^\sigma, \qquad g_{\mu\nu} u^\mu u^\nu = -1, \tag{1}$$

where $u^\mu = dx^\mu/d\tau$ is the four-velocity of the particle, $\Gamma^\mu_{\alpha\beta}$ are Christoffel symbols for a Kerr black hole metric and $F_{\mu\nu}$ is the tensor of the electromagnetic field. The magnetic field B is weak (it does not contribute to the metric), but the magnetic field influence on the charged particles motion can be fairly large depending on the specific particle charge. The "charged particle" can represent matter ranging from electron to some charged inhomogeneity orbiting in the innermost region of the accretion disk. The specific particle charge q/m for any such structures will then range from the electron maximum to zero. The dimensionless quantity b (magnetic parameter) can be introduced as relative Lorenz force $b = qBGM/2mc^4$. For a stellar mass black hole $M \approx 10$ M$_\odot$, we can have an electron e$^-$ in the magnetic field $B = 10^{-5}$ Gs, or charged dust grain (one electron lost, $m = 2 \times 10^{-16}$ kg) in the field $B = 10^9$ Gs – the absolute value of the magnetic field parameter is the same in both cases, $b = 0.004$.

Ionized particle acceleration - model of jet

Relativistic jets, i.e. collimated streams of escaping charged particles (velocities $v \sim c$) are observed in a wide variety of astrophysical systems. Many models have been proposed for a relativistic jet engine (jets driven by the accretion disk / driven by the central black hole); the exact mechanism is still unknown,

but it is generally accepted that large scale magnetic fields play a fundamental role in the jet formation. In Stuchlík & Kološ (2016) we study the dynamics of neutral particles forming an accretion disk that are ionized and start to feel the magnetic field. Chaotic scattering in combined black hole gravitational and uniform magnetic field then occurs and interchange between velocity around the black hole u^{ϕ} and velocity along the rotational axis u^{z}, providing mechanism for charged particle acceleration and escape along the magnetic field lines. Relativistic escape velocity of light particles can be obtained even for relatively small magnitudes of magnetic fields.

Magnetic field and microquasar quasi-periodic oscillations

Microquasars are binary systems composed of a black hole and a companion (donor) star, demonstrating quasi-periodic oscillations (QPOs) of the X-ray power density. Different types of QPOs were distinguished: these are the high frequency (HF) and low frequency (LF) QPOs in the timing spectra. The HF QPOs are sometimes detected with the twin peaks (upper f_{U} and lower f_{L}) which have frequency ratio close to $3:2$. In addition to HF QPOs, some sources display simultaneous existence of the low frequency LF QPOs f_{low} in the timing spectra. In Kološ et al. (2017) we examine the magnetic field influence on the QPOs phenomena, determining mass and spin of the black hole inside the GRS 1915+105, XTE 1550-564 and GRO 1655-40 sources.

Radiation reaction of a charged particle - synchrotron radiation

Synchrotron radiation emitted by a charged particle leads to appearance of the back-reaction force which can significantly affect its motion. In Tursunov et al. (2017) we study the dynamics of a charged particle undergoing radiation reaction force in combined Schwarzschild black hole gravitational field and an external asymptotically uniform magnetic field. The final state of the particle depends on the orientation of the Lorentz force with respect to the black hole. In case where the Lorentz force is directed towards the black hole, the radiation reaction leads to the fall of the charged particle from initially stable orbit into the black hole. Inversely, when the Lorentz force is repulsive, the orbit of the charged particle remains bounded while oscillations decay.

References

Kološ, M., Tursunov, A., & Stuchlík, Z. 2017, *ArXiv e-prints* [arXiv:1707.02224]

Stuchlík, Z. & Kološ, M. 2016, *European Physical Journal C*, **76**, 32

Tursunov, A., Kološ, M., Stuchlík, Z., & Gal'tsov, D. V. 2017, *Astrophys. J.*, submitted

Contrib. Astron. Obs. Skalnaté Pleso **48**, 284 – 286, (2018)

Monitoring and modelling magnetic variability in two white dwarfs with very weak magnetic fields

J. D. Landstreet[1,2], S. Bagnulo[2] and G. Valyavin[3]

[1] *Dept. of Physics & Astronomy, University of Western Ontario, London, Ontario N6A 3K7, Canada*

[2] *Armagh Observatory and Planetarium, College Hill, Armagh BT61 9DG, Northern Ireland, UK*

[3] *Special Astrophysical Observatory, RAS, Nizhnij Arkhiz, Zelenchukskij Region, 369167 Karachai-Cherkessian Republic, Russia*

Received: November 5, 2017; Accepted: November 9, 2017

Abstract. We have measured the magnetic field strengths $\langle B_z \rangle$ and $\langle |B| \rangle$ of two very weak field magnetic white dwarfs WD 2047+372 and WD 2359-434, and have used these data to obtain simple magnetic field models.

Key words: white dwarfs – magnetic fields

Only a few fields weaker than 1 MG are known in white dwarfs (WDs) We have been carrying out the most sensitive survey to date for weaker fields, in the range of a few kG up to 1 MG, using ISIS at the WHT, FORS at the ESO VLT, ESPaDOnS at the CFHT, and the MSS at the BTA/SAO. This survey discovered a field of $\langle |B| \rangle \sim 60$ kG in the bright DA3.4 WD2047+372 ($T_{\rm eff} = 14710$ K), the third weakest MWD field securely detected. For our results so far, see Landstreet et al. (2012, 2015, 2016, 2017); Bagnulo et al. (2015); and references in these articles.

We have obtained time series for WD2047+372 and WD2359-434 (DAP5.8, $T_{\rm eff} = 8540$ K). We measure the mean line-of-sight field $\langle B_z \rangle$ and the mean field modulus $\langle |B| \rangle$ averaged over the visible hemisphere, as well as the equivalent width of the core of Hα. These measured values are then searched for periodic variability due to rotation of the underlying WD.

The results are as follows. WD2047+372: $\langle B_z \rangle$ varies periodically, +15 to –11 kG, $P = 0.243$ d; $\langle |B| \rangle \approx 60$ kG $\approx$ constant. WD2359-434: $\langle B_z \rangle$ is almost constant at +5 kG; Hα core equivalent width varies strongly with $P = 0.112$ d; $\langle |B| \rangle$ is hard to measure, but appears to vary between ~ 50 and ~ 100 kG.

Modelling is difficult because (1) the intrinsic width of the Hα core is much wider than vsini broadening, seriously limiting the information in the line profiles about the magnetic field, and (2) our LTE synthesis tools cannot compute accurately the deep Hα line cores of DA stars. Our data for WD2047+372 are consistent with a simple dipole model, $i = 27°$, $\beta = 86.5°$, $B_d = 92$ kG (see the left panels of Fig. 1); however, this model is not strongly constrained. The data

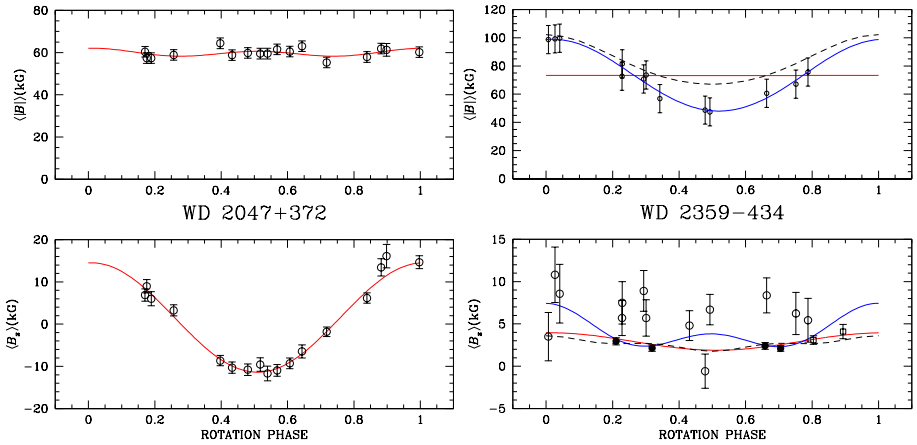

Figure 1. *Left panel:* WD 2047+372: Observed variation of $\langle B_z \rangle$ and $\langle |B| \rangle$ fit by a simple dipolar model. *Right panel:* WD 2359-434: Observed variation of $\langle B_z \rangle$ and $\langle |B| \rangle$ fit by a simple dipolar model (thin red lines), a co-linear dipole-quadrupole-octupole model (dashed black lines) and by a model including the superposition of a dipole with a non linear quadrupole (thick blue lines).

for WD2359-434 do not appear consistent with a simple dipole-like geometry. Red lines in Fig. 1 (right) show the best simple dipole fit found. A better fit is obtained using a combination of a dipole and quadrupole with different axes (blue lines). A model fit to $\langle B_z \rangle$ and $\langle |B| \rangle$ is shown in Fig. 1 (right), and a map of this fit is illustrated in Fig. 2 (thanks to Oleg Kochukhov for the plot routine).

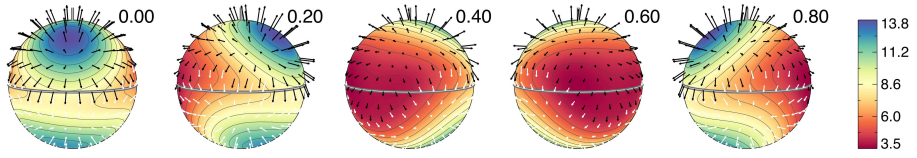

Figure 2. The distribution of magnetic field over the surface the dipole-non-aligned quadrupole model of WD 2359-434, as seen at five successive phases. Black arrows represent outward field, white arrows inward field. The axis of rotation is a small white line segment close to the top of each sphere. The scale at right is in units of Tesla (1 T = 10 kG).

References

Bagnulo, S., Fossati, L., Landstreet, J. D., & Izzo, C. 2015, *Astron. Astrophys.*, **583**, A115

Landstreet, J. D., Bagnulo, S., Martin, A., & Valyavin, G. 2016, *Astron. Astrophys.*, **591**, A80

Landstreet, J. D., Bagnulo, S., Valyavin, G., & Valeev, A. F. 2017, *Astron. Astrophys.*, **607**, A92,

Landstreet, J. D., Bagnulo, S., Valyavin, G. G., et al. 2012, *Astron. Astrophys.*, **545**, A30

Landstreet, J. D., Bagnulo, S., Valyavin, G. G., et al. 2015, *Astron. Astrophys.*, **580**, A120

John Landstreet

Contrib. Astron. Obs. Skalnaté Pleso **48**, 287 – 288, (2018)

HD 185330 – chemically peculiar ^{3}He star in the *Kepler* field

E. Niemczura[1], S. Vennes[2], T. Różański[1], A. Pigulski[1], K. Hełminiak[3] and H. Lehmann[4]

[1] *Astronomical Institute, University of Wrocław, 51-622 Wrocław, Poland (E-mail: niemczura@astro.uni.wroc.pl)*

[2] *Astronomical Institute of the Czech Academy of Sciences 251 65 Ondřejov, The Czech Republic*

[3] *Nicolaus Copernicus Astronomical Center, Polish Academy of Sciences, 87-100 Toruń, Poland*

[4] *Thüringer Landessternwarte Tautenburg, D-07778 Tautenburg, Germany*

Received: November 20, 2017; Accepted: November 23, 2017

Abstract. We analyzed high-resolution spectra of the chemically peculiar ^{3}He star HD 185330. We determined its atmospheric parameters ($T_{\rm eff}, \log g, \xi$) and constrained its rotation velocity and abundance pattern. In particular, we found a large ($\times$100) phosphorus abundance excess and evidence of ^{3}He and ^{4}He abundance stratification in the atmosphere.

Key words: stars: chemically peculiar – stars: atmospheres – stars: abundances

Chemically peculiar B-type stars showing unusually high abundances of the ^{3}He isotope in their atmospheres are rare. HD 185330 (KIC 3246460, V= 6.50 mag) was classified as ^{3}He star by Preston (1976). Several ^{3}He and ^{4}He lines are visible in its spectra. We classified HD 185330 as B5 II-IIIp following criteria presented in Gray & Corbally (2009).

The spectra of HD 185330 show weak emission lines (WELs). According to the list presented in Wahlgren & Hubrig (2004) these are, e.g., the Mn II multiplet 13, Fe II and P II lines. Some of the observed WELs remain unclassified. Theoretical explanations for the WELs are based mainly on the interlocked non-local thermodynamic equilibrium (non-LTE) effects. To explain the observed emission of the Mn II multiplet 13, these effects have to be combined with the vertical stratification of the Mn abundance (see Sigut, 2001a,b).

The high-resolution spectra of HD 185330 were taken with the HERMES (Raskin et al., 2011), HIDES (Izumiura, 1999) and TLS (see e.g. Lehmann et al., 2016) spectrographs. The atmospheric parameters were obtained following various methodologies. First, we assumed LTE and used Kurucz ATLAS9 and SYNTHE codes (Kurucz, 2005). We determined the effective temperature $T_{\rm eff} = 16300 \pm 200$ K and surface gravity $\log g = 3.7 \pm 0.1$ from Balmer and Fe II/Fe III lines, and the microturbulence $\xi = 0.5 \pm 0.5$ km s^{-1} from Fe II lines.

Next, a hybrid non-LTE method was applied, in which we combined LTE Kurucz atmospheric models and non-LTE line formation procedures (DETAIL and SURFACE codes, see Przybilla & Butler, 2004). Using this method, we derived $T_{\rm eff} = 16400 \pm 400\,{\rm K}$ and $\log g = 3.8 \pm 0.1$ from Si II/Si III and Balmer lines, and $\xi = 0.5 \pm 0.2\,{\rm km\,s^{-1}}$ from S II and Si III lines. Finally, we applied a full non-LTE method using TLUSTY and SYNSPEC (Hubeny & Lanz, 2017) for the atmospheric model and synthetic spectra calculations. A variable abundance stratification of He isotopes and other elements was included in the model atmosphere calculations to fit the observed lines. We found that the ^{3}He and ^{4}He abundances decrease with height and that the overall abundance of ^{3}He is lower than that of ^{4}He. The abundance analyses using all these methods generally agree. In particular, the P abundance determined from LTE and full non-LTE approaches is a factor of 100 above solar. This is a typical characteristic of He-weak PGa stars, but Ga lines were not identified in the spectra of HD 185330.

HD 185330 was observed by the *Kepler* satellite during all quarters, which corresponds to a time span of about four years. A total number of 50291 data points were collected in the long-cadence mode. The analysis of the light curve gave a rotation period $\rm P_{rot} = 37.64307 \pm 0.00003\,d$. The rotation period and projected rotation velocity $v \sin i = 3.0 \pm 0.5\,{\rm km\,s^{-1}}$ obtained from the spectroscopic analysis allow us to estimate a minimum stellar radius of about $6\,{\rm R_\odot}$.

Acknowledgements. EN and TR acknowledge the National Science Centre grant no. 2014/13/B/ST9/00902. Calculations have been carried out at the Wrocław Centre for Networking and Supercomputing (http://www.wcss.pl), grant No. 214. KH and AP acknowledge support provided by the National Science Center through grants no. 2016/21/B/ST9/01613 and 2016/21/B/ST9/01126. SV acknowledges support from the Czech Science Foundation (15-15943S).

References

Gray, R. O. & Corbally, J., C. 2009, *Stellar Spectral Classification* (Princeton University Press)

Hubeny, I. & Lanz, T. 2017, *ArXiv e-prints* [arXiv:1706.01859]

Izumiura, H. 1999, in *Obs. Astroph. in Asia and its Future*, ed. P. S. Chen, 77

Kurucz, R. L. 2005, *Mem. Soc. Astron. Ital. Suppl.*, **8**, 14

Lehmann, H., Borkovits, T., Rappaport, S. A., et al. 2016, *Astrophys. J.*, **819**, 33

Preston, G. W. 1976, *Carnegie Yrb., 1975, p. 288*

Przybilla, N. & Butler, K. 2004, *Astrophys. J.*, **609**, 1181

Raskin, G., van Winckel, H., Hensberge, H., et al. 2011, *Astron. Astrophys.*, **526**, A69

Sigut, T. A. A. 2001a, *Astron. Astrophys.*, **377**, L27

Sigut, T. A. A. 2001b, *Astrophys. J., Lett.*, **546**, L115

Wahlgren, G. M. & Hubrig, S. 2004, *Astron. Astrophys.*, **418**, 1073

Contrib. Astron. Obs. Skalnaté Pleso **48**, 289 – 291, (2018)

Frequency of CP2 (CP4) stars in open clusters compared to the Galactic field

M. Rode-Paunzen

Institut für Astrophysik, Universität Wien, Türkenschanzstraße 17, 1180 Vienna, Austria, (E-mail: monika.rode-paunzen@oeaw.ac.at)

Received: January 17, 2018; Accepted: January 20, 2018

Abstract. More than ten percent of all A- and B-type stars are chemically peculiar objects and about five percent are well known magnetic chemically peculiar (mCP) stars. This project explores the occurrence of the magnetic CP star groups (CP2 and CP4) in open clusters and in the Galactic field. In a first step, their positions in the Milky Way were analyzed. The next step will include a study of the dependence between various parameters and the Galactic position to identify Galactic environments that might favour the formation of mCP stars. The final goal of the project is to provide evidence for the evolution of the magnetic field by means of the mCP star incidence and their Galactic position.

Key words: stars: chemically peculiar – open clusters and associations: general – Galaxy: stellar content

1. Introduction

The group of mCP stars combines some important properties, such as strong magnetic fields, slow rotation, and chemical surface abundance inhomogeneities (see e.g. Netopil et al., 2017). We used the Michigan Catalogue of spectral types (vol. I–V, the latest by Houk & Swift, 1999) and the Catalogue of Ap, HgMn and Am Stars (Renson & Manfroid, 2009) to extract a list of CP2 and CP4 stars. The Michigan Catalogue is based on a spectral sky survey (108 Å/mm at Hβ) and covers the southern sky ($-90° < \delta < +5°$). It includes about 50 000 stars which are classified as B, A and early F-type objects. Furthermore, the catalogue by Renson & Manfroid (2009) lists more then 8000 known CP stars (spectral type: B to early F), compiled from many different sources. Open clusters were extracted from the online-database WEBDA[1] and the online-database Simbad served as an additional data source.

2. Data analysis

Renson & Manfroid (2009) list 3321 CP2 and CP4 stars, including about 1800 objects from the Michigan Catalogue. WEBDA lists about 1200 open cluster

[1] http://webda.physics.muni.cz

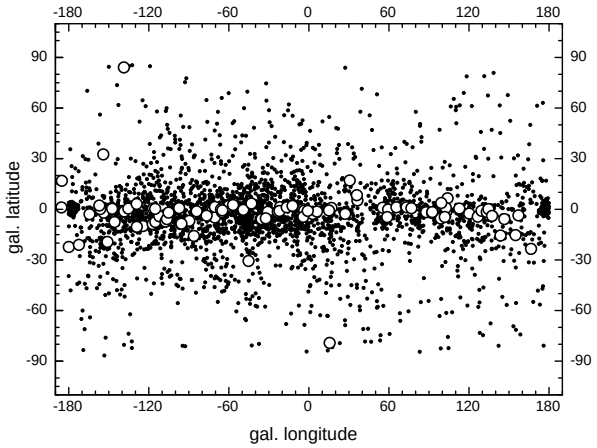

Figure 1. The Galactic positions of all identified mCP field stars (dots) and open clusters with known mCP member stars (open circles).

with 50 000 member stars in total, provides basic information (such as coordinates) and includes numerous photometric and astrometric data for the cluster stars. We identified 245 mCP cluster stars in 95 open clusters. The analysis of field stars is based on the Michigan Catalogue and Renson & Manfroid (2009). Open clusters with mCP star members are more concentrated to the Galactic plane, which also holds for the group of mCP field stars. Only the clusters Blanco 1 in the southern hemisphere and Coma Berenices in the north do not follow the general trend (see Fig. 1).

The sample of cluster mCP stars certainly still requires some improvement. The photometric Δa peculiarity index was developed to identify mCP stars in an economic way (Maitzen, 1976). This three-filter-system (g_1, g_2, y) makes use of a flux depression at 5200 Å, a typical characteristic for this group of stars. Generally, objects showing $\Delta a > 20$ mmag can be classified as mCP star candidates. Paunzen et al. (2005) derived a detection efficiency of up to 95 %, depending on the detection limit. We compiled Δa measurements for about 500 field and cluster mCP stars in our sample. However, not all of the spectroscopic mCP stars also show a remarkable Δa value (see right panel of Fig. 2), which might be a result of spectroscopic misclassification and a lower detection efficiency towards cooler objects. Nonetheless, this photometric system is a valuable tool to detect mCP star candidates which are too faint for detailed spectroscopic surveys; it even allowed the detection of mCP stars in the Large Magellanic Cloud (e.g. Paunzen et al., 2011).

A first evaluation of our data set does not show a clear correlation between the number of detected mCP stars in the individual open clusters and the number of cluster members, the cluster diameter, the distance, or the position.

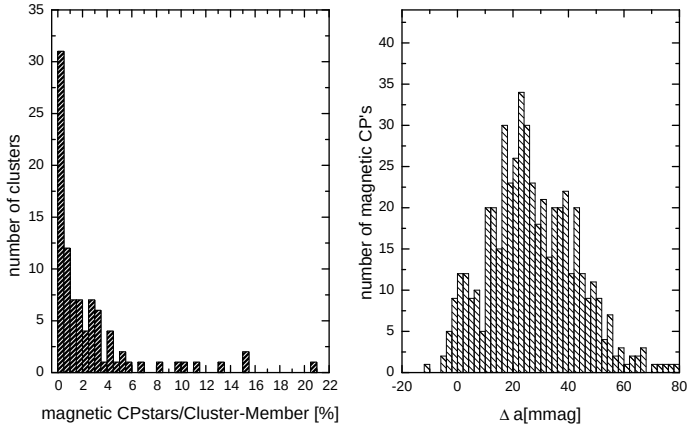

Figure 2. *Left*: Relationship between peculiar and non-peculiar stars in 95 cluster. *Right*: Distribution of the Δa values of spectroscopically identified mCP stars.

3. Conclusions

We know of 95 open clusters that host one or more mCP member stars. Most open clusters (80 objects) show a mCP star incidence between 0.5 % and 5% (left panel of Fig. 2), which is lower than typically quoted values for the Galactic field. Neither the diameter of the open clusters nor the distance seem to show a correlation with the number of detected mCP stars. An improvement of the cluster sample is certainly needed, but a spectroscopic survey is not a practicable option. Photometric measurements and long based time series will help to identify new mCP cluster stars.

References

Houk, N. & Swift, C. 1999, *Michigan catalogue of two-dimensional spectral types for the HD Stars; vol. 5*

Maitzen, H. M. 1976, *Astron. Astrophys.*, **51**, 223

Netopil, M., Paunzen, E., Hümmerich, S., & Bernhard, K. 2017, *Mon. Not. R. Astron. Soc.*, **468**, 2745

Paunzen, E., Netopil, M., & Bord, D. J. 2011, *Mon. Not. R. Astron. Soc.*, **411**, 260

Paunzen, E., Stütz, C., & Maitzen, H. M. 2005, *Astron. Astrophys.*, **441**, 631

Renson, P. & Manfroid, J. 2009, *Astron. Astrophys.*, **498**, 961

Contrib. Astron. Obs. Skalnaté Pleso **48**, 292 – 293, (2018)

Investigating stellar magnetism (in evolved stars) in Mexico

L. Sabin, J. Ramiréz Veléz, D. Hiriart, J. H. Castro Chacón, M. Nuñez and J. Valdez

Universidad Nacional Autónoma de México, Instituto de Astronomía, Km 103 Carretera Tijuana - Ensenada C.P. 22860, Ensenada, B.C, México (E-mail: lsabin@astro.unam.mx)

Received: November 9, 2017; Accepted: November 14, 2017

Abstract. We present the latest instrumental and theoretical developments performed at the Universidad Nacional Autónoma de México (UNAM) regarding the search and analysis of magnetic fields in various type of stars among the more evolved ones. This work is the prelude to a wider assessment of magnetism across the Hertzsprung-Russell diagram.

Key words: polarization – magnetic fields – radiative transfer – instrumentation: polarimeters – stars: magnetic field

1. Introduction

Polarimetric data have been used to determine the geometry and intensity of magnetic fields of astronomical objects along the Hertzsprung-Russell diagram. However, in the case of intermediate evolved stars (e.g. Post-AGB stars and PNe), few observational data regarding the measurement of the magnetic fields intensity using optical spectropolarimetry (Sabin et al., 2015), have been so far obtained. We therefore present the latest instrumental and theoretical developments performed at UNAM regarding the detection and analysis of magnetic fields in various stars and particularly the evolved ones.

2. FICUS: The FIber Coupled Unit System

The 2.1m telescope at the San Pedro Mártir Observatory in Mexico (OAN-SPM) is now equipped with a polarimetric unit designed and built at the Institute of Astronomy of UNAM in Ensenada (Mexico). FICUS, the FIber Coupled Unit System, is a polarization module that can be connected to the spectrographs of the OAN via a set of optical fibers (Fig. 1–left). This system would thus provide good quality polarimetric data. Only the polarimetric module is attached to the telescope, and since the spectrograph is detached, more stability is obtained for the spectropolarimetric data. Finally, as its name suggests, FICUS can be coupled to any spectrograph located at the OAN, implying that either low, medium or high resolution are achievable. FICUS is now in its ultimate commissioning phase with the low resolution Boller & Chivens spectrograph.

3. Spectropolarimetic data analysis with the PCA/ZDI method

In order to analyse the data obtained with FICUS (or any other spectropolarimeter) and study the magnetic fields, a new data inversion code has been developed at IA-UNAM (Fig. 1–right). The latter is based on the technique of Principal Components Analysis (PCA) associated to theoretical radiative transfer models (PCA/ZDI). It will therefore be possible to have a robust estimation of the intensity (Ramírez Vélez et al. 2016; Ramiréz Veléz, in prep.).

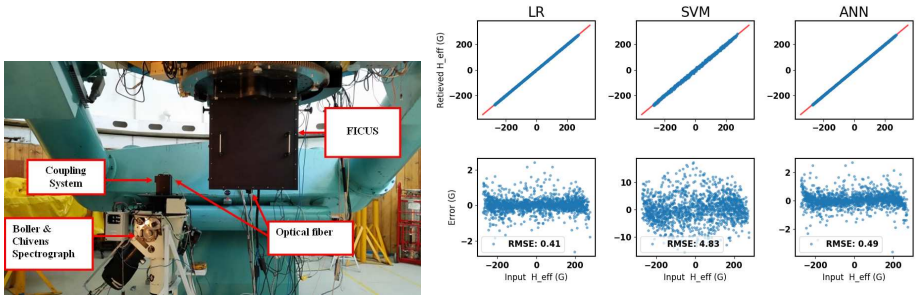

Figure 1. *Left*: Full polarimetric system mounted on the 2.1m with the Boller & Chivens spectrograph. *Right*: Accuracy of the inversions of a sample of 1 500 MZS, using three different algorithms, all based in a machine learning approach. With LR: Linear Regression (Bayesian Ridge), SVM: Support Vector Machine, ANN: Artificial Neuronal Network. (Ramírez Vélez et al., in prep).

Acknowledgements. The authors thank the personal of the OAN-SPM for their help in all the different aspects of this project. We are supported by the CONACYT project 180817.

References

Ramírez Vélez, J. C., Stift, M. J., Navarro, S. G., et al., 2016, *Astron. Astrophys.*, **596**, A62

Sabin, L., Wade, G. A., & Lèbre, A. 2015, *Mon. Not. R. Astron. Soc.*, **446**, 1988

Contrib. Astron. Obs. Skalnaté Pleso **48**, 294 – 295, (2018)

Physical properties of three young magnetic chemically peculiar stars

E. Semenko[1] **and E. Semenova**[2]

[1] *Special Astrophysical Observatory, Nizhnii Arkhyz, Russia, 369167, (E-mail: sea@sao.ru)*

[2] *Kazan Federal University, Kazan, Russia, 420008*

Received: November 9, 2017; Accepted: January 2, 2017

Abstract. We report the recent measurements of a longitudinal effective magnetic field and the estimations of physical parameters for three young chemically peculiar stars.

Key words: stars: atmospheres – stars: magnetic field

1. Stars selection and observations

The origin of magnetic fields in early-type stars remains an open question, and magnetic chemically peculiar stars are perfect test-beds here.

We have searched the catalog by Renson & Manfroid (2009) for young magnetic stars based on the criteria of objects having outlying SrCrEu-type anomalies banded with early spectral classes, and selected two poorly studied stars: HD 50341 and HD 63347. Later we added HD 201174, previously known from observations to be A0 SrCrEu magnetic star.

The current study is based on spectropolarimetric observations carried out with the 6-m telescope at the Special Astrophysical Observatory. Raw data was reduced with the use of ESO-MIDAS system.

2. Physical parameters and magnetic field

We have attempted to estimate basic physical parameters from the H_β spectral region using the SME code (Piskunov & Valenti, 2017) assuming the stars to be non-magnetic. If present, we also used Geneva or Strömgren photometric data to estimate $T_{\rm eff}$ and $\log g$.

Stellar physical parameters obtained from different sources are reviewed in Table 1. According to the listed values of the effective temperature and luminosity, the stars lay near ZAMS on a theoretical HR diagram.

Magnetic properties of the stars were obtained from time series of the effective magnetic field (B_l) measurements. For HD 50341 and HD 63347, we have found the presence of the magnetic field for the first time. Also, we found rotational periods derived from magnetic measurements to be in perfect agreement

Table 1. Derived physical parameters and rotational characteristics of sample stars.

	HD 50341	HD 63347	HD 201174
$T_{\rm eff}$ (phot), K	10 870	–	9 690
$\log g$ (phot)	4.3	–	3.8
$T_{\rm eff}$ (spec), K	10 800	11 600	9 600
$\log g$ (spec)	4.0	4.5	4.0
$v_{\rm e} \sin i$, km s^{-1}	50	43	< 20
$\log L/{\rm L}_\odot$	1.67	1.66	1.45
$P_{\rm rot}$, days	2.5094	1.7495	2.4300

with those mentioned in the literature. Rotational period of HD 201174 was derived, to our knowledge, for the first time.

The best-fit model for longitudinal field phase curves of HD 63347 and HD 201174 is a two harmonic extension of periodic functions (see Fig. 1). HD 50341 has the weakest field in the sample, which does not allow to draw any conclusions about its topology.

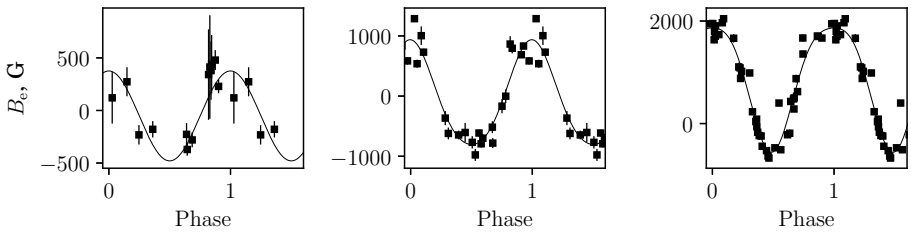

Figure 1. From left to right: phase curves of the longitudinal field of HD 50341, HD 63347, and HD 201174.

Acknowledgements. This work is supported by the Russian Science Foundation, grant No.14-50-00043.

References

Piskunov, N. & Valenti, J. A. 2017, *Astron. Astrophys.*, **597**, A16

Renson, P. & Manfroid, J. 2009, *Astron. Astrophys.*, **498**, 961

Contrib. Astron. Obs. Skalnaté Pleso **48**, 296 – 297, (2018)

O-type magnetic stars space distribution

S. V. Shulman and A. F. Kholtygin

Saint Petersburg State University, Saint Petersburg, Russia

Received: November 8, 2017; Accepted: December 20, 2017

Abstract. We have compiled the measurements from Hubrig et al. (2011), Hubrig et al. (2013), Grunhut et al. (2017), Schöller et al. (2017) into a catalog of 150 stars and distinguished the "magnetic" stars according to the condition: $\langle B \rangle > 3\sigma$ at least for one measurement, and explored their space distribution. The catalog contains 28 "magnetic" stars, 91 stars with measured parallaxes, and only 15 of them are "magnetic".

Key words: stars: magnetic field – stars: distances

1. Spatial Density

The spatial density of stars is calculated as the ratio of stars number in spherical layer centered on the Sun to its volume (Fig. 1).

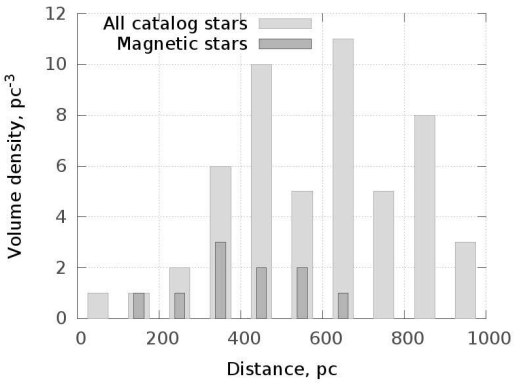

Figure 1. The spatial density of stars vs. their distances to the Sun. Magnetic stars are labeled by dark--gray color, all catalog stars – by light-gray. A large fraction of the catalog stars has no measured parallaxes. We suppose that they are located farther than 1 kpc from the Sun.

2. Surface density

We determine the stars surface density as the ratio of the number of stars in the zone of sphere to its area in steradians. Latitude and longitude distributions of the surface density are shown in Fig. 2 (a, b).

It is also useful to consider the ratio of magnetic stars density to all catalog stars density to estimate directions in Galaxy, where the magnetic stars fraction is maximal. Figure 2 (c, d) shows this ratio as function of the galactic latitude and longitude.

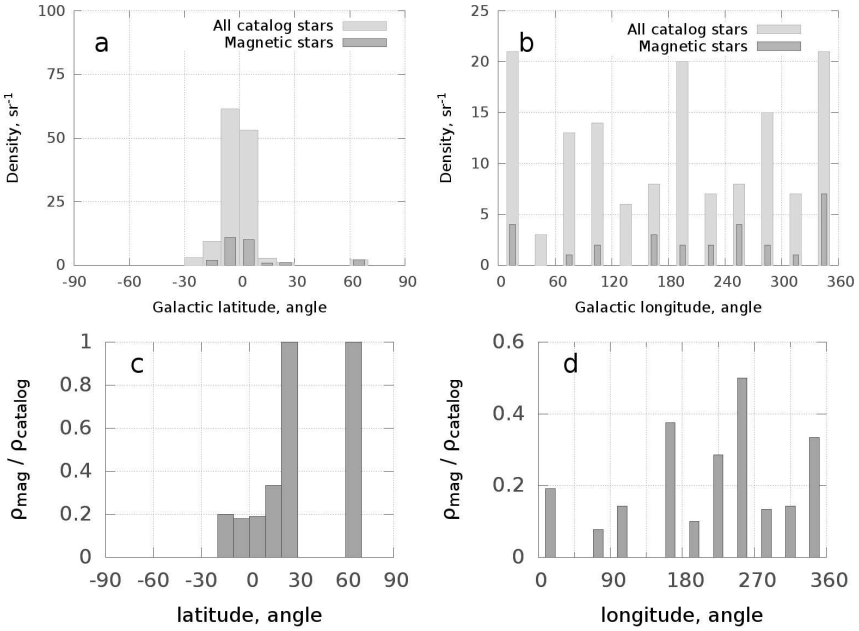

Figure 2. The stars surface densities (a, b) and their ratio (c, d) vs. galactic coordinate. Panel a, c: latitude distribution, panel b, d: longitude distribution.

3. Conclusions

There is a strong selection of the magnetic field measurements on the galactic latitude. There are no measurements for stars with $|b| > 30°$. The ratio of the angle densities of magnetic to all stars in the solar vicinity for $|b| < 30°$ is nearly constant.

Acknowledgements. This work was supported by the Russian Scientic Foundation grant N 16-02-00604 A.

References

Grunhut, J. H., Wade, G. A., Neiner, C., et al. 2017, *Mon. Not. R. Astron. Soc.*, **465**, 2432

Hubrig, S., Schöller, M., Ilyin, I., et al. 2013, *Astron. Astrophys.*, **551**, A33

Hubrig, S., Schöller, M., Kharchenko, N. V., et al. 2011, *Astron. Astrophys.*, **528**, A151

Schöller, M., Hubrig, S., Fossati, L., et al. 2017, *Astron. Astrophys.*, **599**, A66

Contrib. Astron. Obs. Skalnaté Pleso **48**, 298 – 299, (2018)

HD 156324: A Tidally Locked Magnetic SB3 With an Orbitally Disrupted Centrifugal Magnetosphere

M. Shultz[1], Th. Rivinius[2], G. A. Wade[3], E. Alecian[4], O. Kochukhov[1] and the BinaMIcS Collaboration

[1] *Department of Physics and Astronomy, Uppsala University, Box 516, Uppsala 75120, (E-mail: matt.shultz@gmail.com)*

[2] *ESO - European Organisation for Astronomical Research in the Southern Hemisphere, Casilla 19001, Santiago 19, Chile*

[3] *Department of Physics, Royal Military College of Canada, Kingston, Ontario K7K 7B4, Canada*

[4] *Univ. Grenoble Alpes, CNRS, IPAG, F-38000 Grenoble, France*

Received: November 8, 2017; Accepted: December 22, 2017

Abstract. Period analysis of radial velocity, equivalent width, and magnetic measurements of the SB3 system HD 156324 yield identical results in all cases, indicating the system is tidally locked with orbital and rotational periods of 1.58 d. Its Hα emission profile exhibits marked morphological departures from the usual pattern observed amongst magnetic B-type stars, which can plausibly be ascribed to tidal disruption of the gravitocentrifugal potential.

Key words: stars: individual: HD 156324 – stars: magnetic field – binaries: spectroscopic – binaries (including multiple): close – stars: massive

HD 156324 is a triple Spectroscopic Binary (SB3) system (Alecian et al., 2014) in the Sco OB4 association (Kharchenko et al., 2005), consisting of a He-strong B2V primary, a B6V secondary, and a PGa B6V tertiary; since the system is a hierarchical triple we designate these components Aa, Ab, and B, respectively. The primary (Aa) has a strong magnetic field, and displays Hα emission indicative of a Centrifugal Magnetosphere (CM; Petit et al. 2013). We have obtained a large dataset of high-resolution ESPaDOnS spectropolarimetry and FEROS spectroscopy with which to determine the system's orbital, rotational, and magnetic properties.

Radial velocities (RVs) were measured from the Mg II 448.1 nm line, in which all three components are clearly detected, using a parametric fitting algorithm described by Grunhut et al. (2017). The RVs of the He-strong star and the secondary vary in antiphase, as expected. Frequency analysis of the Aab RVs using Lomb-Scargle statistics yields a period of 1.5805(10) d, which we take to be the orbital period $P_{\rm orb}$. The same analysis of the B component's RVs yields two significant periods: one around 2 years, and the second of 6.67(2) d. We interpret the short-term variation as orbital motion with an undetected, low-

mass fourth star, and the long-term variation as the orbit of the B sub-system around the more massive A sub-system.

The longitudinal magnetic field $\langle B_z \rangle$ of the Aa component was evaluated from Least-Squares Deconvolution (LSD; Kochukhov et al. 2010) profiles which we disentangled using the iterative process described by González & Levato (2006) so as to remove the contributions of Ab and B from the Stokes I profiles. $\langle B_z \rangle$ varies between 0 and 3 kG, with a typical uncertainty of ∼300 G. Period analysis of $\langle B_z \rangle$ yields a rotational period $P_{\rm rot} = 1.5804(3)$ d, identical within uncertainty to $P_{\rm orb}$.

Since the magnetospheric Hα emission should also be modulated with $P_{\rm rot}$, we measured the Hα equivalent width, and found $P_{\rm rot} = 1.5806(3)$ d, again identical within uncertainty to $P_{\rm orb}$. We infer that Aab is tidally locked. Consistent with this, the eccentricity $e \sim 0$, the rotational and orbital inclination angles are both about 25°, and the semi-major axis and Kepler corotation radius are both at about 3 R_*.

The Hα emission is notable in that it shows only a single emission bump, i.e. there is evidence for only one plasma cloud, whereas two are expected theoretically (Townsend & Owocki, 2005), and invariably observed in CM-host stars (Petit et al., 2013). Maximum RV separation of the Aab components occurs at the same phase as maximum Hα emission, indicating that the plasma cloud and the Ab component are directly opposite one another, i.e. Ab occupies the expected position of the missing cloud. This suggests that modification of the gravitocentrifugal potential by the presence of a close companion may explain the missing emission cloud.

References

Alecian, E., Kochukhov, O., Petit, V., et al. 2014, *Astron. Astrophys.*, **567**, A28

Donati, J.-F., Semel, M., Carter, B. D., Rees, D. E., & Collier Cameron, A. 1997, *Mon. Not. R. Astron. Soc.*, **291**, 658

González, J. F. & Levato, H. 2006, *Astron. Astrophys.*, **448**, 283

Grunhut, J. H., Wade, G. A., Neiner, C., et al. 2017, *Mon. Not. R. Astron. Soc.*, **465**, 2432

Kharchenko, N. V., Piskunov, A. E., Röser, S., Schilbach, E., & Scholz, R.-D. 2005, *Astron. Astrophys.*, **438**, 1163

Kochukhov, O., Makaganiuk, V., & Piskunov, N. 2010, *Astron. Astrophys.*, **524**, A5

Petit, V., Owocki, S. P., Wade, G. A., et al. 2013, *Mon. Not. R. Astron. Soc.*, **429**, 398

Townsend, R. H. D. & Owocki, S. P. 2005, *Mon. Not. R. Astron. Soc.*, **357**, 251

ud-Doula, A. & Owocki, S. P. 2002, *Astrophys. J.*, **576**, 413

Contrib. Astron. Obs. Skalnaté Pleso **48**, 300 – 301, (2018)

On the structure of magnetized accretion flows in the system of Beta Lyrae

M. Yu. Skulsky

Lviv Polytechnic National University, Lviv, Ukraine
(E-mail: mysky@polynet.lviv.ua)

Received: November 14, 2017; Accepted: November 17, 2017

Abstract. In this paper we show the structure of gas flows between the components of the massive interacting system Beta Lyrae.
Key words: stars: individual: Beta Lyrae – magnetic fields – stars: magnetic field – binaries: general

1. Introduction

We show that the structure of gas flows between the components of the well-known massive interacting system Beta Lyrae is due, above all, to the presence of the magnetic field of the donor with an axis directed along the phases 0.35–0.85 P and deflected relative to the gravitational axis of this binary system (Skul'Kij, 1985; Skul'Skij & Plachinda, 1993).

In the phase range around 0.8–0.9 P this field is maximal and the axis of its dipole on the donor surface is closest to the accretion disk. This presumes the presence of more effective shock collisions of the magnetized plasma in the phases of the second quadrature 0.6–0.9 P. This leads to the observation of the hot arc on the accretion disk rim facing the donor (Skulsky, 2015).

The configuration of the donor magnetic field and the gravitation of the massive accretor explain also the hotter region on the accretion disk, which dominates in accordance with Mennickent & Djurašević (2013) in the phases near 0.80 P. This region on the disk can be formed by collision with this disk of magnetized gas which is channeled by the magnetic field of the donor in the direction of the massive accretor. The energy effect from the collision on the disk is significantly strengthened here by the opposite rotation of the disk rim at velocities up to 250 $\mathrm{km\,s^{-1}}$ towards the falling gas flows. The specific configuration of the magnetic field of the donor is an influencing factor on the mass transfer, evidenced by analysis of the absolute spectrophotometry, curves of magnetic field changes, intensities and radial velocities of spectral lines with the phases of the orbital period, and also the study of circumstellar gas structures, their dynamics and energetics (Alekseev & Skulskii, 1989; Burnashev & Skul'Skii, 1991; Skul'Skii & Mal'Kov, 1992).

As a result of high-energy a collision of ionized plasma, which is canalized by the donor's magnetic field, with the accretion disk is generating a scattering gas

shell that partially masks the components of this binary system outside of the Lyman limit and completely in the soft X-ray region (Hack et al., 1977; Polidan, 1989; Kondo et al., 1994; Ignace et al., 2008). The problem of the real existence and physical nature of jet-like structures in the Beta Lyrae system can be solved in a similar way.

References

Alekseev, G. N. & Skulskii, M. Y. 1989, *Astrofiz. Issled. Izv. Spets. Astrofiz. Obs.*, **28**, 18

Burnashev, V. I. & Skul'Skii, M. Y. 1991, *Bull. Crimean Astrophys. Obs.*, **83**, 95

Hack, M., Hutchings, J. B., Kondo, Y., & McCluskey, G. E. 1977, *Astrophys. J., Suppl. Ser.*, **34**, 565

Ignace, R., Oskinova, L. M., Waldron, W. L., Hoffman, J. L., & Hamann, W.-R. 2008, *Astron. Astrophys.*, **477**, L37

Kondo, Y., McCluskey, G. E., Silvis, J. M. S., et al. 1994, *Astrophys. J.*, **421**, 787

Mennickent, R. E. & Djurašević, G. 2013, *Mon. Not. R. Astron. Soc.*, **432**, 799

Polidan, R. S. 1989, *Space Sci. Rev.*, **50**, 85

Skul'Kij, M. Y. 1985, *Pis'ma Astron. Zh.*, **11**, 51

Skul'Skii, M. Y. & Mal'Kov, Y. F. 1992, *Astron. Zh.*, **69**, 291

Skul'Skij, M. Y. & Plachinda, S. I. 1993, *Astronomy Letters*, **19**, 203

Skulsky, M. 2015, *Science and Education a New Dimension. Natural and Technical Sciences*, **54**, 6

Contrib. Astron. Obs. Skalnaté Pleso **48**, 302 – 304, (2018)

Transition disk stars in the NGC 2264 cluster - Accretion diagnostic

A. P. Sousa[1] **and S. H. P. Alencar**[1,2]

[1] *Departamento de Física-ICEx-UFMG Antônio Carlos, 6627, 31270-290. Belo Horizonte, MG, Brazil, (E-mail: alana@fisica.ufmg.br)*

[2] *Univ. Grenoble Alpes, IPAG, F-38000 Grenoble, France*

Received: December 25, 2017; Accepted: December 29, 2017

Abstract. Disk holes are inferred from infrared observations of T Tauri stars, indicating the existence of a transitional phase between thick accreting disks and debris disks. Using data from the observational multiwavelength campaign CSI2264, we analyzed 410 stars belonging to NGC 2264 and found about 7% transition disk candidates. We characterized these star-disk systems using accretion diagnostics and we compared them with star-disk systems with full disks and diskless. We were able to evaluate the influence of disk evolution on the observed accretion characteristics.

Key words: open clusters and associations: individual: NGC 2264 – stars: pre-main sequence – accretion, accretion disks

1. Overview and Results

Transition disks are systems with a hole in the inner disk that are characterized by a lack of emission, above the photospheric level, in near-infrared wavelengths and an excess of emission like thick disk in mid-infrared bands (Owen, 2016). We searched for transitional disk candidates belonging to the young stellar cluster NGC 2264 (~ 3 Myr and d ~ 760 pc; Dahm, 2008) to characterize these systems in terms of accretion diagnostics, such as Hα emission and UV excess.

Our sample is composed of 410 stars that were observed with *Spitzer*/IRAC (Teixeira et al., 2012) and CFHT/Megacam (Venuti et al., 2014). We constructed SEDs (spectral energy distributions) of all these stars and modelled them with the Hyperion SED model (Robitaille, 2017). We found 28 transition disk candidates (stars with an inner hole according to the SED modelling and that have 24 μm flux above the photospheric level), 212 stars with a full disk and 170 diskless stars (see Fig. 1). This number of transition disks (~ 7 % of the total of 410 stars that we analyzed) confirms that the disk dispersal is rapid compared to the disk lifetime, as was also reported in the literature (Owen, 2016).

The Hα emission in a T Tauri star comes mostly from the accretion funnel, then this line is used as accretion diagnostics (White & Basri, 2003). In our sample, 82 % of the transition disk candidates are accreting, which shows the

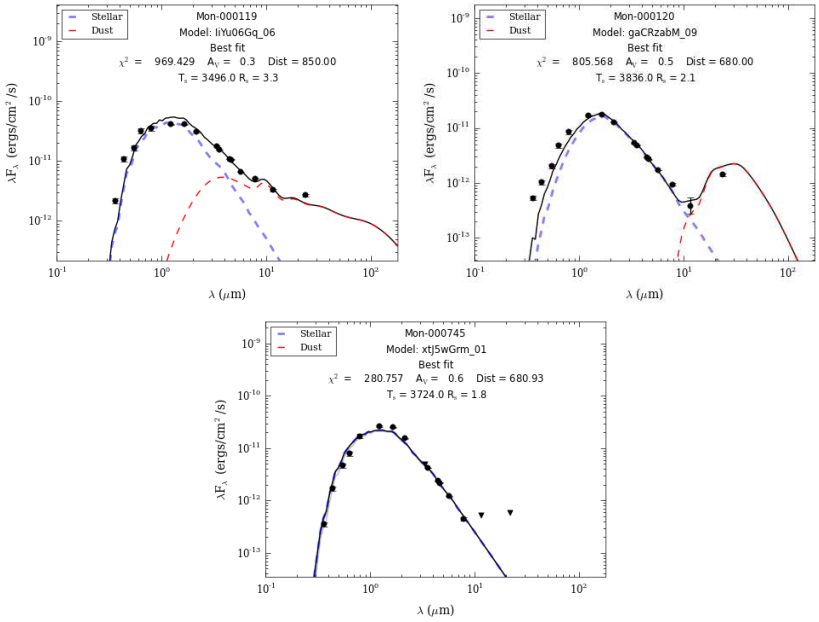

Figure 1. Examples of SEDs for systems with a full disk (left upper panel), a transition disk candidate (right upper panel) and diskless (lower panel). The circles show the observed data published by Rebull et al. (2002) and Wright et al. (2010). The black solid line is the best data fit and the dashed lines are stellar and dust emission components (Robitaille, 2017).

presence of a hole in a disk does not stop the accretion process. The UV excess above the photospheric level, in a T Tauri star, comes from hot spots, consequently the UV excess can also be used as a diagnostic for accretion (Venuti et al., 2014). We deduce from Fig. 2 that diskless systems do not have an UV excess, while full disk systems, which are expected to be accreting, have an UV excess. Transition disk candidates, in general, show an UV excess like full disk systems, and this is consistent with the picture of an active accretion. With the UV excess, Venuti et al. (2014) calculated mass accretion rates for the T Tauri stars in NGC 2264. We show in Fig. 2 that mass accretion rates for stars with transition and full disks are of the same level, the mean values are $(1.78 \pm 0.82) \times 10^{-8}\,\mathrm{M}_\odot\,\mathrm{yr}^{-1}$ and $(1.69 \pm 0.30) \times 10^{-8}\,\mathrm{M}_\odot\,\mathrm{yr}^{-1}$, respectively.

2. Conclusions

The presence of a hole in the inner disk does not stop the accretion process, because 82 % of transition disk stars are accreting and show Hα, UV excess and

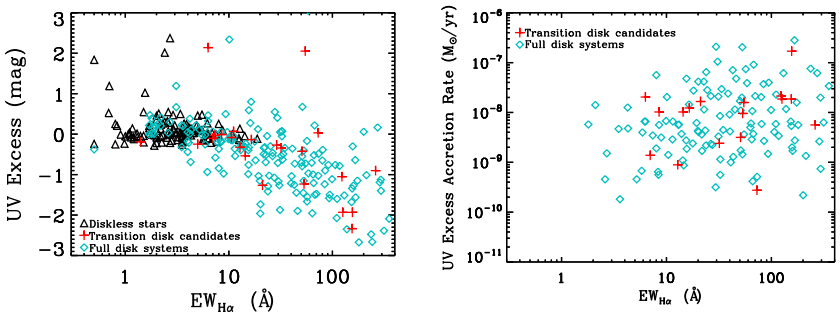

Figure 2. UV excess (left) and mass accretion rates (right) calculated by Venuti et al. (2014) as a function of the Hα equivalent width (Sousa et al., 2016; Dahm & Simon, 2005).

mass accretion rates at the same level as accreting systems.

Acknowledgements. The authors wish to thank Luisa Rebull for sharing with us the photometric data and CNPq, FAPEMIG and CAPES for funding this research.

References

Dahm, S. E. 2008, *The Young Cluster and Star Forming Region NGC 2264*, ed. B. Reipurth, 966

Dahm, S. E. & Simon, T. 2005, *Astron. J.*, **129**, 829

Owen, J. E. 2016, *PASA*, **33**, e005

Rebull, L. M., Makidon, R. B., Strom, S. E., et al. 2002, *Astron. J.*, **123**, 1528

Robitaille, T. P. 2017, *Astron. Astrophys.*, **600**, A11

Sousa, A. P., Alencar, S. H. P., Bouvier, J., et al. 2016, *Astron. Astrophys.*, **586**, A47

Teixeira, P. S., Lada, C. J., Marengo, M., & Lada, E. A. 2012, *Astron. Astrophys.*, **540**, A83

Venuti, L., Bouvier, J., Flaccomio, E., et al. 2014, *Astron. Astrophys.*, **570**, A82

White, R. J. & Basri, G. 2003, *Astrophys. J.*, **582**, 1109

Wright, E. L., Eisenhardt, P. R. M., Mainzer, A. K., et al. 2010, *Astron. J.*, **140**, 1868

Contrib. Astron. Obs. Skalnaté Pleso **48**, 305 – 306, (2018)

Multiple, short-lived "stellar prominences" on the O giant ξ Persei: a magnetic star?

N. Sudnik[1] **and H. F. Henrichs**[2]

[1] *Belarussian State Pedagogical University, 220050, Sovetskaya 18, Minsk, Belarus, (E-mail: snata.astro@gmail.com)*

[2] *Anton Pannekoek Institute for Astronomy, University of Amsterdam, Science Park 904, 1098 XH Amsterdam, The Netherlands*

Received: October 22, 2017; Accepted: November 2, 2017

Abstract. We present strong evidence for a rotation period of 2.0406 d of the O giant ξ Persei, derived from the N IV λ1718 wind line in 12 yr of IUE data. We predict that ξ Per has a magnetic dipole field, with superposed variable magnetic prominences. Favorable dates for future magnetic measurements can be predicted. We also analysed time-resolved He II 4686 spectra from a campaign in 1989 by using the same simplified model as before for λ Cephei, in terms of multiple spherical blobs attached to the surface, called stellar prominences (Sudnik & Henrichs, 2016). These represent transient multiple magnetic loops on the surface, for which we find lifetimes of mostly less than 5 h.

Key words: stars: early-type – stars: individual: ξ Persei – stars: magnetic field – stars: winds, outflows – stars: rotation

1. Stellar rotation and wind variability

The well documented cyclic variability on the estimated rotational timescale in UV wind lines of early-type stars still lack a proper explanation. Except for the $\sim$ 7% of O stars with a dipolar magnetic field (Grunhut et al., 2017), the unknown rotation period often hinders modeling of the many variable surface phenomena, which likely drive the wind variability. To search for the rotation period of the O7.5III(n)((f)) star ξ Per ($v \sin i = 230\,\mathrm{km\,s^{-1}}$) we analysed the equivalent-width (EW) variations of the N IV λ1718 line in 307 IUE spectra over 12 years in the velocity range $[-405\,\mathrm{km\,s^{-1}}, v \sin i]$, which represents the lower wind. In the power spectrum (Fig. 1, top left), we identify the peak at 2.04058 d as the rotation period. We can exclude twice this value, as often used before, because of the constraining stellar radius of $\sim$11 $R_\odot$. The phase-folded data shows a sinusoidal behavior (Fig. 1, bottom left, which includes the ephemeris). The most likely explanation is that the star hosts a magnetic field with maximum strength at maximum EW. For a dipolar field, the footpoints of strong UV DACs should stem from only one of the magnetic poles. With the implied $i = 56°$, and only one pole visible, β should be near $\sim 90° - i = 34°$. Such a field has been hitherto undetected, possibly because of its weakness, and/or because all magnetic measurements so far have been taken at unfavorable phases.

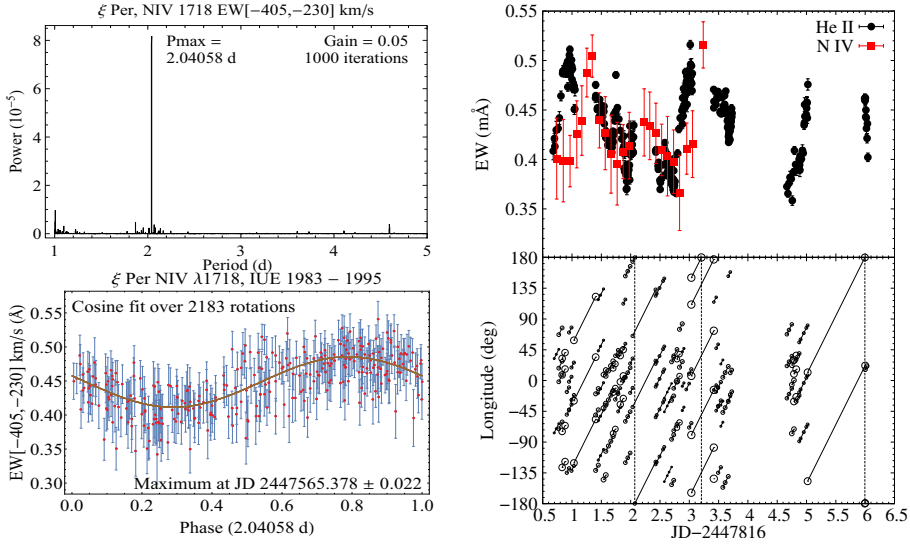

Figure 1. *Top left:* Cleaned power spectrum of N IV λ1718 EWs. *Bottom left:* Phase plot of 307 datapoints over 12 years. *Top right:* Overplot of scaled N IV and He II EWs in 1989, showing a similar trend. *Bottom right:* Model fit results of subsequent quotient He II spectra displayed as circles at the fitted stellar longitude with 0° at the line of sight and size proportional to the fitted optical depth ($0.08 < \tau < 0.38$).

2. Model fits of He II λ4686 spectra

We applied the same stellar prominence model as for λ Cep (Sudnik & Henrichs, 2016) to 322 He II λ4686 spectra with 6 d coverage in 1989 of ξ Per. To fit subsequent quotient spectra, multiple (≤ 5) prominences with lifetimes up to 5 h are needed (Fig. 1, bottom right). These are proposed to be at the footpoints of weaker intermediate DACs. Cancellation effects may make magnetic detection of these prominences difficult (Kochukhov & Sudnik, 2013). Similar behavior is also observed in other O stars, which suggests a common phenomenon.

References

Grunhut, J. H., Wade, G. A., Neiner, C., et al. 2017, *Mon. Not. R. Astron. Soc.*, **465**, 2432

Kochukhov, O. & Sudnik, N. 2013, *Astron. Astrophys.*, **554**, A93

Sudnik, N. P. & Henrichs, H. F. 2016, *Astron. Astrophys.*, **594**, A56

Contrib. Astron. Obs. Skalnaté Pleso **48**, 307 – 311, (2018)

Observing and modelling magnetic fields in white dwarfs

S. Vennes[1], A. Kawka[1], L. Ferrario[2] and E. Paunzen[3]

[1] *Astronomical Institute of the Czech Academy of Sciences*
251 65 Ondřejov, The Czech Republic, (E-mail: vennes@asu.cas.cz)
[2] *Australian National University, Canberra, Australia*
[3] *Masaryk University, Brno, Czech Republic*

Received: October 31, 2017; Accepted: November 6, 2017

Abstract. Our ongoing spectroscopic survey of high proper motion stars is a rich source of new magnetic white dwarfs. We present a few examples among cool white dwarfs showing the effect of field strength and geometry on the observed optical spectrum. Modelling of hydrogen and heavy element spectral lines reveals a range of uniform or markedly offset dipole fields in these objects.
Key words: white dwarfs – magnetic fields – techniques: spectroscopic

1. Observations

Magnetic white dwarfs account for a substantial fraction of the population of white dwarf stars (Kawka et al., 2007). Spectroscopic surveys (Kawka & Vennes, 2012) routinely uncover new candidates showing a great diversity in field strength and geometry (Landstreet et al., 2017). Our most recent observations were obtained with ESO's FOcal Reducer and low-dispersion Spectrograph 2 (FORS2) and the intermediate-dispersion X-shooter spectrograph both on ESO's Very Large Telescopes (VLTs). Detailed modelling of spectroscopic time series often reveals complex surface field structures or the presence of a close degenerate companion, as observed in the case of NLTT 12758 (Kawka et al., 2017).

2. Modeling and analysis

We followed a methodology described in Martin & Wickramasinghe (1984) and Achilleos & Wickramasinghe (1989) and modelled the field distribution in magnetic hydrogen-rich white dwarfs, known as DAH white dwarfs, using a dipole of strength B_p which may be offset along the polar axis by a fraction of the radius a_z and inclined with respect to the viewer at an angle i. We divided the surface into 450 elements along the surface longitude and latitude and integrated the emergent intensity spectrum. These model spectra describe average surface field properties at a particular time and do not account for possible blurring caused by a short rotation period.

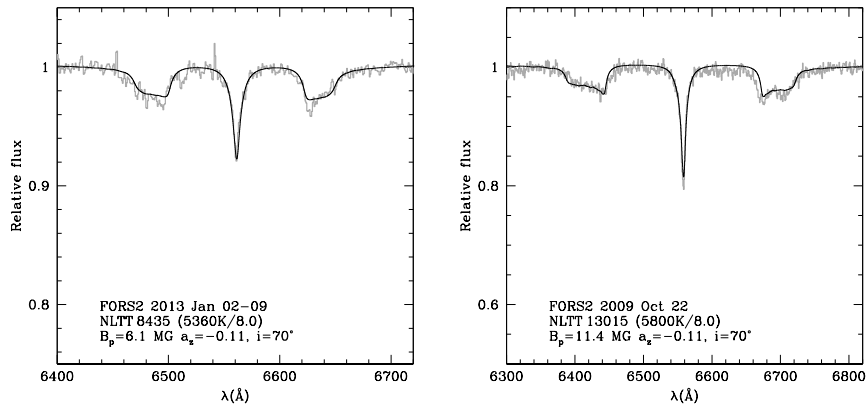

Figure 1. Observation and modelling (Hα) of the DAH white dwarfs NLTT 8435 (left) and NLTT 13015 (right).

2.1. Hydrogen Balmer lines

The hydrogen Balmer spectra were computed using line strengths and Zeeman shifts from Garstang & Kemic (1974). The following examples illustrate the method. The new magnetic white dwarf NLTT 8435 ($B_p = 6.1$ MG) is relatively cool ($\approx$ 5360 K) and hydrogen-rich (Fig. 1). Photometric time series obtained with the Danish 1.54-m telescope revealed a likely rotation period of 95 minutes (Fig. 2). We also observed radial velocity variations of at least 60 km s^{-1} that are not related to surface field variations but, instead, caused by the presence of a close, unseen companion. The cool magnetic white dwarf NLTT 13015 is also hydrogen-rich and exhibits marked field variations around a mean polar field of $\approx$12 MG. Figure 1 shows one of the three individual exposures obtained with FORS2: The best-fitting model implies a field strength of 11.4 MG and a small offset along the polar axis of -11%.

2.2. Heavy elements

White dwarf atmospheres are often contaminated with trace heavy elements (Zuckerman et al., 2003). Some cool and polluted hydrogen-rich white dwarfs known as DAZH white dwarfs such as NLTT 7547 (Kawka et al. 2018, in preparation) and NLTT 53908 (Kawka & Vennes, 2014) show strong CaH&K lines imbedded in a magnetic field with strengths ranging from $\approx 10^5$ to 10^6 G. Other trace elements are also seen in the spectra of these objects (e.g., sodium, magnesium, aluminum, and iron) and modelling of spectral line shapes should provide additional constraints on the strength and structure of the magnetic field.

We computed detailed line profiles following the procedure described in Kawka & Vennes (2011) but updated with offset dipole field distributions de-

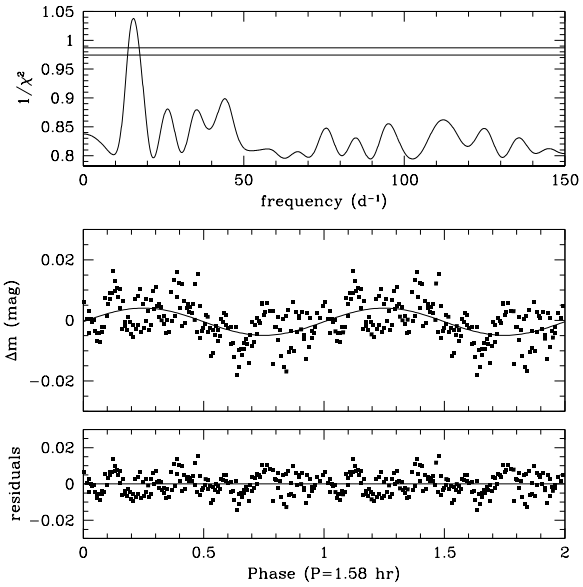

Figure 2. Photometric (R-band) time series (middle panel) and residuals (bottom panel) of NLTT 8435 obtained with the Danish 1.54-m telescope. The period analysis finds a significant periodicity near 95 minutes (top panel).

scribed above and assuming quadratic Zeeman line splitting following Landi Degl'Innocenti & Landolfi (2004). The updated Zeeman patterns agree with earlier calculations employing Kemic (1975). Figure 3 shows the calcium K line in two polluted, magnetic white dwarfs. In the case of NLTT 7547, the broad line shape requires a field spread characteristic of a centered dipole ($a_z = 0$) of 240 kG, while in the case of NLTT 53908, the narrow Zeeman components require a marked offset ($a_z = -0.2$) and a dipole field of 635 kG.

3. Discussion

Kawka & Vennes (2014) found evidence of field enhancement among cool, polluted hydrogen-rich white dwarfs. This simple fact can be interpreted either as evidence of a correlation between magnetic field strength and heavy element pollution, or as a field enhancement in *all* cool white dwarfs.

Ultimately, this project aims at delivering field structure and binary properties for a large sample of magnetic white dwarfs and constrain population statistics. In particular we seek to determine the fraction of magnetic white dwarfs as a function of age, companionship, and spectral type.

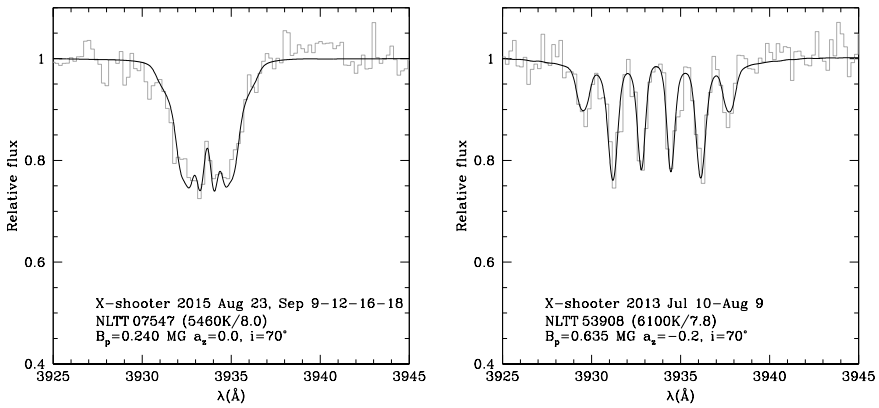

Figure 3. Observation and modelling (Ca K) of the DAZH white dwarfs NLTT 7547 (left) and NLTT 53908 (right).

Acknowledgements. A.K., L.F. and S.V. acknowledge support from the Czech Science Foundation (15-15943S). This work is based on observations made with ESO telescopes at the La Silla Paranal Observatory under programme IDs 84.D-0862, 90.D-0473, 091.D-0267 and 095.D-0311, and at Kitt Peak National Observatory and Cerro Tololo Inter-American Observatory (National Optical Astronomy Observatory).

References

Achilleos, N. & Wickramasinghe, D. T. 1989, *Astrophys. J.*, **346**, 444

Garstang, R. H. & Kemic, S. B. 1974, *Astrophys. Space Sci.*, **31**, 103

Kawka, A., Briggs, G. P., Vennes, S., et al. 2017, *Mon. Not. R. Astron. Soc.*, **466**, 1127

Kawka, A. & Vennes, S. 2011, *Astron. Astrophys.*, **532**, A7

Kawka, A. & Vennes, S. 2012, *Mon. Not. R. Astron. Soc.*, **425**, 1394

Kawka, A. & Vennes, S. 2014, *Mon. Not. R. Astron. Soc.*, **439**, L90

Kawka, A., Vennes, S., Schmidt, G. D., Wickramasinghe, D. T., & Koch, R. 2007, *Astrophys. J.*, **654**, 499

Kemic, S. B. 1975, *Astrophys. Space Sci.*, **36**, 459

Landi Degl'Innocenti, E. & Landolfi, M., eds. 2004, Astrophysics and Space Science Library, Vol. **307**, *Polarization in Spectral Lines*

Landstreet, J. D., Bagnulo, S., Valyavin, G., & Valeev, A. F. 2017, *Astron. Astrophys.*, **607**, A92

Martin, B. & Wickramasinghe, D. T. 1984, *Mon. Not. R. Astron. Soc.*, **206**, 407

Zuckerman, B., Koester, D., Reid, I. N., & Hünsch, M. 2003, *Astrophys. J.*, **596**, 477

Relaxing in front of the Brno Observatory and Planetarium

Awaiting the concert of the Chamber Wind Harmony Brno